NISTIR 5120

NIST REACTOR: Summary of Activities July 1991 through September 1992

U.S. DEPARTMENT OF COMMERCE
Technology Administration
National Institute of Standards
and Technology
Materials Science and Engineering Laboratory
Reactor Radiation Division
Gaithersburg, MD 20899

NIST

NISTIR 5120

NIST REACTOR: Summary of Activities July 1991 through September 1992

U.S. DEPARTMENT OF COMMERCE
Technology Administration
National Institute of Standards
and Technology
Materials Science and Engineering Laboratory
Reactor Radiation Division
Gaithersburg, MD 20899

February 1993

U.S. DEPARTMENT OF COMMERCE
Ronald H. Brown, Secretary

NATIONAL INSTITUTE OF STANDARDS AND TECHNOLOGY
Raymond Kammer, Acting Director

FOREWORD

This annual report incorporates two major changes. First, the dates covered have been changed, so that from now on, the report year will coincide with the fiscal year—October 1 to September 30. Second, this report contains highlights from each divisional research area, which are described in enough detail to allow an assessment of the progress made in key areas. In addition, experiment titles are listed under each section. These titles may represent one or a number of blocks of beam time. This change was necessitated by the large number of individual experiments now being performed annually, which made even a brief description of all topics impossible. Further information on any topic of interest can be obtained by writing either to the authors directly, or to Mrs. Carol O'Connor, who will contact the appropriate person.

Within Reactor operations, this has been an uneventful and therefore successful year. The reactor has operated well, with better than 95% reliability overall. Fabrication of the new main heat exchangers is almost complete, and planning for their installation (presently scheduled for the end of 1993) is well underway. This installation will involve an extended shutdown, as we intend to install the new hydrogen cold source and the remaining three cold neutron guides at the same time. In order to minimize the disruption to experimental programs, every effort will be made to perform all tasks in parallel to the extent possible.

Within the Cold Neutron Project, progress has been steady. By early 1993, there will be eleven instruments installed in the CNRF, including the two instruments which comprise the NSF-funded Center for High Resolution Neutron Scattering (CHRNS). The formal CNRF user program was successfully initiated this past year, with more than 80 proposals received. Use of the facilities continues to grow as capability increases, a trend which to date shows no signs of saturating. A new pass system, which greatly simplifies access by non-NIST researchers, is now operational, and has proved to be a significant improvement for all concerned. No additional instruments will be installed before the end of 1993, when the new hydrogen source is scheduled for installation. However, design, construction, and R&D continue.

The Neutron Condensed Matter Science program continues to produce outstanding results, with notable examples in the study of fullerenes (with one paper on C_{60} named as a "hot paper" by *The Scientist*), in studies of the magnetic properties of high T_c superconductors, in studies of surfaces and interfaces by reflectrometry, and with the *ab initio* determination of one of the most complex crystal structures yet solved by powder methods, among many others. Two new thermal neutron facilities are well under way—the new 32 detector powder diffractometer now being commissioned at BT-1, and a dedicated instrument for residual stress measurements which is now being designed and constructed.

This has been a year of steady progress throughout the division, and I want to thank every one of the dedicated people who has contributed to it. I also thank Carol O'Connor for her dedicated efforts in the Guest Researcher program and for editing this report.

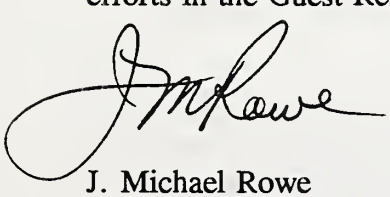

J. Michael Rowe
Chief, Reactor Radiation Division

ABSTRACT

This report summarizes all the programs which use the NIST reactor. It covers the period for July 1991 through September 1992. The programs range from the use of neutron beams to study the structure and dynamics of materials through nuclear physics and neutron standards to sample irradiations for activation analysis, isotope production, neutron radiography, and nondestructive evaluation.

KEY WORDS: activation analysis; cold neutrons; crystal structure; diffraction; isotopes; molecular dynamics; neutron; neutron radiography; nondestructive evaluation; nuclear reactor; radiation.

DISCLAIMER

Certain trade names and company products are identified in order to adequately specify the experimental procedure. In no case does such identification imply recommendation or endorsement by the National Institute of Standards and Technology, nor does it imply that the products are necessarily the best available for the purpose.

CONTENTS

CHEMICAL PHYSICS OF MATERIALS

Research at the NBSR which falls into this category typically involves inelastic neutron scattering measurements of the dynamics of molecular solids, various inclusion compounds, and structurally disordered materials. These studies yield detailed information on the atomic and molecular interactions responsible for many properties of these systems. For cases involving either rotational excitations or hydrogen motions or both, this information is difficult, if not impossible, to obtain by other means. Furthermore since thermal neutron wavelengths are comparable to interatomic spacings, one is able to ascertain the geometry of the various motions in a way unmatched by other spectroscopic probes. Each of these attributes is featured in one or more of the examples that are highlighted here.

Fullerenes and Fullerides

Fullerenes, the third allotrope of carbon, are closed cage molecules consisting of triply connected atoms which form 12 pentagons and any number of hexagons other than 1. Because of the strained nature of the carbon bonding when pentagons are adjacent, the soccer ball-shaped C_{60} (buckminsterfullerene) is particularly stable, it being the smallest fullerene in which no pentagons are adjacent. Work on the solid state properties of the fullerenes started following the discovery of a method by which bulk quantities of C_{60} could be produced [1]. It was quickly shown that at room temperature C_{60} crystallizes into an fcc structure [2] in which the molecules are orientationally disordered and that solid C_{60} undergoes a transition at $T_c \sim 256$ K to a low temperature, mostly ordered simple cubic phase [3].

C_{60} can also be intercalated with alkali metals resulting in several stochiometric compounds, known as fullerides, including A_3C_{60} and A_6C_{60} where A = K or Rb [4]. Here electrostatic guest-host interactions favor orientational ordering of the C_{60} molecular units. A_3C_{60} crystallizes in a face-centered-cubic structure with the C_{60}^{3-} ions randomly distributed between two orientations, related to each other by 90°-rotations [5]. These compounds are metallic and become superconducting at 19 K [6] and 28 K [7] for K_3C_{60} and Rb_3C_{60}, respectively. Saturation-doping results in the insulating phase A_6C_{60} which adopts a body-centered-cubic structure with the C_{60}^{6-} units orientationally ordered at room temperature [8]. Motivated by the nearly spherical shape of C_{60}, work at NIST has addressed the question of how these "balls" rotate and how the rotational excitations are related to orientational order and disorder in these systems.

- **Rotational dynamics above T_c**

Before discussing the spectroscopy of orientational motions, it is convenient to refer to powder diffraction data in the disordered phase [9] (see also Crystallography section). Figure 1 shows that, in addition to the Bragg peaks arising from the fcc structure of the solid, there is a diffuse scattering component with two prominent peaks at Q values of 3.4 and 5.7 Å^{-1}. Figure 2(a) shows an inelastic neutron scattering (INS) spectrum obtained at Q = 5.67 Å^{-1} which demonstrates that the diffuse scattering above T_c is entirely quasielastic. The widths and intensities of the quasielastic peaks are strongly Q-dependent, as shown in Figure 3.

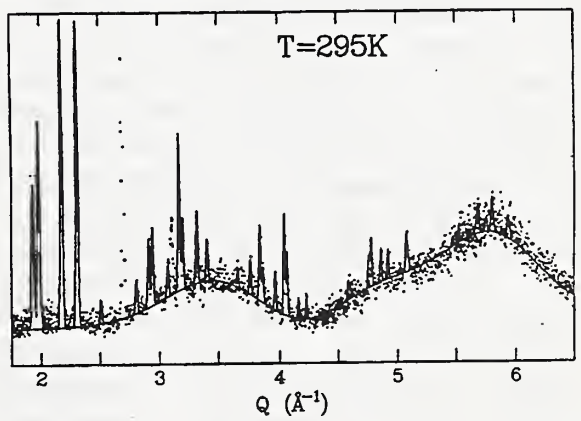

Figure 1. Room temperature neutron diffraction pattern for C_{60}. Points represent measurements at NIST, normalized to a fixed monitor count. The line was calculated assuming that the orientations of molecules are random and uncorrelated.

The quasielastic scattering can be accurately described within a remarkably simple model of rotational diffusion [10]. The reorientational motions of adjacent molecules are regarded as

completely uncorrelated, and each molecule tumbles randomly through a continuum of orientations rather than executing jumps among some set of discrete orientations. The powder-averaged rotational component of the coherent neutron scattering function $S_r(Q,\omega)$ can then be expressed as a sum of Lorentzians

$$S_r(Q,\omega) = \sum_{\ell=1}^{\infty} a_\ell \, (2\ell + 1) \, j_\ell^2 \, (QR) \cdot \frac{1}{\pi} \frac{\tau_\ell}{1 + \omega^2 \tau_\ell^2} \qquad (1)$$

where

$$\tau_\ell = \frac{1}{\ell \, (\ell + 1) \, D_r}, \qquad (2)$$

j_ℓ is a spherical Bessel function, R is the radius of the C_{60} molecule, D_r is the rotational diffusion constant, and the coefficients a_ℓ are given by

$$a_\ell = \sum_{n,n'=1}^{60} P_\ell \, (\cos \theta_{nn'}). \qquad (3)$$

Here P_ℓ is a Legendre polynomial and $\theta_{nn'}$ is the angle subtended at the molecular center by atoms n and n' within the same molecule [11]. This sum reflects the molecular geometry and completely accounts for the fact that motions between atoms within a single molecule are correlated. Due to the high degree of symmetry of C_{60}, one finds that all odd-ℓ and many even-ℓ terms are identically zero. In fact, the only terms that significantly contribute to the scattering in the Q-range of these experiments, are those with ℓ = 6,10,12,16,18 and 20.

The Q dependences of the quasielastic intensities and energy widths, shown in Figure 3, are quantitatively described by the predictions of this model. Only an overall scale factor has been used to adjust the calculated intensities in comparing with experiment, while an additional parameter, D_r, describes the Q dependence of the widths at each temperature. It has been found that at 260 K, $D_r = (1.4 \pm 0.4) \times 10^{10} s^{-1}$. Different values of D_r affect only the magnitude of the widths, but the shape of Γ vs. Q remains the same.

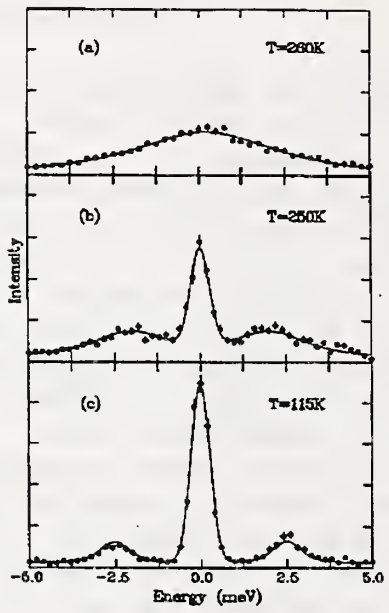

Figure 2. Inelastic neutron scattering spectra taken at Q = 5.65 Å^{-1} at 260 K, 250 K, and 115 K. Above T_c the spectrum consists of a single Lorentzian centered at zero energy transfer, characteristic of diffusion. Below T_c the spectra show peaks at non-zero energy transfers, corresponding to librations of C_{60} molecules about their equilibrium positions.

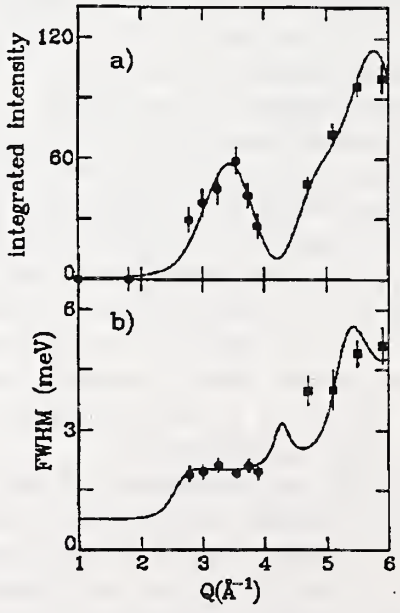

Figure 3. Q-dependences of the integrated intensity and the energy width of the quasielastic scattering at 260K. Points represent experimental data. The solid lines are calculated for isotropic rotational diffusion. For (b), a value of $D_r = 1.4 \times 10^{10} s^{-1}$ has been used in the calculation.

Comparing the widths for different temperatures yields an activation energy of (35 ± 15) meV.

In spite of its good agreement with the neutron results, the rotational diffusion model cannot be the complete picture of the disordered phase. The orientational ordering must ultimately arise from dynamic orientational correlations above T_c. It is possible that such correlations would be detectable in a neutron scattering experiment on a single crystal. In fact recent x-ray diffraction results obtained from a single crystal show that the scattering distribution is not completely spherical in the high temperature phase, but that at room temperature it differs from spherical symmetry by at most 15% [12].

- **Rotational dynamics in the ordered phase**

At 256 K, long-range orientational order develops in solid C_{60}. The high-temperature fcc structure ($Fm\bar{3}m$) lowers its symmetry to a simple cubic ($Pa\bar{3}$) structure [13], in which there are four molecules per unit cell. One can generate this structure by first aligning all molecules in the same orientation, with three orthogonal twofold axes parallel to the cubic axes, and then rotating each ball 22° about a specific {111} direction. The molecules then face each other so that, for each pair of nearest-neighbor balls, a twofold axis on one ball is aligned with a pentagonal face on a neighboring ball.

The orientational potential which secures this structure gives rise to librations of the balls about the equilibrium configuration. We have observed a well-defined excitation with an energy of 2.8 meV at 20 K [14]. The scans shown in Figure 2 illustrate the broadening and softening that take place as the temperature is raised from 115 to 250 K. The librational peaks are significantly broadened above experimental resolution at all temperatures, but the natural width increases by a factor of six between 20 and 250 K, accompanied by a softening of about 30% in the energy of the mode.

The assignment of the observed inelastic scattering to librations is based primarily on the Q dependence of the energy-integrated intensities (Fig. 4). Assuming that librations of individual molecules are neither coupled to one another nor to other types of excitation, and that angular displacements from equilibrium are equally likely

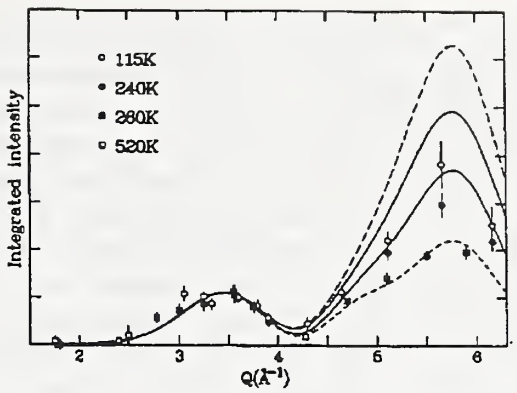

Figure 4. Q dependence of the total integrated rotational scattering. Points represent data at various temperatures. The lower dashed line corresponds to complete rotational disorder (or extremely large amplitude librations). The upper dashed line corresponds to vanishingly small amplitude librations. Upper and lower solid lines correspond to librations with amplitudes of 4.0° and 6.7°, respectively. Calculations and data are arbitrarily scaled to the ℓ = 10 peak at Q ~ 3.5Å^{-1}.

to occur about any axis, an analytic expression can be derived for these intensities in the limit of small librational amplitudes. The energy integral of this expression, $S_r(Q)$, resembles the result for rotational diffusion (Fig. 3) except that equation 3 now contains an additional factor $\ell(\ell+1)$ which lends extra weight to the higher ℓ terms [15]. The theory gives good qualitative agreement with experiment, but overestimates the scattering at larger Q, because no angular Debye-Waller factor has been taken into account. An alternative approach to the calculation of $S_r(Q)$ is to use a Monte Carlo technique, in which one calculates the scattering from an assembly of molecules which have been randomly displaced from the equilibrium configuration according to a Gaussian probability distribution in angle. Simulations of this type describe the Q dependence of the librational intensity very well as shown in Figure 4 [15]. This unambiguously identifies the excitations as librations. In addition, they demonstrate the pronounced effect of the angular Debye-Waller factor on the Q-dependence of the rotational scattering intensity, emphasizing the importance of including it in all calculations of the scattering from C_{60}, including the Bragg intensity.

The neutron scattering experiments performed at NIST give a fairly complete picture of the orientational dynamics of solid C_{60} in the solid phase. Below T_c the molecules librate about their equilibrium positions while above T_c the molecules reorient randomly through a continuum of orientations. Thus the high temperature phase can be considered to be an orientational liquid and the orientational order-disorder transition may be regarded as "rotational melting" since it separates this "liquid" phase from a phase in which oscillations occur about an equilibrium orientation.

- **Rotational Dynamics in K_3C_{60} and Rb_6C_{60}**

Representative INS spectra for K_3C_{60} below and above the superconducting transition temperature T_c (=19.3 K) and at 300 K, at Q = 5.72 Å^{-1} are shown in Figures 5(a)-(c). Figure 5(d) shows the corresponding Rb_6C_{60} spectrum at room temperature at Q = 5.93 Å^{-1} [16]. In both systems, the librations soften as the temperature increases; however, the softening is markedly smaller in K_3C_{60} and Rb_6C_{60} than in C_{60}. The widths of the librational peaks are not resolution-limited, but are essentially temperature-independent indicating the presence of dispersion effects and anisotropies in the rotational potential.

Of particular interest is the behavior of the librational modes in K_3C_{60}, as the sample is cooled below T_c. Measurements performed at 25 K and 12 K demonstrate that within the experimental uncertainty, neither the energy nor the width is affected. The superconductivity gap, 2Δ, is known to be greater than or equal to the energy of the librations. Therefore Γ_{ep}, the lifetime contribution to the width due to the electron-phonon interaction, disappears in the superconducting state, and the peaks should narrow by approximately Γ_{ep} as the sample becomes superconducting. The observed linewidth changes are only consistent with small values of Γ_{ep} in contrast to the predictions of some theories of libration-mediated electron pairing in the fullerides, which predict $\Gamma_{ep} \sim 0.5$-0.7 meV. This result indicates that coupling of electrons to librations does not contribute significantly to the formation of Cooper pairs.

The energy of the librational mode increases as the ionicity of the C_{60} unit is increased. This is due to an increase in the interaction strength in going from C_{60}, where the predominant forces are

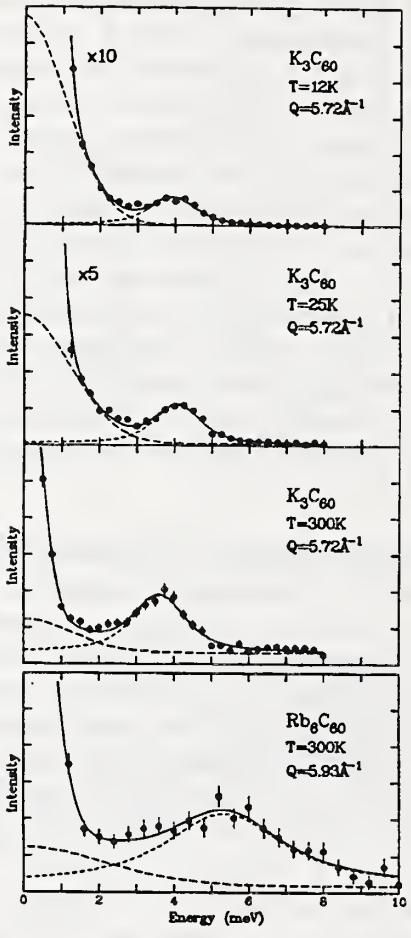

Figure 5. Representative INS spectra at constant Q. K_3C_{60}, Q = 5.72 Å^{-1}, with (a) T = 12 K, (b) T = 25K, and (c) T = 300 K, (d) Rb_6C_{60}, Q = 5.93 Å^{-1}, with T = 300 K. The solid circles are experimental points and the solid lines are best fits.

of van der Waals origin, to Rb_6C_{60}, where Coulomb forces between highly charged ions dominate. In addition, the energy of the C_{60} librations is slightly larger for Rb-intercalated systems then for those intercalated with K. Presumably this is due to steric effects since Rb ions are slightly larger that K ions.

The integrated intensities of the librational peaks of K_3C_{60} and Rb_6C_{60} at room temperature are shown as a function of Q in Figure 6. Calculations for completely orientationally disordered molecules (dashed line), and for uncorrelated isotropic molecular librations with a root-mean-square amplitude $\theta_{rms} = 6.7°$ (solid line), are also included. The calculations were arbitrarily scaled to the Q~5.75 Å^{-1} peak. There is satisfactory agreement between the experimental data and the

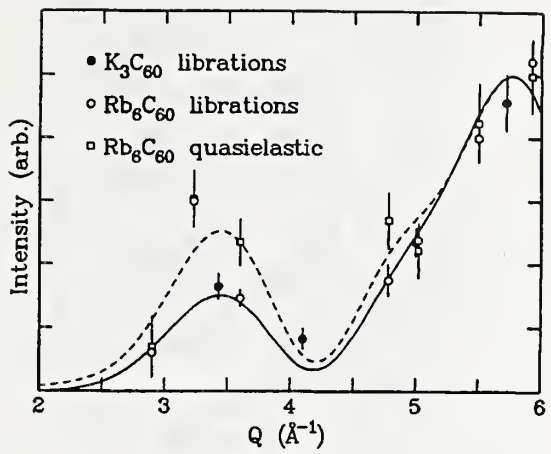

Figure 6. Q-dependence at 300 K of the intensity of the librational mode in K_3C_{60} (solid circles), the librational mode in Rb_6C_{60} (open circles), and the zero-energy-transfer centred Gaussian component in Rb_6C_{60} (open squares). The dashed line is the intensity variation calculated for complete orientational disorder while the solid line is for uncorrelated isotropic librations with a root-mean-square amplitude of 6.7°. Calculations are arbitrarily normalized to the Q = 5.75 Å^{-1} peak.

librational model calculation, confirming the assignment of the inelastic scattering peak to molecular librations.

- **Microscopic Theory of Orientational Disorder in C_{60}**

If one includes atoms, single bond centers, and double bond centers within a C_{60} molecule, there are a total of 150 interaction sites. Therefore a brute-force calculation of the potential felt by a molecule in solid C_{60} for just 1 orientation of the molecule and its 12 neighbors requires performing a sum with more than 250,000 terms. In the orientationally disordered phase one must then average over all orientations. The numerical complexity of the problem can be greatly reduced by utilizing the symmetry of the molecule and of the molecular site through the use of appropriate symmetry adapted functions. The interaction between two molecules may then be written as a multipole expansion with a greatly reduced number of terms. The computational saving is particularly remarkable because of the very high symmetry of the C_{60} molecule. The leading terms, as we have seen previously, are those with $\ell = 6$ and $\ell = 10$.

These types of calculations have been performed assuming a Lennard-Jones potential between atoms, requiring a significant extension of earlier work on symmetry adapted functions since only terms up to $\ell = 3$ had been considered previously [17]. In particular it was shown that multipolar functions of T_{2g} symmetry with $\ell = 10$ are dominant in driving the phase transition while the most significant contribution to the crystal field is the A_{1g} symmetry component belonging to the $\ell = 6$ manifold. Furthermore, the phase transition is first order (as observed experimentally) and occurs at the X point of the Brillouin zone.

While the calculated transition temperature was somewhat below the observed value the above results are general and do not depend on the particular choice of the potential. The importance of this work is not so much in the numerical results, which are based on a particular choice of interatomic potential, but rather in the symmetry consequences, and as a formalism for performing calculations based on more realistic interatomic potentials as they become available.

Hydrogen in Metals

It is well-known that a number of hcp rare-earth metals (e.g., Sc, Lu, and Y) can retain substantial amounts of hydrogen at low temperatures without precipitation of ordered hydride phases. The dissolved hydrogen atoms reside in the tetrahedral interstices of the metal lattice. Despite this tetrahedral symmetry, INS studies have indicated that an anharmonic, anisotropic soft mode typically exists for H vibrations polarized along the c axis, 25%-30% lower in energy than the doubly-degenerate modes polarized in the basal plane. Moreover, the high-resolution lineshape of the c-axis mode at high H concentrations is broad and essentially split into two components, namely, local lower-energy "acoustic" and higher-energy "optic" branches caused by hydrogen pairs dynamically coupled across metal atoms along the c direction. The details of the lineshape depend on temperature, H concentration, and host metal and directly reflect the extent of short-range ordering of hydrogen pairs into finite chains along the c direction and possible 3-d ordering of the chains themselves. Further efforts at NIST have been directed to

concentration-dependent studies of the vibrational dynamics of α-LuH_x and its deuterated analog in order to establish a more complete comparison of the nature of H and D dissolved in Sc, Lu, and Y. Figure 7 compares the H-concentration dependence of the c-axis vibration at low temperature for α-YH_x and α-LuH_x. The change in lineshape with H concentration for α-LuH_x mimics that for α-YH_x: the progression from high to low H concentration causes a smearing out of the higher-energy optic component of the spectral doublet, reflecting the broader distribution of H-H interactions due to the reduction in hydrogen pairing order. This behavior has also been observed for α-ScH_x and α-LuD_x.

As in the rare-earth/hydrogen α-phase studies, neutron vibrational spectroscopy of the superstoichiometric rare-earth dihydrides is found to be a sensitive probe of the order that occurs in the octahedrally-coordinated hydrogen sublattice. For example, the low-temperature hydrogen vibrational spectra of β-TbH_{2+x} (which possesses 2 tetrahedral-site and x octahedral-site H atoms per Tb atom, see Fig. 8) indicate that the o-site hydrogen (H_o) and associated optical vibrations are sensitive to the value of x (see Fig. 9). For x = 0.03 (as well as for x = 0.09), the majority of the low-concentration o-site hydrogens are isolated in a local cubic environment and exhibit a relatively sharp vibrational density of states at 80.8 meV, in accord with the presence of triply-degenerate normal modes. In contrast, for x = 0.19, a more complex density of states is evident, consistent with the type of long-range order that is known to occur in the H_o sublattice at this higher concentration. This density of states is present at the lower H_o concentrations only as minor spectral wings. In this ordered sublattice, each o-site hydrogen (H_o) is an intersecting member of identical $[-H_o-Tb-]_n$ chains in the (100) and (001) directions and a $[-H_o-Tb-\square-Tb-]_n$ chain (where $\square$ represents an o-site vacancy) in the (010) direction. This yields what may be a dispersion-broadened bimodal lineshape consisting of doubly-degenerate vibrations at higher energy (~82.7 meV) associated with the (100)- and (001)-polarized modes and a singlet vibration at lower energy (~78.0 meV) associated with the (010)-polarized mode. Nonetheless, we are also exploring the possibility that the breakup of vibrational degeneracy is due to a high-concentration, low-temperature shift in o-site

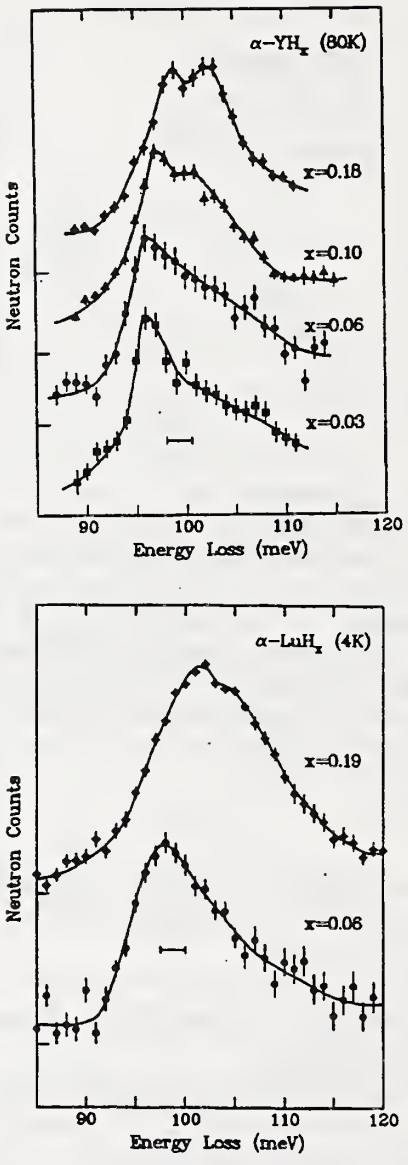

Figure 7. High-resolution INS spectra of α-YH_x at 77 K and α-LuH_x at 4.2 K as functions of H concentration measured on the BT-4 spectrometer with the Be/PG/Be-filter analyzer. Solid lines are intended only to guide the eye.

hydrogens away from their ideal positions, leading to a lowering of the o-site symmetry, as has been observed in other superstoichiometric rare-earth dihydrides.

The vibrational density of states of hydrogen trapped by interstitial nitrogen impurities in $NbN_{0.007}H_{0.004}$ have been measured to more fully characterize, under higher-resolution conditions, the lineshape of the broad 106-meV feature previously observed for $NbN_{0.004}H_{0.003}$. The lineshape measured at 4.2 K exhibits clear

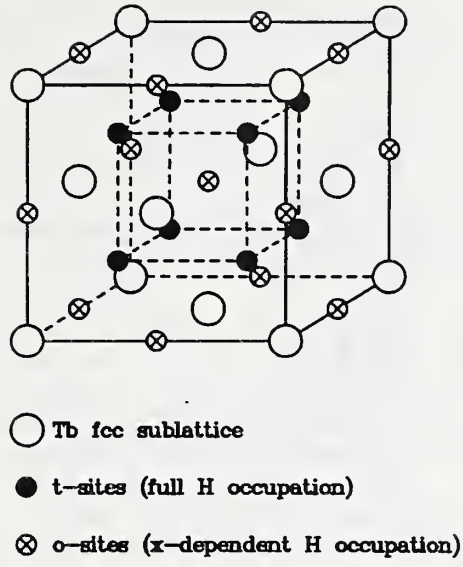

Figure 8. Unit cell geometry of TbH_{2+x}.

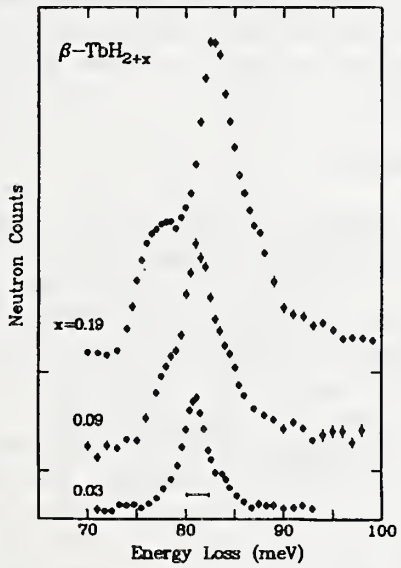

Figure 9. A comparison of the vibrational density of states of the H_o sublattice in β-TbH_{2+x} for different values of the excess hydrogen x. The instrumental resolution (FWHM) is denoted by the horizontal bar accompanying the spectra.

evidence of a spectral doublet that is absent at 77 and 296 K (see Fig. 10). This result is interpreted as the first experimental observation of excited-state tunnel splitting, indicating a separation of 4 $\pm$0.3 meV. The splittings of the ground state and first-excited state tunneling levels and the $E_{0\to1}$ vibration can simultaneously be fit with a 1-d

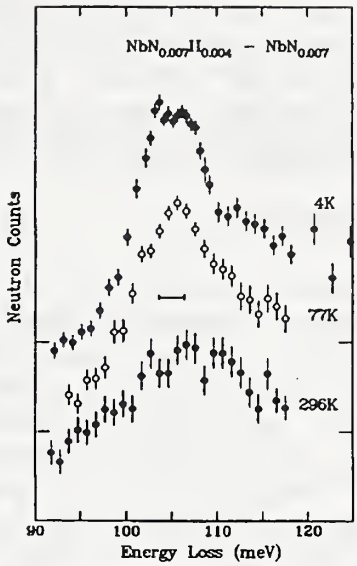

Figure 10. The effect of temperature on the high-resolution INS difference spectra of the low-energy H vibrational mode in $NbN_{0.007}H_{0.004}$. The instrumental resolution (FWHM) is illustrated by the horizontal bar beneath the spectra.

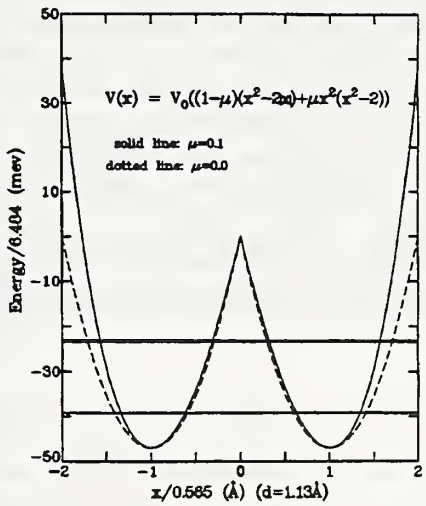

Figure 11. Model potential and energy levels. The levels shown are for the case μ = 0.1, a small but significant quartic anharmonicity. The splittings are 0.20 meV for the ground state, and 4.5 meV for the excited state. The vibrational transition is 100 meV. The tunneling site separation is d = 1.13 Å.

function for the double-well potential comprised of harmonic and quartic terms (see Fig. 11). The interpretation of the fit is complicated by two important factors. First, the line joining the tunneling sites is not along a normal mode

direction, so a 3-d analysis of the motion may be required. Second, and more difficult, the many-body effects which have been shown to be significant for the ground state tunneling have yet to be worked out for the excited state splittings.

Microporous Materials

The neutron vibrational spectrum of sodium hydroxosodalite dihydrate $Na_8(Al_6Si_6O_{24})(OH)_2 \cdot 2H_2O$ has revealed a novel $[HO \cdots H \cdots OH]^-$ (i.e., $H_3O_2^-$) anion stabilized within the Na^+ cation tetrahedron occupying each sodalite cage. The spectrum resembles that of the $[H_2O \cdots H \cdots OH_2]^+$ (i.e., $H_5O_2^+$) cation present in dodecatungstophosphoric acid hexahydrate $H_3PW_{12}O_{40} \cdot 6H_2O$ (see Fig. 12), suggesting that both ions possess a very similar central hydrogen bond, consistent with the comparable short $O \cdots O$ distance (0.236-0.237 nm) for each ion. These spectra were qualitatively unlike vibrational spectra measured for other molecular compounds containing $H_3O_2^-$-type complexes: namely, $CsOH \cdot H_2O$ and the natrochalcite-type compound $Cu_2K(H_3O_2)(SO_4)_2$, which possess longer $O \cdots O$ distances (0.264 and 0.2486 nm, respectively) and significantly noncentered hydrogens in the $HO \cdots H \cdots OH$ entities, and exhibit features indicative of separate H_2O and OH^- vibrations of an $HOH \cdots OH^-$ complex. Spectroscopic measurements of the deuterated analogs of the $H_3O_2^-$ and $H_5O_2^+$ complexes are in progress.

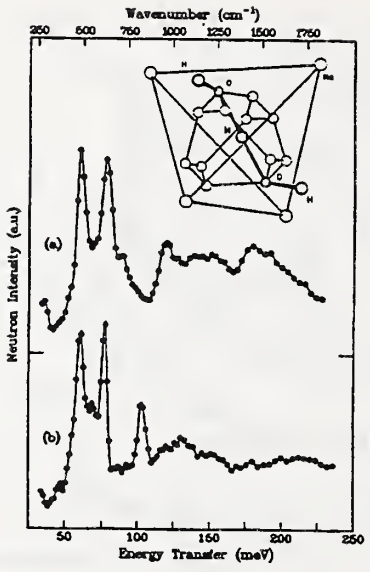

Figure 12. The INS spectra of a) $[Na_4(H_3O_2)]_2[Al_6Si_6O_{24}]$ at 4.2 K and b) $[H_5O_2]_3[PW_{12}O_{40}]$ at 10 K measured on the BT-4 spectrometer with the Be-filter analyzer. The inset illustrates the truncated tetrahedron of the O atomic positions of the disordered $H_3O_2^-$ anion, the larger Na_4 tetrahedron, and one possible anion orientation.

References

[1] W. Krätschmer, L. D. Lamb, K. Fostiropolous, and D. R. Huffman, Nature 347, 354 (1991).

[2] R. M. Fleming, T. Siegrist, P. M. Marsh, B. Hessen, A. R. Kortan, D. W. Murphy, R. C. Haddon, R. Tycko, G. Dabbagh, A. M. Mujsce, M. L. Kaplan, and S. M. Zahurak, Mater. Res. Soc. Symp. Proc. 206, 691 (1991).

[3] P. A. Heiney, J. E. Fischer, A. R. McGhie, W. J. Romanow, A. M. Denenstein, J. P. McCauley, Jr., A. B. Smith, III, and D. E. Cox. Phys. Rev. Lett. 66, 2911 (1991).

[4] O. Zhou and D. E. Cox, J. Phys. Chem. Solids 53, 1373 (1992).

[5] P. W. Stephens, L. Mihaly, P. L. Lee, R. L. Whetten, S.-M. Huang, R. B. Kaner, F. Diederich, and K. Holczer, Nautre, 351, 632 (1991).

[6] A. F. Hebard, M. J. Rosseinsky, R. C. Haddon, D. W. Murphy, S. H. Glarum, T.T.M. Palstra, A. P. Ramirez, and A. R. Kortan, Nautre 350, 660 (1991).

[7] M. J. Rosseinsky, A. P. Ramirez, S. H. Glarum, D. W. Murphy, R. C. Haddon, A. F. Hebard, T.T.M. Palstra, A. R. Kortan, S. M. Zahurak, and A. V. Makhija, Phys. Rev. Lett. 66, 2830 (1991).

[8] O. Zhou, J. E. Fischer, N. Coustel, S. Kycia, Q. Zhu, A. R. McGhie, W. J. Romanow, J. P. McCauley, Jr., and A. B. Smith III, Nature 351, 462 (1991).
[9] J.R.D. Copley, D. A. Neumann, R. L. Cappelletti, W. A. Kamitakahara, E. Prince, N. Coustel, J. P. McCauley, Jr., N. C. Maliszewskyj, J. E. Fischer, A. B. Smith III, K. M. Creegan, and D. M. Cox, Physica B 180-181, 706 (1992).
[10] D. A. Neumann, J.R.D. Copley, R. L. Cappelletti, W. A. Kamitakahara, R. M. Lindstrom, K. M. Creegan, D. M. Cox, W. J. Romanow, N. Coustel, J. P. McCauley, Jr., N. C. Malisewskyj, J. E. Fischer, and A. B. Smith III, Phys. Rev. Lett. 67, 3808.
[11] V. F. Sears, Can. J. Phys. 45, 237 (1967).
[12] P. C. Chow, X. Jiang, G. Reiter, P. Wochner, S. C. Moss, J. D. Axe, J. C. Hanson, R. K. McMullan, R. L. Meng, and C. W. Chu, Phys. Rev. Lett. 69, 2943 (1992).
[13] R. Sachidanandam and A. B. Harris, Phys. Rev. Lett. 67, 1467 (1991).
[14] D. A. Neumann, J.R.D. Copley, W. A. Kamitakahara, J. J. Rush, R. L. Cappelletti, N. Coustel, J. E. Fischer, J. P. McCauley, Jr., A. B. Smith III, K. M. Creegan, and D. M. Cox, J. Chem. Phys. 96, 8631 (1992).
[15] J.R.D. Copley, D. A. Neumann, R. L. Cappelletti, and W. A. Kamitakahara, J. Phys. Chem. Solids 53, 1353 (1992).
[16] C. Christides, D. A. Neumann, K. Prassides, J.R.D. Copley, J. J. Rush, M. J. Rosseinsky, D. W. Murphy, and R. C. Haddon, Phys. Rev. B. 46, 12088 (1992).
[17] K. H. Michel, J.R.D. Copley, and D. A. Neumann, Phys. Rev. Lett. 68, 2929 (1992).

Experiments

Neutron Spectroscopic Study of Excited-State Tunnel-Splitting for Hydrogen in $NbN_{0.007}H_{0.004}$
J. J. Rush, T. J. Udovic, N. F. Berk, D. Richter, and A. Magerl.

Neutron Spectroscopic Studies of α-LuH_x and α-LuD_x Solid Solutions
T. J. Udovic, J. J. Rush, I. S. Anderson, J. N. Daou, P. Vajda, and O. Blaschko.

Neutron Spectroscopic Studies of α-ScH_x and α-ScD_x Solid Solutions
T. J. Udovic, J. J. Rush, N. F. Berk, and I. S. Anderson.

Neutron Spectroscopic Studies of β-TbH_{2+x}, β-YH_{2+x}, and their Deuterated Analogs
T. J. Udovic, J. J. Rush, and I. S. Anderson.

Neutron Spectroscopic Study of Hydrogen and Deuterium Site Occupation in Nb-rich BCC NbV Alloys
T. J. Udovic, J. J. Rush, R. Hempelmann, and D. Richter.

Diffuse and Inelastic Neutron Scattering Study of a Quenched $Fe_{0.5}Cr_{0.5}$ Crystal
J. L. Robertson, L. Reinhard, D. A. Neumann, and S. C. Moss.

Modeling of the Structure of Icosahedral Phase Alloys
J. L. Robertson.

Quasielastic Neutron Scattering Study of Dilute Alloys of Liquid Al
I. Penfold, J. L. Robertson, S. C. Moss, and D. L. Price.

Neutron Spectroscopic Study of Hydrogen Site Geometry in $ZrCoH_3$
R. Hempelmann, T. J. Udovic, and T. Schober.

Neutron Spectroscopic Study of Hydrogen in Nanocrystalline Pd
U. Stuhr, H. Wipf, and T. J. Udovic, J. J. Rush.

Neutron Spectroscopic Study of Hydrogen in $YBa_2Cu_3O_x$
U. Knell, C. Heid, H. Wipf, T. J. Udovic, and J. J. Rush.

Neutron Spectroscopic Study of Hydrogen in $La^{60}Ni_5H_x$
C. Schönfeld, R. Hempelmann, T. J. Udovic, and J. J. Rush.

Inelastic Neutron Scattering Studies of Heteropolyanions of Tungsten and Molybdenum and Their Deuterated Analogues
T. J. Udovic and J. M. Nicol.

Neutron Vibrational Spectroscopy of Sodium Hydroxosodalite Dihydrate $Na_8[Al_6Si_6O_{24}](OH)_2 \cdot H_2O$
O. Elsenhans, J. M. Nicol, T. J. Udovic, W. Bührer, J. Felsche, P. Sieger, and M. Wiebcke.

Neutron Vibrational Spectroscopy of $CsOH \cdot H_2O$
T. J. Udovic and J. M. Nicol.

A Study of the $H_3O_2^-$ Anion in $Cu_2K(SO_4)_2H_3O_2$ and $Cu_2Na(SO_4)_2H_3O_2$ by Inelastic Neutron Scattering Spectroscopy

J. M. Nicol and T. J. Udovic.

On Why, Apart From Spin Incoherence, n Itinerant Hydrogen (Deuterium) Atoms in Metals Do Not Engender n^2 Coherent Neutron-Scattering Cross Sections as Proposed in the Literature

R. C. Casella.

The Neutron Vibrational Spectroscopy of the Interstitial Hydrogen Ligand in $HRu_6(CO)_{18}Cs$

J. Eckert, S. Johnson, J. M. Nicol, and U. A. Jayasooriya.

A Study of the Temperature Dependence of the N-H bending mode in Acetanilide ($C_6D_5NH(D)$ $COCD_3$) by Neutron Vibrational Spectroscopy

S. W. Johnson, J. Eckert, M. Barthes, and J. M. Nicol.

A Study of Protonic Species Present in Partially Dehydroxylated Kaolinites by Inelastic Neutron Scattering Spectroscopy

J. M. Nicol, R. F. Meinhold, T. Davis, and R.T.C. Slade.

Characterization of Cyclopropane Adsorbed in Na-X Zeolite by Inelastic Neutron Scattering Spectroscopy

J. M. Nicol, T. J. Udovic, R. R. Cavanagh, and S. Suib.

Inelastic Neutron Scattering of OH groups in $Mg_3(Si_2O_5)(OH)_4$

J. M. Nicol, T. J. Udovic, G. D. Stucky.

Inelastic Neutron Scattering Studies of Iridium Clusters in Na-Y and K-L Zeolites

J. M. Nicol, R. R. Cavanagh, T. J. Udovic, Z. Xu, S. Kawi, N. Triantafillow, B. C. Gates, and X. Smith.

Rotational Dynamics of C_{60} in The Orientational Liquid Phase

D. A. Neumann, J.R.D. Copley, R. L. Cappelletti, W. A. Kamitakahara, K. M. Creegan, D. M. Cox, N. Coustel, J. P. McCauley Jr., N. C. Maliszewskyj, J. E. Fischer and A. B. Smith III

Rotational Dynamics of C_{60} in The Low Temperature Phase

D. A. Neumann, J.R.D. Copley, R. L. Cappelletti, W. A. Kamitakahara, K. M.Creegan, D. M. Cox, N. Coustel, J. P. McCauley Jr., N. C. Maliszewskyj, J. E. Fischer and A. B. Smith III

Rotational Dynamics of C_{60} in $K_{0.5}$ $Rb_{2.5}$ C_{60}

D. A. Neumann, J.R.D. Copley, W. A. Kamitakahara, Otto Zhou, and J. E. Fischer

Rotational Dynamics of C_{60} in K_3 C_{60}

C. Christides, D. A. Neumann, K. Prassides, J.R.D. Copley, J. J. Rush, M. J. Rosseinsky, D. W. Murphy, and R. C. Haddon

Rotational Dynamics of C_{60} in Rb_6C_{60}

C. Christides, D. A. Neumann, K. Prassides, J. R. D. Copley, J. J. Rush, M. J. Rosseinsky, D. W. Murphy, and R. C. Haddon

Rotational Dynamics and Diffuse Scattering from Solid C_{70}

C. Christides, T.J.S. Dennis , K. Prassides, R. L. Cappelletti, D. A. Neumann, and J.R.D. Copley

Rotational Dynamics of $C_{60}Br_{24}$

K. Prassides, D. A. Neumann, J.R.D. Copley, and J. J. Rush

Rotational Dynamics of C_{60} in C_{60} $(I_2)_2$

K. Prassides, C. Christides, D. A. Neumann, and J.R.D. Copley

Search for Orientational Melting in K_3C_{60}

C. Christides, D. A. Neumann, J.R.D. Copley, W. A. Kamitakahara, K. Prassides, M. J. Rosseinsky, D. W. Murphy and R. C. Haddon

High Resolution Inelastic Neutron Scattering Study of Intramolecular Modes in C_{60}

W. A. Kamitakahara, D. A. Neumann, J.R.D. Copley, J. J. Rush, and R. L. Cappelletti

Maximum Entropy Determination of the c-axis Scattering Profile from Layered Materials

Philippe Depondt, D. A. Neumann, and S. F. Trevino

Rotation-Translation Coupling in $CsC_{24}(ND_3)_{3.7}$

Philippe Depondt, D. A. Neumann, and S. F. Trevino

Inelastic Neutron Scattering Study of Methyl Torsions in Acetonitrile

S. F. Trevino, C. S. Choi, and D. A. Neumann

Microscopic Theory of Orientational Disorder and the Solid C_{60}

K. H. Michel, J.R.D. Copley and D. A. Neumann

Neutron and X-ray Scattering Cross Sections of Orientationally Disordered Solid C_{60}
J.R.D. Copley and K. H. Michel

Dynamics of Cubic and Hexagonal Boron Nitride
W. A. Kamitakahara, D. A. Neumann, G. Doll, and A. W. Moore

Dynamics of Carbon Foams
W. A. Kamitakahara, B. Frick, D. A. Neumann, and R. Lagasse

Quasielastic Neutron Scattering from a Tetrahydrofuran-Water Solution
N. Wada, W. A. Kamitakahara, and B. Frick

Participants

Anderson, I. S.	Institut Laue-Langevin
Barthes, M.	U. of Montpellier II, France
Berk, N. F.	Reactor Radiation Division
Blaschko, O.	Institut für Experimentalphysik der Universität Wien
Bührer, W.	Paul Scherrer Institut
Cappelletti, R. L.	Ohio University, Athens, OH
Cavanagh, R. R.	Surface & Microanalysis Science Division
Choi, C. S.	Army Res. Devel. & Eng. Ctr. and NIST
Christides, C.	University of Sussex (UK)
Copley, J.R.D.	Reactor Radiation Division
Coustel, N.	University of Pennsylvania
Cox, D. M.	Exxon Research & Engineering
Creegan, K. M.	Exxon Research & Engineering
Daou, J. N.	Universite Paris-Sud
Dennis, T.J.S.	University of Sussex, UK
Depondt, Ph.	U. Pierre et Marie Curie
Doll, G.	General Motors Research Lab
Eckert, J.	Los Alamos National Lab
Elsenhans, O.	Paul Scherrer Institut
Frick, B.	Institut Laue-Langevin
Felsche, J.	U. of Konstanz, Germany
Fischer, J. E.	University of Pennsylvania
Gates, B. C.	University of Delaware
Gehring, P.	Reactor Radiation Division
Haddon, R. C.	AT&T Bell Laboratories
Heid, C.	Technische Hochschule Darmstadt, Germany
Hempelmann, R.	KFA Julich, Germany
Jayasooriya, U. A.	U. of East Anglia, UK
Johnson, S.	Los Alamos National Lab
Kamitakahara, W. A.	Reactor Radiation Division
Kawi, S.	University of Delaware
Knell, U.	Technische Hochschule Darmstadt, Germany
Lagasse, R.	Sandia National Laboratories
Magerl, A.	Institut Laue-Langevin
Maliszewskyj, N. C.	University of Pennsylvania
Michel, K. H.	University of Antwerp
McCauley, Jr., J. P.	University of Pennsylvania
Moore, A. W.	Union Carbide Coatings Service Corp.
Murphy, D. W.	AT&T Bell Laboratories
Neumann, D. A.	Reactor Radiation Division
Nicol, J. M.	Reactor Radiation Division
Prassides, K.	University of Sussex, UK
Rice, B.	Army Research Lab
Richter, D.	KFA Julich, Germany
Robertson, J. L.	Oak Ridge National Lab
Rosseinsky, M. J.	AT&T Bell Laboratories
Rush, J. J.	Reactor Radiation Division
Santodonato, L. J.	Reactor Radiation Division
Schober, T.	KFA Julich, Germany
Schönfeld, C.	KFA Julich, Germany
Sieger, P.	U. of Konstanz, Germany
Smith III, A. B.	University of Pennsylvania
Smith, X.	Amoco
Stucky, G. D.	U. of California, Santa Barbara
Stuhr, U.	Technische Hochschule Darmstadt, Germany
Suib, S.	University of Connecticut
Triantafillow, N.	University of Delaware
Trevino, S. F.	Army Res. Devel. & Eng. Ctr. and NIST
Udovic, T. J.	Reactor Radiation Division
Vajda, P.	Universite Paris-Sud
Wada, N.	Colorado School of Mines
Wiebcke, M.	U. of Konstanz, Germany
Wipf, H.	Technische Hochschule Darmstadt, Germany
Xu, Z.	University of Delaware
Zhou, O.	University of Pennsylvania

Research in these areas has covered a rather diverse range of topics, from the nature of magnetic ordering and spin dynamics in low dimensional systems, high-T_c superconductors, artificially structured materials and heavy fermion systems, to the interaction of magnetism with superconductivity, to the superconducting properties themselves. Following are a few highlights of the ongoing work.

Magnetism

- **Low Dimensional Systems**

One of the fundamental problems in magnetism concerns the nature of the ground state in antiferromagnetic materials. In 3-d systems the Néel state, where spins are alternatively up and down, is a good approximation to the ground state, but the precise nature of the ground state is still unknown. In low-dimensional systems, on the other hand, the Néel state is not a good approximation in some cases, and qualitatively new many-body ground states are anticipated. Hence a considerable effort has been made to investigate the spin dynamics of 2-d magnets related to the high-T_c oxide superconductors, and the magnetism of 1-d "chain" magnets such as $Ni(C_2D_8N_2)_2NO_2ClO_4$ (NENP), $CsMnI_3$, $[(CD_3)_3ND]FeCl_3 \cdot 2D_2O$ (FeTAC), and $EuNi_3P_5$.

For 1-d antiferromagnetic spin chains, Haldane has conjectured that there is a fundamental difference between the behavior of chains constructed with half-integer spins rather than whole-integer spins. In particular, half-integer spin systems have a ground state with quasi-long-range order, while integer-spin antiferromagnetic chains have a qualitatively new ground state characterized by a singlet, disordered, spin configuration, which possesses a gap (the Haldane gap) in the excitation spectrum. The existence of such a gap at wave vector $\tilde{q}$ has been indicated by experiments on quasi-1-d model materials as well as numerical simulations. Figure 1 shows the dispersion relation and instantaneous spin correlation function for such a model material, the S = 1 system NENP. The spin wave excitations are well defined even though there is no static long range order. Note that the dispersion relation retains the

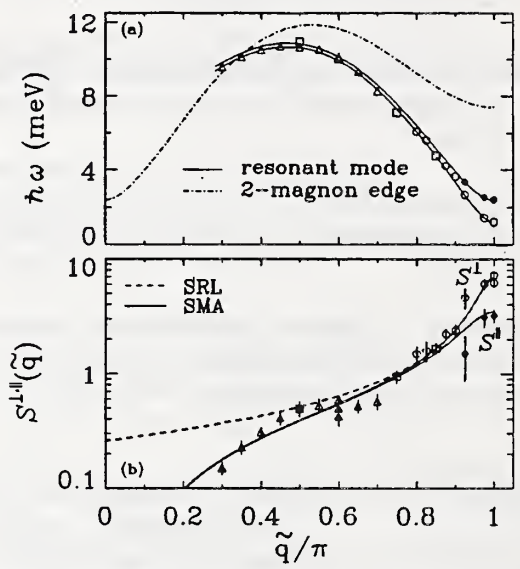

Figure 1. (a) Experimental dispersion relation (circles, triangles, squares, and solid curve) for the long-lived modes in the S = 1 Haldane gap system NENP. The dot-dashed curve is the lower edge of the corresponding two-magnon continuum. (b) Instantaneous spin correlation function. The dashed curve is for the Square-Root Lorentzian theory, and the solid curve is for the Single-Mode Approximation.

fundamental 2π periodicity of the lattice, in contrast to the case for the Néel antiferromagnet where the translational symmetry is broken and the spin wave dispersion relation is π periodic. An interesting consequence of this unbroken symmetry is that the two-magnon continuum intersects the resonant mode. The instantaneous spin correlation function (Fig. 1b) is consistent with the Square-Root-Lorentzian (SRL) form predicted by continuum field theories for large $\tilde{q}$, but deviates significantly from this form for smaller $\tilde{q}$ because such theories do not account correctly for near-neighbor correlations. The solid curve is a theoretical calculation based on the Single Mode Approximation (SMA) and the measured dispersion relation (Fig. 1a). The almost perfect agreement emphasizes that a single resonant mode dominates the spectrum for the spin-1 chain.

The Haldane conjecture for the fundamental nature of the ground state in 1-d is now relatively well documented experimentally, and interest is beginning to focus on whether these ideas can be extended to systems in higher dimensions. Indeed

when the interchain coupling exceeds a critical value these 1-d systems in fact become ordered three-dimensionally at sufficiently low temperatures, and one route to address these questions is to investigate the spin dynamics in the ordered phase. One class of materials of central interest is represented by $CsNiCl_3$ and $RbNiCl_3$, which are spin-1 chain antiferromagnets, and isostructural $CsMnI_3$, which is spin 5/2 (half-integer). These materials were in fact the first to be studied in detail with regard to the Haldane conjecture. For the S = 1 Ni materials spin wave theory failed to account for the dynamics in the low-T ordered phase, and this failure was anticipated based on the 1-d results for this Haldane-gap system. In particular, polarized neutron data had revealed that the gap at the zone center consists of a singlet ground state with a triplet excited state above it, in agreement with field theory results based on expectations for the 1-d integer spin dynamics.

One of the surprises in this class of materials, on the other hand, was that spin wave theory also failed to account for the spin dynamics of the half-integer spin system $CsMnI_3$. We therefore have carried out inelastic polarized beam experiments to determine the nature of the excitations in this system, and the possible reasons for this failure. Figure 2 shows the polarization dependence of the magnetic scattering observed close to the zone center, (001). At low field the data reveal that there are two magnon modes at (001) that are degenerate or nearly degenerate in energy, but with different widths, while spin wave theory would predict two sharp modes with a ratio of energies of $\sqrt{2}$. At higher field, on the other hand, we see that there is a clear separation in energy for these two modes. These results for this half-integer spin system are remarkably similar to those for the integer-spin systems, where our understanding is based on the existence of a Haldane gap. The degenerate modes in $CsMnI_3$ must have a different physical origin than those in $CsNiCl_3$ if our present understanding is correct, and it will be particularly interesting to see how these questions are resolved as future experiments unfold.

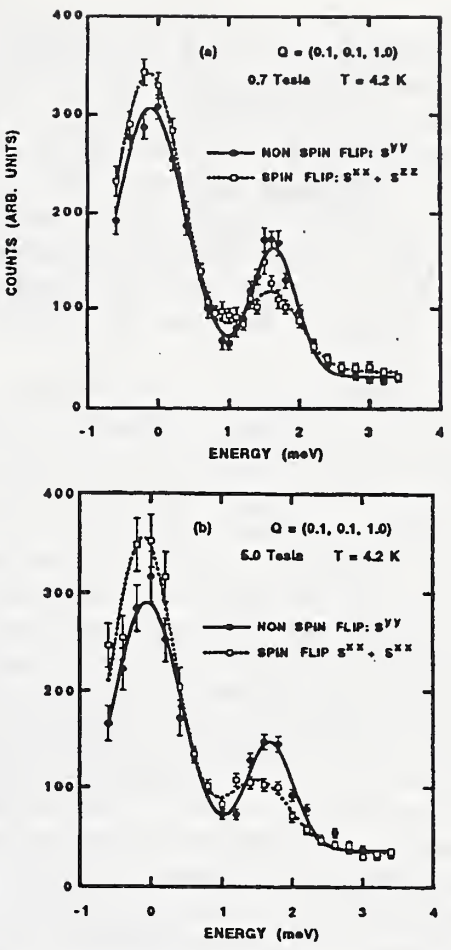

Figure 2. Spin-flip and non-spin-flip inelastic magnetic scattering in the half-integer spin chain compound $CsMnI_3$. At low field (top) the magnetic excitations are nearly degenerate in energy but differ in width, while spin wave theory predicts an energy ratio of $\sqrt{2}$. At high field (bottom) the excitations are clearly shifted in energy. These results are unexpectedly similar to the results for the integer-spin Haldane gap systems.

- **Invar**

In contrast to the low dimensional systems discussed above, spin wave theory is known to work extremely well for 3-d isotropic ferromagnets. For example, the temperature dependence of the spin wave dispersion relations, magnetization, spin wave linewidths, etc., are in quantitative agreement with theory in the expected energy and temperature regimes. There is a singular exception to this good agreement, and that is for Invar systems such as crystalline $Fe_{65}Ni_{35}$ (Invar) or amorphous $Fe_{86}B_{14}$. Recall that an Invar system is an isotropic ferromagnet which exhibits a magneto-expansion below the Curie temperature, that is so

large that it actually compensates for the usual thermal contraction so that the density is independent of temperature over a wide range. We have found previously that spin wave theory also works very well for Invar systems in terms of the temperature dependence of the spin wave dispersions relation, magnetization, spin wave linewidths, etc., except that the magnetization varies much more quickly with temperature than expected based on the measured dispersion relations.

One explanation for this "Invar anomaly" is that there are additional "hidden" magnetic excitations which participate in reducing the magnetization. If this explanation is correct, then the magnetization and neutron results already place stringent conditions on the form that such excitations might take, since there is no freedom to change the *form* of the theory, viz. the $T^{3/2}$ behavior of M(T), the $T^{5/2}$ behavior for the spin wave renormalization, etc. Hence we must have a density of states for the "hidden" excitations which has precisely the same form as the conventional spin wave excitations themselves. One possibility is that the (transverse) spin wave excitations couple to the longitudinal fluctuations, yielding either longitudinal excitations which peak near the spin wave energies, or diffusive modes which peak at E = 0 but have a width which varies as q^2. We have been carrying out inelastic polarized beam experiments on both of these Invar systems, as well as related non-Invar materials, to determine if such longitudinal excitations exist, and if so, over what temperature regime. In the amorphous $Fe_{86}B_{14}$ material we indeed find longitudinal propagating excitations, which would go a long way toward explaining this Invar behavior. However, we also find such "longitudinal" excitations in amorphous $Fe_{40}Ni_{40}P_{14}B_6$, which is a non-Invar material. Hence it is not clear whether these excitations are related to Invar, or are new excitations related to the amorphous magnetic state. Moreover, polarized beam inelastic measurements have recently been taken on crystalline $Fe_{65}Ni_{35}$ (Invar), and an example is shown in Fig. 3. In this vertical field configuration ($\mathbf{P} \perp \mathbf{Q}$), the conventional spin waves are observed in the spin-flip cross sections (solid circles) both for energy gain (E < 0) and energy loss (E > 0), as expected, while the longitudinal magnetic scattering

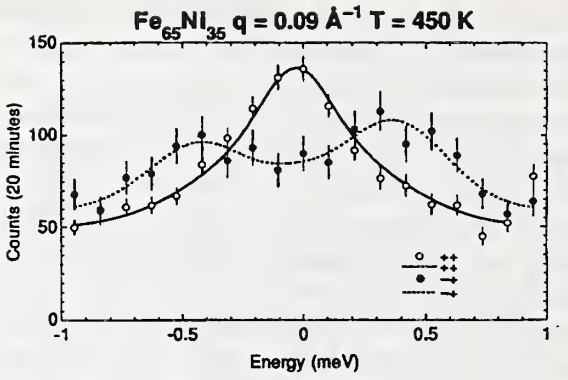

Figure 3. Spin-flip (solid circles) and non-spin flip (open circles) scattering for the crystalline $Fe_{65}Ni_{35}$ (Invar) isotropic ferromagnet. The customary spin waves are observed in energy gain (E < 0) and energy loss (E > 0) in the spin flip scattering, while longitudinal spin diffusion is observed in the non-spin-flip scattering.

is revealed in the non-spin-flip scattering. It is clear that the longitudinal response at this temperature is diffusive in nature, peaking at E = 0. Furthermore, at lower temperatures we do not observe longitudinal propagating excitations near the spin wave positions, in contrast to the results for amorphous $Fe_{86}B_{14}$. Indeed the longitudinal scattering observed in Figure 3 increases with increasing temperature as the Curie temperature is approached, and may be related to the natural evolution of the spin dynamics as the paramagnetic state is approached, rather than being associated with the Invar properties. Clearly further work is required to fully understand the dynamics in these isotropic ferromagnets, especially in the amorphous materials, and to resolve the long-standing puzzle of Invar.

Artificial Materials

- **Magnetic Multilayers**

Artificially layered systems have provided important information about the type, strength and range of coupling across different types of interfaces, and also the effects of interfacial epitaxy on the magnetic structures. We have studied systems with local-moment long-range RKKY coupling (rare-earths), itinerant magnets (transition metals) and local-moment short-range superexchange coupling (transition metal oxides).

While the rare-earth studies directly demonstrate the long range oscillatory nature of the RKKY interaction and its strong dependence on the nature and details of the band structure, the effects of interfacial epitaxy on the magnetic structures have also been of interest, since the bulk rare earths exhibit some of the largest known magnetoelastic strains. Epitaxial-layer growth produces a unique tetragonal distortion via planar compression or expansion, which is difficult to produce by other means. For example, in c-axis growth of hcp rare-earths, this produces large perturbations of the c/a lattice constant ratio compared to those found in the bulk. By studying the magnetic structures in Dy|Y and Dy|Lu superlattices the c/a ratio can be varied by approximately -2% to +3.5%. The helix turn angle of the magnetic structure in the Dy layers just below the ordering temperature is found to change from 46° for epitaxy with yttrium to about 30° for epitaxy with lutecium, as shown in Figure 4. This suggests magnetoelastic origins for the temperature and strain dependence of the magnetic structure in Dy, even at high temperatures. Theories of the temperature dependence of the magnetic structure in Dy have previously concentrated on superzone-gap band effects. The rare-earth superlattice systems clearly provide quantitative means to include the magnetoelastic effects.

A second dramatic effect of epitaxial strain in Dy|Y and Dy|Lu superlattices is the suppression of any ferromagnetic transition for yttrium, and a factor of two enhancement of the Curie temperature for lutecium (from 85 K in the bulk to 160 K). The bulk transition is known to be driven by magnetoelastic energy which produces a 0.7% basal plane orthorhombic distortion. In a superlattice such a distortion would remove the layers from the substrate. However, neutron and X-ray measurements have shown that a similar distortion takes place, but with a domain size of only a few hundred Å. This prevents the production of large numbers of atomic dislocations. The dipolar coupling strength between these small domains has been calculated to be on the order of 0.1 Tesla. This energy is likely responsible for the long range antiferromagnetic coupling observed between the Dy ferromagnetic layers. We expect that a complete magnetoelastic energy calculation

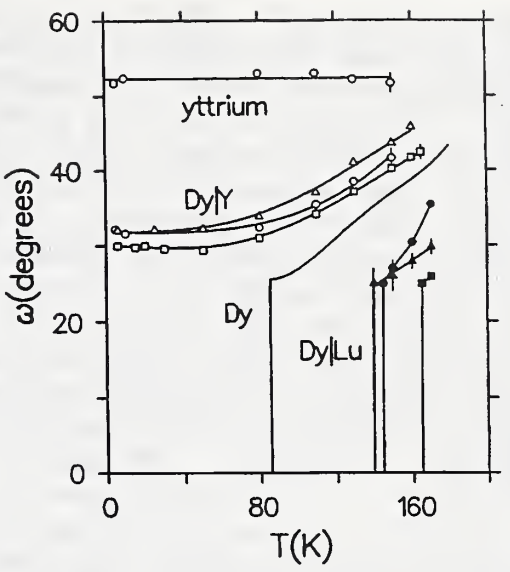

Figure 4. The magnetic structures in Dy superlattices with ytrium and lutecium as the nonmagnetic spacer layer are compared to bulk Dy by plotting the helix turn angle versus the temperature. The large changes in the high-temperature turn angles and Curie temperatures arise from the epitaxial compression (Lu) or expansion (Y) of the basal plane.

will reproduce the observations of the magnetic structures in the Dy|Y and Dy|Lu superlattices.

While the major focus of magnetic superlattice research has been on long-range coupling between layers, we have recently initiated investigations of magnetic coupling in short-range interaction systems, such as transition-metal oxides, which typically have antiferromagnetic superexchange interactions.

It is known that for sufficiently thin alternating layers of two different antiferromagnetic oxides, a single phase transition is found at a temperature intermediate between the bulk values. As the layers become thicker, the ordering of the separate layers becomes more evident and for sufficiently thick layers distinct peaks may be observed in the specific heat and susceptibility. We would like to understand how the mean-field prediction of a single phase transition to a long-range ordered state breaks down in real systems.

We have performed neutron diffraction experiments on several metal-oxide systems to study the temperature and layer thickness dependence of the antiferromagnetic order. One of the systems we have studied is CoO|NiO superlattices. These superlattices were grown by

reactive sputtering and exhibit strong in-plane order with sharp layer interfaces. The bulk ordering temperatures are 291 K (CoO) and 520 K (NiO). For superlattices with a 36 Å bilayer thickness, the neutron diffraction analysis shows that the order parameter is not substantially different between the layers, with the measured transition temperature between the Néel temperatures for the bulk materials. The antiferromagnetic order is coherent through several bilayers.

In contrast, the Ni and Co order parameters are separately bulk-like in a 72 Å period sample, with effective ordering temperatures shifted from the bulk Néel temperatures. Furthermore, the coherence of the antiferromagnetic order monotonically decreases as the temperature increases to 450 K, but remains greater than the width of a single bilayer. The Ni and Co moment values were extracted from the diffraction data by comparing the integrated intensities of the (1/2,1/2,1/2) and (111) peaks within the framework of a damped-wave superlattice model. The temperature dependence of the separate moments are shown in Figure 5a. There is a large temperature range where the Co moments are zero within experimental error, yet the magnetic order remains coherent across the Co layers. These data are in agreement with the mean-field calculations as shown in Figure 5b, which predict a single transition to long range order, although that calculation does not explain the temperature dependence of the coherence length. The mean-field calculation also does not explain the complete loss of coherence above the CoO transition, observed in samples with thicker CoO layers. The breakdown of magnetic coherence has been shown to be entirely reversible with temperature. We are continuing to investigate this long-range order in other oxide superlattices.

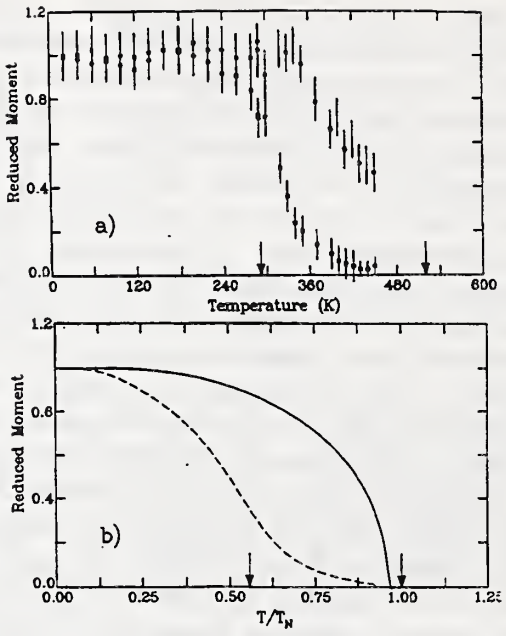

Figure 5. (a) Temperature dependence of the Co (open squares) and Ni (filled squares) moments, in the center of the CoO and NiO layers, respectively, for a [NiO(43Å)|CoO(29Å)] superlattice, extracted from fits of the (1/2,1/2,1/2) and (111) diffraction data. The Néel temperatures of bulk NiO and bulk CoO are marked by arrows. (b) Temperature dependence of the Ni (solid line) and Co (dashed line) moments calculated from mean field theory for a bilayer with 8 atomic planes of NiO and 8 atomic planes of CoO.

- **Nanosized Magnetic Particles**

Another type of system where interface and surface effects are important is in small particles. Thus, composites of nanometer-size magnetic particles in varying matrices have been the subject of recent interest. Ferromagnetic particles of this size are typically below the critical size for domain formation, and the dynamics of these small, relatively uncoupled domains have been described by the classical theory of superparamagnetism. The systems which have been prepared recently are ideal superparamagnets in the sense that the particle size distribution is quite monodispersed. We have prepared such a material by cosputtering iron and alumina.

We have been interested in studying both the interparticle superparamagnetic fluctuations and the intraparticle dynamics by neutron scattering. Previously we have measured the instantaneous two-spin correlation function assuming that the quasistatic approximation is valid. It was found that the correlation length increases to approximately the particle size at low temperature, and the amplitude associated with this scattering concomitantly decreases. We suggested that this indicates a gradual freezing of spins probably initiating at the surface of the particles. Recently, to look for direct evidence of this freezing, inelastic neutron scattering measurements have been made near the small-angle peak in the

structure factor. The quasi-elastic magnetic scattering was found, with a wave-vector and temperature dependent width. The quasi-elastic peak widths decrease with decreasing temperature and the integrated quasi-elastic intensity concomitantly decreases. This confirms that the scattering arises from a freezing phenomenon. We hope to confirm that this freezing occurs at the particle surface spins from the wave-vector dependence of the quasielastic linewidth. We are also currently attempting to measure the intraparticle magnetic dynamics, which are expected to appear at energies above several meV.

Magnetic Superconductors

One of the striking properties of the oxide superconductors and related parent compounds is that there is a magnetic moment associated with the Cu ions, and this is the same electron system where the Cooper pairing occurs. Historically, of course, magnetic ordering is known to coexist with superconductivity in Chevrel phase systems such as $DyMo_6S_8$, but the conventional reasoning for this behavior is that the rare earth ions are electronically isolated from the superconducting electrons moving on the Mo sublattice. Hence the usual spin-depairing mechanism which is so detrimental to conventional superconductivity is circumvented. For the copper oxide superconductors this is clearly not the case, and the presence of these Cu spins, along with the enormous energy scale associated with their spin dynamics, has fueled speculation that the Cu spins are intimately related to the formation of the superconducting state. Thus the nature of the Cu magnetism in these materials has naturally drawn intense interest both experimentally and theoretically, but the rare earth magnetism is also quite interesting, both in terms of the superconductivity and in its own right.

- **Non-collinear Spin Structure**

All the insulating cuprate oxides order antiferromagnetically, and the nature of the magnetic ordering and exchange interactions is of fundamental importance. In the parent compounds of the electron superconductors, such as Nd_2CuO_4, Sm_2CuO_4, and Pr_2CuO_4, the Cu spins occupy a body-centered tetragonal lattice, and order at ~ 280 K with nearest-neighbor spins in the basal plane antiparallel (as found in all the other oxide systems). However, due to the tetragonal symmetry there are two possible orientations of the spins in adjacent planes, one where the spins are collinear, and another non-collinear structure where the spins in adjacent layers are orthogonal. In a multidomain crystal these two magnetic structures are impossible to distinguish with neutron scattering. Hence diffraction experiments have been carried out as a function of applied magnetic field in order to establish which structure is correct. Some results are shown in Figure 6, where the intensity of the (3/2,1/2,1) and (3/2,-1/2,-1) peaks are plotted as a function of H, with the direction of H tilted an angle α away from the (100) axis. For the collinear structure H would be tilted $\sim 45°$ from the moment direction, and thus the behavior of the magnetic peaks should be qualitatively the same irrespective of the sign of α. However, we see that one peak decreases in intensity as the other peak increases, while the sense reverses when α changes sign. This is the expected behavior if the structure is non-collinear. Extensive field-dependent measurements such as these have now established that the correct magnetic structure in both Nd_2CuO_4 and Sm_2CuO_4 is the non-collinear one, and we anticipate that the same is true for Pr_2CuO_4.

- **Sm Magnetic Ordering in Sm_2CuO_4**

One of the interesting aspects of these electron superconductors is that there is no clear separation of the rare earth and copper sublattices. In fact, in Nd_2CuO_4 we have already shown that the rare earth magnetic moments are clearly coupled with the Cu spins. Sm_2CuO_4 is an even more interesting example, as the ordering temperature for the Sm is relatively high (T_N = 5.95 K), while the ordered moment is small ($< 1\ \mu_B$). The dipole energy is thus two orders-of-magnitude too small to cause the rare earth ordering, and one is led to the inescapable conclusion that exchange interactions dominate. These are the same interactions that cause the depairing in conventional electron-phonon mediated systems. The magnetic structure of the Sm has been investigated, and it was found that the Sm spins in the *a-b* plane are coupled ferromagnetically, while adjacent layers are

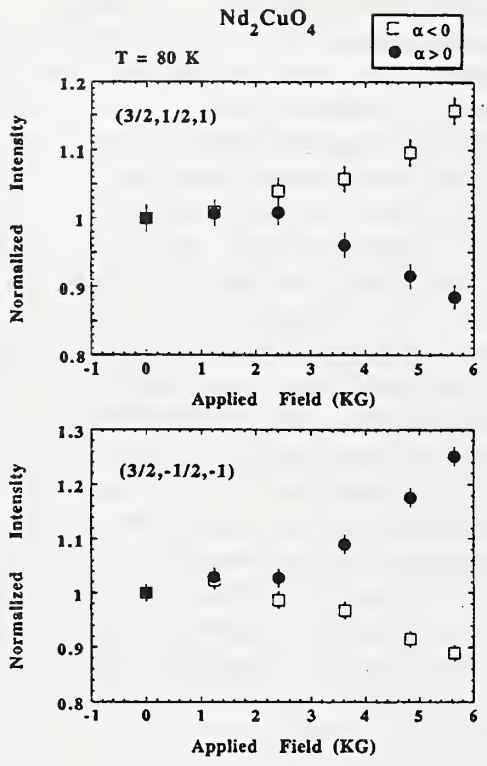

Figure 6. Magnetic Bragg peak intensity for the (3/2,1/2,1) and (3/2,-1/2,-1) peaks of Nd_2CuO_4 as a function of field. The solid circles are for the field tilted an angle $+\alpha$ away from the (100) direction, while the open aquares are for an angle $-\alpha$. For the collinear spin structure all peaks should behave in the same way, but we see that the (3/2,1/2,1) peak increases in intensity for $\alpha < 0$ and decreases for $\alpha > 0$, while the sense reverses for the (3/2,-1/2,-1) peak, as expected for the non-collinear magnetic structure. Hence the non-collinear spin structure is the correct one for these electron superconductors.

antiferromagnetically coupled. In between these layers is the Cu-O superconducting layer. Then in the superconducting state, but above the Sm Néel temperature, the Cooper pairs must obey a mirror symmetry, while below T_N the pairs must obey an antimirror symmetry. In addition, the exchange interaction must be mediated through these layers. If the conventional theory is invoked, it is clear that this system would not be expected to be superconducting at all, instead of being a high T_c superconductor ($T_c \sim 25$ K). In fact, measurements reveal no anomalies in the superconducting properties as the sample is cooled through the Néel point. Thus even if we ignore the fact that there are Cu spins in the superconducting phase, the rare earth magnetism should be sufficient to inhibit superconductivity if the superconductivity is BCS like. These results strongly suggest that a new mechanism for superconductivity is operating in these copper-oxide superconductors.

- **Oxygen Dependence of the Rare Earth Order in 123 Systems**

In the 123 systems, there is one rare earth ion in the unit cell, and since *c* is three times longer than *a* or *b*, it is not surprising that these are good representations of 2-d systems. Early superconductivity measurements indicated that T_c was not strongly affected by the rare earth spins (with the exception of Pr), and this observation coupled with the low ordering temperatures (~ 1 K) suggested that the rare earth ions are electronically isolated from the superconducting layers. Indeed the ordering for the heavy rare earths (e.g. Dy, Er, Gd) can be understood with the assumption that dipole interactions dominate the energetics. However, rather dramatic effects are observed as the oxygen content is varied: changes in T_N, changes in the magnetic structure, and even the destruction of long range order. The most interesting case to date is $NdBa_2Cu_3O_{6+x}$, as the moment is small and exchange interactions are important. In the fully oxygenated state it orders at $\sim 1/2$ K. However, with the reduction of x by only 0.1, where superconductivity is still well established, long range magnetic order is completely inhibited, and only 2-d short range correlations are observed. Yet these correlations develop at a temperature which is three times higher. Long range order is only reestablished when x is reduced below ~ 0.3, with a magnetic structure which is the same, but with a Néel temperature (at x = 0) of 1.7 K. These results show that the oxygen content in the chain layer has a dramatic effect on the rare earth (and Cu) magnetic order and exchange interactions. Again this contradicts the conventional wisdom about "magnetic-superconductors".

Superconductivity

- **Vortex Lattice**

Two neutron techniques have been employed to initiate studies of the superconducting properties directly. One technique is small angle neutron

scattering (SANS), which can be used to directly observe the symmetry of the vortex structure (or lack of structure), and its field and temperature dependence. Figure 7 shows the observed diffraction data at 4.4 K and 0.5 T on a single crystal of Nb. These data were collected in 2 min, and they show the very high quality of data that can now be achieved on the new 30-m instruments. A background subtraction is unnecessary for these data, as the signal-to-noise ratio is excellent. We note that these data are plotted on a log scale, and the observed intensities of the peaks actually vary by several orders-of-magnitude. The width of each Bragg peak (rocking curve) is ~0.3°, which is the expected width based on instrumental considerations. The bottom part of the figure shows the peak position as a function of field, where the solid curve is the expected functional dependence. Excellent agreement is obtained.

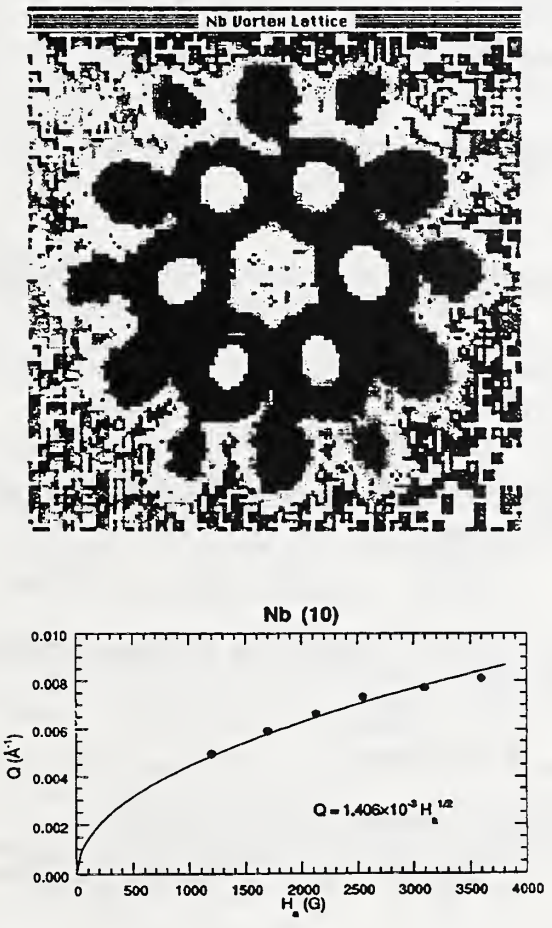

Figure 7. (top) Vortex lattice in Nb observed on the SANS 2-D detector. (bottom) Position of the magnetic Bragg peak of the vortex lattice as a function of applied field.

Nb is of course an ideal material to study, as the penetration depth is short, and large, high quality, and properly shaped single crystals are available. Hence it is essential to be able to obtain high quality data on this system if one has a hope of obtaining useful results on the high-T_c systems where the crystals are smaller, the screening length is longer, and there are competing cross sections in the SANS range such as from "background" grain and twin boundaries, etc. We have also made exploratory measurements of the vortex lattice in $DyBa_2Cu_3O_7$, $ErBa_2Cu_3O_7$ and $Ba_{1-y}K_yBiO_3$ (BKBO), and we anticipate that considerable progress can be made as larger, higher quality samples become available.

One fundamental question concerns the behavior of the vortices at elevated temperatures, and in particular whether the lattice "melts". These are very challenging experiments, as the melting is expected to occur just when the signal is becoming very small. So far, neutron experiments to directly observe the melting have not been successful; what would be expected in Figure 7 is a liquid-like ring of scattering, rather than Bragg spots. However, melting may not be restricted to high T_c systems, and indeed the best chance to observe it may be in a low T_c elemental superconductors such as Nb. Another fundamental question concerns the effect of the rare earth ordering on the vortex state. In the paramagnetic state, the rare earth moments should follow the field of the fluxoid, and should thus contribute to the scattering intensity. This is important as the vortex scattering in the oxide superconductors is quite weak relative to systems such as Nb, since the magnetic screening length λ is large and the scattering intensity is proportional to $1/\lambda^4$. More importantly, though, it is the total magnetic flux that should be quantized, and this leads to a number of possible new phases at low temperatures where the rare earth ions order.

- **Magnetic Screening Length**

The second technique that has been used to investigate the superconducting properties is polarized neutron reflectometry, which can be used to measure the magnetic screening length λ (London penetration depth) in thin film superconductors. The merit of the method lies in the fact that it provides an absolute measurement of λ

and therefore has the capability in principle to make a model-independent determination of $\lambda(T)$. The basic idea is that there is a critical angle θ_c due to nuclear scattering from the film, and then there is a small shift of this critical angle due to the diamagnetic screening of the superconducting electrons. This shift is proportional to the applied field (below H_{C1}), and is spin-dependent; θ_c is shifted to larger scattering angle for one neutron spin state, and to smaller angle for the other. One way to present the data is then to plot the (flipping) ratio of the two cross sections. Figure 8 shows some data taken on a Nb film. The first large dip is due to the shift in the critical angle, and then the oscillations are due to interference effects caused by the finite thickness (3100 Å in this case) of the

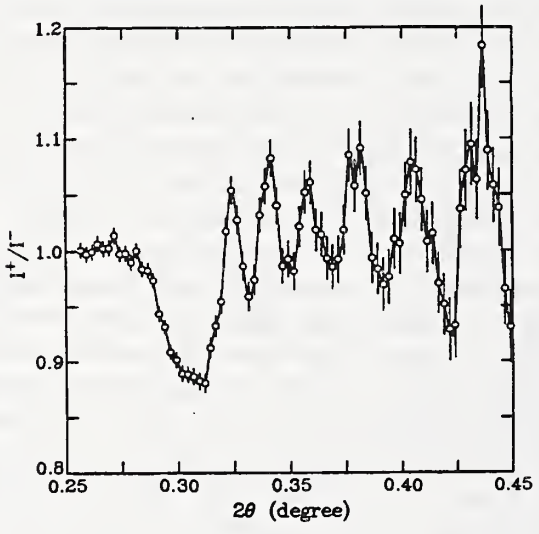

Figure 8. Observed polarized reflectivity ratio as a function of scattering angle on a superconducting Nb film of thickness 3100 Å.

film. Clearly data of this type are rich in information in terms of film thickness, surface and interface roughness, and functional form of the supercurrent screening.

We have also made significant theoretical progress on modeling this type of scattering. In the (local) London theory the strength of the magnetic field inside the superconductor decreases exponentially with distance. The scattering problem is then described by a 1-d Schrödinger equation, where the neutron experiences a step potential, along with an exponential increase or decrease to an asymptotic value which depends on the neutron spin. We have found an exact solution to this scattering problem, which contains two transmission effects. One is the usual velocity-dependent one which is caused by interference effects arising from the spatial variation of the potential. Thus, as the kinetic energy of the neutron increases above the potential threshold, the reflectivity oscillates due to these wavelength-dependent interference effects. However, for an increasing potential an anomalous transmission is found to occur, where the reflectivity vanishes and the beam is completely transmitted. This new anomalous transmission effect does not depend on the neutron wavelength, but rather depends only on the *shape* of the potential. It will be interesting to see if this anomalous transmission effect can be observed experimentally.

Experiments

Two Dimensional Magnetic Correlations and Magnetic Ordering of Dy and Er in $DyBa_2Cu_3O_7$ and $ErBa_2Cu_3O_7$

T. W. Clinton, J. W. Lynn, J. Z Liu, X. Jia, and R. N. Shelton.

Polarization Analysis of the Magnetic Inelastic Scattering of Invar $Fe_{86}B_{14}$

J. W. Lynn, N. Rosov, and G. Fish.

Magnetic Order of the Rare Earth in $Dy_2Ba_4Cu_7O_{15}$

Z. Zhang, J. W. Lynn, and D. E. Morris.

Resolution Considerations For Polarized Triple-Axis Spectrometry

N. Rosov, J. W. Lynn, and R. W. Erwin.

Antiferromagnetic Ordering of $BaPrO_3$ Via Neutron Diffraction

N. Rosov, J. W. Lynn, Q. Lin, G. Cao, J. W. O'Reilly, P. Pernambuco-Wise, and J. E. Crow.

Temperature Dependence of the Magnetic Order in UPdSn

R. A. Robinson, A. C. Lawson, J. W. Lynn, and K.H.J. Buschow.

Magnetic Ordering of Sm in Sm_2CuO_4

I. W. Sumarlin, S. Skanthakumar, J. W. Lynn, J. L. Peng, W. Jiang, Z. Y. Li, and R. L. Greene.

Neutron Powder Diffraction Study of the Nuclear and Magnetic Structures of $YBa_2Fe_3O_8$ at Room Temperature

Q. Huang, V. Karen, P. Karen, A. Kjekshus J. W. Lynn, A. D. Mighell, N. Rosov, and A. Santoro.

Incommensurate Magnetic Order in UPtGe

R. A. Robinson, A. C. Lawson, J. W. Lynn, and K.H.J. Buschow.

London Penetration Depth λ_L in Superconductors by Polarized Neutron Reflectometry: Theory

H. Zhang and J. W. Lynn.

Magnetic Ordering of the Cu Spins in $PrBa_2Cu_3O_{6+x}$

N. Rosov, J. W. Lynn, G. Cao, J. W. O'Reilly, P. Pernambuco-Wise, and J. E. Crow.

Field-Induced Transition in UPdSn At 3T

H. Nakotte, R. A. Robinson, J. W. Lynn, E. Brück, and F. R. de Boer.

Neutron Powder Diffraction Study of the Nuclear and Magnetic Structures of $YBa_2Fe_3O_{8-\delta}$ (δ = 0, 0.36) as a Function of Temperature

Q. Huang, P. Karen, V. L. Karen, A. Kjekshus, J. W. Lynn, A. D. Mighell, N. Rosov, and A. Santoro.

Field Dependence of the Magnetic Ordering of Cu in R_2CuO_4 (R = Nd, Sm)

S. Skanthakumar, J. W. Lynn, J. L. Peng, and Z. Y. Li.

Quasi-Elastic and Inelastic Neutron Scattering Studies of $[(CD_3)_3ND]FeCl_3 \cdot 2D_2O$: A One-Dimensional Ising Ferromagnet

N. Rosov, J. W. Lynn, J.J.M. Williams, and C. P. Landee.

Polarization Analysis of the Magnetic Excitations in Invar and Non-Invar Amorphous Ferromagnets

J. W. Lynn, N. Rosov, and G. Fish.

Oxygen Dependence of the Magnetic Order of the Rare Earth Ions in $RBa_2Cu_3O_{6+x}$

T. W. Clinton, J. W. Lynn, B. W. Lee, M. Buchgeister, M. B. Maple.J. Z. Liu, Y. X. Jia, R. N. Shelton, and J. L. Peng.

Phonon Density-Of-States in R_2CuO_4 and Superconducting $R_{1.85}Ce_{0.15}CuO_4$ (R = Nd, Pr)

I. W. Sumarlin, J. W. Lynn, D. A. Neumann, J. J. Rush, C.-K. Loong, J. L. Peng, and Z. Y. Li.

Two-And Three-Dimensional Magnetic Order of Er in Superconducting $ErBa_2Cu_3O_7$

T. W. Clinton, J. W. Lynn, J. Z. Liu, Y. X. Jia, and R. N. Shelton.

Magnetic Field Penetration Depth in Superconductors by Polarized Neutron Reflectometry

H. Zhang, J. W. Lynn, C. F. Majkrzak, S. K. Satija, C. J. Lobb, and J. H Kang.

Crystallographic and Magnetic Properties of UAuSn

R. A. Robinson, J. W. Lynn, V. Nunez, K.H.J. Bushcow, H. Nakotte, and A. C. Lawson.

A Polarization Analysis of Magnetic Excitations in $CsMnI_3$

Z. Tun, J.-G. Lussier, R. W. Erwin, J. W. Lynn, and A. Harrison.

Longitudinal and Transverse Magnetic Fluctuations Below T_c in Fe-Ni Alloys

J. W. Lynn, N. Rosov, and M. Acet.

Magnetic Fluctuations in U-Cu-Pd Alloys

M. Aronson, R. A. Robinson, J. W. Lynn, C. Seaman, and M. B. Maple.

Magnetic Ordering of Eu in $EuNi_5P_3$

J. V. Badding, J. Luce, A. M. Stacy, J. W. Lynn, and R. W. Erwin.

Propagation of Antiferromagnetic Order Across Paramagnetic Layers in CoO/NiO Superlattices

J. A. Borchers, M. J. Carey, R. W. Erwin, A. E. Berkowitz, and C. F. Majkrzak.

Structural Characterization of Fe_3O_4/NiO Single Crystal Superlattices by X-Ray Diffraction, RHEED and Neutron Diffraction

D. M. Lind, S. D. Berry, R. W. Erwin, and J. A. Borchers.

Polarization of Pd Interlayers in Co/Pd Superlattices

J. A. Borchers, J. F. Ankner, C. F. Majkrzak, B. N. Engel, and C. Falco.

Magnetic Structure in Dy/Sc Superlattices

F. Tsui, C. P. Flynn, R. S. Beach, M. B. Salamon, J. A. Borchers, R. W. Erwin, and J. J. Rhyne.

Stuctural Analysis of Rare-Earth Superlattices by X-Ray Diffraction Techniques

J. A. Borchers, R. W. Erwin, A. Matheny, R. S. Beach, C. P. Flynn, and M. B. Salamon.

Magnetic Coherence in Dy/Lu Superlattices
R. S. Beach, J. A. Borchers, A. Matheny, R. W. Erwin, M. B. Salamon, J. J. Rhyne, and C. P. Flynn.

Structure of MBE Grown Er/Y and Er/Lu Films
B. Everitt, J. Borchers, R. S. Beach, A. Matheny, R. W. Erwin, M. B. Salamon, C. P. Flynn, J. J. Rhyne.

Cu Magnetic Order and Spin Dynamics in Pr_2CuO_4
I. W. Sumarlin, J. W. Lynn, and T. Chattopadhyay.

Magnetic Flux Lattice in Nb and High T_c Superconductors
J. W. Lynn, T. W. Clinton, H. Zang, and N. Rosov.

Cerium and Oxygen Dependence of the Nd and Cu Order in $Nd_{2-x}Ce_xCuO_{4-y}$
S. Skanthakumar, J. W. Lynn, J. L. Peng, and Z. Y. Li.

Dominance of Long-Lived Excitations in the Antiferromagnetic Spin-1 Chain NENP
S. H. Ma, C. Broholm, D. H. Reich, B. J. Sternlieb, and R. W. Erwin.

Helimagnetism in Metallic $V_{2-y}O_3$ Under Pressure
W. Bao, C. Broholm, S. A. Carter, T. F. Rosenbaum, G. Aeppli, J. M. Honig, J. Spalek, and S. F. Trevino.

Antiferromagnetism in the Stacked Kagome Antiferromagnet $KCr_3(OH)_6(SO_4)_2$
S. H. Lee, C. Broholm, M. F. Collins L. Heller, C. Kloc, E. Bucher, and R. W. Erwin.

Magnetic Fluctuations in Metallic $V_{2-y}O_3$
W. Bao, C. Broholm, S. A. Carter, T. F. Rosenbaum, G. Aeppli, J. M. Honig, and J. Spalek.

Incommensurate Antiferromagnetic Order in Strained Layer MnSe/ZnTe Superlattices
T. M. Giebultowicz, P. Klosowski, N. Samarth, H. Luo, J. K. Furdyna, J. J. Rhyne.

Investigation of ZnMnTe Weakly Diluted FCC Magnetic Semiconductor
P. Klosowski, T. M. Giebultowicz, N. Samarth, H. Luo, J. K. Furdyna, and J. J. Rhyne.

Magnetic Critical Phenomena in fcc Antiferromagnets: Role of Strain and Dimensionality
P. Klosowski, T. M. Giebultowicz, N. Samarth, H. Luo, J. K. Furdyna, and J. J. Rhyne.

Antiferromagnetism in ZnSe/MnSe Strained Layer Superlattices
N. Samarth, P. Klosowski, H. Luo, T. M. Giebultowicz, J. K. Furdyna, J. J. Rhyne, B. E. Larson, N. Otsuka.

Antiferromagnetism in Epilayers and Superlattices Containing Zinc-Blende MnSe and MnTe
P. Klosowski, T. M. Giebultowicz, J. J. Rhyne, N. Samarth, H. Luo, and J. K. Furdyna.

X-ray Structural Refinement of a Co/Pt(III) Superlattice Exhibiting Perpendicular Magnetic Anisotropy
J. F. Ankner, J. A. Borchers, R. F. C. Farrow, and R. F. Marks.

Analysis of Antiferromagnetic Spin Coupling in Co/Cu Superlattices Using Polarized Neutron Diffraction
A. Schreyer, J. A. Borchers, J. F. Ankner, H. Zabel, and C. F. Majkrzak.

Participants

Acet, M.	Duisburg University, Germany
Aeppli, G.	AT&T Bell Laboratories
Ankner, J. F.	Reactor Radiation Division
Aronson, M.	University of Michigan
Badding, J. V.	Pennsylvania State U.
Bao, W.	Johns Hopkins University
Beach, R. S.	University of Illinois
Berkowitz, A. E.	U. of California, San Diego
Berry, S. D.	Florida State University
Borchers, J. A.	Reactor Radiation Division
Broholm, C.	Johns Hopkins University
Brück, E.	University of Amsterdam
Bucher, E.	AT&T Bell Laboratories
Buchgeister, M.	U. of California, San Diego
Buschow, K.H.J.	Philips Research Labs
Cao, G.	Florida State University
Carey, M. J.	U. of California, San Diego
Carter, S. A.	University of Chicago
Chattopadhyay, T.	Institut Laue-Langevin
Clinton, T. W.	University of Maryland
Collins, M. F.	McMaster University
Crow, J. E.	Florida State University
de Boer, F. R.	University of Amsterdam
Engel, B. N.	Arizona State University
Erwin, R. W.	Reactor Radiation Division

Everitt, B.	University of Illinois
Falco, C.	University of Arizona
Farrow, R.F.C.	IBM Almaden
Fish, G.	Allied Signal Corp.
Flynn, C. P.	University of Illinois
Furdyna, J. K.	University of Notre Dame
Giebultowicz, T. M.	University of Notre Dame
Greene, R.L.	University of Maryland
Harrison, A.	Oxford University
Heller, L.	McMaster University
Honig, J. M.	Purdue University
Huang, Q.	U. of Maryland and NIST
Jia, Y. X.	U. of California, Davis
Jiang, W.	University of Maryland
Kang, J. H.	Westinghouse
Karen, P.	University of Oslo
Karen, V.	Reactor Radiation Division
Kjekshus, A.	University of Oslo
Kloc, C.	AT&T Bell Laboratories
Klosowski, P.	University of Maryland
Landee, C. P.	Clark University
Larson, B. E.	Thinking Machines Corp.
Lawson, A. C.	Los Alamos National Lab
Lee, S. H.	Johns Hopkins University
Lee, B. W.	U. of California, San Diego
Li, Z. Y.	University of Maryland
Lin, Q.	Beijing Inst. of Physics
Lind, D. M.	Florida State University
Liu, J. Z.	U. of California, Davis
Lobb, C. J.	University of Maryland
Loong, C.-K	Argonne National Lab
Luce, J.	U. of California, Berkeley
Luo, H.	University of Notre Dame
Lussier, J.-G	McMaster University
Lynn, J. W.	U. of Maryland and NIST
Ma, S. H.	Johns Hopkins University
Majkrzak, C. F.	Reactor Radiation Division
Maple, M. B.	U. of California, San Diego
Marks, R. F.	IBM Almaden
Matheny, A.	University of Illinois
Mighell, A. D.	Reactor Radiation Division
Morris, D. E.	Morris Research, Inc. (CA)
Nakotte, H.	University of Amsterdam
Neumann, D. A.	Reactor Radiation Division
Nunez, V.	University of Maryland
O'Reilly, J. W.	Florida State University
Otsuka, N.	Purdue University
Peng, J. L.	University of Maryland
Pernambuco-Wise, P.	Florida State University
Rhyne, J. J.	University of Missouri
Reich, D. H.	Johns Hopkins University
Robinson, R. A.	Los Alamos National Lab
Rosenbaum, T. F.	University of Chicago
Rosov, N.	U. of Maryland and NIST
Rush, J. J.	Reactor Radiation Division
Salamon, M. B.	University of Illinois
Samarth, N.	University of Notre Dame
Santoro, A.	Reactor Radiation Division
Satija, S. K.	Reactor Radiation Division
Schreyer, A.	Ruhr Universität, Germany
Seaman, C.	U. of California, San Diego
Shelton, R. N.	U. of California, Davis
Skanthakumar, S.	University of Maryland
Spalek, J.	Purdue University
Stacy, A. M.	U. of California, Berkeley
Sternlieb, B. J.	Columbia University
Sumarlin, I. W.	University of Maryland
Trevino, S. F.	ARDEC and NIST
Tsui, F.	University of Illinois
Tun, Z.	Atomic Energy of Canada
Williams, J.J.M.	Clark University
Zhang, H.	University of Maryland
Zabel, H.	Ruhr Universität, Germany

CRYSTALLOGRAPHY

Instrumentation

Much effort during the past year has been directed to getting as much data as possible out of the powder diffractometer at BT-1, in anticipation of the period during which it would be out of service for installation and calibration of the new, upgraded instrument. After many years of sporadic activity, the final components necessary for the upgrade were delivered in the spring and summer of 1992; installation took place in September/October to be followed by checkout and calibration in the winter.

Figure 1 shows a layout of the new instrument. It has 32 detectors, arranged at 5° intervals around a circle in an assembly that can scan a 12° 2θ range, so that powder diffraction patterns can be collected over the entire range from 0° to 167°. The Soller slit collimator in front of each detector has a divergence of 7′ of arc, defined by stretched Mylar sheets impregnated with Gd_2O_3. The collimators are 125 mm high, but they can be masked down for the low angle detectors to minimize the peak shape distortions caused by the finite curvature of the Debye-Scherrer cone. There is a choice of three monochromator take-off angles, so that the peak-width minimum can be matched to the d-spacing range that is most important for each sample. Because of the excellent results from the old instrument for samples with large, but high symmetry, unit cells, one of the takeoff angles is 75°, with a Cu 220 monochromator. A Si 531 monochromator at a takeoff angle of 120° gives high resolution for small, low symmetry unit cells, while a Cu 311 monochromator at a takeoff angle of 90° can be used for intermediate size unit cells. All choices have a neutron wavelength close to 1.54 Å.

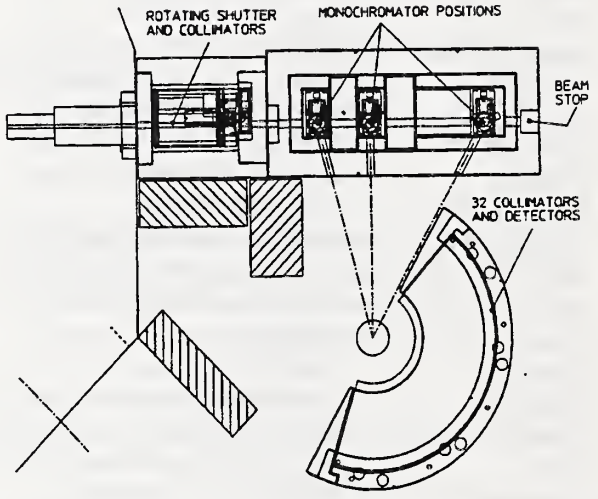

Figure 1. Layout of the new BT-1 high resolution powder diffractometer.

Structure Determination and Refinement from Powder Data

- **Buckyballs**

One of the most interesting crystallographic studies during the year was a powder diffraction study of the room temperature and low temperature structures of C_{60}, "buckminsterfullerene", whose highly symmetrical molecules are known as "buckyballs". At room temperature the powder pattern is that of a face centered cubic lattice with a_o = 14.17 Å, but the background is not flat, as is usual with well-crystallized samples on this instrument (see Chemical Physics section). Instead it has broad peaks, characteristic of an amorphous material. These peaks were shown to correspond to what would be expected from a spherical shell the size of the C_{60} molecule, as if the centers of the molecules occupied the fcc lattice positions, but their orientations were perfectly random. At about 255 K the crystals undergo a phase transition, with an abrupt contraction of the lattice (Fig. 2) from a_o = 14.15 Å to 14.11 Å, to a simple cubic structure, space group Pa3. In this phase threefold symmetry axes of the molecules line up with threefold axes of the lattice, but each of the four molecules in the unit cell lines up with a different [111] direction of the lattice. Below the transition temperature the diffuse background peaks are much smaller, but they do not disappear altogether.

A Rietveld refinement in which the molecule was constrained to have its full icosahedral symmetry converged to a model in which the molecule is rotated away from the position where

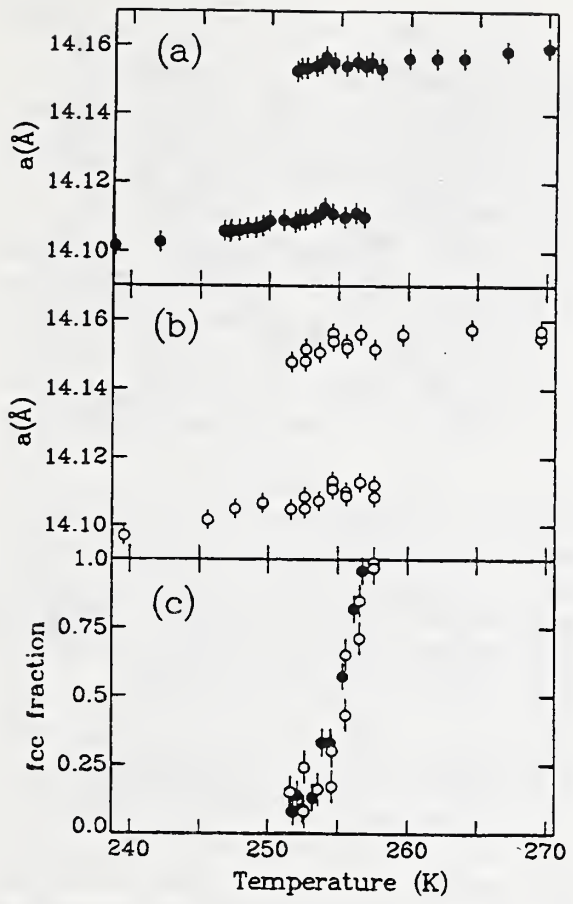

Figure 2. a) The cubic lattice constant of C_{60} as determined by X-rays. b) The lattice constant of C_{60} as determined by neutrons. c) The proportion of the high temperature phase as a function of temperature, as determined by X-rays (closed circles) and neutrons (open circles).

three of its twofold axes are aligned with the fourfold axes of the lattice by about 22°, in agreement with other calculations. However, the fit was not satisfactory. Models that allow the molecule to be significantly distorted seem unlikely in view of the weakness of intramolecular (van der Waals) forces compared with the covalent intermolecular bonds. A possible alternative model has molecules randomly distributed, with unequal probability, between two different values of the angle of rotation around the threefold axis. This model also explains the residual disorder scattering in the low temperature phase.

- **$Ga_2(HPO_3)_3 \cdot 4H_2O$**

Although the Rietveld method has been developed over the past 20 years as a tool for *refinement* of structures of considerable complexity, the *determination* of structure from powder diffraction data is more difficult. The determination and subsequent refinement of a framework structure with the composition $Ga_2(HPO_3)_3 \cdot 4H_2O$ and 29 atoms in the asymmetric unit is therefore a major advance [1]. The unit cell is monoclinic, with a = 8.13 Å, b = 10.02 Å, c = 7.70 Å, and β = 111.5°. The initial model was determined from synchrotron X-ray powder diffraction data, whose high resolution enabled the measurement of a sufficient number of individual structure factor values to use direct methods to determine phases. Refinement of the X-ray data (assuming, initially, only three water molecules per formula unit) did not give a satisfactory fit. Rietveld refinement of neutron diffraction data, taken at 8.7 K on a deuterated sample, located an additional water molecule and all of the deuterium atoms. The final refinement gave R_B = 2.91%, R_{wp} = 4.39%.

Figure 3 shows the structure, which consists of GaO_6 octrahedra linked by corner-sharing HPO_3 tetrahedral groups and hydrogen bonds into a three dimensional framework.

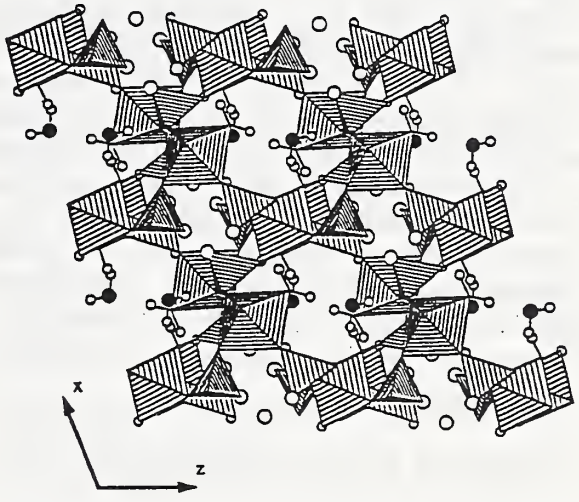

Figure 3. The structure of $Ga_2(HPO_3)_3 \cdot 4H_2O$ viewed down the *b* axis.

- **High T_c Superconductors**

In the search for higher temperature superconductors many mixed-oxide compounds have been synthesized, and some of them have rather surprising structures. An example is the compound $YSr_2A\ell Cu_2O_7$, which is derived from

the "123" superconductor $YBa_2Cu_3O_{7-\delta}$ by replacement of barium by strontium and one third of the copper by aluminum. The aluminum atoms selectively replace the copper atoms in the "chain" positions, and they are coordinated by four oxygen atoms in a tetahedral configuration. A tetrahedron does not fit in the origin site of the apparent space group (P4/mmm), so the environment of the aluminum atom must be disordered. As is shown in Figure 4, there are four orientations for the tetrahedron, two of which are occupied in local regions, with orthorhombic symmetry, so that $A\ell O_4$ tetrahedra_share corners to form chains along [110] or [1$\bar{1}$0]. It appears that the strain on a twin boundary separating domains with the chains in these directions is so small that microtwins form very easily, and, although the local environment has orthorhombic symmetry, the crystal is effectively tetragonal.

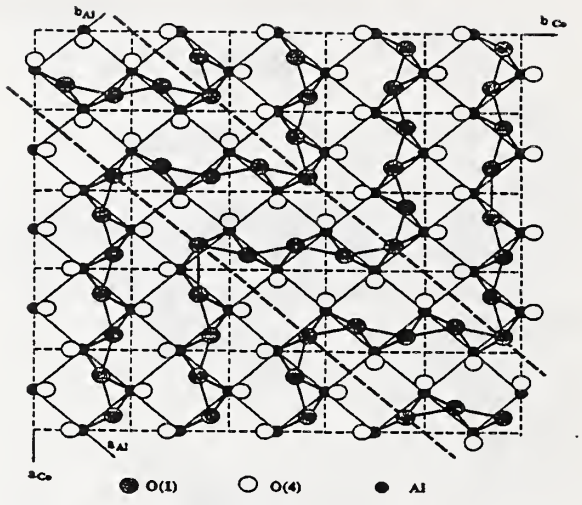

Figure 4. A slice of the structure of $YSr_2A\ell Cu_2O_7$ near the z = 0 plane, showing the chains of $A\ell O_4$ tetrahedra. O(1) lies in the z = 0 plane and O(4) lies above and below it to give tetrahedral coordination to $A\ell$. The direction of the chain changes along "twin planes" marked by the heavy, dashed lines.

- **Alloys**

In the Zr-Pd alloy system it had been known that there were several intermetallic phases, but the actual phase diagram in the vicinity of ZrPd was uncertain. In an alloy of composition $Zr_{0.45}Pd_{0.55}$ selected area electron diffraction showed two phases, one the known orthorhombic ZrPd phase and the other a previously unknown rhombohedral phase. Because scanning electron microscope observations showed that the rhombohedral phase was palladium rich, a structure was postulated that had the composition Zr_3Pd_4. A Rietveld refinement showed that the postulated structure was essentially correct, although details of atomic positions were slightly different. This intermetallic phase is only the second example of a structure type that was discovered in 1983 in the Pu-Pd system.

Accuracy in Powder Diffraction II

In a special highlight of the past year the Reactor Radiation Division was host, at the end of May, to an international conference, Accuracy in Powder Diffraction II. The first international conference on Accuracy in Powder Diffraction was held at NIST (then NBS) in 1979. At this year's conference 177 registrants from 18 countries on five continents discussed developments in the intervening 13 years on phase identification and quantification; accuracy and standards; new developments in software and data analysis; profile fitting; decomposition and microstructural effects; novel applications and structural science; and new developments in hardware; including detectors; and studies under non-ambient and time-resolved conditions. There were 26 invited talks and 72 contributed papers, as well as two tutorial workshops, organized by JCPDS-International Centre for Diffraction Data, one on powder diffractometer sensitivity and one on indexing methods.

Maximum Entropy

Work on the development of maximum entropy as a phasing tool in macromolecular crystallography continued during the year. The earlier promising results on recombinant bovine chymocin were reproduced using a many times faster version of the computer program, and various strategies for choosing a starting set of phases were explored. Substantial progress was made toward the goal of a computer program that will generate maximum entropy density maps using fast Fourier transform routines that utilize the symmetries of 20 space groups that include more than 90% of known protein crystals.

Diffraction Data Center

The NIST Crystal Data File and search software have now been integrated into commercial single-crystal X-ray diffractometers. As an integral part of every structure determination with the X-ray diffractometer, the database is routinely searched, using lattice matching techniques, to establish if the compound under investigation is the same as or related to existing materials. More importantly, the integration of the Crystal Data File with the diffractometer creates a new analytical tool for materials characterization. With this new automated tool, the identification of an unknown crystal can be carried out within a few minutes.

The Electron Diffraction Database has been built into the work stations associated with several commercial Analytical Electron Microscopes. Unknown phases are identified by chemical/lattice matching procedures as soon as experimental elemental and d-spacing data have been recorded. With this analytical tool, extremely small samples can be readily characterized.

Reference

[1] R. E. Morris, W.T.A. Harrison, J. M. Nicol, A. P. Wilkinson, and A. K. Cheetham, Nature 359, 519-522 (1992).

Experiments

The Structure of $YBa_2Fe_3O_{8-\delta}$
Q. Huang, I. Natali Sora, V. L. Karen, A. D. Mighell, J. W. Lynn, N. Rosov, A. Santoro, P. Karen,and A. Kjekshus.

The Structure of $(Y_{1-x}Ca_x)Ba_2Fe_3O_8$
Q. Huang, I. Natali Sora, V. L. Karen, A. D. Mighell, J. W. Lynn, N. Rosov, A. Santoro, P. Karen, and A. Kjekshus.

The Structure of $YSr_2A\ell Cu_2O_7$
Q. Huang, A. Santoro, S. Sunshine, and R. J. Cava.

The Structure of $YBa_2Cu_{3-x}Co_xO_{6-\delta}$
A. Santoro, M. Marezio, P. Bordet, and J. L. Hodeau.

The Structure of $LaVO_3$
Q. Huang, A. Santoro, R. J. Cava, and M. Marezio.

The Structure of $Pb_2Sr_2YCu_3O_{8-\delta}$
Q. Huang, A. Santoro, J. J. Capponi, O. Chmaissen, R. J. Cava, and M. Marezio.

The Structure of $BaSrCuO_{2+x} \cdot CO_3$
Q. Huang, A. Santoro, C. Chaillout, J. Chenavas, P. Bordet, J. L. Hodeau, R. J. Cava, J. J. Krajewski, J. P. Levy, M. Marezio, and W. F. Peck.

The Structure of $MA\ell Si_2O_6$ (M = Cs, Rb, K)
Q. Huang, I. Natali Sora, A. Santoro, R. S. Roth and C. Rawn.

The Structure of $La_{0.5}Ba_{0.5}Co_{0.7}Cu_{0.3}O_{2.8}$
Q. Huang, I. Natali Sora, J. Lynn, S. Russeck.

The Structure of $Ba_3In_2RO_8$ (R = Zr_3Ce)
Q. Huang, I. Natali Sora, J. Lynn, S. Adler.

The Structure of $YBaCoCuO_5$
Q. Huang, V. L. Karen, A. D. Mighell, J. Lynn, N. Rosov, I. Natali Sora, A. Santoro, P. Karen, and A. Kjekshus.

The Structure of MBi_2O_4 (M = Ca, Sr); $Sr_4Bi_5O_{11.5}$; $Sr_{4.3}Bi_{4.7}O_x$
I. Natali Sora, Q. Huang, A. Santoro, R. S. Roth, and C. Torardi.

The Structure of $LaCuO_{2.64}$; $Y_{0.95}Ca_{0.05}CuO_{2.55}$
I. Natali Sora, Q. Huang, A. Santoro, and R. J. Cava.

The Structure of $Sr_2Nd_{1.5}Ce_{0.5}NbCu_2O_{10}$; $Sr_2Nd_{1.35}Ce_{0.65}GaCu_2O_9$
I. Natali Sora, Q. Huang, A. Santoro, R. J. Cava.

The Structure of $Li_xNb_{1-x}O_y$
I. Natali Sora, Q. Huang, A. Santoro, and M. Zocchi.

The Structure of a Cobalt Containing Aluminophnosphate (AℓPO-5) Zeolite.
E. Prince and S. C. Tang.

Maximum Entropy Phase Determination and Extension in Macromolecular Crystallography
L. Sjölin and E. Prince.

Fast Fouier Transorm Routines Utilizing Space Group Symmetry
E. Prince, C. Lu, M. An, and R. Tolimieri.

Neutron Diffraction Study of $Y(Ba_{1-x}La_x)_2Fe_3O_8$, x = 0.05, 0.10, 0.15, 0.20, 0.30.
I. Natali-Sora, Q. Huang, A. Santoro, and R. J. Cava.

Neutron Rietveld Analysis of Anion and Cation Disorder in the Fast-Ion Conducting Pyrochlore System $Y_2(Zr_xTi_{1-x})_2O_7$, x = 0.3, 0.45, 0.6, and 0.9
C. M. Heremans, B. J. Wuensch, J. K. Stalick, and E. Prince.

Neutron Rietveld Analysis of Cation Disorder in the Pyrochlore Systems $Tb_2Ti_2O_7$ and $(Nd_{0.5}Yb_{0.5})Ti_2O_7$
T. Hyuga, B. J. Wuensch, J. K. Stalick, and E. Prince.

Determination of the Crystallographic and Magnetic Structure of $Nd_2Fe_{17}N_{2.8}$ at 295 and 4K
J. K. Stalick, S. F. Cheng, J. Cullen, and A. E. Clark.

Neutron Diffraction Analysis of the Zr-Pd System Near the 1:1 Composition: Structure Determination of ZrPd and Zr_3Pd_4
J. K. Stalick, L. A. Bendersky, and R. M. Waterstrat.

Determination of the Structure of $SrHfO_3$ by Neutron Rietveld Refinement
M. F. Garbauskas, G. L. Bryant, Jr., and J. K. Stalick.

Neutron Diffraction Characterization of a New SiO_2 Catalyst
J. B. Higgins, M. E. Leonowicz, G. D. Stucky, J. K. Stalick, and J. J. Rush.

A Neutron Powder Diffraction Study of the Structure of Hydrated Sodium Zinc Arsenate
T. M. Nenoff, W.A.T. Harrison, J. M. Nicol, and G. D. Stucky.

Neutron Powder Diffraction of a $Na_3(Zn_3P_3O_4)_3$ Phase
T. M. Nenoff, J. M. Nicol, and G. D. Stucky.

Cation Locations in the Novel, Open-Framework, Non-Linear Optical Material K(2/3)Ag(1/3)Nb_2PO_8
W.T.A. Harrison, C. S. Liang, J. M. Nicol, and G. D. Stucky.

An Investigation of the Structure of Dehydrated Li-A Zeolite by Neutron Powder Diffraction
B. H. Toby, J. MacDougall, C. Coe, and J. M. Nicol.

Structural Characterization of a Be Exchanged Na/Cs-Rho Zeolite
T. M. Nenoff, W.T.A. Harrison, J. M. Nicol, and G. D. Stucky.

A Neutron Powder Diffraction Study of Deuterated 6-0-8 Sodalite
O. Elsenhans, J. M. Nicol, T. J. Udovic, W. Bührer, P. Sieger, and J. Feische.

Complex Structures by Powder Diffraction Methods; The Structure of Gallium Phosphite: $Ga_2(HPO_3)_3 \cdot 4H_2O$
R. E. Morris, A. P. Wilkinson, W.T.A. Harrison, J. M. Nicol, and A. K. Cheetham.

Powder Neutron Diffraction Study of the Li-ABW Type Phase Lithium Zinc Phosphate Hydrate Location of Lithium Cations and Proton Positions
W. A. T. Harrison, T. E. Gier, J. M. Nicol, and G. D. Stucky.

Crystal Structure of a New Sodium Zinc Arsenate Phase Solved by Simulated Annealing
T. M. Nenoff, W. T. A. Harrison, J. M. Nicol, G. D. Stucky, and J. M. Newsam.

A Structural Characterization of the Location of Cyclohexane in Na-Y Zeolite at 10K by Neutron Powder Diffraction
L. Bull, N. Henson, A. K. Cheetham, J. M. Nicol, J. Ripmester, and C. Ratcliffe.

Discontinuities in Cation Distribution in the Double Perovskite System $Ba_{(2-X)}Bi_{(1+X)}O_{4+\Delta}$
K P. Resis, A. J. Jacobson, W. T. A. Harrison, and J. M. Nicol.

Stuctural Chacterization of YbBePO-Faujasite by Neutron Powder Diffraction
T. M. Nenoff, W.T.A. Harrison, J. M. Nicol, and G. D. Stucky.

Structural Studies of $YbH(SeO_3)_2 \cdot 2H_2O$ by Neutron Powder Diffraction
R. E. Morris, J. M. Nicol, and A. K. Cheetham

Diffuse Scattering from C_{60} in the Orientationally Disordered Phase.

J.R.D. Copley, R. L. Cappelletti, W. A. Kamitakahara, D. A. Neumann, J. P. McCauley, Jr., N. Coustel, N. Maliszewskyj, J. E. Fischer, A. B. Smith III, K. M. Creegan, and D. M. Cox.

Diffuse Scattering from C_{60} in the Low Temperature Phase.

J.R.D. Copley, R. L. Cappelletti, W. A. Kamitakahara, D. A. Neumann, J. P. McCauley, Jr., N. Coustel, N. Maliszewskyj, J. E. Fischer, A. B. Smith III, K. M. Creegan and D. M. Cox.

Discontinuous Volume Change at the Orientational Order-Disorder Transition in C_{60}.

J.R.D. Copley, D. A. Neumann, W. A. Kamitakahara, P. A. Heiney, J. P. McCauley, Jr., N. Coustel, J. E. Fischer, A. B. Smith III, K. M. Creegan, and D. M. Cox.

Neutron Diffraction Studies of the Temperature-dependent Magnetic Structure of β-$TbH(D)_{2+x}$

T. J. Udovic, J. A. Borchers, and I. S. Anderson.

Neutron Powder Diffraction From $C_{60}(HSO_4)_8$.

J.R.D. Copley, D. A. Neumann, A. Qasba, W. A. Kamitakahara, G. Miller, K. M. Creegan, and D. M. Cox.

Neutron Powder Diffraction From C_{70}.

C. Christides, K. Prassides, T.J.S. Dennis, J.R.D. Copley, D. A. Neumann, R. L. Cappelletti, M. J. Rosseinsky, D. W. Murphy, and R. C. Haddon.

Neutron Scattering Study of Orientational Disorder in K_3C_{60}.

C. Christides, K. Prassides, J.R.D. Copley, D. A. Neumann, M. J. Rosseinsky, D. W. Murphy, and R. C. Haddon.

Search for an Orientational Order-Disorder Transition in K_3C_{60}.

D. A. Neumann, J.R.D. Copley, W. A. Kamitakahara, C. Christides, K. Prassides, M. J. Rosseinsky, D. W. Murphy, and R. C. Haddon.

The NIST X-ray and Electron Diffraction Data Center.

A. Mighell, V. Karen, and M. Mrose.

Participants

Adler, S.	U. of California, Berkeley
An, M.	Aware, Inc.
Anderson, I.S.	Institut Laue-Langevin, France
Bendersky, L. A.	Metallurgy Division
Borchers, J. A.	Reactor Radiation Division
Bordet, P.	C.N.R.S., France
Bryant, Jr., G. L.	General Electric Company
Bührer, W.	Paul Scherrer Institute, Switz.
Bull, L.	U. of California, Santa Barbara
Cappelletti, R. L.	Ohio University
Capponi, J. J.	C.N.R.S., France
Cava, R. J.	AT&T Bell Laboratories
Chaillout, C.	C.N.R.S., France
Cheetham, A. K.	U. of California, Santa Barbara
Chenavas, J.	C.N.R.S., France
Cheng, S. F.	Naval Surface Warfare Center
Chmaissen, O.	C.N.R.S., France
Christides, C.	University of Sussex, UK
Clark, A. E.	Naval Surface Warfare Center
Coe, C.	Air Products and Chemicals,
Copley, J.R.D.	Reactor Radiation Division
Coustel, N.	University of Pennsylvania
Cox, D. M.	Exxon Research & Eng. Co.
Creegan, K. M.	Exxon Research & Eng. Co.
Cullen, J.	Naval Surface Warfare Center
Dennis, T.J.S.	University of Sussex, UK
Elsenhans, O.	Paul Scherrer Institute, Switz.
Feische, J.	U. Konstanz, Germany
Fischer, J. E.	University of Pennsylvania
Garbauskas, M. F.	General Electric Company
Gier, T. E.	U. of California, Santa Barbara
Haddon, R. C.	AT&T Bell Laboratories
Harrison, W.A.T.	University of Houston
Heiney, P. A.	University of Pennsylvania
Henson, N.	U. of California, Santa Barbara
Heremans, C. M.	MIT
Higgins, J. B.	Mobil R&D Corp., Princeton NJ
Hodeau, J. L.	C.N.R.S., France
Huang, Q.	University of Maryland
Hyuga, T.	MIT
Jacobson, A. J.	University of Houston
Kamitakahara, W. A.	Reactor Radiatin Division
Karen, V. L.	Reactor Radiation Division
Karen, P.	University of Oslo
Kjekshus, A.	University of Oslo
Krajewski, J. J.	AT&T Bell Laboratories
Leonowicz, M. E.	Mobil R&D Corp, Paulsboro NJ
Levy, J. P.	AT&T Bell Laboratories
Liang, C. S.	U. of California, Santa Barbara
Lu, C.	Towson State University
Lynn, J. W.	University of Maryland & NIST
MacDougall, J.	Air Products & Chemicals, Inc.
Maliszewskyj, N.	University of Pennsylvania

Marezio, M.	AT&T Bell Laboratories
McCauley, Jr., J. P.	University of Pennsylvania
Mighell, A. D.	Reactor Radiation Division
Morris, R. E.	U. of California, Santa Barbara
Murphy, D. W.	AT&T Bell Laboratories
Natali-Sora, I.	Universita di Brescia, Italy
Nenoff, T. M.	U. of California, Santa Barbara
Neumann, D. A.	Reactor Radiation Division
Newsam, J. M.	Biosym Technologies, Inc., CA
Nicol, J. M.	Reactor Radiation Division
Peck, W. F.	AT&T Bell Laboratories
Prassides, K.	University of Sussex, UK
Prince, E.	Reactor Radiation Division
Qasba, A.	Montgomery Blair High School
Ratcliffe, C.	Nat'l Res. Council, Canada
Rawn, C.	Ceramics Division
Resis, K. P.	University of Houston
Ripmester, J.	Nat'l Res. Council, Canada
Rosov, N.	Reactor Radiation Division
Rosseinsky, M. J.	AT&T Bell Laboratories
Roth, R. S.	Ceramics Division
Rush, J. J.	Reactor Radiation Division
Russeck, S.	U. of California, Berkeley
Santoro, A.	Reactor Radiation Division
Sieger, P.	U. Konstanz, Germany
Sjölin, L.	Chalmers U. of Tech., Sweden
Smith III, A. B.	University of Pennsylvania
Stalick, J. K.	Reactor Radiation Division
Stucky, G. D.	U. of California, Santa Barbara
Sunshine, S.	AT&T Bell Laboratories
Tang, S. C.	Shell Development Co.
Toby, B. H.	Air Products & Chemicals, Inc.
Tolimieri, R.	Aware, Inc.
Torardi, C.	DuPont
Udovic, T. J.	Reactor Radiation Division
Waterstrat, R. M.	American Dental Association
Wilkinson, A. P.	U. of California, Santa Barbara
Wuensch, B. J.	MIT
Zocchi, M.	Universita of Brescia, Italy

SURFACE AND INTERFACIAL STUDIES

The measurement of neutron reflectivity at glancing angles of incidence has a wide variety of scientific and technical applications [1]. In this section we will highlight a few of the many interesting neutron reflectivity experiments performed in the last year at the NBSR in the fields of magnetism, electrochemistry, surfactants, superconductivity, Langmuir-Blodgett films, and polymer science. For polymer-polymer interfaces the emphasis has been on the study of block copolymer films, polymer brushes and inter-diffusion of polymers. In the area of surfactant films neutron reflectivity was used to examine the self-assembly of surfactant monolayers in thin fluid films attached to bulk reservoirs of surfactant solutions. A summary of some of our ongoing work in the general analysis of reflectivity data will also be given. More detailed accounts of our data analysis efforts, as well as other instrumentation development projects we have been involved in, including multilayer polarizers and supermirror guide coatings, can be found in the Proceedings of the International Society of Optical Engineering's Technical Symposium on Optical Applied Science and Engineering held in San Diego, July 1992 [2]. Some reflectivity measurements are also described in other sections of this report.

Magnetic Multilayers

A topic of current interest in the field of magnetism is the novel behavior of artificially grown magnetic multilayered structures, particularly those consisting of alternating thin films of a technologically important ferromagnetic 3-d transition metal (e.g., Fe or Co) and an antiferromagnetic (e.g., Cr) or nonmagnetic metal (e.g., Cu). Some of these superlattices exhibit pronounced or giant magnetoresistance effects ascribed to an antiferromagnetic interlayer coupling of the ferromagnetic films.

One valuable technique often employed to measure the magnetization of thin films and multilayered structures is the "surface"-sensitive, magneto-optic Kerr effect (SMOKE) wherein the rotation of the polarization of a reflected beam of light is used to infer a given magnetization. Nonetheless, the SMOKE technique is not inherently surface-sensitive for the case of magnetic multilayers with 20-100 Å bilayer thicknesses since the optical penetration depth in metals is of the order of a few hundred Å. In effect, the magnetization measured by SMOKE for such a multilayer is that averaged over several bilayer periods. Thus, it is not unambiguous whether an antiferromagnetic response, for example, is due to antiparallel interlayer magnetic coupling or the presence of intralayer, oppositely oriented ferromagnetic domains.

Spin polarized neutron reflectivity measurements, on the other hand, can reveal directly and unambiguously the microscopic magnetic structure of theses multilayers. As is well-known, the strength of the neutron-atomic moment interaction is proportional to the magnitude of the moments. Furthermore, given a structure in which the magnetic moments lie in the plane of the film (or normal to the wavevector transfer $\vec{Q}$), specular reflection of polarized neutrons without spin flip (NSF) is due to projections of the atomic moments along the direction of a magnetic field applied in the plane. Conversely, spin flip scattering (SF) is associated with atomic magnetic components normal to the applied field [3]. Thus, not only can the magnitudes of the atomic moments be obtained by polarized neutron reflection, but their orientations as well. In an actual case where an antiferromagnetic SMOKE response was clearly observed for a particular Co-Cu superlattice, it was subsequently shown using polarized neutron reflectivity measurements that an ordered, coherent interlayer antiparallel coupling of Co slabs did not, in fact, exist.

As a specific illustration of the power of polarized neutron reflectivity measurements as a probe of multilayer magnetism, consider the raw specular neutron reflectivity data for an Fe-Cr multilayer, plotted in Figure 1 as a function of the wavevector transfer Q. The presence of ferromagnetic Fe slabs is clearly manifest by the appearance of two distinct critical cutoff angles for total external mirror reflection near $Q = 0.02$ and in the vastly different intensities of the NSF scattering for the primary multilayer diffraction peak at a Q of approximately 0.09 $Å^{-1}$ (corresponding to an Fe-Cr bilayer spacing of about 70 Å).

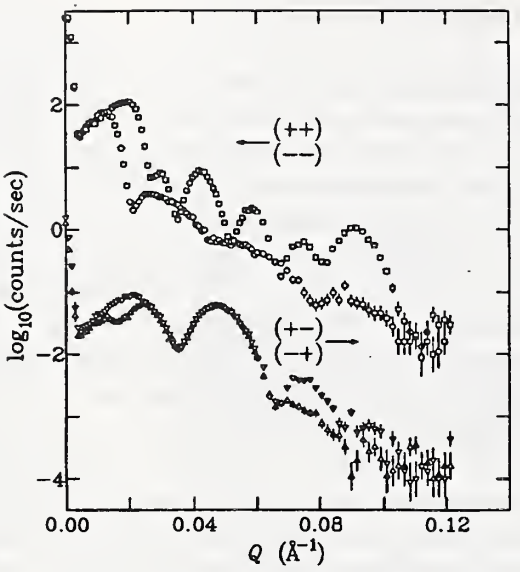

Figure 1. Raw polarized neutron reflectivity data for the Fe-Cr multilayer with noncollinear interlayer magnetic coupling as described in the text. (++,--) = NSF; (+-,-+) = SF.

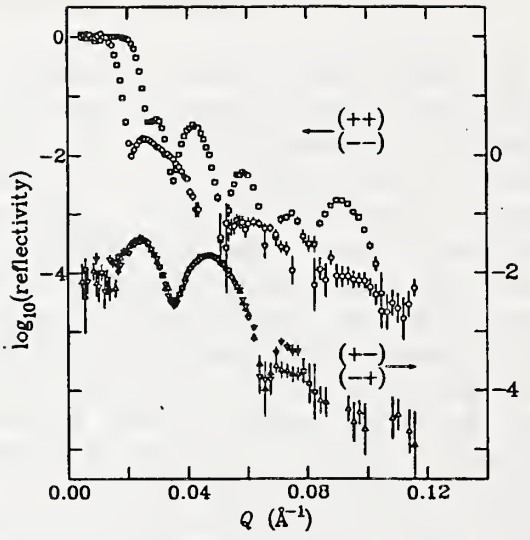

Figure 2. Polarized neutron reflectivity data for the Fe-Cr multilayer shown in Figure 1 after correction for geometrical effects, instrumental polarization and flipping efficiencies.

The respective splitting and difference in intensities, I, for these features are due to the interference between nuclear and magnetic scattering densities ρ_N and ρ_M: $I_{++} \propto \rho_N + \rho_M$ and $I_{--} \propto \rho_N - \rho_M$. Note the N - 2 (e.g., N = 6 in the case of Fig. 1) subsidiary peaks, where N = # of bilayers, between the mirror reflection region and the primary multilayer diffraction peak. This well-resolved profile indicates that the magnetic and chemical structures are coherent over the entire thickness of the multilayer. Correcting for refractive shifts, a pronounced peak appears in the SF reflectivity data at a Q corresponding to a doubling of the fundamental chemical bilayer period. Since in this configuration the SF scattering is entirely magnetic in origin, it can be immediately inferred that the magnetic unit cell is twice that of the chemical spacing and that adjacent ferromagnetic Fe layers have relative moment orientations which are not parallel. Figure 2 shows the result of correcting the raw data for background, finite sample size, and instrumental polarizing and spin flipping efficiencies. Note in particular that the difference in the +- and -+ reflectivities in the region about Q = .02 for the raw data of Figure 1 is an instrumental artifact arising from slightly different front and rear polarizer and flipper efficiencies and is absent in

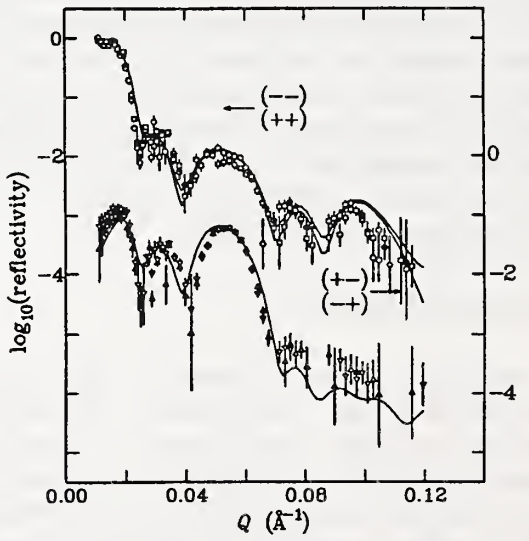

Figure 3. Polarized neutron reflectivity data (symbols) for a different Fe-Cr multilayer with nearly perfect antiparallel coupling between Fe layers. The solid curves are fits generated with the spatial density profiles and moment orientation shown schematically in Figure 4.

the corrected data of Figure 2. In Figure 3 is shown a quantitative fit to corrected reflectivity data for a different Fe-Cr multilayer with nearly perfect antiparallel coupling between Fe layers. The corresponding spatial chemical, magnetic, and moment orientation angle profiles are depicted in

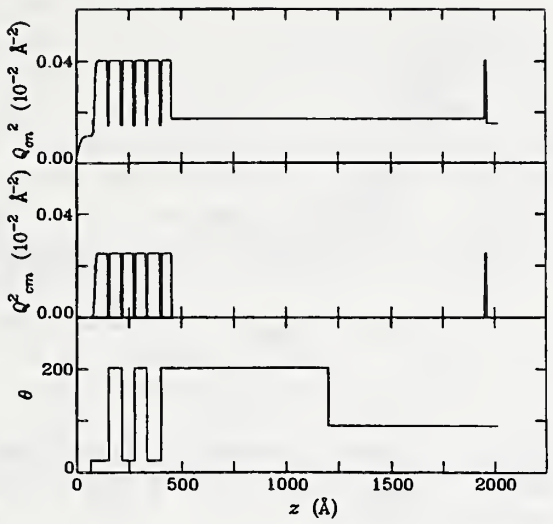

Figure 4. Schematic scattering density profiles and magnetic moment orientation for the Fe-Cr multilayer whose reflectivity data is shown in Figure 3. $Q_{CM}^2 = 16\pi\rho_M$ where CN corresponds to nuclear, CM to magnetic.

Figure 4. Both qualitatively and quantitatively, the polarized neutron reflectivity measurements give a detailed microscopic picture of the magnetic structure of this novel artificially layered material. The polarized neutron reflectivity work described here on the Fe-Cr and Co-Cu multilayers was performed at the NBSR in collaboration with A. Schreyer, Ch. Morawe, and H. Zabel of the Ruhr-Universität, Bochum, Germany.

Langmuir-Blodgett (LB) Films

LB films are created by first forming a monomolecular layer of surfactant molecules on a water surface and then transferring this monolayer onto a solid substrate which is slowly translated through the air-water interface. Repetition of this process results in the formation of a multilayered structure. High quality LB multilayers of various compositions, consisting of such organic substances as fatty acids and their bivalent metallic salts, polymers and polymerizable compounds, and lipids, as well as proteins and nucleic acids, can now be prepared.

The applications of LB films are many. For example, LB films are used for orienting coatings in liquid crystal displays, high-resolution resists for electron and photon lithography, thickness standards, optical lens coatings, molecular lubricants for magnetic and optical storage discs, high capacity electrical capacitors, calibrated radioactivity sources, microelectronic devices such as field-effect transistors, and biosensors. A sophisticated pyroelectric detector system for thermal radiation has even been proposed which can be used in fast infra-red television cameras. LB films containing proteins and DNA can also now be prepared. These biomolecular LB films and superlattices are particularly interesting when composed of compounds which do not grow as single crystals, since the artificial periodicity created in the LB films along the film normal makes it possible to obtain unique structural information from glancing angle reflectivity measurements.

Despite all of the above-mentioned existing and potential applications, relatively little is known about the detailed, microscopic structure of these films. Such knowledge is essential for a proper understanding of the properties of LB films. While scanning tunnelling microscopy (STM), atomic force microscopy (AFM), and electron diffraction can be used to extract in-plane structural information about the topmost surface, the chemical density depth profile normal to the surface can be obtained by neutron and x-ray reflectivity measurements. Again, because the LB films are largely composed of hydrogenous organic compounds, neutrons are, in many cases, the probe of choice. By performing neutron reflectivity measurements, then, we can obtain the chemical density profile normal to the film with a spatial resolution of a few Å, so that such important phenomena as interdiffusion and phase transitions can be probed.

We have been performing structural investigations of a number of LB systems using neutron reflectometry on films prepared by groups led by W. Knoll and L. Feigin at the Max Plank Institute for Polymer Research, Mainz, Germany, and the Institute of Crystallography, Moscow, Russia, respectively. We will describe below one particular study in some detail.

The "as deposited" microstructure and thermal stability of LB composite multilayers containing both a 'hairy-rod' polyglutamate copolymer, poly(γ-methyl-L-glutamate)-co-(γ-n-alkyl-L-glutamate) [4], (PG), and cadmium arachidate (CdA) have been studied using neutron and x-ray

reflectometry (NR & XR). Protonated (p-) and deuterated (d-) species of the two molecules were used to provide contrast between layers for NR. XR was insensitive to the distinction between protonated and deuterated layers, but was sensitive to the slight (ca. 5%) electron density difference between the PG backbone and side chains within a layer, thus providing a complementary sensitivity.

Evidence of interlayer interdiffusion in CdA LB multilayers at 85 °C has been reported by others [5]. These reports, along with studies demonstrating the promise of PG for use in various ultra thin film applications [6], have raised the possibility of improving microstructural stability by using PG multilayers and nanocomposite systems combining PG and smaller, classical LB molecules such as CdA. Earlier measurements in the present study suggested that multilayer 'sandwiches' containing a PG bilayer (n=18) between two multilayers of CdA changed substantially upon annealing at 84 °C, while multilayers containing a single d-CdA/p-CdA interface changed only slightly [7].

A series of experiments was performed to discriminate between actual movement of CdA molecules across the polymeric barrier and interfacial diffuseness due to interdigitation at layer/layer interfaces. A sample composed of eight d-PG (n=18) layers atop six layers of p-CdA supported on a silicon wafer (sample 'CdA/PG') was measured before and after annealing to determine the degree to which a single interface between PG side chains and CdA aliphatic tails changed with annealing. In this case there was no reason to anticipate diffusion across the PG. However, the neutron reflectivity changed markedly with annealing as shown in Figure 5, suggesting a broadening of the PG/CdA interface due to interdigitation alone.

The effect of side chain density and length upon the composite microstructure and stability was also investigated using comparable sandwich samples with different types of PG. The first type of sample contained PG with about 30% n-alkyl substituted residues and different side chain lengths: n = 12, 18, 20, 22. These materials do not exhibit side chain crystallization, even at temperatures substantially below room temperature. A second sample type included a PG with n = 18, but 60% substitution. Side chain crystallization in

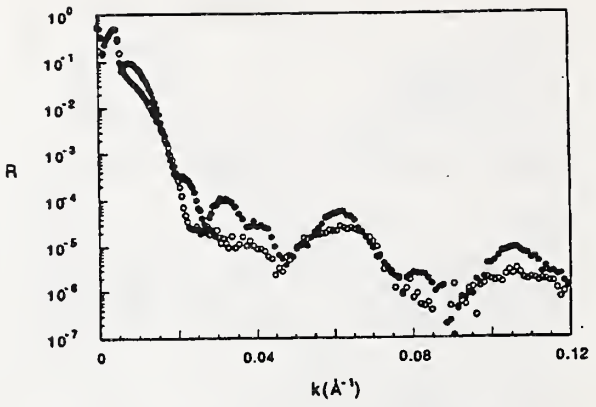

Figure 5. Neutron reflectivities of the CdA/PG multilayer as deposited (•) and after (o) annealing 44 hrs at 84 ±1.5 °C.

the bulk was much easier for this molecule. The change in microstructure with annealing for the sample with n = 22, 30% substitution and that with n = 18, 60% substitution was distinctly different from that of the other samples. A more quantitative interpretation of this difference awaits further detailed analysis of the neutron reflectivity data. This specific work, as described above, was performed in collaboration with M. D. Foster and T. Vierheller of the University of Akron, A. Schmidt, K. Mathsauer, W. Knoll, and G. Wegner of the Max Planck Institute for Polymer Research. A special note of thanks is due W. Schrepp of BASF AG for assistance in the preparation of the multilayer.

Developments in Data Analysis

This "law" of nature also applies to the world of neutron reflectivity data analysis. Because of the relatively high reflectivity (approaching unity at low wavevector transfers), a dynamical theory of reflection which accounts for the appreciable distortion of the incident wave is required to correctly extract density profiles from the reflectivity data. In practice, a direct comparison between measured reflectivity data and that calculated for a particular model of the real space density profile is often performed with varying degrees of agreement by trial and error. J. Ankner has improved upon this process by developing a sophisticated non-linear least squares program which can be used to automatically vary parameters to obtain the best model fit to the

observed reflectivities. In some cases, however, the loss of phase information (the measured reflectivities or intensities are proportional to the square of the structure factor) is sufficiently great that a unique real space density profile cannot be accurately obtained from a given reflectivity profile. We are currently working on phase shifting techniques, analogous to the method of isomorphic substitution employed in conventional crystallography.

It is in principle possible to recover phase information regarding an unknown, non-magnetic film structure in reflectivity measurements with polarized neutrons if the film is deposited on a substrate with a buried ferromagnetic layer of known thickness. We have shown that the subtraction method for inverting polarized neutron reflectivities to obtain real space density profiles works, in principle, in the kinematic limit. However, if the reflectivity data are in the dynamical regime, an analogous subtraction scheme within the Distorted Wave Born Approximation (DWBA) is of questionable value. In the neighborhood of the critical angle, crucial reflectivity information can be sufficiently perturbed in position and magnitude to significantly increase the probability of ambiguous results. Nonetheless, Norm Berk has very recently made progress in adapting mathematical simplex techniques to better fit neutron reflectivity in the dynamical case.

It has also been found that by simultaneously fitting plus and minus polarized neutron reflectivity data, the number of possible scattering density profiles can be reduced. This applies to the determination of both chemical and magnetic density profiles. During the past year we have expanded the capability of our specular reflectivity modeling software to include the simultaneous refinement of polarized neutron data sets. This new software complements the existing non-polarized beam programs REFFIT, MLAYER, and TAILS (see last year's report) and allows us to model quantitatively most specular reflectivity measurements that can be performed on the BT-7 reflectometer. The programs MAGLAYER and MAGBLOCKS allow one simultaneously to fit the two-cross section specular reflectivity of simple ferromagnetic samples with moment orientation parallel or antiparallel to the neutron polarization. Program MAGBLOCKS4 treats the case of moments oriented arbitrarily in the plane of the sample surface by refining the four cross sections that can be measured for the incident and reflected neutron beams.

The refractive index of polarized neutrons incident on a ferromagnetic material depends on both nuclear and magnetic interactions [8],

$$n_{\pm} = [1-\lambda^2 N(b\pm p)/\pi]^{1/2} \qquad (1)$$

where λ is the wavelength of the incident neutrons, N the number density of the scatterers, and b and p their nuclear and magnetic scattering amplitudes. The magnetic amplitude is related to the net moment per scatterer, $p = C\mu$, where $C = 0.2695 \times 10^{-4}$ Å/μ_B with μ given in units of Bohr magnetons. The plus and minus of equation (1) refer to neutrons polarized parallel and antiparallel to the sample magnetic moment.

By simultaneously fitting the plus and minus data sets, one can determine the nuclear and magnetic density profiles. Figure 6 shows the measured reflectivities from an Fe/Si multialyer [9]. The solid lines in Figures 6a and 6b are model curves generated (using MAGBLOCKS) from the profiles in Figures 7a and 7b using the parameters in Table 1 (see refs. [10,11] for a general discussion of specular reflectivity fitting). The essential structural detail needed to reconcile plus and minus fits is the difference in thickness between the nuclear and magnetic iron layers, the effect of which can be seen most clearly in Figure 7b. From Table 1, note that the fitted average nuclear thickness d_b for the iron layers is 58.6 Å, while the thickness d_p of the layers exhibiting the bulk iron moment is only 46.2 Å. We therefore must have 6.2 Å of magnetically dead iron at each interface. The profiles in Figure 7 demonstrate how these dead layers give rise to the observed scattering. The magnetic scattering density (7d) is added to the nuclear (7c) to produce the plus profile (7a). This profile differs only subtly from one in which the nuclear and magnetic thicknesses are the same, so the reflected intensity in Figure 6a resembles that from a simple bilayer of total thickness 107.9 Å. In the minus profile, on the other hand, the thinner magnetic layer incompletely cancels the nuclear density (7b=7c-7d), resulting in regions of greater density at the interfaces. The

Table 1.

ℓ	Type	Re(nb) (10^{-6} Å^{-2})	d_b (Å)	σ_b (Å)	Re(Np) (10^{-6} Å^{-2})	d_p (Å)	σ_P (Å)
1	FeOx	7.1	52.5	8.9	0.3	52.5	8.9
2	Si	1.9	48.4	7.3	0	54.6	7.3
3,5,...,25	Fe	7.9	58.6±1.8	6.3	5.0	46.2±1.8	6.3
4,6,...,26	Si	1.7	49.3±2.6	6.3	0	61.7±2.6	6.3
27	Fe	7.9	28.9	6.3	5.0	22.7	6.3
28	glass	3.6	____	3.0	0	____	3.0

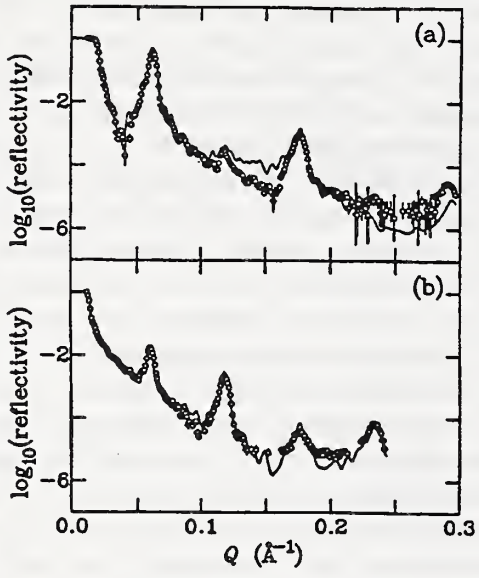

Figure 6. Spin up (a) and spin down (b) polarized neutron reflectivity data (circles) and model curves (solid lines) generated from the spatial profiles of Figure 7 for an Fe-Si multilayer as described in the text.

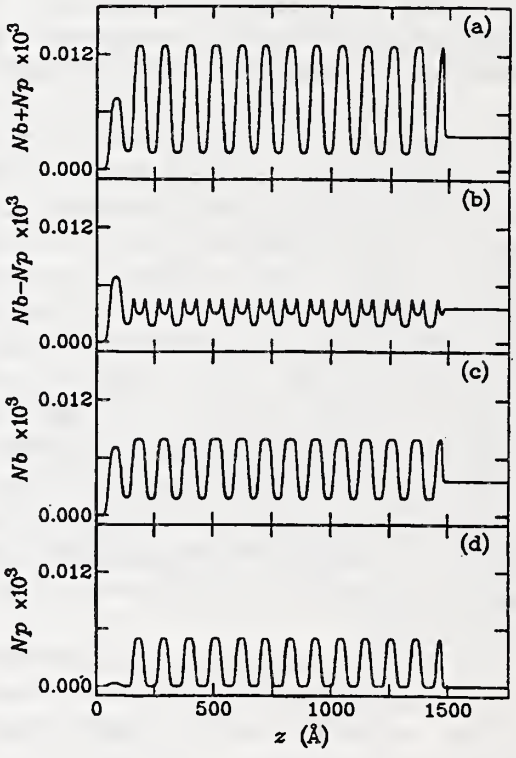

Figure 7. Real space density profiles for the Fe-Si multilayer.

minus profile (7b) goes through twice as many maxima and minima as the plus, producing enhanced even-order diffraction peaks. The observed diffraction patterns manifest directly the underlying magnetic profile.

Polymers

- **Chain Configurations in Ordered Block Copolymers**

In thin films of symmetric diblock copolymers, the preference of one copolymer component for an interface induces a strong orientation of the lamellar domains parallel to the interface, generating a multilayered structure. In an earlier study, neutron reflectivity was performed on thin films of poly(styrene-b-methyl methacrylate) on silicon, in which either the PS or the PMMA blocks were fully deuterated to provide contrast between the layers [12]. This labeling scheme gave detailed information on the average thickness of the domains and the interfacial width as a function of copolymer molecular weight. In the present study, P(S-b-MMA) copolymers were synthesized with selected portions of the blocks deuterated, to allow the study of chain configurations within the lamellar morphology.

Copolymers were anionically synthesized with small fractions (5-10%) of either the PS or PMMA blocks deuterated at the chain end or adjacent to the PS/PMMA junction. Copolymer films 1300-1600 Å thick were spin cast from solution in toluene onto silicon and annealed to achieve ordering. Specular reflectivity measurements were made on the BT-7 reflectometer. Scattering length density profiles giving best fits to the data were deconvoluted to generate volume fraction profiles for the labeled and unlabeled components of the copolymer.

From the reflectivity analysis the junction points were found to be essentially confined to the PS/PMMA interfacial regions. Chain ends, however, are well-distributed through their respective domains, exhibiting only a weak maximum in concentration at the domain centers. This is well illustrated in Figure 8, which shows the volume fraction profile for a film of 70 K P(S-b-MMA-b-MMA_{d8}) where 5 vol% of the total copolymer is deuterated. Results from this study differ significantly from those obtained from small-angle scattering of selectively labeled PS-b-PVP copolymers [13], where the chain ends were inferred to be highly localized within the domain centers.

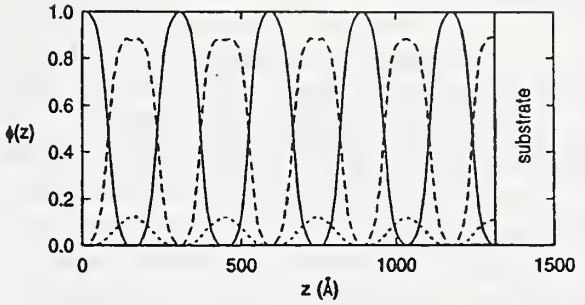

Figure 8. Volume fractions of PS (solid), PMMA (dashed) and $PMMA_{d8}$ (dotted) for 70 K end-labeled copolymer.

- **Entropically Driven Surface Segregation in Block Copolymer Melts**

The morphology of block copolymer films near surfaces can be significantly affected by the difference in surface free energy of the two blocks and their affinity for the substrate. Depending on the interaction between the two blocks, the copolymer can be either homogeneously mixed or separated into microdomains. In properly annealed thin films these microdomains orient parallel to the surface. In block copolymer films of polystyrene-polymethymethacrylate (PS-PMMA) on silicon, the first PMMA layer is in contact with a $Si\text{-}SiO_2$ surface while the air interface contains only PS segments. This is a result of very strong chemisorption of PMMA to oxide surfaces as well as the lower surface tension of the PS at the polymer-air interface. The surface segregation in this case and many other cases that are known is primarily driven by the enthalpic factors [14].

Recently, we have studied thin block copolymer films where the same block segregates to both the solid and the air interface [15]. This behavior was found in both poly(ethylene-propylene)-poly(ethyl-ethylene) (PEP-PEE) block copolymers where PEE is the surface active species as well as poly(ethylene)-poly((ethylene-propylene)(PE-PEP) block copolymers where PEP is the surface active species. The enthalpic driving force for surface segregation is rather small in these cases since both blocks in PEP-PEE as well as PE-PEP block copolymers are simple saturated hydrocarbons. The entropic force thus plays a significant role in surface segregation in these block copolymer systems.

This was shown by studying three different combinations of block copolymers of PEP-PEE, PE-PEE and PE-PEP. All were compositionally symmetric samples with one block deuterated for neutron contrast. All three blocks have different statistical segment lengths, these being 8.3, 6.8 and 5.1 Å for PE, PEP and PEE respectively. Neutron reflectivity from films of these copolymers on a silicon substrate are shown in Figure 9. The solid lines represent the best fit to the data assuming that in each case the block having the smaller statistical segment length goes to both the air and Si interface. The best fits assuming that the longer segment length goes to both surfaces are shown as dashed lines. PEP-PEE films were also grown on polystyrene, Ag and quartz as the substrates. The results for all the combinations of polymers and substrates studied are shown in Table 2. On all of these substrates with widely varying substrate energies the smaller statistical segment length block goes to both the air and substrate interface.

Surfactants

The molecular order in aqueous solutions near interfaces and in thin films can be different from the ordering in coexisting bulk phases. By examining the structure of interfaces and thin films as a function of concentration in coexisting bulk surfactant solutions, we can probe the influence of the interfacial constraints on the self-assembly mechanisms responsible for surfactant aggregation in films and in bulk surfactant solutions.

We have used neutron reflectivity to examine the self-assembly of surfactant monolayers in thin fluid films attached to bulk reservoirs of surfactant solutions. These ultrathin films are examples of "precursing" films which form in front of macroscopic menisci and control macroscopic wetting phenomena. We have examined aqueous solutions of sodium dodecyl sulphate (SDS) in contact with an SiO_2 surface. The SiO_2 is the native oxide on a silicon crystal and has a negative surface charge in pH7 water. Enclosed in a vapor-sealed and temperature-controlled chamber, the sample is fixed vertically with only its bottom edge touching a small reservoir of bulk surfactant solution. Since the native charge of the SiO_2 surface and the wetting properties of the surface are extremely sensitive to contamination, control of the sample surface chemistry is essential. We have achieved this level of cleanliness via a multi-step process involving acid washes, ultraviolet exposure, and a final coating of the substrate with a physisorbed monolayer of SDS. To achieve the contrast needed in the experiment, the SDS was perdeuterated.

In complementary experiments, we probed the surfactant concentration on the bulk SiO_2/solution interface. Using a different cell designed for examining the interface between the solid surface and a bulk liquid, we found that the reflectivity from the interface with a solution at 2 times the critical micellar concentration (CMC) is the same as that from a pure water phase (see Fig. 10). If a significant fraction of a perdeuterated surfactant monolayer had been present, these spectra would have been clearly different. Fitting of these reflectivity spectra confirm the absence of surfactant at this interface. Thus, at the bulk solid/liquid interface, the surfactant anion is repelled by the negatively charged SiO_2 surface

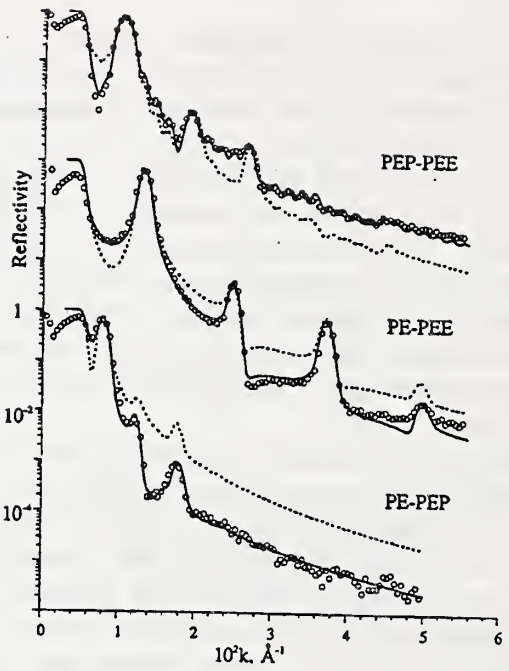

Figure 9. Experimental neutron reflectivity data (open symbols) for three polyolefin block copolymer films on Si. The solid (dashed) lines are fits to the data assming that the smaller (larger) statistical segment length block goes to both the air and Si surfaces.

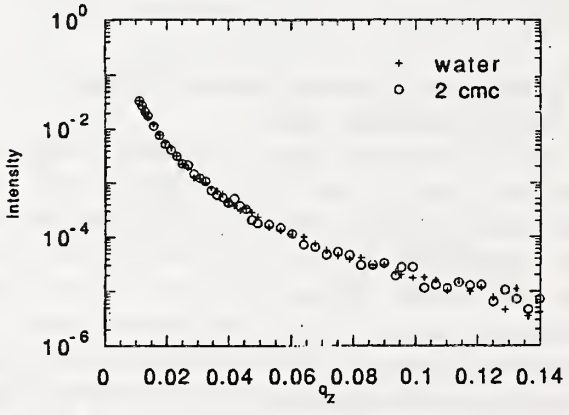

Figure 10. Reflectivity of bulk silica/fluid interface.

even at concentrations where self-assembly in the form of micelles has occurred in the bulk solution.

In the precursing films, the preadsorbed SDS monolayer is desorbed from the solid/liquid interface but a monolayer has appeared at the liquid/vapor interface of the film. Figure 11 shows a representative spectrum of a film connected to a reservoir with a solution at 2 CMC. The film grows over 12 to 72 hrs after contacting the bulk solution. Connected to bulk solutions with concentrations from 1/4 to 2 CMC, the film

Table 2. Thin film characteristics					
diblock copolymer	substrate	lamellar period, d, Å	number of bilayers, n	surface block	surface concentration, $Ø_s$
PEP-PEE(d_6)	*Si	348 ±5	5	PEE(d_6)	0.90
	Poly-styrene	330	3	PEE(d_6)	0.87
	Ag	325	5	PEE(d_6)	0.83
	Quartz	330	5	PEE(d_6)	0.87
PE(d_6)-PEE	*Si	255	12	PEE	0.87
PE(d_6)-PEE	*Si	535	6	PEP	0.72

*Stripped with a 10% aqueous HF solution

has a water core on the order of 10^2 Å and a monolayer at about the molecular density reported to exist at the bulk liquid/vapor interface. The films extend at least 7 cm above the level of the bulk solution and are uniform in thickness to about 5% to 10%.

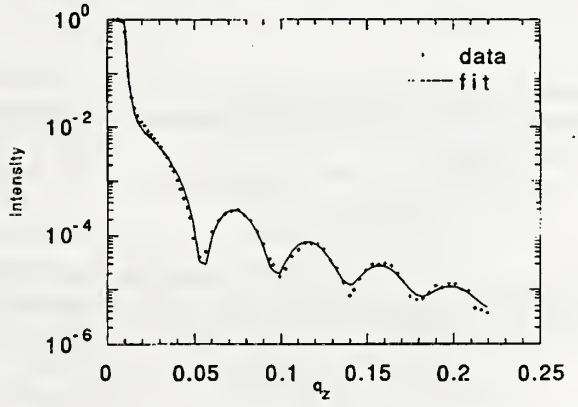

Figure 11. Reflectivity of film connected to 2 cmc bulk fluid.

References

[1] See, for example, C. F. Majkrzak and G. P. Felcher, MRS Bulletin Vol. XV, Nov. 1990, p. 65.

[2] "Neutron Optical Devices and Applications", SPIE Conference Proceedings Volume 1738, ed. C. F. Majkrzak and J. L. Wood (SPIE, Bellingham, WA, in press).

[3] See, for example, C. F. Majkrzak et al., Advances in Physics, 40, 99 (1991).

[4] G. Duda, A. J. Schouten, T. G. Lieser, G. F. Schmidt, C. Bubeck, G. Wegner, "Thin Solid Films", 159, 221 (1988).

[5] M. Shimomura, K. Song, J. F. Rabolt, "Langmuir", 8, 887 (1992).

[6] A. Mathy, K. Mathauer, G. Wegner, C. Bubeck, "Thin Solid Films" 215, 98 (1992).

[7] M. Foster, T. R. Vierheller, A. Schmidt, W. Knoll, K. Mathauer, G. Wegner, S. Satija, C. F. Majkrzak, "Mat. Res. Soc. Symp. Proc.," 248 (1992).

[8] G. P. Felcher, Phys. Rev. B 24, 1595 (1981).

[9] J. F. Ankner, C. F. Majkrzak and H. Homma, J. Appl. Phys. in press.

[10] J. F. Ankner, in "Surface X-Ray and Neutron Scattering", Edited by H. Zabel and I. K. Robinson, Springer Proceedings in Physics, Vol. 61 (Springer-Verlag, New York, 1992), p. 105.

[11] J. F. Ankner and C. F. Majkrzak, in "Neutron Optical Devices and Applications, SPIE Conference Proceedings, Vol. 1738 (SPIE, Bellingham, WA), in press.

[12] S. H. Anastasiadis, T. P. Russell, S. K. Satija, and C. F. Majkrzak, J. Chem. Phys. 92, 5677 (1990).

[13] Y. Matsushita, K. Mori, R. Saguchi, I. Noda, M. Nagasawa, T. Chang, C. Glinka, and C. C. Han, Macromol. 23, 4317 (1990).

[14] G. Coulon, B. Collin, D. Asserre, D. Chatenay, and T. P. Russell, J. Phys. (Paris) 51, 2801 (1990).

[15] M. D. Foster, M. Sikka, N. Singh, F. S. Bates, S. K. Satija, and C. F. Majkrzak, J. Chem. Phys. 96, 8605 (1992).

Experiments

Neutron Reflectivity Studies of the Passive Oxide Film on Fe
L. A. Krebs, S. Krueger, G. G. Long, J. F. Ankner, C. F. Majkrzak, S. K. Satija, and D. G. Wiesler.

Using Polarized Neutrons to Determine Non-Magnetic Chemical Density Profiles of Thin Films
C. F. Majkrzak, N. F. Berk, J. F. Ankner, S. K. Satija, and T. P. Russell.

Distributions of Chain End and Junction Points in Ordered Block Copolymers
A. M. Mayes, T. P. Russell, S. D. Smith, S. K. Satija, and C. F. Majkrzak.

Homopolymer Distributions in Ordered Block Copolymers
A. M. Mayes, T. P. Russell, S. K. Satija, and C. F. Majkrzak.

Neutron Reflectivity Studies of Triblock Copolymer Films
A. M. Mayes, T. P. Russell, S. D. Smith, S. K. Satija, and C. F. Majkrzak.

Polarized Neutron Reflectivity Studies of Magnetic Interlayer Coupling in Co-Cu Superlattices
A. K. Schreyer, H. Zabel, Bochum, J. F. Ankner, and C. F. Majkrzak.

Neutron Reflectivity Studies of Protein Channels in Mitochondrial Outer Membrane
S. Krueger, M. Colombini, D. Gurley, J. F. Ankner, S. K. Satija, and C. F. Majkrzak.

Neutron Reflectivity Studies of Pressure-induced Polymer Surface Contact
W.-L. Wu, W. Orts, S. K. Satija, and C. F. Majkrzak.

Neutron Reflectivity Studies of the Si-PMMA Interface
W.-L. Wu, W. Orts, S. K. Satija, and C. F. Majkrzak.

Temperature Dependence of the Density Profile of End-Grafted Polystyrene in Cyclohexane
D. Perahia, L. Fetters, D. Wiesler, and S. K. Satija.

Molecular Weight Dependence of the Brush Height for End-Grafted Polystyrene in Cyclohexane
S. K. Satija, J. F. Ankner, C. F. Majkrzak, R. Composto, and T. Mansfield.

Magnetization Profile of Co-Pt Multilayers
J. F. Ankner, J. A. Borchers, C. F. Majkrzak, R. Farrow, and R. F. Marks.

Magnetization Profile of Fe-Pd Multilayers
J. F. Ankner, T. Jach, C. F. Majkrzak, and C. Falco.

Magnetization Profile of Co-Cu Superlattices
T. Jach, J. F. Ankner, C. F. Majkrzak, and R. Clarke.

Neutron Reflectivity Study of Acrylo-Nitrile Polymers on Polycarbonate
T. Mansfield and R. Composto.

Neutron Reflectivity Studies of PS-PMMA Diblock Copolymer Mixtures of Different Molecular Weights
A. M. Mayes, T. P. Russell, S. K. Satija, and C. F. Majkrzak.

Installation and Testing of Linear Position Sensitive Detector for Use in Non-Specular Reflectivity Measurements
J. F. Ankner, W. J. Orts, A. Schreyer, S. K. Satija, and C. F. Majkrzak.

Competition for Absorption Between Ionic and Non-Ionic Surfactants at a Quartz-Water Interface
A. R. Rennie, D. Kanelleas, D. C. McDermott, S. K. Satija, and C. F. Majkrzak.

Neutron Reflectivity Studies of Homopolymer-Copolymer Blends of PS and PMMA
A. M. Mayes, T. P. Russell, S. K. Satija, and C. F. Majkrzak.

Polarized Neutron Reflectivity Measurements of Fe_3O_4/NiO Multilayers
J. A. Borchers, J. F. Ankner, C. F. Majkrzak, S. Berry, and D. Lind.

Neutron Reflectivity Studies of PEP-PEE Block Copolymers on Si
M. Sikka, N. Singh, A. Karim, F. Bates, S. Satija, and C. F. Majkrzak.

Neutron Reflectivity Studies of Thick PMMA and PS Films on Si
B. Sauer, W.-L. Wu, W. Orts, and J. Van Alsten.

Characterization of Langmuir-Blodgett Films
M. Foster, S. K. Satija, and C. F. Majkrzak.

Neutron Reflectivity Studies of Surfactants
S. Garoff and S. K. Satija.

Neutron Reflectivity Studies of Langmuir-Blodgett Films of Stearic and Behenic Acids
L. Feigin, J. F. Ankner, D. G. Wiesler, S. K. Satija, A. Karim, and C. F. Majkrzak.

Block Copolymer Blends of PEP-PEE
A. Karim.

Neutron Reflectivity Studies of Triblock Co-polymer Blends
M. Sikka, N. Singh, A. Karim, F. Bates, S. Satija, and C. F. Majkrzak.

Participants

Ankner, J. F.	Reactor Radiation Division
Bates, F. S.	University of Minnesota
Berk, N. F.	Reactor Radiation Division
Berry, S. D.	Florida State University
Borchers, J. A.	Reactor Radiation Division
Brocker, C. W.	University of Maryland
Carey, M.	U. of California, San Diego
Clarke, R.	University of Michigan
Colombini, M.	University of Maryland
Composto, R.	University of Pennsylvania
Falco, C.	University of Arizona
Farrow, R.	IBM Corp.
Feigin, L.	Academy of Science (Russia)
Fetters, L.	Exxon
Foster, M.	University of Akron
Garoff, S.	Carnegie Mellon University
Gurley, D.	University of Michigan
Jach, T.	Surface & Microanalysis Sci. Div.
Kanelleas, D.	Oxford University
Karim, A.	University of Maryland
Krebs, L. A.	Johns Hopkins University
Krueger, S.	Reactor Radiation Division
Lind, D. M.	Florida State University
Long, G. C.	Ceramics Division
Lynn, J. W.	University of Maryland
Majkrzak, C. F.	Reactor Radiation Division
Mansfield, T.	University of Pennsylvania
Marks, R. F.	IBM Corp.
Mayes, A. M.	IBM Corp.
McDermott, D. C.	Oxford University
Orts, W. J.	Polymers Division
Perahia, D.	Exxon
Rennie, A. R.	University of Bristol (UK)
Russell, T. P.	IBM Corp.
Satija, S. K.	Reactor Radiation Division
Sauer, B.	University of Delaware
Schreyer, A. K.	Rühr University, Germany
Sikka, M.	University of Minnesota
Singh, N.	University of Minnesota
Smith, S. D.	Procter & Gamble
Van Alsten, J.	E. I. DuPont
Wiesler, D. G.	Reactor Radiation Division
Wu, W.-L.	Polymers Division
Zabel, H.	Rühr University, Germany
Zhang, H.	University of Maryland

MACROMOLECULAR AND MICROSTRUCTURE STUDIES

In the past year, studies of macromolecular structure and materials microstructure in solutions and bulk solids have been carried out on both the CNRF's 30 m NIST/Exxon/U. Minnesota small angle neutron scattering (SANS) instrument and the 8 m Reactor/Polymers Divisions' SANS instrument. In its first full year of operation, approximately 80 experiments were carried out on the 30 m SANS by more than 110 scientists including 20 from NIST. Among the 80 experiments, about 20 were done by research groups who responded to the CNRF's first official call for proposals and were allocated time by the CNRF's Program Advisory Committee. Results of these studies appear in several places in this report. Some of the areas in which Reactor scientists, usually in collaborations with visiting groups, have had a major involvement are described here.

Polymers

Recent research efforts have dealt with the following topics: the interactions that affect the miscibility of polymer blends; the effects of shear flow on the conformation of linear polymers in solution; novel polymer architectures produced by dendritic growth; and the phase behavior of polymer-liquid crystal mixtures.

- **Polymer Blends**

In order to tailor the physical properties of polymeric materials, one has to mix (i.e., blend) many polymers together. It is important, however, that the mixture remains in the single-phase region for mechanical performance considerations. The spinodal line has been investigated for many "compatible" blend mixtures, such as deuterated polystyrene/poly(vinyl methylether), using the SANS technique. It is known (from cloud point measurements) that the deuteration needed for SANS measurements brings about temperature shifts of the spinodal line. The goal of this project was to better understand this effect of deuteration on the interaction of polymer blends. We have performed SANS measurements from ternary blends of deuterated polystyrene (PSD), hydrogenated polystyrene (PSH), and poly(vinyl methylether) (PVME) at various compositions. The three Flory-Huggins "chi" parameters corresponding to the interaction of any two polymer pairs have been obtained as well as their temperature variation. This method has allowed a direct measurement of the interaction parameter of two hydrogenated polymers (PSH/PVME) which was found to be appreciably different from that of PSD/PVME.

- **Polymer Solutions**

It is known from light scattering that shearing favors mixing in polymer blends (above the glass-rubber transition temperature) while it promotes demixing in solutions of some high molecular weight polymers. The purpose of this project is to better understand the conformational changes that accompany such a demixing process in high molecular weight polystyrene in semidilute dioctyl phthalate solution under shear. Shearing, in this system, induces a "transition" to the two-phase region as evidenced by the sudden increase in SANS intensity. To our great surprise, it was found that the SANS patterns showed no anisotropy even at the highest shear rates. This is due to the fact that the length scale observed corresponds to chain portions which relax faster than the shearing process. A sharp dependence of the second virial coefficient on shear rate was found. No theory can currently predict such behavior. This project involves a collaboration with the Polymers Division.

- **Polymer Gels**

Starburst dendrimers are synthesized through a multifunctional polymerization with branching at each generation so that a "cauliflour" gel is grown from an initial core. These polymeric materials are finding applications as drug carriers, cosmetic additives, lubricants, adhesives, etc. Starburst dendrimers with 3, 5, 7, or 9 generations have been measured in heavy water solutions by the SANS technique. Single-"particle" (Fig. 1) and interparticle structure factors have been extracted. Reliable particle sizes have been obtained in each case. Also, it was found that the addition of acid or salt weakens the interparticle interactions. The particle sizes found using SANS were more precise than ones previously reported using intrinsic

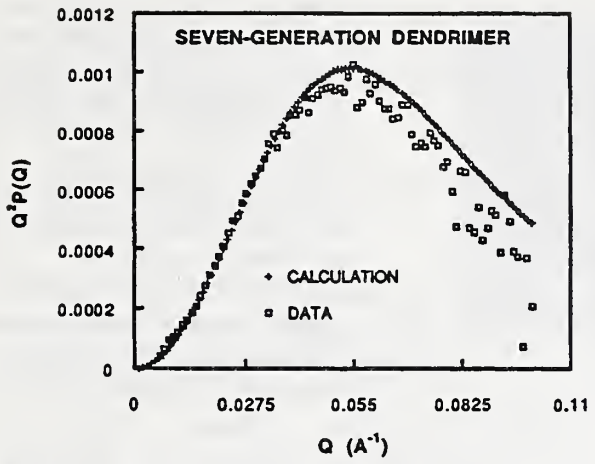

Figure 1. Kratky plot of SANS data from solutions of seventh generation starburst polyamidoamine dendrimers in deuterated water, extrapolated to zero concentration, compared with the calculated single-particle scattering for a dendrimer model with gaussian blocks. Salt was added to the solutions to screen out coulombic interactions.

viscosity or size exclusion chromatography measurements. All of our SANS measurements so far made use of "normal" (i.e., nondeuterated) dendrimers in heavy water. Our goal is to measure dendrimers with one deuterated generation on the outside. Such dendrimers will hopefully allow us to assess whether there is a depletion of the monomer density close to the particle core as predicted by de Gennes. Computer simulations by Muthukumar have shown that, on the contrary, monomer density decreases smoothly with the particle radius. This project involves a collaboration with the Polymers Division and the University of Maryland.

- **Liquid Crystals**

Progress has been made in the modeling of mixtures of liquid crystals and flexible polymers. The structure factor for such a mixture has been derived using the Random Phase approximation (RPA). Lyotropic as well as thermotropic mixtures can be described by this simple model which is a generalization of the deGennes formula to include chain stiffness. Isotropic-to-nematic and spinodal lines are predicted. SANS data will be taken from mixtures of liquid crystals and flexible polymers and this model will be used to analyze such data. It is hoped that the Maier-Saupe interaction parameter (which represents nematic interactions) can be obtained along with its temperature behavior.

Complex Fluids under Shear Flow

The availability of a couette flow scattering cell, built for the CNRF by NIST's Thermophysics Division, has stimulated a growing interest in using SANS to relate the bulk rheological behavior of fluids consisting of strongly interacting particles and macromolecules to their underlying microstructure. In collaboration with the Thermophysics Division and the University of Illinois, both dilute and concentrated aqueous suspensions of uniform polystyrene latex particles have been studied over a wide range of shear rates. When properly prepared, these model systems can be induced to form highly ordered crystalline-like structures (see, for example, Fig. 2) that exhibit a remarkable degree of stability under shear flow. A 4% (by volume) suspension of 91 nm latex spheres, for example, was observed to have long range orientational order at shear rates up to ten thousand hertz before shear melting into a liquid-like state. At high concentrations ($\sim$ 50%), the suspensions show striking rheological behavior including an abrupt drop in steady state viscosity (shear thinning) at moderate shear rates, and a steep rise in viscosity (shear thickening) at high shear rates. The SANS measurements have identified distinct changes in the suspension microstructure associated with each aspect of the rheological response. The SANS data have, for example, provided the first direct evidence to support the hypothesis that the shear thinning is associated with a nonequilibrium structural transition between two distinct states with long range orientational order. The shear thickening, on the other hand, is associated with a gradual disordering of the suspension, or melting, into a liquid-like structure.

SANS measurements of fluid behavior under shear are being extended to the study of interparticle correlations in binary colloidal mixtures and of the phases and structural transitions that occur in systems of self-associating amphiphilic molecules. The ability to observe the effects of shear on the underlying microstructure in such systems will enhance our understanding and ability to control fluid properties.

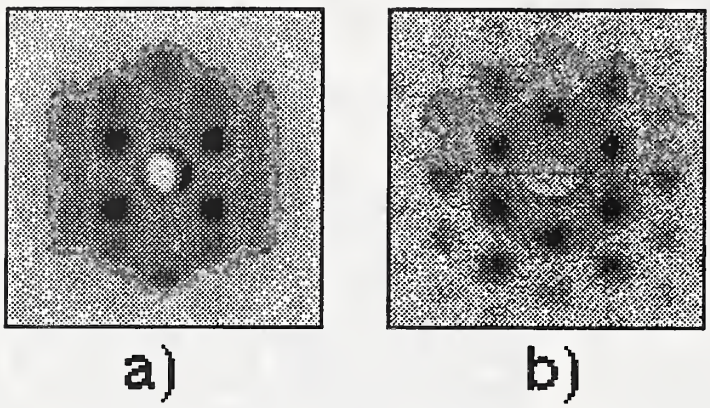

Figure 2. Small angle neutron scattering from polystyrene latex suspensions at rest after shearing to induce ordering. The patterns are gray scale images of the scattered neutron intensity as recorded on the 2-d detector on the 30-m NIST/Exxon/U. Minnesota SANS instrument. The pattern on the left is for a 4% (by volume) suspension of 91 nm particles; that on the right a 53% suspension of 239 nm particles.

Biological Macromolecules

The availability of the NIST/Exxon/U. of Minnesota 30m SANS and, most recently, the CHRNS 30m SANS has brought about a renewed interest in the study of biological macromolecules at the CNRF. These high resolution instruments have made possible the measurement of biopolymers which form large polymer networks. Polysaccharide gels such as agarose have been measured in collaboration with the National Institutes of Health. SANS measurements were performed on 3% agarose in D_2O as a function of temperature from room temperature through its melting point (~ 85 °C). The behavior of the gel in D_2O followed closely its known behavior in H_2O. The transition from gel (at room temperature) to sol is gradual, starting above 70 °C through the melting point. Measured correlation lengths ranged from 70 nm for the gel at room temperature down to 6 nm at the melting point. The gel is completely melted at 95 °C where the scattered intensity was weak and did not follow the form expected for a polymer network. When the sol was allowed to cool back down to room temperature, the expected hysteresis was observed as gelation took place rapidly at ~35 °C.

It is hoped that agarose can be used as a model system for the study of junction formation in physiologically important biological gels such as heparin, which is found in connective tissue. The polymerization of actin, which is found in muscle tissue, has also been measured with the intent of studying the effects of shear on the polymer structure.

The relatively high flux available on the sample also makes possible the study of dilute solutions of small globular complexes. The nucleosome, a 10 nm diameter protein/DNA complex which forms the basic subunit of chromatin, has been measured in collaboration with Los Alamos National Laboratory (LANL) and the University of California at Davis. Protein/ DNA interactions are being investigated by varying the length of the DNA segment which is bound to the protein core. A scarcity of synthesized material as well as a tendency for the complexes to aggregate make measurements at low concentrations essential for the study of such small complexes. In order to model the small conformational changes which may be occuring during acetylation of the protein core, data must be obtained over a wide angular range and under a variety of solvent conditions.

Also in collaboration with LANL, preliminary SANS measurements have been made on the Troponin C/Troponin I (TnC/TnI) complex, a 6 nm diameter protein complex which plays a role in the calcium regulation of muscle contraction. Deuterated TnC was complexed with nondeuterated TnI and measured at low concentration under a variety of solvent conditions. Initial results from both the chromatin and TnC/TnI experiments show promise that reliable data can be obtained even in cases where the signal-to-noise ratio is expected to be fairly low.

Biological samples often require special care in handling and processing prior to measurement. Final sample preparations such as centrifugation and dialysis sometimes must be made immediately before each SANS measurement. Thus, protein or DNA concentrations are not always known at the time of the SANS measurement and must be

determined independently afterwards. The CNRF is in the process providing more of the equipment which is necessary to meet these specialized needs of the biology community.

Microstructure Evolution of Ceramics During Densification

The evolution of the pore size distribution during densification of powder compacts is of great practical importance in relating the role of processing variables to the final microstructure. The SANS technique provides statistically significant data relating to pore volume and number distributions. Conventional SANS techniques typically measure pore sizes up to 100 nm, making it suitable for characterizing the later stages of sintering. The large pores that are generally present during early and intermediate stages of sintering make it necessary to use the multiple small-angle scattering (MSANS) technique which extends the range of measured pore sizes to 10 μm. While complete volume and number distributions cannot be obtained from the MSANS technique, both MSANS and SANS combined can give important information relating to the largest and smallest pores in the size distribution, respectively.

- **Conventional Ceramics**

Conventional ceramics are compacts which have been formed from powders which contain particles in the 0.1 μm to 1 μm size regime. In collaboration with Dow Chemical Company, the MSANS technique is being used at the CNRF to examine the pore evolution during sintering of silicon nitride. Measurements have been made on both yttria and magnesia-doped silicon nitride during the intermediate sintering stages. Plans are currently underway to measure these samples through the final sintering stages and to examine the role of multiple dopants on the microstructure evolution.

In addition, MSANS studies examining the role of powder particle sizes in the sintering of alumina have been performed in collaboration with Southwest Research Institute using research-grade powders containing monodisperse 0.8 μm particles, monodisperse 0.25 μm particles and a 3:1 mixture of 0.8:0.25 μm particles. These powders were chosen in order to make a direct comparison between theoretical models of sintering and experimental results. Such comparisons have been impossible in the past due to the complicated nature of commercial powders which contain polydisperse particle size distributions.

The results are shown in Figure 3 in the form of effective MSANS-derived pore radius as a function of percent theoretical density. The first points at the lowest density represent measurements on the green body. Although the two monodisperse samples had a green density of ~61%, while the mixture had a higher green density of 68%, the associated pore size was found to be smallest for the 0.25 μm sample, largest for the 0.8 μm sample and in-between for the mixed sample. As observed in earlier MSANS studies of sintered commercial (Baikowski) powder compacts, all samples showed a constant or declining effective pore radius during intermediate stage sintering. At high densities, the 0.8 μm material shows the best microstructure (i.e., the smallest pores) while the 0.25 μm material shows the worst microstructure. These results are not what was expected since the 0.25 μm material had the smallest initial porosity. Finally the mixture appears to be intermediate where it should have shown the best microstructure, according to conventional wisdom. Once the data points between 86% and 95% TD are measured for the 0.25 μm sample, the turnover region between intermediate and final stage sintering can be compared for all three samples.

- **Nanostructured Ceramics**

Nanostructured ceramics are those compacts which have been formed from powders with nano-sized particles of diameters typically less than 10 nm. Nanostructured powders are of technological interest because they can be processed to small-grained, fully-dense ceramics which exhibit novel properties related to their unique microstructures. Since nanostructured compacts contain small pores, conventional SANS techniques can be used to measure pore size distributions as a function of densification. Such an experiment was performed on nanostructured yttria in collaboration with Rutgers University. The results, shown in Figure 4, confirm that pores in the 7 nm size range are present in the as-pressed compacts (60-65%

theoretical density) and in the material which had been sintered at temperatures up to 600 °C. Higher sintering temperatures produced material with increasingly larger pore sizes until, at 1200 °C, the measured scattering curve resembled that of a conventional ceramic material containing micron-sized pores. In contrast, compacts which had been hot-pressed (550 °C) to a higher density without sintering retained the original 7 nm-sized pores. Further SANS studies of isochronally and isothermally sintered nanostructured yttria and zirconia are presently underway.

In addition, SANS measurements of nanostructured alumina have been performed in collaboration with Nanophase Technologies Corp., a participating company in NIST's Advanced Technology Program. This preliminary work represents the beginning of a systematic investigation of nanophase microstructure evolution during processing of extremely small-grained alumina and silicon nitride.

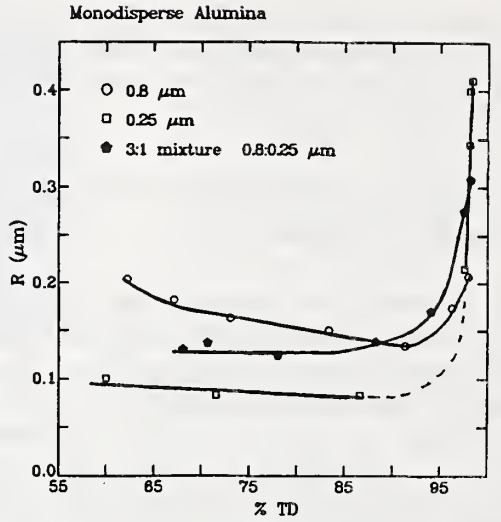

Figure 3. Effective pore radii extracted from MSANS measurements of compacted research-grade alumina powders at various stages of sintering. The abscissa is the bulk density of each sample as a percentage of the theoretical density of alumina.

Precipitate Growth and Morphology

In a classic application of the SANS technique, the kinetics of growth of semiconductor crystallites in a glass matrix have been studied in collaboration with the University of Pavia. Borosilicate glasses doped with a fraction of a percent of either CdTe or CdS_xSe_{1-x} were measured following isochronal anneals at temperatures ranging from 800 to 1000K to induce precipitation of the dopant. The size distribution of the resulting crystallites affects the nonlinear optical properties of these glasses which are presently the object of extensive research in view of their potential applications. The scattering patterns measured for the various annealing temperatures exhibited a scaling behavior indicative of late stage growth, called coarsening, in which the semiconductor is fully precipitated and has a size distribution whose shape is time-independent. At this stage of growth, the only time-dependent parameter is the average crystallite size.

Similar studies of precipitate morphology have been carried out on metal alloys, in particular steels, where the magnetic contrast between a precipitate and the surrounding matrix material can provide additional information on the composition

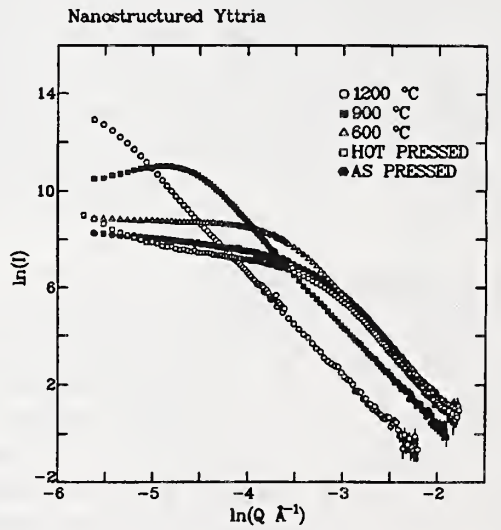

Figure 4. Log-log plot of the small angle scattering from compacts of nanoscale yttria particles that were subsequently sintered to higher density at the temperatures indicated.

of the inhomogeniety. This approach has been used successfully to identify and characterize irradiation-induced precipitates in reactor pressure vessel steels, in collaboration with the University of California at Santa Barbara, and small carbides in prototype high strength, low alloy steels, in collaboration with Northwestern University.

Experiments

Structure of Mesoporous Molecular Sieves
C. J. Glinka, J. M. Nicol, J. J. Rush; G. Stucky, E. Ramli, J. B. Higgins, and M. E. Leonowicz.

Small Angle Neutron Scattering Study of Crystal Growth in Semiconductor-Doped Glasses
G. P. Banfi, V. Degiorgio, A. R. Rennie, and J. G. Barker.

Carbide Size Distribution Evolution with Aging of a Model High Strength and Toughness Steel Alloy
P. J. Jemian, C. Kuehn, G. Olsen, J. R. Weertman, and J. G. Barker.

Cavity Size and Density Evolution in Creep Cavitated Silicon Nitride
W. Luecke, S. Wiederhorn, G. Long, and J. G. Barker.

Structural Changes and Orientational Order in a Sheared Colloidal Suspension
L. B. Chen, M. K. Chow, C. F. Zukoski, B. J. Ackerson, H.J.M. Hanley, G. C. Straty, J. G. Barker, and C. J. Glinka.

Thermodynamics of Deuterated Polystyrene/ Protonated Polystyrene/Polyvinyl Methyl Ether Ternary Polymer Blends
B. Hammouda, R. Briber, and B. Bauer.

High Molecular Weight Polystyrene Solutions under Shear
B. Hammouda, A. Nakatani, and C. C. Han.

Molecular Chain Dimensions in Ionomer Solutions
E. Karayani, S. Cooper, and B. Hammouda.

Interaction Parameter in Polystyrene/Polyxylenyl Ether Polymer Blends
R. Composto, Q. Pan, and B. Hammouda.

Single Particle and Interparticle Structure Factors in Starburst Dendrimers
B. Bauer, R. Briber, and B. Hammouda.

Small Angle Neutron and X-Ray Scattering Study of the Onset and Nature of Fracture of Uniaxially Compressed Gun Propellants
S. F. Trevino, R. J. Lieb, and J. D. Barnes.

Characterization of the Effect of Water Adsorption by the Biological Polymer Chitosan by Small Angle Neutron Scattering
S. F. Trevino and J. Walker.

SANS Studies of Shear Induced Melting of Colloidal Crystals
H.J.M. Hanley, G. C. Straty, J. G. Barker, and C. J. Glinka.

SANS Study of the Growth of Cylindrical Micelles under Shear Flow
M.-W. Kim, S. K. Sinha, M. Y. Lin, H.J.M. Hanley, and G. C. Straty.

Effects of Low Shear on 'Hard-Sphere' Colloidal Systems
R. H. Ottewill, A. R. Rennie, H.J.M. Hanley, and G. C. Straty.

Interparticle Correlations in Colloidal Suspension Mixtures
H. J. M. Hanley, G. C. Straty, A. R. Rennie, and R. H. Ottewill.

Search for Fluxoid Lattices in High Tc Superconductors
J. W. Lynn, H. Zhang, T. Clinton, and N. Rosov.

Micelle-Vesicle Transition in Model Bile Systems
E. W. Kaler, M. A. Long, A. Full, and S. Kline.

Mixed Surfactant Microemulsions
E. W. Kaler, M. A. Long, A. Full, and S. Kline.

Compatibility of PI/PVE Polymer Blends
D. Tomlin and C. M. Roland.

Reentrant Ferromagnetism is $LuFe_{10}Mo_2$
R. W. Erwin and C. Christides.

Microstructure of Photoluminescent Porous Silica
B. J. Heuser and C. J. Glinka.

Structure of Liquid Crystal Polymers under Shear Flow
N. Wagner, L. Walker, and J. Bender.

Phase Transitions in Concentrated Microemulsions
S. H. Chen, D. Lee, and C. Y. Ku.

Conformation of Tethered Block Copolymers
A. Gast, M. Fair, J. Huang, and M. Y. Lin.

Scattering from Dislocations in Deformed Copper Single Crystals
B. J. Heuser.

Chain Interactions in Bimodal Polymer Blends
M. R. Landry.

Particle Size Distribution and Superparamagnetism in Nanodispersed Magnetic Particles
J. R. Childress, C. L. Chien, R. W. Erwin, J. J. Rhyne.

Irradiation Induced Microstructural Evolution in Pressure Vessel Steels
G. R. Odette, E. Mader, D. Klingensmith, J. G. Barker, and C. J. Glinka.

Junction Structure in Biological Matrices—Agarose
S. Krueger and R. Nossal.

Interactions in Chromatin Complexes
P. Yau, J. Gatewood, B. Imai, J. Trewhella, S. Krueger, and E. M. Bradbury.

Conformational Changes in Troponin C/Troponin I Complexes
G. Olah, J. Trewhella, S. Blechner, S. Rokop, and S. Krueger.

Mechanism of Triethanolamine Interaction in Zeolite Nucleation
R. Thompson, E. Coker, G. Long, and S. Krueger.

Microstructure Evolution during Sintering of Monodispersed Alumina Powder Compacts
R. Page, Y. Pan, G. Long, and S. Krueger.

Microstructure Evolution in Early and Intermediate Stage Sintering of Silicon Nitride
J. Hwang, S. Krueger, G. Long, and A. Allen.

Microstructure Evolution of Nanostructured Yttria
H. Hahn, S. Krueger, G. Long, H. Kerch, and A. Allen.

Microstructure Evolution of Nanostructured Alumina
J. Parker, S. Krueger, J. Barker, G. Long, and H. Kerch.

Microstructure of Leached and Unleached Colloidal Silica Precursor Sol-gels
H. Kerch, G. Long, A. Allen, and S. Krueger.

Cement Microstructure Evolution and Aging in Mortars
A. Allen and R. Livingston.

Participants

Ackerson, B. J.	Oklahoma State University
Allen, A.	University of Maryland
Banfi, G. P.	Universata di Pavia, Italy
Barker, J. G.	Reactor Radiation Division
Barnes, J. D.	Polymers Division
Bauer, B.	Polymers Division
Bender, J.	University of Delaware
Blechner, S.	Los Alamos National Laboratory
Bradbury, E. M.	University of California, Davis
Briber, R.	University of Maryland
Chen, L. B.	University of Illinois
Chen, S. H.	MIT
Chien, C. L.	Johns Hopkins University
Childress, J. R.	Johns Hopkins University
Chow, M. K.	University of Illinois
Christides, C.	University of Sussex, UK
Clinton, T.	University of Maryland
Coker, E.	Worchester Polytechnic Inst.
Composto, R.	University of Pennsylvania
Cooper, S.	University of Wisconsin
Degiorgio, V.	Universata di Pavia, Italy
Erwin, R. W.	Reactor Radiation Division
Fair, M.	Stanford University
Full, A.	University of Delaware
Fuller, E.	Ceramics Division
Gast, A.	Stanford University
Gatewood, J.	Los Alamos National Laboratory
Glinka, C. J.	Reactor Radiation Division
Hammouda, B.	Reactor Radiation Division
Hahn, H.	Rutgers University
Han, C. C.	Polymers Division
Hanley, H.J.M.	NIST Boulder
Heuser, B. J.	MURR, Columbia, MO
Higgins, J. B.	Mobil R&D Corp.
Huang, J.	Exxon Research & Eng. Co.
Hwang, J.	Dow Chemical
Imai, B.	Los Alamos National Laboratory
Jemian, P. J.	Argonne National Laboratory
Kaler, E. W.	University of Delaware
Karayani, E.	University of Wisconsin
Karim, A.	University of Maryland
Kerch, H.	Ceramics Division
Kim, M.-W.	Exxon Research & Eng. Co.
Kline, S.	University of Delaware
Klingensmith, D.	U. of California, Santa Barbara
Krueger, S.	Reactor Radiation Division
Ku, C. Y.	MIT
Kuehn, C.	Northwestern University
Landry, M. R.	Eastman Kokak

Lee, D.	MIT
Leonowicz, M. E.	Mobil R&D Corp.
Lieb, R. J.	U.S. Army Research Lab
Lin, M. Y.	Exxon Research & Eng. Co.
Livingston, R.	Building Materials Division
Long, M. A.	University of Delaware
Long, G.	Ceramics Division
Luecke, W.	Ceramics Division
Lynn, J. W.	University of Maryland
Mader, E.	U. of California, Santa Barbara
Nakatani, A.	Polymers Division
Nicol, J. M.	Reactor Radiation Division
Nossal, R.	NIH
Odette, G. R.	U. of California, Santa Barbara
Olah, G.	Los Alamos National Laboratory
Olsen, G.	Northwestern University
Ottewill, R. H.	University of Bristol, UK
Page, R.	Southwest Research Institute
Pan, Q.	University of Pennsylvania
Pan, Y.	Southwest Research Institute
Parker, J.	Nanophase Technologies, Inc., Darien, IL
Ramli, E.	U. of California, Santa Barbara
Rennie, A. R.	University of Bristol, UK
Rhyne, J. J.	MURR, Columbia, MO
Rokop, S.	Los Alamos National Laboratory
Roland, C. M.	Naval Research Lab
Rosov, N	University of Maryland
Rush, J. J.	Reactor Radiation Division
Sinha, S. K.	Exxon Research & Eng. Co.
Straty, G. C.	NIST Boulder
Stucky, G.	U. of California, Santa Barbara
Thompson, R.	Worchester Polytechnic Inst.
Tomlin, D.	Naval Research Lab
Trevino, S. F.	U.S. Army Research Development & Engineering Ctr.
Trewhella, J.	Los Alamos National Laboratory
Wagner, N.	University of Delaware
Walker, L.	University of Delaware
Walker, J.	U.S. Army Natick Research Develop. & Eng. Ctr.
Weertman, J. R.	Northwestern University
Wiederhorn, S.	Ceramics Division
Yau, P.	University of California, Davis
Zhang, H.	University of Maryland
Zukoski, C. F.	University of Illinois

Neutron Diffraction Measurement of Residual Stress

- **New Alignment Techniques**

A stress measurement by means of neutron diffraction consists of a series of a scans of one or more Bragg peaks at some specific location within an orientation of the specimen. This calls for very accurate positioning of the specimen in the neutron beam, defined by apertures in the primary and diffracted beams. At NIST a new set of high-precision procedures has been developed and tested which employ the neutron beam itself as the geometrical reference against which the final alignment is made. Furthermore, these procedures have been developed within a framework in which the neutron measurements are performed at the scattering angle to be used for the specimen to be investigated (typically 90°). This ensures that no tilt of the sample table with counter rotation will affect beam positioning in the sample.

To find the center of rotation of the diffractometer a dial gauge is read out at three angular positions, 45° apart, on a hollow aluminum cylinder containing a powder close in composition to that of the specimen material. The diameter of the cylinder is comparable to the size of the beam apertures. A computer program has been written to solve the set of equations, with dial gauge readings as input, from which the orientation and position of the cylinder in the instrument axis system is obtained. The *x,y* table is then used to reposition the cylindrical sample such that its axis coincides with the spectrometer axis. With this procedure, the center of rotation is determined to $\leq$ 0.01 mm, the accuracy of the dial gauge.

With the Bragg reflection, wavelength, and scattering angle selected, the powder specimen is step-scanned perpendicularly through the incident beam, defined by the primary beam aperture, with no secondary beam aperture in place. The measured intensity profile is fit with a model which includes the size of the aperture, the size of the powder sample, its position and its absorption coefficient as parameters, and yields the primary beam slit position with respect to the spectrometer center. After centering the primary beam aperture, a scan perpendicular to the diffracted beam, and similar analysis, yields the position of the secondary beam aperture (Fig. 1). After these two alignment steps, the center of gravity of the sampling volume as defined by the aperture system coincides with the spectrometer axis to a precision as indicated in Figure 2.

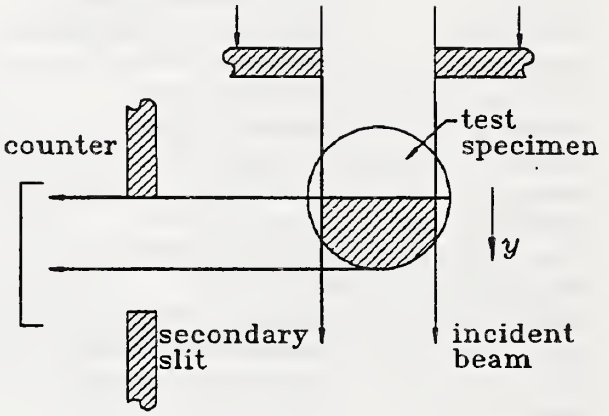

Figure 1. Experimental lay-out during the diffracted beam alignment.

To align the specimen of interest on the diffractometer, geometric positioning relative to the known center of the sampling volume is employed. A check of this positioning is made by measuring an "entering curve" of the sampling volume from lying fully outside the specimen to fully inside the specimen which creates an S-shaped intensity profile as a function of specimen position. The S-curve has been modeled based on the geometry of the sampling volume, beam attenuation, and the neutron beam widths. Path-length attenuation plays an especially important role in reflection geometry. A fitting procedure shows where the specimen surface is with respect to the sampling volume center, completing the alignment.

The new procedures and software described above allow the user to align instrument and specimen for residual stress measurements with quantifiable high precision not previously possible.

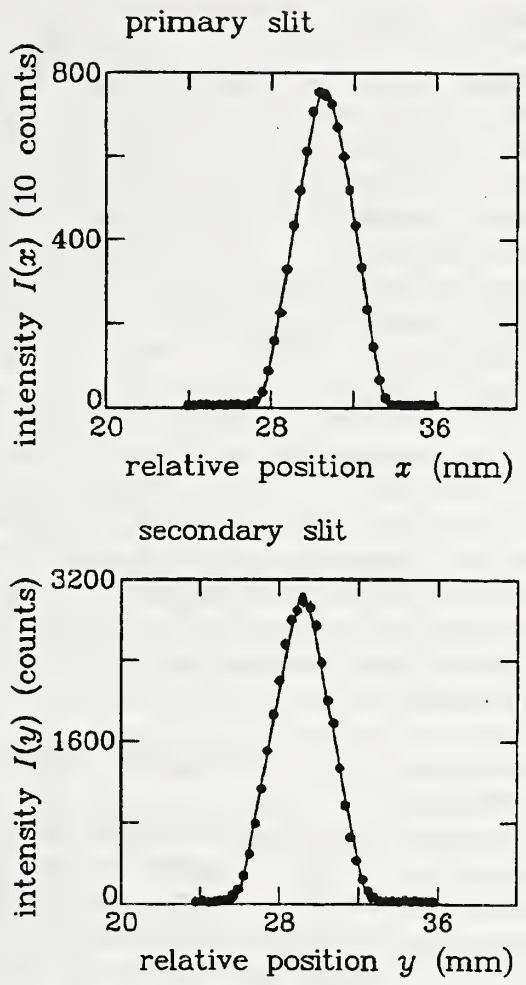

Figure 2. Fit results for the horizontal positioning of the primary (x_o = 30.53 ±0.01 mm) and the secondary (y_o = 29.17 ±0.02 mm) slits.

- **New Data Reduction Software**

A comprehensive neutron residual stress data reduction program called "STRESS" has been developed which takes stress measurement data files as raw input and produces a stress tensor as output.

The program is designed around the concept of an "environment" which includes the following information:

1. A nonambiguous list of input data such as filenames or lattice spacing values.
2. Which corrections should be applied and how data should be fitted.
3. Mechanical constraints such as plane stress or plane strain conditions.
4. Diffraction elastic constants.
5. Measurement details, eg., orientation of the sample, neutron path lengths etc.

The user can create and save an environment that represents a whole class of measurements. In this way one can just input new data files and than fit and solve without having to define the environment again. Other valuable tools which have been incorporated include:

1. Network transfer of data.
2. A sophisticated "search directory" which selects data files that satisfy certain conditions such as settings of particular motors.
3. Statistical handling of current data input according to various bootstrap approaches.
4. Graphic and/or text output.

The program has already proved to be very valuable in facilitating data reduction in a variety of neutron residual stress measurements.

- **A New Double-Axis Spectrometer for Single-Crystal Diffraction, Texture, and Residual Stress Measurement (DASSATS)**

DASSATS is a multipurpose neutron diffraction instrument that is projected to be installed in 1993 on BT-8. A number of features are noteworthy.

A basic US-1 (BNL-design: Universal Spectrometer 1) drum is being modified to allow take-off angles up to 120° ($2\theta_M$) for residual stress measurements. Texture and single-crystal diffraction will utilize a take-off angle of ~25°. An extensive primary and secondary beam handling system will be employed, that allows the choice of potential sampling volumes from 25 × 25 × 25 mm³ to 1 × 1 × 1 mm³, with a beam limiter to reduce the size of the reactor beam before it enters the monochromator drum. The primary system will slide in and out of the plug that is placed in the monochromator drum. The diffracted beam system will slide between the counter and the sample table. The sliding action is meant to allow for objects on the sample table to freely move in space, while going from one scan to another or even while performing some classes of scans. When required, the slides will accommodate a set of Soller slit blades.

An automated monochromator system with remote controlled rocking, translation, etc., and four different monochromators (on an elevator system) is planned. An elevator device to shift a pyrolytic graphite filter in and out of the beam will

be incorporated. Its purpose is to suppress the higher orders in the monochromatized beam for single crystal and texture measurements. Candidate position sensitive detector systems are currently being evaluated.

On completion it is expected that DASSATS will increase throughput for residual stress measurements by at least a factor of five.

- **d_0 and Residual Stress Determination in a Shell Base**

Stress measurements by means of neutron diffraction provide a powerful tool to establish the residual stress state at different locations inside a workpiece nondestructively. A critical parameter in all determinations of triaxial stress distributions is the unstressed d-spacing, d_0, upon which strain and stress depend directly. In this reporting period a new method for determination of d_0 has been developed. Its initial application has been made in stress determination in a shell base of considerable current interest to the Army.

The shell base is cylindrical in shape with gross diameter 160 mm, length 80 mm, and minimum sidewall thickness 5 mm; one end is open and the other has an end plate 10 mm thick. It is made of a hardened and tempered steel with heat treatment applied after machining. Residual stress measurements have been performed on the specimen at eight different positions: one at the midpoint of the sidewall; three at successive depths at R/2 of the base part; four along the intersection region of the cylindrical and base parts. The probe volume for all measurements was $\sim 3 \times 3 \times 3$ mm^3. The Fe-(110) reflection at a diffraction angle of 90° was scanned for between 14 and 30 different orientations at each of the eight positions. Initially, d_0 was taken to be the measured d-spacing in the axial direction in the sidewall position. However, the stresses obtained were in gross disagreement with x-ray measurements which utilized layer removal to probe subsurface stresses.

To assure that the d_0 used for the neutron measurements was reasonably correct, a new "random-walk" method was used to redetermine d_0. Three cylindrical samples (1.5 mm diam and 4 mm long) were cut by EDM from the shell base in the three regions of interest. All three samples were put on the spectrometer with which the stress measurements were made and scanned at 200 (random-walk) orientations. This approach simulates a powder of the material of interest—usually almost impossible to obtain—by using a portion of the end-item itself. The average of each group of 200 scans at each position yields an average value for the stress free lattice parameter d_0 at that position. The results from this determination show a maximum variation in d_0 of 0.00007 Å over the three positions (equivalent to 25 MPA in stress value), and confirm the initial choice of d_0.

The residual stresses obtained from the neutron measurements show that the region of the shell base where base joins sidewall contains very high tensile stresses ($\geq$ 500 MPa) for radial, tangential, and axial directions—suggesting a potential site for failure under firing conditions. More importantly, the neutron results show that for *complex geometries* considerable care must be used in extracting residual stresses when layer removal is employed.

- **Residual Stress Standard Reference Materials**

Design, fabrication, and characterization of shrink-fit, ring-plug specimens as standard reference samples for subsurface residual stress measurement techniques is a new project supported by NIST's Office of Standard Reference Materials and EPRI. Four samples are planned: one of 6061 aluminum, one of a special small-grain, (relatively) texture-free aluminum alloy, one of A533B steel (as used in reactor vessels), and one of titanium. Design, fabrication, and neutron diffraction confirmation of the analytical stress distribution has been completed for the 6061 aluminum sample.

It is interesting that although larger-than-desired grains are present—as seen in a simple rocking curve—residual stress values obtained with neutrons are in excellent agreement with the stresses calculated from the analytical model, known elastic modulus, and measured dimensions of the ring and plug.

On completion of fabrication and characterization of all four specimens, a round robin of measurements at other neutron facilities will be made, after which the specimens will be made available as SRMs for other stress measuring techniques such as ultrasonics.

- **Evolution of Residual Stresses Around Weldments**

The fracture safety of welds may be compromised by the residual stress state which is usually unknown, the microstructure which may contain crack nuclei, and compositional gradients, especially that of hydrogen. Neutron techniques can, in principle, provide critical measurements of the above three phenomena and thus guide the development of rational solutions to the associated welding problems. Utilizing the nondestructive character of neutron diffraction, the study of the evolution of residual stress patterns on an almost pass-by-pass basis was begun in this past year for a model system.

The test specimen—a bainite plate, 15 × 15 × 1.9 cm^3, with a v-notch weld channel—is shown in Figure 3. Measurements have been made in the indicated central plane around the notch before welding and after one weld pass, utilizing a 3 × 3 × 3 mm^3 sampling volume and the (110) reflection. At each of 21 sampling points in the base metal, one or two Bragg peak scans were made in the reflection geometry, and at least four scans were made in transmission. This provided sufficient information to extract three normal stress components and one shear stress component. A few points, not included in this discussion, were also examined in the weld metal.

An initial d_0 was taken to be the average d-spacing of all peak scans for all orientations of the 0-pass (unwelded) plate. This will be refined using the "random-walk" procedure described in the previous section after measurements are completed for all weld passes. Results for σ_{yy} (where y corresponds to the weld-channel direction) are shown in Figure 4 for the 0- and 1-weld-pass conditions. Because of the asymmetry of the weld metal in the channel the residual stress distribution is also asymmetric in the base metal. Certain features are noteworthy:

1. A clear, highly-tensile stress field is produced in the base metal in the region neighboring the channel. Although not confirmed by neutron measurement, a balancing compressive stress region must be present farther from the channel which then would be expected to relax to near zero stress far from the channel.

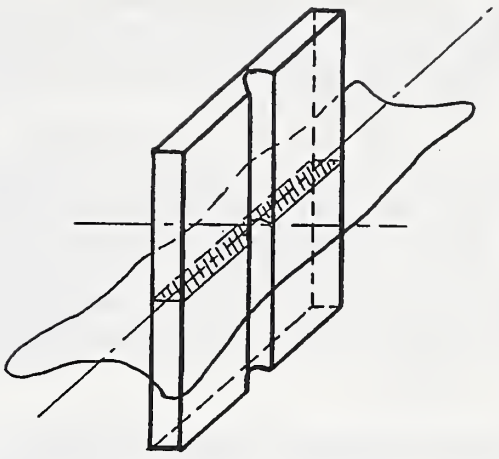

Figure 3. Bainite plate for weldment residual stress studies. The plate is 15.2 × 15.2 × 1.9 cm^3 with a rounded v-notch, 2.2 cm maximum width and 1.3 cm deep.

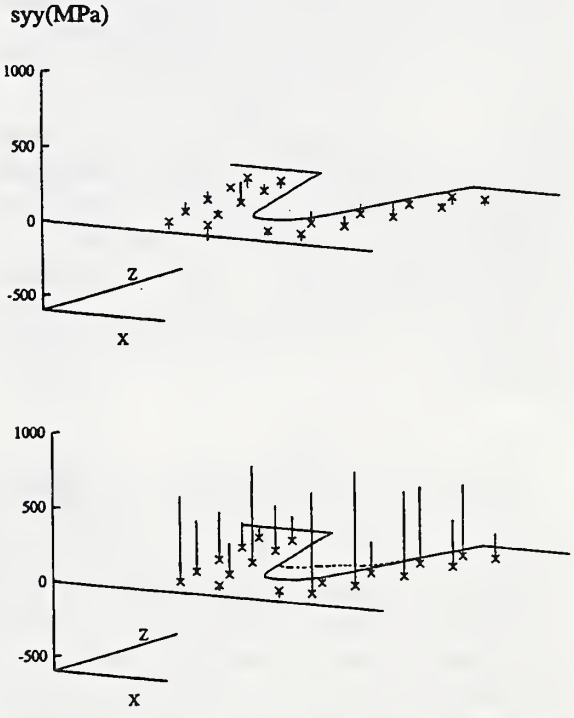

Figure 4. The σ_{yy} residual stresses inferred from neutron diffraction measurements for the unwelded (upper) and single-pass welded bainite plate. The measurements were made at points within the cross-hatched area shown in Figure 3. Points adjacent to the surfaces were 3 mm into the material; in the x direction, columns of points were 5 mm apart; in the z direction, rows were 3 mm apart.

2. The measured stresses—particularly below the tip of the v-notch—become more tensile well into the base metal rather than at the weld-metal/base-metal interface.

The results for the axial direction are qualitatively similar to the character of changes in stresses in the other directions in the bainite plate. The neutron results for the axial and transverse directions in the central plane of the plate are in good agreement with results obtained by x-ray diffraction for surface stresses around a bead weld on a steel plate.

Neutron Diffraction Measurement of Texture

- **Data Reduction Capabilities**

The Preferred Orientation Package—Los Alamos (popLA) is operational at the NBSR. It comprises a comprehensive set of utility programs which is independent of measurement hardware, handles sample symmetries, crystal symmetries down to orthorhombic, and provides excellent graphics. A most important feature of the software is the capability to infer three-dimensional crystallite orientation distributions (ODs) from a set of pole figures by either WIMV (Williams; Imhof; Matthies and Vinel) or harmonic-method analysis. It also facilitates the confirmation of ODs by comparison of measured pole figures with pole figures calculated from the inferred ODs.

- **Shaped-Charge Liners**

Since the mechanical properties of metals are dependent on material anisotropies, a program has been in-place at the NBSR to investigate possible correlations of mechanical properties with texture for a variety of metals and production processes. Recent work has focused on tantalum and molybdenum.

Tantalum is a heavy metal with a high melting point, high ductility, and moderate tensile properties. Recently this material has attracted considerable interest as a prime candidate material for armor penetrators. Current studies have characterized two texture specimens from a powder-sintered bar prepared at ARDEC: one from the periphery (Ta92-7A) and the other from the center (Ta92-7B). The predominant texture of the Ta92 sample was found to be the [111] fiber texture with the fiber axis oriented parallel to the normal direction (ND). There is also a small amount of [100] fiber texture in the periphery of the sample. The texture of the Ta92 sample was similar to that of the TaG1 and TaG2 specimens, reported previously and compared in Table 1. In view of the deep drawing application, the Ta92 sample has almost the ideal texture, i.e. the [111] fiber texture. However, the degree of texture (or the texture index) is still much lower than those of the TaQ2 samples, also shown in Table 1.

The textures of two different conically shaped Mo liners were studied by neutron diffraction measurements and three-dimensional ODF (orientation distribution function) analysis. One of them was fabricated from a vacuum arc-cast (C) ingot, and the other from a powder-metallurgically sintered (S) ingot. Both cones were fabricated by using the same forming processes, including the stress-relief annealing. Two 1 cm^2 plate-like specimens were cut from each liner for the texture study, one from a location 3 cm from the base of the cone, and the other at 8 cm from the base. The specimens were labeled MoC3, MoC8, MoS3 and MoS8 for cast and sintered, 3 and 8 cm positions, respectively. The pole figure data were measured over an entire orientation hemisphere with 1.25 Å neutrons.

The orientation distribution function (ODF) of the samples were obtained by the WIMV method, using triclinic sample symmetry. The agreement between the experimental and the recalculated pole figures was excellent for all the specimens. The major texture components obtained for the four samples are summarized in Table 2. The SOD (sample orientation distribution) of all the samples showed two major texture types: (111)[uvw] and (100)[uvw]. The Ψ-angular distributions of the (100)[uvw] for the cast and sintered liners are shown in Figure 5. Texture gradients with changing distance from the base are evident.

The (111)<uvw> type texture is considered to be the most critical component since (111) texture is known to improve ductility in BCC metals, which for a shaped charge would improve jet performance.

By this criterion the two liners examined are not optimized, and contain, for example, too much (100)<uvw> texture. Further work is planned in

which the effect on texture and performance will be evaluated for liners formed and annealed differently.

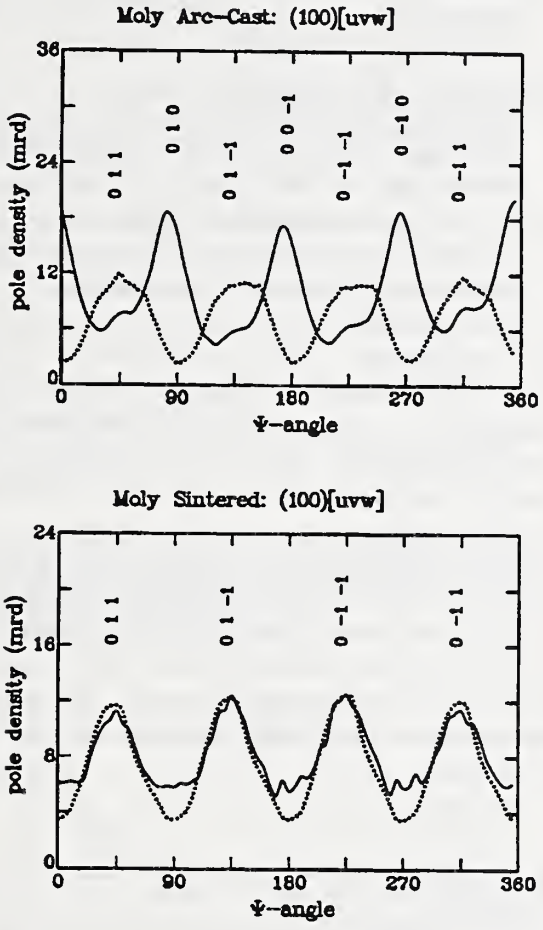

Figure 5. The (100) [uvw] orientation distributions of the two liners are presented as a function of the Ψ-angles, with the Arc-cast liner at the top and the powder-sintered at the bottom. The solid lines represent the distribution at the 3 cm height and the dotted lines are those at the 8 cm height of each liner, respectively. The Miller indices of the (100)[uvw] corresponding to each peak orientation are also shown.

Table 1(a) and 1(b). Summary of the major texture components found in the Ta liner samples including the Ta92 samples. The pole densities are given in multiples of the random distribution (mrd) units

a)

(hkl)[uvw]	TaG[1]	TaQ2-S1[2]	TaQ2-S2[3]
(111)[211]	-	160	140
(111)[211]	-	40	120
[111]fiber	12	20	15
(100)[011]	-	-	-
(100)[032]	-	3	3
[100]fiber	7	-	-

b)

(hkl)[uvw]	TaQ2-S4[4]	Ta92-7A	Ta92-7B
(111)[211]	100	-	-
(111)[211]	80	-	-
[111]fiber	20	23	29
(100)[011]	5	-	-
(100)[032]	-	-	-
[100]fiber	-	3	1

[1] From uniaxially compressed powder-metallurgy ingot; 90% RiA.
[2] Like TaG except from commercial VAC ingot; r = 0 position.
[3] Like TaQ2-S1; intermediate radial position.
[4] Like TaQ2-S1; peripheral radial position.

Table 2. Major texture components of the two conical molybdenum liners, arc-cast (MoC-type) and powder-sintered (MoS-type). The [111] and [100] fiber axes are oriented perpendicularly to the cone surface

	MoC3	MoC8	MoS3	MoS8
(111)<$\bar{1}$10>	9	19	-	10
(111)<$\underline{1}0\underline{1}$>	-	14	-	15
(111)<121>	-	-	3	-
[111]-fiber	6	-	7	-
(100)<010>	14	-	-	-
(100)<011>	2	12	6	8
[100]-fiber	5	2	6	4
(112)<$\bar{1}$10>	-	5	-	5

Neutron Autoradiography of Paintings

The Smithsonian-NIST autoradiography research program has concentrated in three areas: the continuing study of paintings by 19th century American artists, methodology development to improve the efficiency of the autoradiography process, and the renovation of a second laboratory.

Of the four paintings studied this past year, two were attributed to Albert P. Ryder and the other two were by Thomas W. Dewing. Significant reworks have been found in the two Ryder

paintings, the long suspected image of Arial and a shipwreck were revealed in the autoradiographs of the painting "Tempest" depicting the famous Shakespeare's play. The two Dewings were the first in looking into his works in landscape paintings, providing a good comparison to the ten portraits that have been studied.

In the area of methodology development, the feasibility study of using scintillation screens for improving the efficiency of registering the painting autoradiographic signatures on films, and for direct capturing of images on video/electronic means showed good potential. Film speed enhancement of more than 10 was confirmed with actual painting study and there was no discernable loss in image quality. The use of cold neutrons for painting activation was also investigated with very good results. Utilizing a scintillation screen for film speed enhancement and a glancing-angle geometry for activation by cold neutrons could give a painting adequate radioactivity for autoradiography study in an amount of time comparable to that which would be required at a thermal column. A cold neutron guide has much lower level of undesirable gamma rays and high energy neutrons and offers further advantages in greater activation sensitivity and easier accessibility.

In summary, methodology developments provide opportunities:

1. To reduce the total exposure to the paintings under study while maintaining autoradiography quality.
2. To reduce painting activation requirements through more efficient use of neutrons and improved radioactivity detection/imaging systems, thus making possible the autoradiography studies of painting at many other reactor facilities. Traditionally, a minimum physical size and neutron intensity are required before a successful activation can be carried out for autoradiography study of paintings. These requirements are considerably relaxed by:
   a) Using neutron guides where instead of placing a painting perpendicular to the incoming neutrons, the painting is placed almost parallel to the beam, significantly increasing the exposed area.
   b) Improved efficiency of the imaging system requiring lower radioactivity in the painting.
3. To improve the painting pigment identification process by increasing the time resolution in the autoradiography exposure sequence—possible because of the improved efficiency of the activation and imaging procedures.
4. To incorporate computer image processing enhancement in the filmless approach for dissemination of autoradiography information.
5. To make autoradiography information more accessible for distribution and comparison with other painting analysis techniques.

The remodification of a second laboratory has been completed. The environment is tightly controlled to ensure the safety of paintings. This additional space and the aforementioned development work will increase throughput and make the facility at NIST more available to outside users.

The Conservation Analytical Laboratory's facility for neutron induced autoradiography at the National Institute of Standards and Technology is under the direction of Jacqueline S. Olin, Assistant Director for Archaeometric Research, Conservation Analytical Laboratory, Smithsonian.

Experiments

Evaluation of New Neutron Area-Detectors for NDE Applications

P. C. Brand, Y. T. Cheng, and H. J. Prask.

Design and Construction of a New Neutron Diffractometer for Single-Crystal Diffraction, Texture Determination, and Residual Stress Measurement

P. C. Brand, C. S. Choi, J. W. Lynn, L. P. Robeson, E. Prince, and H. J. Prask.

'STRESS': A Comprehensive Code for Data Reduction in Neutron Diffraction Residual Stress Measurements

P. C. Brand.

New Methods for Aperture and Specimen Alignment for Neutron Diffraction Residual Stress Studies

P. C. Brand and H. J. Prask.

A New Approach to the Determination of d_0 for Neutron Diffraction Residual Stress Measurements
P. C. Brand and H. J. Prask.

Subsurface Residual Stresses in Al_2O_3/Al_2TiO_5 Ceramic Composites
A. J. Allen, P. C. Brand, and H. J. Prask.

Neutron Diffraction Characterization of 7000-Series Aluminum Alloy Plate for Aircraft Applications
H. J. Prask, P. C. Brand, and D. Walker.

Evolution of Residual Stresses Around a V-notch Multipass Weld in a Steel Plate
J. Blackburn, P. C. Brand, R. J. Fields, and H. J. Prask.

Determination of Subsurface Residual Stresses in a 150 mm Steel Shell Base
P. C. Brand, H. J. Prask, W. Sharpe, and C. S. Choi.

The Effect of Beam-Entering and -Exiting Surface Orientations on *d*-Spacing Determinations in Neutron Residual Stress Measurements
P. C. Brand and H. J. Prask.

Fabrication and Characterization of a 6061 Aluminum-Alloy Ring/Plug Standard Reference Specimen for Residual Stress Measurement Techniques
H. J. Prask, P. C. Brand, and T. M. Proctor.

The Effect of Whisker Size and Concentration on Residual Microstresses in SiC-Whisker-Reinforced Alumina
E. Fuller, A. Krawitz, and H. J. Prask.

Textures of Tantalum Metal Sheets by Neutron Diffraction
C. S. Choi, J. Orosz, and H. J. Prask.

Texture Study of Powder-metallurgical Ta Liner Samples
C. S. Choi and J. Orosz.

Texture Study of Molybdenum Shaped-Charge Liners by Neutron Diffraction
C. S. Choi, J. Orosz, and H. J. Prask.

The Effect of Texture and Sample Geometry on the r-Value of Heavy Gauge Tantalum Plate
C. Michaluk, C. S. Choi, and J. Bingert.

Examination of the Paintings of Thomas Wilmer Dewing
S. Hobbs, R. Cunningham, and Y.-T. Cheng.
[Paintings on loan from the National Museum of American Art].

Examination and Authentication of the Paintings of Albert Pinkham Ryder*
I. Alexander, R. Cunningham, Y.-T. Cheng, E. Broun, B. Heller, M. Quick.
*[Source of studied paintings—National Museum of American Art, Detroit Institute of Art, and Los Angeles County Museum of Art]

The Use of Scintillation Screens and Cold Neutron Guide in Autoradiography of Paintings
Y.-T. Cheng, W. Leuther, and C. Fischer.

Filmless Autoradiography and Image Processing
Y.-T. Cheng, W. Leuther, C. Fischer, I. Alexander, A. Calmes, and M. Ormsby.

Participants:

Alexander, I.	Smithsonian Institution
Allen, A. J.	University of Maryland
Bingert, J.	Los Alamos National Laboratory
Blackburn, J.	U.S. Navy David Taylor Research Center
Brand, P. C.	University of Maryland
Broun, E.	National Museum of Art
Calmes, A.	National Archives
Cheng, Y. T.	Smithsonian Institution
Choi, C. S.	Army Armament RD&E Ctr.
Cunningham, R.	Smithsonian Institution
Fields, R. J.	Metallurgy Division
Fischer, C. O.	Hahn-Meitner Institut, Germany
Fuller, E.	Ceramics Division
Heller, B.	Detroit Institute of Art
Hobbs, S.	Smithsonian Institution
Krawitz, A.	University of Missouri
Leuther, W.	Hahn-Meitner Institut, Germany
Lynn, J. W.	University of Maryland and Reactor Radiation Division
Michaluk, C.	Cabot Corp., PA
Ormsby, M.	National Archives
Orosz, J.	Army Armament RD&E Ctr.
Prask, H. J.	Reactor Radiation Division
Prince, E.	Reactor Radiation Division
Proctor, T. M.	T-Prosci Co.
Quick, M.	LA County Museum of Art
Robeson, L. P.	Reactor Radiation Division
Sharpe, W.	Army Armament RD&E Ctr.
Walker, D.	Boeing Corp.

Nuclear Methods Group

The development and application of nuclear analytical techniques for elemental compositional analysis of greater accuracy, higher sensitivity and better selectivity are the goals of the Nuclear Methods Group. A high level of competence has been developed in both instrumental and radiochemical neutron activation analysis (INAA and RNAA). In addition, the group has the capability of using neutron beams as analytical probes with both prompt gamma activation analysis (PGAA) and neutron depth profiling (NDP). PGAA measures the total amount of an analyte present throughout a sample by the analysis of the prompt gamma-rays emitted during neutron capture. NDP, on the other hand, determines concentrations of several important elements (isotopes) as a function of depth within the first few micrometers of a surface by energy analysis of the prompt charged-particles emitted during neutron bombardment. These techniques (INAA, RNAA, PGAA and NDP) provide a powerful combination of complementary tools to address a wide variety of analytical problems of great importance in science and technology.

During the past few years, a large part of the Group's efforts has been directed at the exploitation of the analytical applications of cold neutrons. These efforts are needed to take full advantage of the guided cold-neutron beams now available at the new Cold Neutron Research Facility (CNRF). The Group's involvement has been to design and construct state-of-the-art instruments for both PGAA and NDP using cold neutrons.

- **SRM Analysis and Certification**

The use of a variety of nuclear methods has continued to contribute to the Standard Reference Material (SRM) certification effort; this year's efforts include measurements performed on a number of SRMs including: Fly Ash, Automobile Catalysts, Cokes, Tomato Leaves, Spinach Leaves, and three Soils. Group members are serving as Technical Champions for several of these new SRMs, and as such are responsible for scientific decisions made throughout the production and certification processes of these materials. This year marked the first use of the NDP for certifying a NIST SRM. The abundance of ^{10}B was determined in a set of silicon wafers which subsequently will be sectioned and distributed for calibrating analytical instruments such as secondary ion mass spectrometers (SIMS) or Fourier transform infrared spectrometers (FTIR).

Another highlight of the Group's SRM work has been the application of three nuclear analytical techniques (INAA, RNAA, and PGAA) to the determination of 30 different elements in the Tomato Leaves, SRM 1573a. These techniques provided data on 19 elements by INAA, 7 elements by RNAA, and 10 elements by PGAA, with some overlap between techniques. Of the 36 elemental determinations made by these techniques, more than 40% had total overall analytical uncertainties of 2.5% (relative) or less at the 95% confidence level, and almost three-quarters had uncertainties of 5% or less. In addition, the INAA analyses were made on samples sizes of 150 mg, providing homogeneity information important for certification.

- **Neutron Activation Analysis Method Development**

Although NAA has been in use for many years, new developments continue to provided improvements in detection sensitivities, elemental specificity, precision, and overall accuracy. Particularly in the last few years, the NAA technique has become one of the primary analytical techniques for the certification of elemental concentrations in biological SRMs. One important reason is that NAA has unique quality assurance (QA) characteristics which provide the capability for accurate analyses and which often allow the analytical values obtained to be internally evaluated and cross checked. In addition, the capability of INAA for non-destructive analyses (eliminating dissolution errors) and for homogeneity determinations of ng/g level concentrations at samples sizes as low as 100 mg in biological materials has made this technique an important contributor to trace element analyses at NIST. Further, the relative matrix independence of NAA has resulted in applications to many other materials as well, including high temperature

superconductors, soils and fly ash samples, rocks and ores, etc.

Optimizing the gamma-ray counting conditions for the various forms of NAA can generally improve precision or increase sample throughput, or both. This is especially important when counting the very small amount of radioactivity from the analysis of ultratrace quantities of impurities, for example in semiconductor silicon or (after radiochemistry) noble metals in human tissue. Sensitivity can be gained by using high-efficiency, low-background detectors; a subsidiary benefit is that less radioactive material needs to be generated, handled, and discarded. The sources of background in gamma-ray detectors have been reexamined at NIST and elsewhere in recent years, with improved understanding. It is now clear that with care in the selection of the materials from which the detector and the shield are constructed, the only important source of gamma-ray background is the interaction of cosmic ray particles with the shield and the detector itself. Experiments are underway to reduce this component by active, anti-cosmic ray shielding.

- **Specimen Bank Research**

The Biomonitoring Specimen Bank Research Project has continued to support other agencies' monitoring programs. These programs include the EPA Human Liver Project (HLP), the NOAA National Status and Trends (NS&T) program, the NCI Micronutrient program, the IAEA/NIST/FDA/USDA Total Diet Study, the NOAA Alaska Marine Mammal Tissue Archival Project (AMMTAP), and the National Marine Mammal Tissue Bank (NMMTB). Research has centered on specimen banking protocols and improved analytical methodology. The Group uses instrumental and radiochemical neutron activation analysis to determine element compositions of tissues included in the National Biomonitoring Specimen Bank (NBSB). In addition, participation in intercalibration exercises with the project participants and the development of QA materials for various marine analyses has helped to enhance the quality of the analytical results used in the assessment of the environmental health of the nation. During the past year samples were collected, processed, and archived in the NBSB for the HLP, NMMTB and AMMTAP. Some samples were analyzed and concentrations (or upper limit values) for approximately 35 elements were determined using INAA for ten human livers and for 18 marine mammal livers. For the human liver tissues RNAA for Sn was performed.

One part of the NOAA's continuing NMMTB program is a QA in chemical measurements program. To assist in this program, we have prepared a fresh-frozen QA material, pilot whale (Globicephela melaena) liver homogenate, to determine whether this type of material would be suitable for preparation as a fresh frozen SRM. Instrumental neutron activation analysis was performed to determine the trace element content and to assess the homogeneity of the material. The QA material appears to be homogeneous with respect to most elements measured with the exceptions of Al and Cr. This homogenate is currently being used for an international inter-laboratory comparison.

- **Dietary Studies**

A world-wide research program was initiated by the International Atomic Energy Agency (IAEA) in 1985 to obtain reliable data on the average daily dietary intake of nutritionally important elements in various developed and developing countries. The United States is represented in this project by three agencies with multidisciplinary expertise: FDA (sampling strategy), NIST/Nuclear Methods Group (analytical expertise), and the USDA (planning dietary studies). All three agencies will provide expertise for a meaningful interpretation of data. The program will be completed by the end of 1992, by which time approximately 450 samples will have been analyzed. This international diet study is unique in that all samples have been collected and analyzed by identical, or strictly comparable, procedures in each country.

For this study, typical total diets have been collected in 15 countries and analyzed for more than 20 elements. After sample collection, the diets were prepared and freeze-dried locally and then transferred to the IAEA laboratory at Seibersdorf (Austria) for homogenization, division into smaller aliquots, and distribution to a network of experienced analytical laboratories which use a wide variety of analytical techniques. The analytes of interest included practically all the minor and trace elements considered to be essential or of

interest as possible food contaminants, viz. Al, As, Ca, Cd, Cl, Cr, Cu, F, Fe, Hg, I, K, Mg, Mn, Mo, Na, Ni, P, Pb, Se, Sn, V and Zn. The Nuclear Methods Group used INAA and RNAA to determine Cr, Fe, Hg, Mo, Se, Zn in all the samples, and Cd in selected groups of samples. A preliminary evaluation of the results yielded a number of interesting observations. For example, the variability in intakes of essential elements among countries is relatively small (factor of 2 or less between highest and lowest) for Cr, Cu, K, Mg and Zn, and relatively large (around factor of 4 or more) for I, Mn and Se. Three countries (Japan, Norway and Spain) appear to exceed the Provisional Tolerance Intakes (PTIs) for As. However, this may be due to a high consumption of organically-bound As in fish where the toxic effect is minimal and the PTI does not apply. Apparent high intake of Hg in the Iranian and Turkish diets may indicate a cause for concern and an extended study (followed by remedial measures) may be warranted.

The experience gained during this project has allowed the development of a NIST Total Diet Standard Reference Material (SRM 1548). This material has been certified for a number of dietary components such as proximates, major and minor inorganic nutrients, and toxic trace elements, thus making this SRM a multipurpose material. It has been widely distributed among food analysis laboratories world-wide, and has proven extremely effective in technology transfer and in improving analytical quality assurance.

- **Neutron Activation—Mass Spectrometry**

The collaboration with Brian Clarke and colleagues at McMaster University on neutron activation-mass spectrometry (NA-MS) has continued to provide valuable information on ultratrace levels of boron and lithium. NA-MS couples nuclear activation to generate ^{4}He and ^{3}He (from ^{10}B and ^{6}Li, respectively) with the high precision of mass spectrometry. Under ideal conditions the detection limits are in the ng/g for boron and in the pg/g range for lithium. It is thus extremely well suited to an investigation of the natural concentration levels of boron and lithium in biomaterials; both elements present difficult analytical problems for other methods. This is especially true for the determination of sub-ppb levels of lithium where other analytical techniques face serious analytical difficulties, mainly due to contamination control and, in some cases, to insufficiently low detection limits.

Over the past year we have determined B and Li concentrations in a wide variety of biological materials, including well over one hundred individual foods items, as well as several different protein components of blood. Blood Li levels may be both genetically and environmentally regulated. An environmental contribution is deduced from the relationship between the blood Li level and the amount of the element ingested. No such information is available for B, another element present in ultra trace amounts in human blood. Unusually high levels of Li and B in the waters of northern Chile offer an opportunity to study the genetic and environmental regulation of these elements in the blood of healthy subjects.

- **Superconductivity Research**

The Group has taken an active role in the NIST program on high-temperature superconductivity research. In cooperation with materials scientists at NIST and elsewhere, we are measuring impurities in superconductor starting materials and final products, as well as determining the stoichiometry of the major constituents. The needs of the superconductivity program have stimulated the development of methods for accurate, rapid analysis of these materials by both NAA and PGAA. In particular, an effort is underway to establish an accurate monitor-activation analysis technique at NIST. Conventional NAA requires the irradiation and counting of a standard for each element to be determined in a sample. Preparing numerous standard solutions requires much labor, and the accurate quantitation of unanticipated activities in the gamma spectrum is not possible. An elegant solution has been pioneered in Europe, which uses a dimensionless compound nuclear constant called k_0, which can be measured much more accurately than the cross sections and other constants that comprise it. We have begun to apply this approach to cold-neutron PGAA, which is especially subject to systematic errors from neutron scattering effects, and have found that the k_0 approach for determining element ratios offers all the advantages of internal standards in other

methods. We intend to apply the k_0 formalism to delayed NAA as well.

- **Neutron Depth Profiling**

The NDP facility has been designed to be adaptable to many different types of experiments. The facility allows remote scanning of 15 x 15 cm samples and rotation of both sample and detector angles relative to the beam. Sample movements are controlled by a desk top computer. Beginning its second year of operation, the instrument is continuing to evolve.

Developments in the processing of NDP data have made it possible to determine the weight percent of elements such as boron in dielectric films without knowledge of the film density or detailed knowledge of the atomic composition. With this technique accuracies of 1% total error or better can be achieved. In addition, through a Director's Reserve grant, Kevin Coakley of the Statistical Engineering Computing Division has been able to work with us to devise optimum sample-detector-beam geometries.

Among the novel and challenging materials analyzed by NDP this year has been diamond films. The NDP technique has been demonstrated to be a suitable technique for measuring boron concentrations as low as 10 ppm and profiles in chemical vapor deposited (CVD) diamond films. A number of diamond samples were measured to illustrate the sensitivity of the neutron depth profiling technique to changes in boron incorporation during chemical vapor deposition of the diamond film. In each instance, the B_2H_6 flow rate had been changed either deliberately or by electronic malfunction during deposition. However, when the flow conditions and diamond growth rate were held constant the boron incorporation was very uniform. Through the use of NDP, the effects of different diamond growing and doping conditions were quantified and correlated with electrical and physical properties.

- **Prompt-Gamma Activation Analysis**

A permanent, full-time instrument for cold-neutron prompt-gamma activation analysis (PGAA) has been constructed as part of the NIST Cold Neutron Research Facility. This new instrument allows accurate nondestructive measurements of a number of elements, including H, B, C, N, S, and Cd. Hydrogen has been particularly emphasized. This capability will be of value in numerous applications where quantitative, nondestructive analysis of small quantities of hydrogen in materials is necessary. Detection limits, constrained by background, of a few tens of micrograms have already been achieved. Further background reduction by one to two orders of magnitude is probable in the near future. Sensitivities (counting rate per gram of analyte) for a number of elements have been compared using the new cold-neutron instrument to those obtained with the thermal-neutron Maryland-NIST instrument. Sensitivities for most elements are a factor of four better with the cold-neutron apparatus, as a result of its compact sample-detector geometry. Installation of a Compton suppression system will greatly lower background radiation and substantially improve measurements.

The PGAA system has been used for the analysis of hydrogen in a number of samples originating from NIST programs and from academic and industrial laboratories with whom NIST collaborates. For example, hydrogen was measured in 1-g specimens of hydrothermally grown single-crystal quartz, with fused quartz used as a blank. The concentrations determined were found to be less than 10 μg/g. In another application, hydrogen was sought for in a 1.0-μm phosphosilicate glass film deposited on a quarter of a 15-cm silicon wafer; the effective sample mass was 1 mg. The net hydrogen content in this sample was <3 $\mu g/cm^2$. Hydrogen was also measured in NIST SRM 354 (Titanium). In a 2.6-hour irradiation of a 234-mg sample we measured 235 ± 30 μg/g; the certified concentration is 215 ± 6. In addition we have analyzed numerous specimens of pure and substituted C_{60} fullerenes ("buckyballs") have been analyzed for hydrogen (and simultaneously for other elements such as C, S, K, and Rb) in support of neutron scattering and chemical experiments.

- **Focused Neutrons**

A long-range program to explore and develop the analytical applications of focused beams of cold neutrons has been initiated within the Group. The ultimate goal of this research is to produce beams of neutrons which have intensities several orders of magnitude greater than previously available. Such

beams will greatly enhance the capabilities of both PGAA and NDP, and may ultimately lead to a neutron probe for microanalysis. The neutron microguide appears to be one promising approach to achieve analytically useful focused neutrons. As a first approach, a device will be developed and tested using a stack of ultrathin, nickel-coated single-crystal silicon wafers as focusing elements. The silicon wafers act as the transmission medium for the neutrons, which reflect from the 1000 Å nickel surface coatings. The superposition of the individual outputs becomes the focal point. The wafers have been characterized with X-ray reflectivity measurements at a synchrotron source. Cold-neutron measurements using a polychromatic beam at CNRF have shown that these wafers can deflect the neutron trajectories successfully. More precise measurements have been performed using monochromatic neutron beams at BT-6 (NIST) and at ILL, Grenoble.

Another focusing concept involves the use of capillary optics, an idea which has proven successful with X-rays, and which allows for the possibility of two dimensional focusing. In collaboration with scientists from the USSR and SUNY-Albany, we have begun testing this concept with cold neutrons. Our work in this area is described elsewhere in this report.

- **Detector Imaging Research**

The Nuclear Methods Group, working with the Surface and Microanalysis Science Division has developed a video radiation detector (VRD) based upon a charge injection device (CID) camera and image processing system. This system allows live-time high resolution imaging of neutron and charged particle fields. The charge injection device (CID) is an imaging sensor used to detect visible, x-ray and UV photons; however, when an energetic charged particle passes through the capacitance volume of a pixel, it generates electron-hole pairs in the silicon matrix. Based on commercially available image processing hardware and software, the system is easy to use, inexpensive, and data interpretation is simple. Results are five-dimensional, providing information on x-y position, counts received, energy deposited per count, and time. The VRD system is essentially 100% efficient for the detection of alpha particles above 4 MeV energy and emission rates as small as 10^{-5} Bq have been localized. The system allows discrimination between triton, alpha, and fission particles. Spatial resolution of less than 12 μm is achieved by interpolating between pixels. This has been confirmed by correlation of sample position information with transmission electron microscopy data.

We have used the VRD for characterizing neutron focusing components for neutron intensity, determination of the focal plane, and analyzing individual elements in the focusing device. Neutron field maps produced by the VRD have been indispensable for the project. The location and size of the focus can be determined much more quickly with the VRD than by using a series of photographic films. It has also been used for detecting spontaneous emission of naturally radioactive materials from minerals or contaminants in the analysis of environmental samples.

- **Group Interactions**

The strong interaction with industrial scientists using NDP, PGAA, and NAA has continued during the year with a growing number of guest workers, research associates, and joint publications. For example, working this year with researchers from Texas Instruments, we have used NDP to study various aspects of quality control using CVD (chemical vapor deposition) reactors. These measurements will be useful in optimizing process yield and reliability. The Nuclear Methods Group is also collaborating with scientists from the NIST Physics Laboratory in a new measurement of the neutron lifetime. Our work in this area is described elsewhere in this report.

Food and Drug Administration

(D. L. Anderson, W. C. Cunningham, S. G. Caper and T. R. Lindstrom)

The Food and Drug Administration (FDA) maintains a neutron activation analysis facility in the reactor building of NIST. This facility is directed by FDA's Center for Food Safety and Applied Nutrition and provides agency-wide analytical support for special investigations and applications research. NAA complements other analytical techniques used at FDA and serves as a reference technique and confirmatory quality

assurance (QA) tool. Instrumental, neutron-capture prompt-gamma, and radiochemical NAA procedures (INAA, PGAA, and RNAA, respectively) continue as the prime nuclear analytical approaches. A radioisotope-induced X-ray emission (RIXE) spectrometer provides support for FDA programs which monitor toxic elements in housewares (especially Pb), and the low-level gamma-ray counting facility developed by the Nuclear Methods Group of the NIST Inorganic Analytical Research Division is used to determine the radionuclide content in various matrices. This combination of analytical techniques enables diverse multielement and radiological information to be obtained for foods and related materials.

The continued development and production of biological standard reference materials (SRMs) is vital to FDA's analytical programs. FDA's PGAA findings for B, N, and Cl were used (along with inductively-coupled plasma-isotope dilution mass spectroscopy [ICP-IDMS], Kjeldahl, and INAA, respectively, performed by NIST personnel) to certify the concentrations of these elements in SRM 1515 (Apple Leaves) and SRM 1547 (Peach Leaves). PGAA also supplied S, Sm, and Gd concentrations which aided in setting information values for these elements, as well as concentrations for H, C, K, and Ca. Since PGAA was the only source for H and C concentrations, no certified or information values were issued. PGAA findings for K and Ca were in excellent agreement with the concentrations certified by NIST personnel using INAA and IDMS. This year, analytical information for the same elements was provided for the Tomato Leaves renewal reference material (SRM 1573a). Portions of a mixed-diet slurry were also analyzed by PGAA. The slurry is a candidate reference material resulting from a NIST/U.S. Department of Agriculture (USDA)/ FDA project to provide a wet composite SRM. FDA will also use this technique to contribute analytical information for the Spinach renewal reference material (SRM 1570a).

PGAA counting and standardization methods using very high energy gamma-rays (10.3-10.8 MeV) were developed to improve nitrogen determination capability. Total relative uncertainty using low energy gamma-rays for materials containing 3% N (w/w) (*e.g.*, SRM 1573a) was ~7-10%. This has been improved to about 3%. The quantitation limit (corresponding to 10% analytical uncertainty) for the new method is ~1% N (w/w).

To meet a need in the analytical community for infant formula RMs, a multi-agency effort began last year to develop a large batch of powdered infant formula as an RM (to become SRM 1846). FDA, the USDA, and NIST are combining their efforts to make this material available with both element concentration and organic nutrient concentration information. FDA completed INAA and PGAA analyses of a preliminary sample of the powdered infant formula. These analyses indicated very good homogeneity characteristics. Efforts on this SRM will continue next year.

General analytical support was provided for many programs and projects. For example, the purity of bulk sodium fluoride was verified by NAA before the material was used in a Developmental Toxicological Study of Reproductive and Developmental Hazard Effects of Food Additives. This study is under FDA's Risk Assessment and Research Policy Development Program. In another instance a three-layer section of a flexographically-printed, dual-ovenable tray (used in heat-in-package meals) was analyzed by RIXE, INAA, and PGAA. This was a routine investigation to obtain basic composition information for the Division of Food Chemistry and Technology.

Presentations dealing with FDA's INAA and PGAA work on foods were given at the Eighth International Conference, Modern Trends in Activation Analysis (Vienna, Austria) and at the American Nuclear Society's 1992 Annual Meeting (Boston, MA). The content of these presentations included multielement analyses of foods and related materials by PGAA and other NAA techniques and background enhancement effects in PGAA.

PGAA analyses of 234 foods from Total Diet Study Collection K11 (November, 1990 - January, 1991) were completed. While the emphasis of the project was B determination, H, Na, S, Cl and K concentrations were also determined in most of the foods, and Ca and Cd concentrations were determined in some of the foods. The findings will be used to calculate daily intakes for B, S and Cl for several age groups. Na and K intakes have been calculated and agree (for all age groups) with

the findings of FDA's Kansas City District Office, to within 5% for Na and 3% for K.

Approximately 100 ceramic test tiles with a wide range of glaze compositions were analyzed by radioisotope (^{109}Cd) induced X-ray fluorescence spectrometry (^{109}Cd XRFS). The technique can easily and quickly (~1 minute) show whether a Pb glaze is present. Analysis is continuing on additional test tiles with underglaze coatings, with glazes over underglazes, and Pb leaching in conjunction with both pre- and post-leaching XRFS. These experiments will determine leaching effects on glaze composition and X-ray attenuation through glazes. Analysis of 46 ceramic coffee mugs (from 18 countries) by ^{109}Cd XRFS showed that 13 mugs had Pb-based glazes, which were subsequently subjected to leaching studies under FDA's Toxic Elements in Housewares Project. A summary of FDA's work with ^{109}Cd XRFS was presented at the 106th AOAC International Annual Meeting, Cincinnati, OH.

Smithsonian Institution

The Conservation Analytical Laboratory of the Smithsonian Institution maintains an INAA research facility within the Nuclear Methods Group at NIST. The facility, which consists of two automated sample changers with gamma detectors and associated electronics, provides high precision, multi-element chemical data for use in a wide range of Smithsonian and Nuclear Methods Group research projects. In the past year, 2000 archaeological samples have been analyzed for up to 30 elements in support of the 10 research projects involving 3 Smithsonian staff members, 2 Smithsonian Fellows, a Nuclear Methods Group Guest Worker and a large number of active research collaborators, both national and international.

One highlight of this year's research involves an ongoing analytical study of the geological obsidian sources and archaeological artifacts from northern Caucasus and Transcaucasia. Currently, 694 obsidian samples have been submitted to neutron activation analysis, 118 of these (17%) being from geological obsidian sources in the Caucasus and the remaining 576 coming from 53 different archaeological sites throughout the area. At least 19 major Caucasian sources of obsidian samples have been chemically distinguished from each other. In all 26 elements were routinely quantified in the obsidian analysis.

Five hundred and two of the 576 (c. 87%) archaeological artifacts analyzed could be chemically assigned to one or another of the identified Caucasian obsidian sources. Four Caucasian artifacts matched the composition of source samples from near the city of Dogabayzit in NE Turkey. Of the remaining 67 analyzed artifacts from Caucasia, 61 could be assigned to one of six chemical defined composition groups containing at least three samples each. These six unknown source groups have been designated: Transcaucasian or TC 2 (n=23); TC 3 (n=18); TC 4 (n=5); TC 5 (n=9); TC 6 (n=4) and TC 7 (n=3). The five remaining artifacts (c. 0.7% of the total number of artifacts analyzed) did not chemically group with any other artifact samples and therefore, were not assigned a group designation.

University of Maryland

With the death of our colleague, Professor Glen E. Gordon early this year, it is, perhaps, appropriate to reflect on the long standing research relationship between the NIST NBSR reactor group and the University of Maryland (at College Park (UMCP)). The University of Maryland aerosol chemistry group has used the NBSR reactor for instrumental neutron activation analysis to characterize atmospheric aerosol particles and gases for more than 20 years. Detailed and accurate multielement analyses are routinely achieved, nondestructively, for up to 40 elements in aerosol particulate samples collected for periods of several hours to a few days on various types of air filters. Some of the elements measured, e.g., As, Se, and Hg, are highly toxic and, therefore, of epidemiological interest. But, more importantly, information on elemental constituents remains a powerful, fundamental tool with which atmospheric sources and processes may be elucidated.

Our group, under Professor Glen Gordon and former UMCP Professor William Zoller, pioneered the development of source-receptor modeling in urban areas and later applied the techniques to elucidate the intricacies of Global aerosol particle transport. The work at UMCP was instrumental in

the acceptance of the receptor-based concept for source attribution by the U.S. Environmental Protection Agency and EPA's subsequent development of a major Laboratory for Source Apportionment which has well served numerous EPA programs of national significance. Our most recent receptor modeling work extends measurement and statistical techniques to very small (i.e., as small as 100 μg, or smaller) samples of submicrometer aerosol particles size-fractionated with low-pressure-drop micro-orifice impactors. We have nearly completed a large 3-d data set composed of the analyses of as many as 25 elements determined by INAA in more than 70 sets of 7-way fractionated samples collected in industrial and urban airsheds. We are applying various multivariate statistical techniques on the data to determine individual sources of airborne particles and to elucidate mechanisms and time-scales for atmospheric aging processes.

Other current projects are summarized below.

- **INAA Procedures**

Analytical sensitivities have been determined by irradiating >25 prepared multielement standards made from 20 NIST-certified standard solutions, except for Al, Br, Mn, and V, which were made from high-purity laboratory reagents, and S and Ti, which were made by irradiating accurately-weighed aliquots of their elemental forms. Accuracy has been checked by analyzing >30 aliquots of NIST SRM 1633A (Eastern Coal).

Net relative uncertainties ($S_{rel,\ net}$) in INAA depend mainly on counting statistics, imprecision in positioning the samples and flux monitors (geometry errors), coincidence errors, spectral background, and the sometimes substantial concentrations of the various elements in the blank filter substrates. In our work, the maximum relative uncertainty associated with geometry, coincidence, and detector intercalibrations and standard preparations are 2.4, 1.5, and 5%, respectively. Uncertainties in counting statistics typically range from <2% (Al) to 20% (S). Filter blank corrections typically contribute less than 10% for from 96% to 100% of the analyses for Al, As, Fe, Mn, S, Se, Zn, V, and Br; but are often significant for Cr and Cu. For these elements, $S_{rel,\ net}$ is typically <20%.

- **Chesapeake Bay Atmospheric Deposition Study**

Atmospheric deposition by wet and dry processes is known to be an important source of several anthropogenic, particulate-bound metals in critically important waters such as the north Atlantic Ocean, the coastal, mid-Atlantic waters, and the Great Lakes. The Chesapeake Bay, perhaps the world's most productive bay, is especially subject to deposition of anthropogenic air pollutants as it lies in close proximity to several heavily polluted urban areas, e.g., Norfolk, VA, Washington, DC, and Baltimore, MD, and receives polluted air masses from the heavily industrialized Ohio Valley.

To investigate spatial and temporal variations in Bay aerosol, airborne particles with diameters <10 μm were sampled weekly, at two rural agricultural land sites in the northern and central regions of the Chesapeake Bay between 5 June and 31 December, 1990. In November, sample collections were initiated at Haven Beach (HB), a third land site, located 500 m from the western shore of the southern portion of the Bay.

We have now completed analyses of more than 185 samples, laboratory blanks, and field blanks, representing the first 18 months of the study. INAA, inductively-coupled plasma-atomic emission spectrometry (ICP-AES), and graphite furnace atomic absorption spectrometry with Zeeman background correction (GFAAS) were utilized. Analyses for Al, As, Cd, Cr, Cu, Fe, Mn, Ni, Pb, S, Se, and Zn in the >130 first-year samples have been used to estimate aerial dry deposition fluxes to Bay surface waters as the product of the annual average concentrations and deposition velocities (V_ds) suitable for water surfaces.

Despite agreement with previously determined values, dry deposition estimates remain uncertain. Aside from uncertainties in V_ds, errors may arise from i) concentration differences between air over land and air over water; ii) deposition of particles >10 μm; and iii) use of inappropriate deposition velocities. In regard to the latter, the underlying physics suggests that dry deposition to water surfaces occurs episodically, i.e., during periods of high turbulence and great atmospheric instability. The disparity between deposition velocities for different wind speeds is so great that the deposition associated with a wind speed of 20 $m \cdot s^{-1}$ for 10

minutes a day would be equivalent to the deposition associated with an entire week at an average wind speed of 5 $m \cdot s^{-1}$. The effect of frequent turbulence episodes would be to drive dry deposition fluxes towards the maximum values.

- **Characterization of Submicrometer Aerosol Particles**

Detailed investigations of the size-distribution and composition of urban aerosols are important to the scientific community because they contain information about the formation, transport, and sources of atmospheric particles. In recent work, size-segregated aerosol samples were collected at three sites in Washington, DC, an area influenced largely by emissions from motor vehicles, utility coal and oil combustion, and municipal incineration; and at two sites in the heavily industrialized Philadelphia area, to determine the spatial variability in elemental size spectra and relationships between modal diameter and atmospheric aerosol origin and age.

Samples were collected daily from 7 am to 6 pm EST at the three Washington sites from 18 August to 26 September 1990, and at the Philadelphia sites from 16 October to 12 November 1990.

Elemental analyses were performed on selected impactor sets from both urban areas by INAA. Results are now complete for short-lived neutron activation products, from which we have produced elemental concentration versus aerodynamic particle diameter spectra for Al, Br, Ca, I, In, Cl, Mn, Mg, Na, S, Ti, V, Cu, Ba, and K.

The results of this study confirms the existence of fine structure in submicrometer aerosol and suggests that particles from various sources remain separated over urban transport scales. It is likely, therefore, that source/receptor distance relationships can be extracted from size-distribution data and that the size-spectra of certain enriched marker elements will permit identification of specific sources. Good analytical accuracy achieved with INAA permitted estimation of log-normal distribution parameters for over 60% of the elements measured in most of the samples analyzed to date. We anticipate that analyses for additional elements, when combined with previously collected data, will permit the elucidation of source/receptor relationships and atmospheric aging processes.

- **Regional and Indigenous Sources of Pollutants from Coal Combustion in Maryland**

Over the past six years various UMCP students have collected and analyzed more than 200 aerosol particles and gases at sites in western and central Maryland. These data are now being used in conjunction with recently completed studies of Ming Han and Glen Gordon at Lewes, Delaware, to determine the portion of the ambient aerosol particulate inventory associated with coal- and oil-fired power plants in the State of Maryland. Results for Lewes are important as they are needed to establish pollutant concentration gradients across the State of Maryland.

A total of 132 sets of airborne particulate and acidic gas samples were collected simultaneously at Lewes, DE, from July 24, 1989, to January 18, 1990. The Lewes samples were collected in two phases: in Phase I, 92 successive 12-hour samples were collected; and in Phase II, 40 samples were collected before, during, and after precipitation. The samples were analyzed for >40 elements by instrumental neutron activation analysis, for particulate S by inductively-coupled plasma atomic emission spectroscopy, and for gas phase SO_2, NO_x, and Cl by ion chromatography.

The concentration patterns were interpreted using Principal Component Analysis which revealed 6 principal components (PCs): PC1 was heavily loaded with crustal elements and elements usually associated with high-temperature combustion sources; PC2 was mainly loaded with Na and Cl and represents marine aerosol; PC3 had a distinctive V signature and was attributed to oil-fired power plants; PC4 was loaded with particulate and gaseous S, and possibly represents nearby coal-fired power plants; PC5 contained Cr, Zn and Sb, which is indicative of an incinerator component; PC6 was loaded with particulate S and Se, and is attributed to regional sulfate.

Despite the large distance from major coal-fired power plants, regional sulfate, which is mainly secondary SO_4^{2-} converted from SO_2 released from coal-fired power plants along with some other minor components, accounted for 59 and 49% of the Lewes aerosol mass in Phase I and Phase II, respectively; followed by seasalt and soil, accounting for 19 and 15% of the aerosol mass in Phase I, and 32 and 13% in Phase II. Oil-fired

power plants and local coal-fired power plants accounted for about 1 and 2% of the total particulate mass in both Phases. The contributions of six other sources totalled <5%. The average concentration ratio of nonmarine particulate S to gas-phase sulfur and was 0.76, indicating that the site may be influenced by local SO_2 emissions.

Federal Bureau of Investigation

The Elemental and Metals Analysis Unit (EMAU) of the Federal Bureau of Investigation (FBI) Laboratory irradiates samples for neutron activation analysis (NAA) at the NIST reactor facility. These samples are evidence in criminal cases being investigated by the FBI, state, and local jurisdictions throughout the United States. The primary analysis is of lead projectiles (bullets and shotshell pellets). In a typical case bullets from a crime scene are compared with the bullets from cartridges found in the possession of a suspect. The samples are irradiated at NIST along with an appropriate standard (SRM 2416, or SRM 2417) and then transported to FBI Laboratory facilities for gamma-ray spectroscopy. By NAA, samples are quantitatively analyzed for trace amounts of copper, antimony, and arsenic. The quantities of these trace elements found thus characterizes each bullet and allows bullets to be compositionally compared within a specific case. Further, the lead data from approximately the last ten years has been stored in a database. With this database new samples can be compared to each other and to all samples the FBI has analyzed to give an idea of how common their composition is. When appropriate, Special Agent Examiners provided expert court testimony in these cases.

The FBI also occasionally irradiates copper and steel samples at NIST. These analyses are also quantitative determinations for the trace elements present, and ultimately inter-sample comparison.

In addition to using NAA to analyze samples from criminal cases several projects of note are being worked on this year. Using NIST facilities EMAU has analyzed bullet lead which was used as a testing standard in a collaborative crime laboratory testing program. EMAU is also participating in a study of the effects of bullet fragments on brain tissue by analyzing bullet lead before and after implantation in the brain tissue of mice. On-going research concerning the quantitative trace analysis of bullet and shotshell pellet lead continues as questions arise in criminal cases.

Experiments

Use of INAA, PGAA, and RNAA to Determine 30 Elements for Certification of an SRM: Tomato Leaves, 1573a

D. A. Becker and D. L. Anderson.

The k_o Approach in Cold-Neutron Prompt Gamma Activation Analysis

R. M. Lindstrom and R. F. Fleming.

Analysis of Boron in CVD Diamond Surfaces Using Neutron Depth Profiling

G. P. Lamaze, R. G. Downing, L. Pilione, A. R. Badzian, and T. Badzian.

Non-Destructive Determination of Weight Percent Boron in Dielectric Films

R. G. Downing and G. P. Lamaze.

Oxygen-17 Implantation and Diffusion Profiles By Cold Neutron Depth Profiling

J. N. Cox, J. Blackmon, G. P. Lamaze, and R. G. Downing.

The IAEA-NIST-FDA-USDA Joint Project on Dietary Intake of Monor and Trace Elements in Different Countries: Results From Preliminary Evaluation

G. V. Iyengar.

Developmemt of Fresh-Frozen, Biological Standard Reference Materials

B. J. Koster and S. A Wise.

Regional and Indigenous Sources of Pollutants From Coal Combustion in Maryland

J. M. Ondov.

Neutron Capture Prompt-Gamma Emmisson Measurement of Hydrogen and Dopants in $KTiPO_4$ and $KTiAsPO_4$

M. Crawford, K. Cheng, A. Ferretti, W. Bindloss, J. M. Nicol, and R. M. Lindstrom.

B Evaluation of BPSG Films Produced in CVD Reactors

R. G. Downing, G. P. Lamaze, T. Hossain, and J. Keenan.

Certification of Standard Reference Materials by Neutron Activation Analysis
R. R. Greenberg, D. A. Becker, R. Demiralp, K. M. Garrity, R. M. Lindstrom, E. A. Mackey, and B. R. Norman.

Improvements to INAA Methodology
R. R. Greenberg, D. A. Becker, R. Demiralp, R. M. Lindstrom, and E. A. Mackey.

Quality Assurance Improvements for NAA
R. R. Greenberg, D. A. Becker, R. Demiralp, R. M. Lindstrom, and E. A. Mackey.

Development of Radiochemical Separation for NAA
D. A. Becker, K. M. Garrity, R. R. Greenberg, E. A. Mackey, and B. R. Norman.

Evaluation of Errors and Interferences in NAA
D. A. Becker, M. J. Blackman, R. R. Greenberg, and R. M. Lindstrom.

Trace Elemental Characterization of Silicon Semiconductor Materials
D. A. Becker and R. M. Lindstrom.

Improvements to PGAA Methodology
R. M. Lindstrom, D. L. Anderson, E. A. Mackey, R. L. Paul, and D. H. Vincent.

Evaluation of Accuracy and Precision in INAA of Botanical Materials
D. A. Becker.

Neutron Scattering Effects in PGAA
R. M. Lindstrom, E. A. Mackey,R. L. Paul, and D. H. Vincent.

New Developments in Monitor Activation Analysis
R. R. Fleming, G. P. Lamaze, R. M. Lindstrom, E. A. Mackey, and R. L. Paul.

Neutron Activation - Mass Spectrometry
R. G. Downing, G. V. Iyengar, and B. Clarke.

Bio Analytical and Specimen Bank Research
R. G. Downing, R. Demiralp, K. A. Fitzpatrick, K. M. Garrity, R. R. Greenberg, G. V. Iyengar, B. J. Koster, J. K. Langland, and E. A. Mackey.

Studies in Elemental Speciation
D. A. Becker and K. M. Garrity.

Multielement Analysis of Foods and Related Materials by NAA
D. L. Anderson, W. C. Cunningham, and T. R. Lindstrom.

High Sensitivity Gamma-Ray Spectrometry
R. M. Lindstrom

Application of Radioisotope-Induced X-Ray Emission to the Identification of Lead and Other Elements in Ceramic Glazes and Housewares
D. L. Anderson, W. C. Cunningham, and T. R. Lindstrom.

Elemental Characterization of High Temperature Superconductors
D. A. Becker, K. M. Garrity, R. R. Greenberg, R. M. Lindstrom, E. A. Mackey, R. L. Paul, and D. H. Vincent.

New Developments in NDP
R. G. Downing, G. P. Lamaze, J. K. Langland, and K. Coakley.

Comparison of Nuclear Reactors for Analytical Chemistry
D. A. Becker.

Determination of Hydrogen by PGAA
D. L. Anderson, R. R. Greenberg, R. M. Lindstrom, E. A. Mackey, R. L. Paul, and D. H. Vincent.

Analytical Applications of Cold Neutrons
H. Chen, R. Demiralp, R. G. Downing, R. R. Greenberg, G. P. Lamaze, J. K. Langland, R. M. Lindstrom, E. A. Mackey, D. F. R. Mildner, R. L. Paul, V. A. Sharov, and D. H. Vincent.

Neutron Focusing for Analytical Chemistry
H. Chen, R. Demiralp, R. G. Downing, J. K. Langland, D. F. R. Mildner, and V. A. Sharov,

Development of a Position-Sensitive Video Radiation Detector
H. Chen, R. G. Downing, and C. J. Zeissler.

Chesapeake Bay Atmospheric Deposition Study
Z. C. Lin, J. M. Ondov, and Z. Y. Wu.

Characterization of Submicrometer Aerosol Particles
F. Divita and J. M. Ondov.

Forensic Applications of NAA
E. R. Peele and R. F. Rebbert.

Archeological Applications of NAA
R. Bishop, M. James Blackman and J. E. Myers.

Analytical Study of the Geological Obsidian Sources and Archaeological Artifacts From the Northern Caucasus and Transcaucasia
R. Bishop, M. James Blackman, J. E. Myers, R. C. Badaljan, Z. K. Kikodze, I.G. Narimanov, and P. Kohl.

Participants

Anderson, D. L.	Food and Drug Admin.
Badaljan, R. C.	Acad. of Sci. (Armenia, FUSSR)
Badzian, A. R.	Pennsylvania State University
Badzian, T.	Pennsylvania State University
Becker, D. A.	Nuclear Methods Group
Bindloss, W.	DuPont
Bishop, R.	Smithsonian Institution
Blackman, M. J.	Smithsonian Institution
Blackmon, J.	University of No. Carolina
Capar, S. G.	Food and Drug Administration
Chen, H.	Nuclear Methods Group
Cheng, K.	DuPont
Coakley, K. J.	Statistical Engineering Div.
Cox, J. N.	INTEL
Crawford, M.	DuPont
Cunningham, W.C.	Food and Drug Admin.
Demiralp, R.	Nuclear Methods Group
Divita, F.	University of Maryland
Downing, R. G.	Nuclear Methods Group
Ferretti, A.	DuPont
Fitzpatrick, K. A.	Nuclear Methods Group
Fleming, R. F.	University of Michigan
Garrity, K. M.	Nuclear Methods Group
Gordon, G. E. (dec.)	University of Maryland
Greenberg, R. R.	Nuclear Methods Group
Han, M.	University of Maryland
Hossein, T.	Cornell University
Iyengar, G. V.	Nuclear Methods Group
Keenan, J.	Texas Instruments
Kikodze, Z. K.	Acad. of Sci. (Georgia, FUSSR)
Kohl, P.	Wellesley College
Koster, B. J.	Nuclear Methods Group
Lamaze, G. P.	Nuclear Methods Group
Langland, J. K.	Nuclear Methods Group
Lin, Z. C.	University of Maryland
Lindstrom, R. M.	Nuclear Methods Group
Lindstrom, T. R.	Food and Drug Admin.
Mackey, E. A.	Nuclear Methods Group
Mildner, D.F.R.	Nuclear Methods Group
Myers, J. E.	Smithsonian Institution
Narimanov, I. G.	Acad. of Science (Azerbaijan, FUSSR)
Nicol, J. M.	Reactor Radiation Division
Norman, B. R.	Nuclear Methods Group
Paul, R. L.	Nuclear Methods Group
Ondov, J. M.	University of Maryland
Pilione, L.	Pennsylvania State University
Peele, E. R.	Federal Bureau of Investigation
Rebbert, R. F.	Federal Bureau of Investigation
Sharov, V. A.	Kurchatov Institute, Russia
Vincent, D. H.	University of Michigan
Wilson, J.	Nuclear Methods Group
Wise, S. A.	Organic Analytical Res. Div.
Wu, Z. Y.	University of Maryland
Zeissler, C. J.	Surface & Micro. Sci. Div.

NEUTRON METROLOGY AND DOSIMETRY

This project develops and applies well-characterized neutron fields and related capabilities for materials dosimetry detector development, methods evaluation, and standardization. It also carries out forefront research at the CNRF in weak interaction physics and testing of fundamental symmetry principles, develops advanced measurement techniques in neutron interferometry, and establishes basic, accurate neutron interaction data by means of benchmark experiments in standard neutron fields. Standards and calibration facilities for primary nuclear targets and fissionable deposits are maintained for fundamental physics research, analytical chemistry, and nuclear technology.

Project work in fundamental neutron physics is reported separately.

Interaction with our constituency in materials dosimetry was enhanced by the preliminary availability of the University of Michigan's Material Dosimetry Reference Facility (MDRF) with larger irradiation volume and its high neutron fluence compared with fission neutron sources at NIST. Characterization of the MDRF neutron spectrum is progressing as a close cooperation between NIST and the Phoenix Memorial Laboratory at the University of Michigan. Fission chambers have been employed extensively to measure neutron fluence rates at the CNRF, notably the NG-3 sample position. Highlight activities are as follows.

- **The Materials Dosimetry Reference Facility (MDRF)**

A new, high-intensity reference neutron field for reactor dosimetry is in early stages of operation at the Ford Nuclear Reactor (FNR) at the University of Michigan. Designed and constructed by the National Institute of Standards and Technology, the facility hosts calibration and validation experiments in support of materials neutron dosimetry for the nuclear power industry and for the metallurgical community engaged in estimating radiation damage in steel. This benchmark is a natural extension of a long-term NIST program to develop standard and reference neutron fields for measurement assurance applications and for testing new detectors and techniques. Field characterization and user operation of the facility is a joint effort by NIST and the Phoenix Memorial Laboratory of the University of Michigan.

The MDRF complements the ^{235}U cavity fission source at NIST by providing a tenfold increase in fast-neutron fluence, a much larger irradiation volume with modest flux gradients, and a neutron spectrum rich in intermediate-energy neutrons. Two spectrum options are available to investigate detector response characteristics and to validate the interpretation of dosimetry measurements.

Essentially, the MDRF is a steel cylinder (15 cm o.d., 5cm i.d., 61 cm long) wrapped in cadmium and mounted in the reactor pool near the face of the FNR. An irradiation thimble, inserted from the top of the reactor pool, locates passive or active detectors (e.g. NIST double fission chambers) at the core midplane. A choice of two thimbles, one with and one without a boron-10 liner, allows a convenient change from a neutron spectrum that extends down to the cadmium cut-off at 0.4 ev to one which cuts off at a few keV. The nominal fast-neutron fluence rate ($E > 1$ MeV) is 3×10^{11} n/cm^{2}s^{-1}. Total fast-neutron fluences for routine facility-user irradiations will normally be limited to about 2×10^{16} n/cm^2.

At the present time, neutron spectra for the two MDRF options are known from 2-d DORT calculations with a homogeneous model of the reactor core. The spectra are indistinguishable above 1 MeV and quite similar to the ^{235}U fission neutron spectrum. The fraction of the spectrum above 1 MeV is 0.23 for MDRF and 0.32 for MDRFw/^{10}B. Below the prominent iron transmission window at 25 keV, the MDRF relaxes into a near-1/E slowing down distribution while the MDRFw/^{10}B cuts off sharply. Calculations with more detailed core and MDRF modeling will be forthcoming. Certified neutron fluences for measurement assurance irradiations are established with $^{58}Ni(n,p)$ activation monitors calibrated in terms of neutron fluence transfer from the NIST ^{252}Cf Fission Neutron Irradiation Facility. It is anticipated that this monitoring scheme, supported by spectrum calculations and diagnostic measurements with threshold detectors, will make it possible to specify the neutron fluence above 1 MeV to 5% or better. The total neutron fluence

will be more uncertain because of a much greater dependence on calculation at low energies.

Initial fission chamber and activation detector measurements [threshold: ^{237}Np(n,f), ^{238}U(n,f), ^{58}Ni(n,p), ^{54}Fe(n,p), ^{46}Ti(n,p); low energy: ^{235}U(n,f)] have been employed to measure spectral indexes and to establish neutron fluence rates in the MDRF. Spectral indexes for the threshold reactions, taken with respect to the ^{238}U fission reaction, agree well with existing calculations for the lowest threshold detector, ^{237}Np(n,f), but exceed calculation by an average of 12% for the higher energy threshold reactions. The spectral index ^{235}U(n,f)/^{238}U(n,f), with a median ^{235}U(n,f) response energy of 20ev, is in surprisingly good agreement (a few percent) with the simplified calculational model. A fast-neutron fluence rate (E>1 MeV), from a weighted average of the values from each of the five threshold detectors, is 2.9×10^{11}n/cm^{2}s^{-1} for a typical reactor core configuration and a power level of 2MW. The experimental standard deviation for this average value is 6%. Most of the threshold detector results are based on neutron fluence transfer from the NIST ^{252}Cf Fission Neutron Irradiation Facility.

- **National Repository for Fissionable Isotope Mass Standards**

This new initiative will include acquiring fissionable, lending deposits, maintaining scientific and regulatory records, and making occasional intercomparisons of well-characterized deposits by fission counting and alpha counting to verify the documented isotopic and mass analyses. The pace of these various activities is expected to increase gradually over the next three years. The acquisition of selected Argonne National Laboratory foil collections and intercomparisons with NIST reference deposits are the first anticipated steps.

- **A New Double Ionization Chamber For Boron Target Mass Comparisons**

As a complement to existing low-geometry charged-particle counters with arrays of surface barrier detectors we have built and tested a new double ionization chamber. Figure 1 shows a cross sectional view of the new chamber. At the central plane of the new chamber, two targets are positioned back-to-back with each target deposit

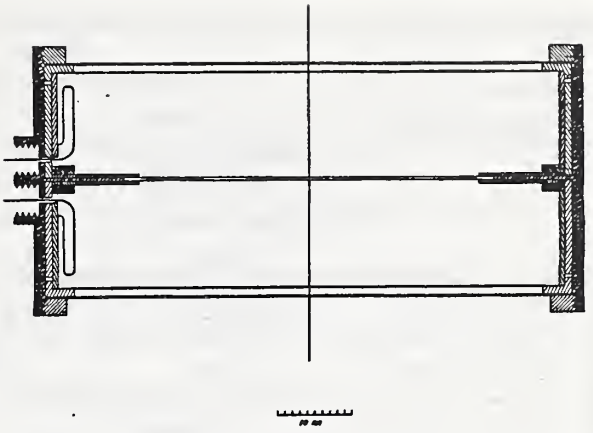

Figure 1. A cross sectional view of the new double ionization chamber.

facing into an independent pulse-mode ionization chamber. The top and bottom halves of the chamber are identical. The chamber is easy to open for changing targets. The chamber operates with a slow continuous flow of P-10 gas (a mixture of 90% argon and 10% methane). For boron or lithium targets, a bias of about 100 volts is sufficient to eliminate charge recombination; fissionable deposits might require somewhat higher bias voltage to prevent recombination.

Figure 2 shows the pulse-height distribution (PHD) from a deposit of mass thickness 10 μg/cm^2. The slight asymmetry in the main alpha peak indicates that the target to anode spacing needs to be increased by about 25% to eliminate some truncation of the ionization on the shortest paths across the chamber.

This ionization chamber design is very similar to that of the NIST double fission chamber. Table 1 shows the results of some mass ratio measurements made with the new chamber compared with mass thickness ratios measured by the 4-detector surface barrier array at NIST. All the ratios are given with respect to the third target, designated B090112-H5. The discrepancy between the uncorrected ionization chamber ratios and the surface barrier detector ratios is found to be roughly linear with the difference in the masses of the two deposits under comparison, as was expected from previous work with the NIST fission chamber. The necessary corrections for self-absorption and extrapolation of the pulse-height

Table 1. Mass ratios derived from the new double ionization chamber and surface barrier detector arrays

^{10}B target label	Fully corrected mass thickness ratio by surface barrier detector array	Uncorrected mass ratio by ionization chamber	Mass thickness difference relative to B0901112-H5 (μg/cm^2)	Discrepancy between ion chamber and surface barrier array ratios
CBNM-H2	0.9086	0.9134	0.89	0.53 %
B0901109-H2	0.9626	0.9634	0.89	0.08 %
B0901112-H5	1	1	0	0
CBNM3-H6	1.756	1.723	-7.31	-1.90 %

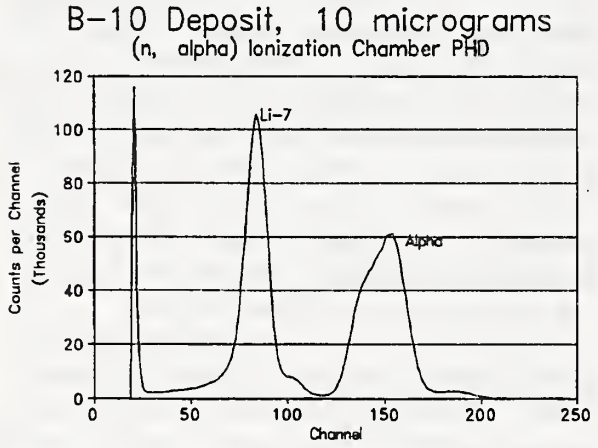

Figure 2. Pulse-height distribution (PHD) from a deposit of mass thickness 10 μg/cm^2.

distribution to zero energy (ETZ) amount to about 0.3% per μg/cm^2 of difference in mass thickness. For sets of six targets all made during the same evaporation at the Belgian Central Bureau for Nuclear Measurement (CBNM), the difference in mass thickness is typically less than 0.1 μg/cm^2 for deposits of 10 μg/cm^2 thickness. The self-absorption and ETZ corrections for the ionization chamber ratios are expected to be of the order of 0.03% for such cases. The ionization chamber can be employed as a sufficiently accurate independent check on the surface barrier array counts in these cases.

The new ionization chamber can also be employed as a true 1/v beam monitor, replacing the previously employed fission chamber monitor. Thus possible effects from changes in Westcott g-factors with reactor temperature could be avoided in the monitor counter.

The primary disadvantages of the new chamber are the much lower amplitude of the pulses (compared with those from a fission chamber) and the large corrections for self-absorption and ETZ in cases where the target masses are not nearly equal. However, the ionization chamber has the advantages of needing less beam intensity, of being free of the requirements of very accurate positioning of the targets, and of needing only a very simple system of data acquisition electronics.

- **Support Structure Experiment at the Trojan Nuclear Power Plant**

Results were obtained this year from a multilaboratory effort to measure neutron exposures for critical pressure vessel support structures at the Trojan nuclear power reactor. In support of this work, certified neutron fluence standards were prepared at the ^{235}U Cavity Fission Source for Westinghouse's Waltz Mill Dosimetry Laboratory. Benchmark irradiations of archive dosimeters for this experiment were also carried out at the NIST MDRF. Detectors irradiated to a known fluence in these irradiations were nickel, iron, titanium, and ^{238}U.

Counting results from Waltz Mills for the neutron fluence standards were found be within $\pm$ 2% to $\pm$ 6.5% of the value obtained by absolute activation counting. Specific disagreement with calculation of Trojan detector results centered on the Fe/Cu spectral index and excessively high values for the ^{238}U detector response. The latter appears to associated with a ^{235}U contaminant in

the ^{238}U that was not accounted for. The MDRF irradiation was undertaken to help establish a correction for the ^{235}U response. Comparison with initial calculations indicates a $^{235}U/^{238}U$ spectral index that is unacceptably high by more than 50%. Results for Solid State Track Recorder (SSTR) dosimeter agreed with corresponding radiometric detector to within about 15%.

Experiments

Characterization of the Materials Dosimetry Reference Facility (MDRF)
J. A. Grundl, C. M. Eisenhauer, E. D. McGarry, A. I. Hawari, P. A. Simpson, and R. Venkatoraman.

Neutron Transmission Through Iron
J. Grundl, C. M. Eisenhauer, and D. Gilliam.

Benchmark Measurements and Calculations for Criticality Safety
D. M. Gilliam and J. F. Briesmeister.

Neutron Fluence Rate Measurements at the CNRF
D. M. Gilliam.

Neutron Irradiations for other Government Agencies, Universities, and Industry
D. M. Gilliam.

New High-Accuracy Alpha Counting Apparatus
D. M. Gilliam.

Certified Neutron Fluence Standards from the Cavity Fission Source
E. D. McGarry and J. A. Grundl.

Quality Assurance Checks on Masses and Impurities in Neutron Dosimeters Used for NRC Pressure-Vessel Exposure Surveillance
E. D. McGarry and J. A. Grundl.

ICRU REPORT 47, Measurement of Dose Equivalents from External Photon and Electron Radiations
R. Schwartz, G. Portal, W. G. Cross, G. Dietze, and J. R. Harvey.

ISDO/CD 10647, Procedures for Calibrating and Determining the Response of Neutron Measuring Devices used for Radiation Protection
R. Schwartz and C. M. Eisenhauer.

Measurement of LET Spectra and Kerma Rates at AFRRI
R. Schwartz.

Measurement of Spectral Response of ROSPEC Rotating Spectrometer
R. Schwartz, C. M. Eisenhauer, and H. Ing.

Determination of Second-Order Scatter Corrections for Instrument Calibrations
R. Schwartz and C. M. Eisenhauer.

Neutron Transport Calculation
C. M. Eisenhauer.

Participants

Briesmeister, J. F.	Los Alamos National Lab
Cross, W. G.	AECL, Canada
Dietze, G.	Phys.-Tech. Bund., Germany
Eisenhauer, C. M.	Ionizing Radiation Division
Gilliam, D.	Ionizing Radiation Division
Grundl, J. A.	Ionizing Radiation Division
Harvey, J. R.	Berkely Nucl. Labs, UK
Hawari, A. I.	University of Michigan
Ing, H.	Bubble Tech. Ind., Canada
McGarry, E. D.	Ionizing Radiation Division
Portal, G.	C.E. Nucleaires, France
Schwartz, R.	Ionizing Radiation Division
Simpson, P. A.	University of Michigan
Venkatoraman, R.	University of Michigan

FUNDAMENTAL NEUTRON PHYSICS

The past year has seen extensive progress in the fundamental neutron physics program at the CNRF. Of particular note was the successful completion of the first set of experimental measurements to be carried out at the end position on NG-6. These included intercomparisons between absolute neutron flux monitors required for the NIST neutron lifetime determination program and the testing of a prototype coincidence detector for the Los Alamos/NIST/Michigan/ Berkeley time reversal experiment. Also of note was the acceptance of the first beam from the in-guide monochromator at NG-7. Construction of the seismic/acoustic isolation system at the interferometer is continuing and the last year has seen the installation of several major subsystems. Planning for the experimental program at NG-6 has also seen considerable progress.

- **Advanced Methods of Neutron Flux Determination**

A series of intercomparisons between two novel, absolute neutron flux monitors were carried out at the end position of NG-6 in the winter of 1991-92. These monitors were designed to achieve an accuracy of 0.1% or below in the measurement of a cold (or thermal) neutron flux. Such an accuracy is significantly below that which is attainable by conventional neutron detectors. The original motivation for this work arose from the NIST program for the measurement of the neutron beta decay lifetime. However, the attainment of the projected accuracy will have additional applications for the calibration of secondary neutron detectors and dosimeters, for the primary calibration of standard neutron sources, for the measurement of neutron cross sections of important nuclear materials and for the accurate assay of primary standards for neutron activation analysis.

The first of these detectors [1] is based on an application of the coincidence method for the absolute determination of detector efficiencies. The method uses the $^{10}B(n,\gamma)$ reaction which produces a 478 kev gamma as well as an alpha particle. In addition to being calibrated by the coincidence method, the new detector's efficiency can also be determined by an independent procedure involving an alpha source of well known activity. A comparison of these two calibration methods provides an objective test of the overall reliability of the final calibration. Data collection was carried out over several reactor cycles in late 1991 and early 1992. These data are currently being reduced, but data analysis indicates an internal consistency at the 0.1% level. The final accuracy of this method will depend on the understanding of a variety of small systematic instrumental effects which are currently being investigated off line.

The second absolute neutron monitor involves the calorimetric determination of the energy released by the capture of neutrons by ^{6}Li in a "black" target [2,3]. Neutron capture by ^{6}Li produces only short range particles, and the reaction has a very well known total energy release. If all the neutrons in a beam are captured by ^{6}Li, and if all the reaction energy appears as a thermal excitation of the target, the incident neutron flux can be determined from a measurement of the heat developed in the target. For typical neutron fluxes this heat will be rather small, on the order of microwatts. However, the accurate detection of such small thermal powers is possible at cryogenic temperatures where the heat capacity of a target may be quite small. In a collaborative project between Harvard University, Los Alamos National Laboratory, and NIST, a cryogenic ^{6}Li calorimeter based on this principal has been constructed. In tests carried out at the CNRF, the sensitivity of this device has been shown to be approximately 2 nanowatts in a 20 min integration time. This performance more than exceeds the initial design goal corresponding to a precision of 0.1%. The ^{6}Li calorimeter was tested on the end position at NG-6 in early 1992. Analysis of the initial data set and comparison with the alpha/gamma coincidence device is currently in progress.

- **Determination of the Free Neutron Lifetime**

The long term NIST program for the determination of the neutron lifetime has made significant progress in the last year. A considerable effort has gone into the construction of a totally rebuilt neutron decay detector. The decay detector is, at the time of this writing, being

installed on the end position NG-6. This apparatus is based on the same measurement principles as that employed in our earlier collaborative efforts carried out at the Insitut Laue Langevin in 1989 [4]. The new apparatus includes a variety of mechanical, electronic and conceptual changes to insure that results will be immune to systematic effects. The aim of this project, which enjoys significant support from the Department of Energy, is to provide a reliable determination of the free neutron beta decay lifetime with an uncertainty at the level of 0.1-0.2%. Such an experimental value of this fundamental parameter will have significance for weak interaction theory, for the understanding of the details of the early universe, and for a variety of issues in astrophysics.

- **Search for Time Reversal Violation in Neutron Beta Decay**

The simplicity of the beta decay process in the free neutron makes it an attractive system for detailed tests of weak interaction theory. One class of test involves investigations of the degree to which the weak interaction satisfies various fundamental symmetries. A particularly interesting test concerns the experimental search for time reversal symmetry violating correlations between the decay products of neutron decay. As part of a collaborative effort between Los Alamos National Laboratory, NIST, Harvard University, and the University of California (Berkeley), a prototype detector, designed to be sensitive to such correlations, was tested for several reactor cycles in early 1992. This device was capable of detecting, in coincidence, the beta electron and the recoil proton emerging from the decay of a free neutron within a cold neutron beam. The initial detector tests employed unpolarized neutrons at NG-6. The final T violation measurement will, however, use polarized neutrons. The results of the prototype test indicate that detector sensitivities and background noise levels in the guide hall are sufficient to allow a complete measurement. Design and construction of the final detector, as well as the neutron polarizers, are now in progress.

- **Neutron Interferometry**

Construction of the neutron interferometry facility in the CNRF guide hall has proceeded over the last year with the installation of several critical components. One major subassembly is the "in-guide" monochromator which is now fully operational. Like conventional crystal monochromators, the recently installed device on NG-7 diffracts a narrow velocity "slice" from the broad velocity distribution within the guide. Final design, installation, and alignment of the monochromator were carried in 1992 with first beam extraction in mid-summer. Currently, detailed measurements of the velocity distribution are under way.

A second major component of the neutron interferometry facility is the seismic and acoustics isolation system which will act as the support for the perfect crystal monochromator itself. This system is a multistage, actively-controlled pneumatic system which will reject high frequency (greater than about 1Hz) floor and airborne vibration while maintaining the long term position to within a few microns. The first stage of this system is built around a 37 ton reinforced concrete platform supported on high capacity pneumatic supports. In the spring of 1992 the base platform was delivered and installed in its well alongside NG-7 at the CNRF. As of this writing the primary pneumatic system has also been fully installed and is undergoing preliminary tests.

References

[1] D. M. Gilliam, G. L. Greene, G. P. Lamaze, Nucl. Instrum. and Methods A248, 220(1989).

[2] R. G. H. Robertson and P. E. Koehler, Nucl. Instrum. and Methods, A251, 307(1986).

[3] J. M. Richardson et al., Nucl. Instrum. and Methods A306, 291(1991).

[4] J. Byrne et al., Phys. Rev. Let. 65, 289(1990).

Experiments

Accurate Determination of Neutron Flux using Alpha-Gamma Coincidence Methods

W. M. Snow, D. Gilliam, M. S. Dewey, G. L. Greene, and J. Richardson.

Measurement of Neutron Flux by Cryogenic Calorimetry

J. Richardson, T. Chupp, W. M. Snow, D. Gilliam, M. S. Dewey, G. L. Greene, R.G.H. Robertson, and J. Wilkerson.

Search for Time Reversal Invariance Violation in Neutron Beta Decay

J. Wilkerson, T. Bowles, R.G.H. Robertson, J. Nico, W. M. Snow, D. Gilliam, M. S. Dewey, G. L. Greene, T. Chupp, E. Wasserman, S. Freedman, and K. Coulter.

On the Unobservability to $O(10^{-8})$ of the Anandan Acceleration of a Neutron Moving in Constant Electric and Magnetic Fields via an Associated Phase Shift in a Neutron Interferometer.

R. C. Casella and S. A. Werner.

Determination of the Neutron Lifetime

W. M. Snow, D. Gilliam, M. S. Dewey, and G. L. Greene.

Participants:

Arif, M.	Physics Laboratory
Bowles, T.	Los Alamos National Laboratory
Casella, R. C.	Reactor Radiation Division
Chupp, T.	University of Michigan
Dewey, M. S.	Physics Laboratory
Freedman, S.	University of California
Gilliam, D.	Physics Laboratory
Greene, G. L.	Physics Laboratory
Heckel, B.	University of Washington
Kaiser, H.	University of Missouri
Klein, A.	University of Melbourne, Australia
Lamaze, G. P.	Nuclear Methods Group
Nico, J.	Los Alamos National Laboratory
Opat, G.	University of Melbourne, Australia
Pauwels, J.	Central Bureau for Nuclear Measurement, Belgium
Richardson, J.	Harvard University
Robertson, H.	Los Alamos National Laboratory
Scott, R.	Scottish Universities Research and Reactor Center
Snow, W. M.	Physics Laboratory
Wasserman, E.	Los Alamos National Laboratory
Werner, S.	University of Missouri
Wilkerson, J.	Los Alamos National Laboratory
Zeilinger, A.	University of Innsbruck, Austria

Single chain characterization in solutions and in bulk states of polymers has been and continues to be a unique strength of the small angle neutron scattering technique. However, the potential of SANS in new areas is also being explored. Two important areas of effort in the last year are time dependence and shear rate dependence studies of various systems. Although we are only studying kinetics and shear rate dependence of polymer mixtures, the potential applications to other fields such as complex fluid and biological systems could be just as important. A few of our projects are summarized below.

Polymer Blends

- **Deviation from Mean-field Behavior in a Low Molecular Weight Critical Polymer Blend**

It is well established that simple binary fluids show static critical behavior characteristic of the three dimensional Ising (d=3, n=1) universality class. Although phase separation in binary polymer mixtures has the same inherent Ising symmetry, de Gennes used the Ginzburg criterion to argue that for sufficiently high degrees of polymerization, the critical regime is confined to a vanishingly small window near T_c and the mean-field (Flory-Huggins) model is adequate to describe the transition. Small angle neutron scattering (SANS) studies of high molecular weight polymer blends have confirmed this prediction. In light of this, it is reasonable to expect that a crossover from mean-field to Ising behavior might be observable in polymer blends with sufficiently low molecular weight. A number of groups have recently reported observing such a crossover in the inverse susceptibility measured from small angle scattering, however, there is some disagreement among their results.

We have carried out SANS measurements of the susceptibility and correlation length as a function of temperature near the phase boundary of a low molecular weight critical mixture of polystyrene and polybutadiene [1]. We have re-examined the Ginzburg criterion for polymer blends. With a proper expression of the Ginzburg criterion and the use of experimentally observed values for the bare-correlation length, ξ_o, and the binary interaction parameter, χ, the cross-over from mean-field to critical behavior of our results as well as those in the literature can be described consistently. This Ginzburg expression we have derived for polymer mixtures is readily applicable to blends of any molecular weight, and its validity in higher molecular weight blends remains to be tested.

- **Inversion of Phase Diagram from UCST to LCST in Deuterated Polybutadiene and Protonated Polybutadiene Blends**

The miscibility of an amorphous mixture of normal (protonated) and perdeuterated polybutadiene (HPB and DPB, respectively) has been extensively studied and was characterized by an upper critical solution temperature (UCST). Some literature reports have interpreted the partial miscibility of isotopic polymer blend in terms of the reduction in carbon-hydrogen bond length resulting from substituting deuterium for hydrogen (isotope effect). For the DPB/HPB blend, however, since polybutadiene consists of a 1,2-unit(vinyl) and a 1,4-unit, the microstructure in the blend should be an important factor in affecting the miscibility of the blend. In an earlier study, we separated the isotope effect from the microstructure effect through a systematic SANS study of DPB/HPB blends with various vinyl contents on the basis of random copolymer mixtures theory. We have regarded the DPB/HPB blend as a blend of A-B copolymer (A and B are the 1,2-unit and the 1,4-unit for DPB, respectively) and C-D copolymer (C and D are the 1,2-unit and the 1,4-unit for HPB, respectively) and showed that the main contribution for miscibility in the blend is due to the intramolecular pairs of A/B and C/D rather than the isotope pairs of A/C and B/D. These intramolecular interactions account for the observation of negative χ's (χ is the binary interaction parameter) for one of the DPB/HPB blend pairs, while the isotope effect can only explain positive χ's. Therefore, it is extremely important to clarify the effect of the microstructure on the miscibility of the DPB/HPB blends.

In this study [2], we carried out SANS measurements for a series of DPB/HPB blends. By holding the vinyl content of the DPB component constant, experimental evidence for

inversion of the phase diagram from UCST to LCST with increasing vinyl content of HPB was obtained (Fig. 1). This inversion is caused by the difference in temperature coefficients for individual pair interaction parameters. All individual pair interaction parameters have positive temperature coefficients (in terms of 1/T) which implies a UCST system; however by taking the difference from intermolecular and intramolecular interactions the sign of the overall χ could change, which results in an inversion from UCST to LCST.

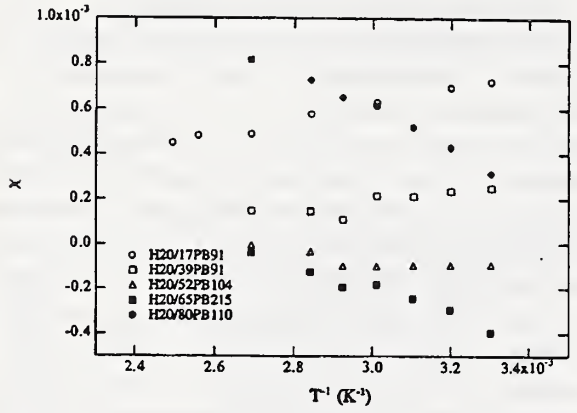

Figure 1. Plots of binary interaction parameters, χ, against reciprocal absolute temperature, T^{-1}, for five different DPB/HPB blends. The deuterated polybutadiene, H20 has a degree of polymerization N_n = 950 and a vinyl content of 15.6 mole %, and the hydrogenated polybutedienes 17 PB 91 has N_n = 1294, and vinyl content 17 mole %, 39 PB 91 has N_n = 1053, and vinyl content 39 mole %, 52 PA 215 has N_n = 3974 and vinyl content 52.2 mole %, 65 PB 104 has N_n = 1922 and vinyl content 64.9 mole % and 80 PB110 has N_n = 2033 and vinyl content 80.4%.

- **Phase Separation in Deuterated Polycarbonate/poly(methylmethacrylate) Blend Near the Glass Transition Temperature**

Small angle neutron scattering study of a deuterated bisphenol-A polycarbonate/ poly(methylmethacrylate) (DPC/PMMA) blend near and above its T_g has been carried out. It is clear from our time resolved SANS study that a 50/50 blend of DPC/PMMA is immiscible above its glass transition temperature. A trapped miscible state can be obtained through fast solution casting of thin film ($\sim 50\mu m$) in THF. A slow spinodal kinetics has been studied by SANS techniques by heating the solvent casted specimen to a temperature above its T_g, (Fig. 2) meanwhile the mobility, M, of the interdiffusion is still slow enough to keep the interdiffusion coefficient, D_{int} ($D_{int} = M\ \partial^2\Delta f/\partial\phi_o^2$) small enough for the time resolved SANS study.

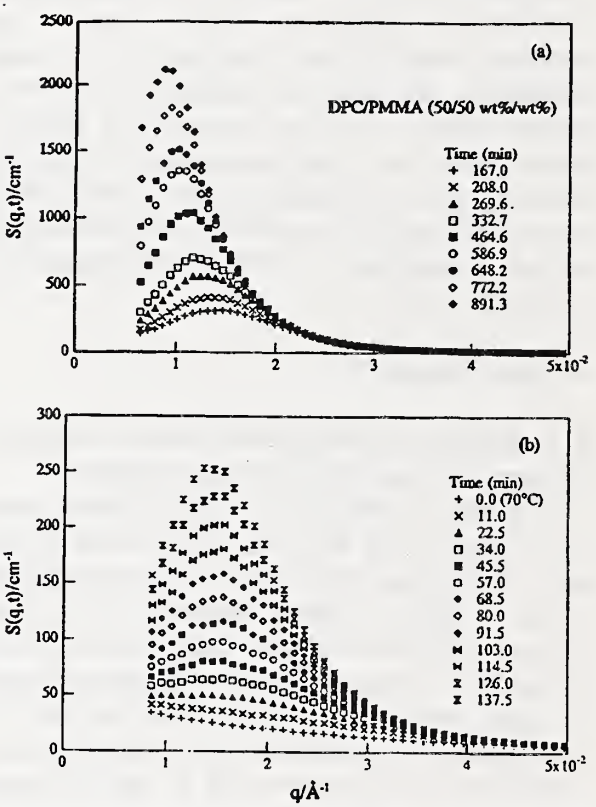

Figure 2. Time-evolution of SANS profiles of DPC/ PMMA blend after a temperature jump from 70 to 110 °C. Time elapses in the order of part (b) to part (a).

The SANS experiment covers a q-range which encompasses the single chain dimension, i.e. from $qR_g > 1$ and $qR_g < 1$. The time dependent structure factor thus obtained provides an unequivocal quantitative measure of the virtual structure factor, $S(q,\infty)$; the relation-ship of q_m and q_c through rate of growth, Cahn-plot analysis and singularity in $S(q,\infty)$; the growth of fluctuation at $qR_g < 1$ and intrachain relaxation at $qR_g > 1$; and finally a clear proof of CHC theory in the very early stage of spinodal decomposition.

This procedure provided a technique of obtaining the functional form of the free energy of mixing of immiscible blends by measuring the temperature dependence of χ parameters at various compositions and final temperatures through measurements of the kinetics of spinodal

decomposition. The phase diagram, which is inaccessible due to the interference of the T_g line, can be obtained through temperature extrapolation of the χ parameter. The intrachain relaxation can in principle be studied from the time and q dependence of S(q) in the region of $qR_g > 1$.

- **Competition of Phase Separation and Transesterification in D-Polycarbonate/Co-Polyester Blends**

Time and temperature dependence of transesterification and phase separation in blends of bisphenol A d-polycarbonate/random copolyester of cyclohexanedimethanol and ethylenediol with terephthalic acid were studied with the small angle neutron scattering technique. Radius of gyration and exponent x in $I \propto q^{-x}$, where q is scattering wave number, showed that phase separation is dominant below 180 °C while transesterification becomes dominant above 220 °C. In the intermediate temperature range, both processes compete so that the interface first becomes very sharp due to phase separation and then broadened by transesterification. It is concluded that relative rates of both processes determine the structure coarsening, melting and stabilization mechanisms.

Shear Studies

- **Polystyrene/DOP Solutions—Single Chain Behavior Under Shear**

Experiments to examine the single chain scattering behavior during shear for a 3% solution of polystyrene in dioctyl phthalate were conducted. Three samples were utilized, each containing 3% total polymer with varying ratios of deuterated to protonated chains (10:90, 20:80, and 30:70). Experiments were performed on the 8 m SANS instrument, at shear rates ranging between 107 and 815 s^{-1}. In contrast to the results obtained previously on the 30 m SANS instrument, where no anisotropy was observed, all samples under all shearing conditions displayed some anisotropic scattering. At low speeds ($< 190\ s^{-1}$), the scattered intensity parallel to the flow direction is suppressed relative to the quiescent scattered intensity. With increasing speeds, the low q scattering increases while the intermediate q range scattering remains suppressed. At the highest speed, the low q scattering for the sheared sample is greater than the quiescent sample, yet the intermediate q range scattering is still lower than the quiescent sample. Normal to the flow direction, an enhancement of the scattering is observed at speeds greater than 190 s^{-1}. The enhancement increases with increasing shear rate, however the q value where the scattering diverges does not change with shear rate.

An estimate of the radius of gyration (R_g) components as a function of shear rate was made using the random phase approximation for polymer solutions. The fits to the structure factors show that R_g increases parallel and normal to flow. The increase along the flow direction is greater than the increase perpendicular to flow. The ratio of $R_{g\parallel}$ to $R_{g\perp}$ is approximately constant (1.1) for the shear rates examined. Due to the fact that the condition $qR_g < 1$ is not satisfied for our experimental conditions, attempts to measure the radius of gyration components parallel and normal to flow using the "high concentration" method and the Zimm plot were unsuccessful.

- **Polystyrene/Polybutadiene/DOP Solutions—Off Critical Shear Rate Behavior**

Studies of the steady shear SANS behavior of the off-critical blend solution that was also examined with the shear light scattering instrument were performed. These results will complement each other to provide a complete picture of the shear induced homogenization observed in this sample. A suppression of concentration fluctuations parallel to the flow direction is observed with the application of sufficiently large shear rates. Normal to the flow direction there is no effect of shear on the fluctuation size. The structure factors were fit to the Ornstein-Zernike function to extract values of the correlation length, ξ, and S(q = 0) as a function of temperature and shear rate. By assuming the system is mean-field in nature and plotting ξ^{-2} versus 1/T, an apparent spinodal temperature may be determined by extrapolating to infinite correlation length. There is a decrease in the apparent spinodal temperature parallel to flow and no change in the apparent spinodal temperature normal to flow. The shear rate dependence of ΔT is much stronger for this off-critical mixture than is predicted by Onuki and Kawasaki for critical mixtures. However, due to the mean field nature of the system there is no true

shift in the spinodal temperature with shear rate, and these results are a reflection of the distortion of the concentration fluctuations with shear.

We have also attempted to determine the smallest concentration fluctuation which is affected by a given shear rate in a manner similar to that used in the analysis of SANS from polymer blends under shear. The critical size is related to q_c, which is determined as the divergence point between sheared and quiescent structure factors. By plotting log q_c versus log $\dot{\gamma}$, power law behavior was observed for different temperatures. However, these power law exponents were less than the 1/3 predicted by mode coupling theory and observed for critical compositions of two component polymer blends. This study highlights the differences between critical and off-critical mixtures and indicates that more work in the area of off-critical mixtures is necessary.

• Crossover to Strong Shear in a Low Molecular Weight Critical Polymer Blend

Small-angle neutron scattering has been used to measure the influence of shear flow on a low-molecular-weight polymer blend near the critical point [3]. When combined with light scattering measurements of the equilibrium ($\dot{\gamma}$ = 0) critical dynamics [4], these measurements reveal that the long-range critical fluctuations begin to break apart when the shear rate becomes comparable to the characteristic relaxation rate τ_c^{-1}, where τ_c is the equilibrium lifetime of the critical fluctuations. In our experiment, $\tau_c = \xi^2/D_c$ for a polystyrene/ polybutadiene blend at critical composition. The correlation length ξ was measured by SANS and D_c was obtained from the DLS experiments. The static structure factor S(q) at various temperatures and shear rates was measured in-situ by SANS experiment. The universal behavior of the shear rate dependence of structure factor or correlation length as a function of reduced shear rate, ($\dot{\gamma}\tau_c$), can be directly related to the decrease in the critical temperature caused by the flow (Fig. 3). Our experimental results are found to be in very good agreement with the theoretical predictions of Onuki and Kawasaki.

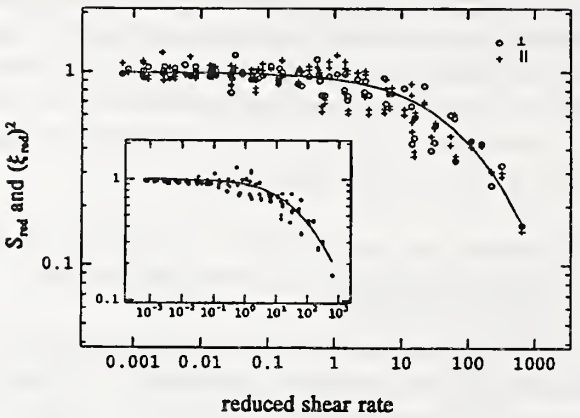

Figure 3. The reduced correlation length squared and the reduced susceptibility as a function of reduced shear rate. The solid line is the behavior predicted to O(ϵ), over six decades in reduced shear rate, with no free parameters. The inset is the same plot using a circular average of the scattering intensity, which is justified by the isotropic nature of the response.

References

[1] D. W. Hair, E. K. Hobbie, A. I. Nakatani and C. C. Han, J. Chem. Phys., 96, 9133 (1992).

[2] H. Jinnai, H. Hasagawa, T. Hashimoto, and C. C. Han, Macromolecules (in press).

[3] E. K. Hobbie, D. W. Hair, A. I. Nakatani and C. C. Han, Phys. Rev. Lett.

[4] D. W. Hair, E. K. Hobbie, J. Douglas and C. C. Han, to be published.

Experiments

Deviation from Mean-field Behavior in a Low Molecular Weight Critical Polymer Blend

D. W. Hair, E. K. Hobbie, A. I. Nakatani. and C. C. Han.

Effect of Crosslinks on the Miscibility of a Deuterated Polybutadiene and Protonated Polybutadiene Blend

H. Jinnai, H. Hasagawa, T. Hashimoto, R. Briber, and C. C. Han.

Inversion of Phase Diagram from UCST to LCST in Deuterated Polybutadiene and Protonated Polybutadiene Blends

H. Jinnai, H. Hasagawa, T. Hashimoto, and C. C. Han.

Phase Separation in Deuterated Polycarbonate/ Poly(methylmethacrylate) Blend Near Glass Transition Temperature
M. Motowoka, H. Jinnai, M. Miyake, T. Hashimoto, Y. Qiu, and C. C. Han.

Competition of Phase Separation and Transesterification in D-Polycarbonate/Co-Polyester Blends
H. Yoon and C. C. Han.

Small Angle Neutron Scattering Studies of Blends Containing Linear and Crosslinked Polymers
B. J. Bauer, R. M. Briber, and C. Cohen.

Conformational Changes in Polystyrene/Poly(vinylmethylether) Blends at Low Polystyrene Composition
B. J. Bauer, R. M. Briber, and B. Hammouda.

Polystyrene/DOP Solutions—Single Chain Behavior Under Shear
A. I. Nakatani, Y.-B. Ban, and C. C. Han.

Polystyrene/Polybutadiene/DOP Solutions—Off Critical Shear Rate Behavior
A. I. Nakatani, Y.-B.Ban, and H. Yajima.

Small Angle Neutron Scattering Studies of Dendrimer Solutions
B. J. Bauer, R. M. Briber, B. Hammouda, and D. A. Tomalia.

Small-Angle Neutron Scattering Study on Weakly Charged Temperature Sensitive Polymer Gels
M. Shibayama, T. Tanaka, and C. C. Han.

Small Angle Neutron Scattering Study on Poly(N-Isopropyl Acrylamide) Gels Near Their Volume-Phase Transition Temperature
M. Shibayama, T. Tanaka, and C. C. Han.

Crossover to Strong Shear in a Low Molecular Weight Critical Polymer Blend
E. K. Hobbie, D. W. Hair, A. I. Nakatani, and C. C. Han.

Participants

Ban, Y.-B.	N.Y. Poly. Inst.
Bauer, B. J.	Polymers Division
Briber, R.	University of Maryland
Cohen, C.	Cornell University
Hair, D. W.	Polymers Division
Hammouda, B.	Reactor Radiation Division
Han, C. C.	Polymers Division
Hasagawa, H.	Kyoto University, Japan
Hashimoto, T.	Kyoto University, Japan
Hobbie, E. K.	Polymers Division
Jinnai, H.	Kyoto University, Japan
Miyake, M.	Kyoto University, Japan
Motowoka, M.	Kyoto University, Japan
Nakatani, A. I.	Polymers Division
Qiu, Y.	East China University of Chemical Technology, China
Shibayama, M.	Kyoto Institute of Technology, Japan
Tanaka, T.	MIT
Tomalia, D. A.	Midland Macromolecular Institute, Michigan
Yajima, H.	Tokyo Science University
Yoon, H.	Polymers Division

EXXON SANS RESEARCH AT CNRF

FY1992 is the first full year in which the NIST/EXXON/U. Minn SANS instrument was fully operational. The Exxon SANS research conducted at NIST in that year can be roughly divided into 3 categories: Polymers, Complex Fluids, and Porous Media. Polymer-related research made up the majority of the SANS experiments, and included studies of thermodynamics of polymer blends, chain dimensions, polymer aggregation, and structure of diblock and grafted copolymers. Complex fluids are solutions of various constituents, e.g., polymer/surfactant mixtures, binary fluids, or micelles solutions. They are studied at different concentrations, temperatures, shear rates, etc, to investigate the corresponding structure changes and their relationship to macroscopic properties. Finally, SANS was used to study the internal structure of various types of microporous materials, including materials with adsorbed fluids. Brief descriptions of the results obtained in some of these experiments are given below. Exxon researchers have also made preliminary studies in the area of neutron tomography and reflectometry.

- **Polyolefin Blends**

The dependence of the Flory-Huggins interaction parameter χ on temperature, composition, and chain length was investigated for binary blends of amorphous model polyolefins, materials which are structurally analogous to copolymers of ethylene and butene-1. The components were prepared by saturating the double bonds of nearly monodisperse polybutadienes with H_2 and D_2, the latter to provide contrast for small angle neutron scattering (SANS) experiments. Polymers with vinyl contents from 8% to 97% were saturated, giving ethylene-butene copolymers ranging over nearly the entire range from polyethylene to polybutene. Values of χ were extracted from SANS data in the single-phase region using the random phase approximation and the Flory-Huggins expression for free energy of mixing. By combining the χ value measured on a blend of the hydrogenous version of one copolymer with the deuterated version of another (HA/DB) with that measured on a blend with the labeling reversed (DA/HB), we have been able to obtain an estimate of the χ between the hydrogenous versions of the two polymers (HA/HB). These values were found to be insensitive to chain length (one test only) and to the component volume fractions for ϕ = 0.25, 0.50, and 0.75. Their temperature dependence (27 - 170 °C) obeys the form $\chi(T) = A/T + B$ with coefficients that connote upper critical solution behavior. These estimates are consistent with SANS pattern changes and supplemental light scattering results that indicate two-phase morphologies at lower temperatures. The $\chi(T)$ coefficients are not consistent with the random copolymer equation. The interaction parameter obtained for branch C_4 - linear C_4 chain units is similar to that found by Crist and coworkers for saturated polybutadienes with lower ethyl branch contents.

- **Structure of Diblock Co-Polymer Aggregates in Solution**

A variety of scattering techniques have been employed to study the structure of diblock copolymer aggregates in solution. The system of interest is an anionically prepared poly(styrene-isoprene) diblock copolymer (PS-PI) with well defined molecular weight and composition. When the diblock copolymer is added to decane, which dissolves the polyisoprene but not the polystyrene, polymeric micelles formation at concentrations above a critical micellar concentration has been observed. The aggregation number is determined by light scattering and neutron scattering to be roughly 120. The micellar aggregate consists of a spherical polystyrene core with a mean radius of 105 Å surrounded by a PI corona. The size distribution is quite narrow (< 10%). The PS core is swollen with the solvent by roughly a factor of 2 in volume. By combining dynamic light scattering and SANS, the thickness of the corona is shown to be 50 Å, which is 70% larger than the radius of gyration of a free PI chain of the same molecular weight in a good solvent. Furthermore, SANS measurements suggest that the aggregates form an ordered phase at the nominal cross-over concentration as expected for highly functionalized star-branched macromolecules in solution.

- **Structure and Ordering Phenomena of Star Polymers in Solution**

Star polymers are built from linear polymers joined covalently to a common center. If they are monodisperse with respect to functionality and arm length they are called regular stars. The conformation of star-shaped polymers has been theoretically examined on the basis of scaling theories. Thereby the starting point was the analogy to semidilute polymer solutions considering, however, the spatially inhomogeneous monomer densities of star polymers. Witten et al. [1] investigated the concentration dependence of the osmotic pressure in star polymer solutions around the overlap concentration. The main outcome of their considerations is the prediction of a repulsive interaction between stars resulting from the large osmotic pressure inside a star molecule. This interaction should lead to ordering phenomena in star polymer solutions around the overlap concen-tration. Dependent on functionality, liquid-like ordering or even the formation of a macrocrystal could be expected. The structure factor S(Q) of such a system should display a peak indicating the preferred spatial distance between particles. Some earlier light and neutron scattering studies have already indicated some evidence of liquid-like ordering phenomena in star polymer solutions.

Detailed investigations of the ordering phenomena in star polymer solutions, varying the functionality of the stars between 8 and 64, have been carried out in this study with SANS. In all cases we observed a structure factor which is most pronounced at the overlap concentration. The ordering tendency increases with increasing functionality; at f-64 there is evidence for formation of a macrocrystal.

- **Aggregation of Associating Polymers**

Small angle neutron scattering measurements were performed on solutions of sodium sulfonated polystyrene in non-polar solvents. The effect of varying the sulfonation level of the ionomers as well as the molecular weight of its precursors on its associating behavior was investigated. Two different molecular weights of single chains were studied in the dilute concentration range. The charge level was varied from low to moderate sulfonation contents. Contrast matched experiments were also carried out in order to investigate the conformation of the single chains within the aggregates. Furthermore, telechelics polymers, which are ionomers with only one ion at each end of backbone, were analyzed to compare with those ionomers containing a very small number of ions randomly attached to the chain backbone.

From these studies, we conclude that no aggregation occurs when low ionic charge levels are randomly situated along the chain. However, marked aggregation is observed when the same level of ionic functionality is placed at the end of the chain. This conclusion correlates well with the rheological behavior of these materials. We have also found that the aggregation phenomenon of ionomers is best described by a closed association and an open association model at relatively low and moderate ionic contents, respectively. It is anticipated that the information on the structure-property relationships of these specific ion-containing polymers are applicable to other associating polymer systems, in general.

- **Polymer-Surfactant Assemblies in Water**

It is well known that nonionic polymers such as poly (ethyleneoxide) (PEO) or poly(vinyl-pyrrolidone) (PVP) form self-assembled water soluble complexes with sodium dodecyl sulfate (SDS). However, questions remain about the effect of SDS on the conformation of the polymer coil in water as well as the interaction of the polymer coil with neighboring coils. Most notably, aqueous solutions containing a mixture of surfactant and polymer exhibit interesting features in terms of their viscosity that could be attributed to conformational changes or to changes in strength of interaction between the charged coils. In this work we attempt to explain the macroscopic viscosity of PEO-SDS solutions on the basis of the configuration of the macromolecules and their mutual interaction. It is found, by SANS experi-ments, that it is the intra-, not inter-, molecular ionic interaction that is responsible for the initial increase of the viscosity of the solution as a function of the surfactant concentration. This is caused by a stretching of the macromolecules due to the attachment of the ionic micelles and their interactions. However, further addition of the surfactants beyond a saturation point only under-

mines these interactions as a result of higher free surfactant concentration in the solution. This explains the dip in the viscosity-SDS concentration plot. The effect of additional salt in the solution is also investigated.

Reference

[1] T. A. Witten, P. A. Pincus, and M. E. Cates, Europhys. Lett. 2, 137 (1986).

Experiments

Thermodynamics of mixing polyolefin blends
D. J. Lohse, L. J. Fetters, R. Krishnamoorti, W. W. Graessley, C. C. Han, and N. Hadjichristidis.

Polymer-surfactant assemblies in water
M. Y. Lin, S. K. Sinha, and K. Chari.

High functionality star polymers
L. J. Fetters, J. S. Huang, M. Y. Lin, D. Richter, O. Jacknischke, L. Willner, J. Roovers, P. Toporowski, and L. L. Zhou.

Formation of worm-like micelles under shear
M.-W. Kim, M. Y. Lin, S. K. Sinha, D. G. Peiffer, H. Hanley, and G. Straty.

Aggregation of associating polymers
D. G. Peiffer, M. Y. Lin, A. Timbo, and J. S. Higgins.

Binary fluid in a fractal silica gel
M. Y. Lin, S. K. Sinha, B. J. Frisken, and D. S. Cannell.

Diblock copolymer aggregates in solution
J. S. Huang, L. J. Fetters, J. Sung, M. Y. Lin, D. Richter, B. Farago, and A. P. Gast.

PEP-PE diblock copolymers in solution
J. S. Huang, S.-L. Chang, and L. J. Fetters.

Crosslinked copolymer membranes
M. Y. Lin, S. K. Sinha, W. S. Ho, G. Satori, and J. P. Stokes.

Wax crystallization
S. K. Sinha, M. Y. Lin, B. G. Silbernagel, and J. P. Stokes.

Grafted copolymers under stretching
D. G. Peiffer, M. Y. Lin, and W. Dozier.

Solid state structure of polyolefin blends
F. C. Stehling and A. Hanyu.

Ordering in microporous silica and silica/alumina
D. E. W. Vaughan, J. W. Johnson, and M. Y. Lin.

Structure of porous Si_3N_4/SiC and their precursors
J. W. Johnson and M. Y. Lin.

Neutron radiography/tomography
J. H. Dunsmuir, S. K. Sinha, and M. Y. Lin.

Neutron reflectivity from polymer on surfaces
D. Perahia, L. J. Fetters, S. K. Sinha, S. K. Satija, and D. Weisler.

Participants

Abeles, B.	Exxon
Balsara, N. P.	Polytechnic University
Cannell, D. S.	U. of California (SB)
Chang, S.-L.	Tsinghua University, Taiwan
Chari, K.	Kodak
Dozier, W.	Argonne National Lab
Dunsmuir, J. H.	Exxon
Farago, B.	ILL, France
Fetters, L. J.	Exxon
Frisken, B. J.	Simon Fraser U., Canada
Gast, A. P.	Stanford University
Graessley, W. W.	Princeton University
Hadjichristidis, N.	University of Athens, Greece
Han, C. C.	Polymers Division
Hanley, H.	NIST, Boulder
Hanyu, I.	Exxon
Higgins, J. S.	Imperial College, UK
Ho, W. S.	Exxon
Huang, J. S.	Exxon
Jacknischke, O.	KFA, Germany
Johnson, J. W.	Exxon
Kim, M.-W.	Exxon
King, H. E.	Exxon
Krishnamoorti, R.	Princeton University
Lin, M. Y.	Exxon
Lohse, D. J.	Exxon
Peiffer, D. G.	Exxon
Perahia, D.	Exxon
Richter, D.	KFA, Germany
Roovers, J.	NRC, Canada

Satori, G.	Exxon	Sung, J.	Exxon
Silbernagel, B. G.	Exxon	Timbo, A.	Imperial College, UK
Sinha, S. K.	Exxon	Toporowski, P.	NRC, Canada
Sirota, E. B.	Exxon	Vaughan, D.E.W.	Exxon
Stehling, F. C.	Exxon	Willner, L.	KFA, Germany
Stokes, J. P.	Exxon	Zhou, L. L.	NRC, Canada
Straty, G.	NIST, Boulder		

UNIVERSITY OF MINNESOTA PROGRAMS

The University of Minnesota, through its Center for Interfacial Engineering, is a member of the CNRF's participating research teams (PRT) in small angle scattering (with NIST and the Exxon Research and Engineering Co.) and reflectometry (with NIST and IBM).

SANS

- **Block Copolymer Phase Behavior Near the Order-Disorder Transition**

Until recently block copolymers were predicted and assumed to conform to a single universal phase diagram described by χN and f where χ is the segment-segment interaction parameter, N is the degree-of-polymerization and f is the composition. Four equilibrium phases have been demonstrated based on polystyrene-polyisoprene (PS-PI) diblock copolymers: cubic packed spheres (S), hexagonally packed cylinders (Hex), lamellae (L) and ordered bicontinuous double diamond (OBDD). A series of polyolefin diblock copolymers consisting of polyethylene (PE), poly(ethylethylene) (PEE), and poly(ethylenepropylene) (PEP) blocks have been polymerized with varying N and f, and studied by SANS. In order to facilitate the identification of phase symmetry, dynamic shearing has been applied to these materials either prior to study or during the scattering experiments. Approximately 40 PEP-PE, PE-PEE, and PEP-PEE diblock copolymers have been investigated at various compositions between f = 0.25 and 0.77. We have discovered a variety of order-order transitions that have been related to rheological transitions. Several new phases, including two modulated lamellar phases and a perforated lamellar phase, have been documented. These results cannot be explained by current theory and are inconsistent with the concept of a universal block copolymer phase diagram based on χN and f alone. Based on these SANS experiments we have concluded that a new parameter, conformational asymmetry, is important in determining phase behavior in block copolymer melts.

- **Influence of Shear on the Block Copolymer Order-Disorder Transition**

Commercially important block copolymers are usually processed by heating through the order-disorder transition (ODT) prior to extrusion, shearing, or some other applied deformation. However, essentially all microscopic structural measurements such as transmission electron microscopy, small-angle x-ray and neutron scattering have been conducted in the undeformed state. This research program is directed at developing a comprehensive understanding of how block copolymer melt phase behavior is influenced by deformation (e.g., shear) rate, amplitude, and proximity to the order-disorder transition. We have designed and constructed a parallel plate shearing device that operates in a simple shear geometry. A series of experiments on a poly(ethylene-propylene) poly(ethylethylene) (PEP-PEE) diblock copolymer, characterized by an ODT at 90 °C revealed an increase in T_{ODT} with increasing shear rate. A second thermodynamic stability limit was also discovered in this material. These findings provide quantitative support for the predictions of Cates and Milner [1] regarding the influence of shear on lamellar forming mesomorphic materials near the ODT.

- **Structure of Core-Shell Latex Particles**

The production of latex particles for use in paints and other coating materials involves a complex sequence of chemical reactions. Controlling the size and composition of the product

requires an understanding of the mobility of the polymeric components within a growing latex particle. Experiments have been designed whereby the sequential addition of deuterated and protonated monomers leads to the formation of isotopically labeled core-shell particles. SANS analysis of these microscopic spherical particles followed by modeling based on classical spherical structure factors that incorporate graded contrast factors has led to a better understanding of the migration of polymer and monomer out of and into the structure during reaction. Initial results suggest a size dependent mobility that may be correlated with the polymer radius-of-gyration.

- **Phase Behavior of Oil/Water/Surfactant Systems**

When surfactants are added to water-oil mixtures, a plethora of complex and often poorly understood phases can result. In this program we are exploring such behavior using a variety of silicon containing nonionic surfactants. Initial experiments have focused on exploiting the contrast variation technique in order to establish the relative location of the hydrophobic moity in spherical micelles at low surfactant concentrations and in bicontinuous structures at high concentrations. In the latter the hydrophobic moity appears to form an interconnected and highly structured network while the water soluble (ethylene oxide) head group assumes a mostly structureless form. The "anomalous" phase (L_3) has also been studied using a new trisiloxane surfactant. This state occurs at low surfactant concentrations and is situated between the water and lamellar liquid crystal phases. Contrast variation experiments revealed that the L_3 phase consists of a watersurfactant bicontinuous microstructure. SANS measurements also confirmed that an isotropic liquid phase (L_1) exists above the cloud-point temperature.

- **Polymer-Surfactant Interactions in Aqueous Solution**

SANS experiments on a dilute lamellar (beta) phase surfactant system composed of sodium dodecyl sulfate/dodecanol/water were performed to measure the water layer and hydrocarbon layer thicknesses. The effect of water soluble polymers (Poly(ethylene glycol) and Poly(acrylic acid)) on the bilayer dimensions was also studied. These systems are used for preparing emulsions of monomers for emulsion polymerization and an important property of these compositions is the interlamellar water layer thickness. The SANS experiments showed that the water layer spacings of these dilute compositions are 40 nm, and the hydrocarbon layer thickness is 3.5 nm. The addition of water soluble polymers to these lamellar dispersions resulted in an osmotic compression of the water layers.

Reflectometry

- **Structure of Block Copolymer Thin Films and Surfaces**

Several principal applications of block copolymers take advantage of the unique surface characteristics achievable in bulk pieces and thin films of these materials. Pressure sensitive adhesives, lubricants, and surface active additives to plastics are representative examples. This program aims to elucidate the complex interplay between molecular weight, composition, block conformation and film dimensions, with microstructure and surface activity. Current applications of block copolymers as interfacial agents are based in large part on an Edisonian approach. Our efforts have begun to reveal a host of interesting and potentially controllable physical phenomena. In a recent discovery, three different model polyolefin block copolymers, containing equal molecular weight blocks, were found to produce thin films in which the same block segregated to both the high energy substrate and air interface. Such symmetric films are not anticipated based on traditional enthalpic arguments, but can be explained on entropic grounds that derive from the differences in block conformations. Experiments with off-symmetry compositions (e.g., $f = 0.75$ where f is the volume fraction of one block) reveal a change in film microstructure from a lamellae to hexagonally packed cylinders. Significantly, this change in microstructure eliminates the islands and holes that occur with the symmetric ($f = 0.50$) films. At intermediate compositions ($f = 0.65$) we have discovered temperature-induced changes in microstructure that can be related to phase transitions that occur in the bulk state. In practice controlling these factors would be accomplished by blending block copolymers with different

compositions. Our initial results with such mixtures leads us to conclude that thin film topology and microstructure can be better optimized with blending, than by producing a single intermediate composition or molecular weight material.

Reference

[1] Cates, M. E. and Milner, S. T. *Phys. Rev. Lett.* **62** (1989) 1856.

Experiments

Order and Disorder in Model Polyolefin Diblock Copolymers
J. Rosedale, I. Hamley, K. Koppi, F. S. Bates, K. Almdal, and K. Mortensen

Order-Order Phase Transitions in Model Polyolefin Diblock Copolymers
J. Rosedale, I. Hamley, K. Koppi, F. S. Bates, K. Almdal, and K. Mortensen

Shear Induced Order in a Nearly Symmetric Model Polyolefin Diblock Copolymer
K. Koppi, M. Tirrell, and F. S. Bates

Limits of Thermodynamic Stability of Disordered Diblock Copolymer Under Dynamic Shearing
K. Koppi, M. Tirrell, and F. S. Bates

Lamellae Orientation in Dynamically Sheared Diblock Copolymer Melts
K. Koppi, M. Tirrell, and F. S. Bates

SANS on Selectively Labeled Polymethylmethacrylate Latex Particles
C. Allen, H.-Y. Parker, and N. Shah

Micelle to Bicontinuous Structure Transition in a Nonionic Silicone Surfactant/Water Binary Solution
M. He, H. T. Davis, L. E. Scriven, F. S. Bates, and R. M. Hill

Microstructure of L_3 Phase of a Trisiloxane Surfactant in Water
M. He, H. T. Davis, L. E. Scriven, F. S. Bates, and R. M. Hill

SANS from Dilute Lamellar Surfactants
K. P. Ananth, F. Hessel, A. Karim, and F. S. Bates

Surface Segregation in Symmetric Polyolefin Diblock Copolymers
F. S. Bates, A. Karim, C. F. Majkrzak, S. K. Satija, M. Sikka, and N. Singh.

Structure of Asymmetric Block Copolymer Thin Films
F. S. Bates, A. Karim, C. F. Majkrzak, S. K. Satija, M. Sikka, and N. Singh.

Phase Transitions in Block Copolymer Thin Films
F. S. Bates, A. Karim, C. F. Majkrzak, S. K. Satija, M. Sikka, and N. Singh.

Structure of Thin-Films Containing Mixtures of Block Copolymers
F. S. Bates, A. Karim, C. F. Majkrzak, S. K. Satija, M. Sikka, and N. Singh.

Participants

Allen, C.	Rohm and Haas Company, PA
Almdal, K.	Risø National Lab., Denmark
Ananth, K. P.	Unilever Co., Minnesota
Bates, F. S.	University of Minnesota
Davis, H. T.	University of Minnesota
Hamley, I.	University of Minnesota
He, M.	University of Minnesota
Hessel, F.	Unilever Co., Minnesota
Hill, R. M.	Dow Corning Corp.
Karim, A.	University of Maryland
Koppi, K.	University of Minnesota
Majkrzak, C.	Reactor Radiation Division
Mortensen, K.	Risø National Lab., Denmark
Parker, H.-Y.	Rohm and Haas Company, PA
Rosedale, J.	University of Minnesota
Satija, S.	Reactor Radiation Division
Scriven, L. E.	University of Minnesota
Shah, N.	Rohm and Haas Company, PA
Sikka, M.	University of Minnesota
Singh, N.	University of Minnesota
Tirrell, M.	University of Minnesota

CNRF INSTRUMENTATION DEVELOPMENT

FY92 saw very significant progress made in a broad spectrum of CNRF instrumentation. This includes the installation and initial operation on NG-3 of the National Science Foundation (NSF)/ NIST 30-m SANS—the principal instrument of the Center for High Resolution Neutron Scattering (CHRNS); the installation and initial operation of the medium-resolution time-of-flight spectrometer; the installation of the cold neutron reflectometer; and the completion of fabrication of the NSF/NIST Cold Neutron Triple-axis Spectrometer. Progress in the development of neutron capillary guides has also been impressive; and design and testing of components of the back-reflection spectrometer and high-resolution time-of-flight spectrometer have continued.

Instrumentation related to Fundamental Neutron Physics and to prompt-gamma activation analysis and cold neutron depth profiling is described elsewhere in this report.

New Instruments

- **The Center for High Resolution Neutron Scattering**

CHRNS was established by a joint agreement between the NSF and NIST in March 1989 to provide state-of-the-art cold neutron scattering instrumentation for use by the general scientific community at NIST's CNRF. Under this agreement, NSF has supported the design and construction by NIST of a general purpose, high resolution, 30-m small angle neutron scattering (SANS) instrument, and is jointly supporting with NIST the construction and operation of a cold neutron polarized beam triple-axis spectrometer (known as SPINS for Spin Polarized Inelastic Neutron Scattering).

The CHRNS 30-m SANS instrument, as shown in Figure 1, was commissioned in August and is operational on a dedicated neutron guide, NG-3. With the NIST/Exxon/U. of Minnesota 30-m SANS instrument, the CNRF has the first SANS instruments in the United States to combine the use of cold (long wavelength) neutrons with efficient beam collimation over long distances to achieve resolution and measurement range that are comparable to that of the best such instruments in the world. The allocation of beam time on the CHRNS SANS instrument is based on peer review of proposals submitted to the Program Advisory Committee (PAC) that allocates time to the general scientific community on all of the CNRF instruments. Up to 75% of the beam time on the CHRNS SANS instrument (amounting to roughly 190 days per year) is available to the general Researcher community.

The principal design features have been described in detail elsewhere [1,2], and are updated in Table 1 to include the actual measured intensity at the sample. It should be noted that this instrument is the first in the United States to utilize a high data rate 2-d position sensitive detector (65 $\times$ 65 cm^2 with 1 cm resolution) of the ILL-type, capable of counting at rates in excess of 30,000/ sec. To take full advantage of this high count rate capability, the instrument's post-sample vacuum flight path has been designed to allow the detector to approach within 1.3 m of the sample. The detector moves along rails inside the flight path to vary the sample-to-detector distance from 1.3 m to 13 m, and in addition, moves transverse to the beam direction (up to 30 cm) to extend the Q-range covered at a particular detector distance. As a result the instrument is not only able to perform high resolution (low-Q) measurements, but also covers a wide Q-range, and significantly improves current capabilities for time-resolved SANS measurements.

- **The NIST/IBM/U. Minn Neutron Reflectometer**

In the past 10 years there has been growing interest in a variety of surface sensitive techniques including, most recently, neutron reflection from surfaces. A neutron reflectivity program using a new thermal neutron reflectometer has already been highly successful. From this, methods and techniques have been developed to be used in the new cold neutron reflectometer installation of which is nearing completion in the guide hall. The design goal for this new instrument is the ability to do measurements of reflectivities of order $\leq 2 \times 10^{-7}$. The spectrometer, shown schematically in Figure 2, utilizes a pyrolytic graphite crystal array to both monochromate and vertically deflect the

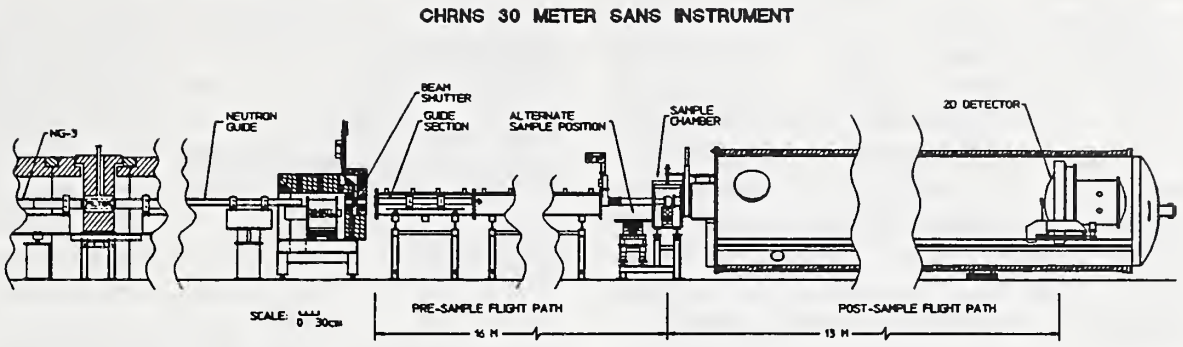

Figure 1. CHRNS 30-m SANS instrument.

Table 1. CHRNS 30-m SANS Characteristics and Performance

Source:	neutron guide (NG-3), 6 × 6 cm^2
Monochromator:	mechanical velocity selector with variable speed and pitch
Wavelength Range:	0.5 nm to 2.0 nm
Wavelength Resolution:	8% to 30% $\Delta\lambda/\lambda$ (FWHM)
Source-to-Sample Dist.:	3.5 m to 16 m in 1.5 m steps via insertion of neutron guide sections
Sample-to-Detector Dist.:	1.3 m to 13 m continuously variable
Collimation:	circular pinhole collimation
Sample Size:	0.5 cm to 2.5 cm diam
Q-Range:	0.01 to 6.0 nm^{-1}
Size Regime:	0.5 nm to 500 nm
Detector:	65 × 65 cm^2 ^{3}He position sensitive proportional counter (1 × 1 cm^2 resolution), ILL type
Ancillary Equipment:	- automatic multispecimen sample changer with temperature control from -10 to 200 C - electromagnet (0 to 15 Kgauss) - couette type shearing cell - cryostats and vacuum furnace (10 to 1800 K)

Neutrons on Sample vs. Q_{min}

$Q_{min}(nm^{-1})$	$I_s a$(n/sec)
0.015	3.7×10^3
0.030	3.4×10^4
0.050	2.6×10^5
0.10	1.0×10^6
0.20	3.5×10^6

[a] for 1.5 cm diam sample and $\Delta\lambda/\lambda$ = .25 at 15MW reactor power.

neutron beam onto a horizontal sample. This configuration allows the measurement of reflectivities of liquid surfaces. The instrument will have two detectors—one at small angles to measure specular reflectivities, and another capable of scanning a large angular range in order to perform surface diffraction measurements. Independent movement of both sample and detector will be provided to allow measurement of off-specular scattering. Some of the important instrumental parameters are listed in Table 2.

- **The Medium Resolution Time-of-Flight Spectrometer [3]**

The medium-resolution Time-of-Flight Spectrometer on the NG-6 guide became operational in February 1992, initially using the double PG(002) monochromators that were previously employed in the Reactor-Hall configuration. To maximize the fluence rate on the sample, these monochromators have recently been replaced by larger PG(002) monochromators which utilize the entire beam cross section. Neutrons

Table 2. Reflectometer characteristics

Monochromator:	Pyrolitic graphite
Wavelength range:	0.235 nm and 0.404 - 0.55 nm
Wavelength resolution:	1% to 2% $\Delta\lambda/\lambda$
Beam size (continuously variable):	.05 × 50 mm to 2 × 50 mm
Q range:	0.03 to 4 nm^{-1}
Q resolution:	Variable with slits from .02 to .15 $\Delta Q/Q$
Polarized beam:	Both initial and reflected beam polarized by multilayer transmission polarizers
Monochromator-to-sample distance:	2 m
Sample-to-detector distance	
a) for reflectivity detector:	2 m
b) for grazing incidence diffraction detector:	1.5 m
Angular range for grazing incidence diffraction detector:	5°- 140°

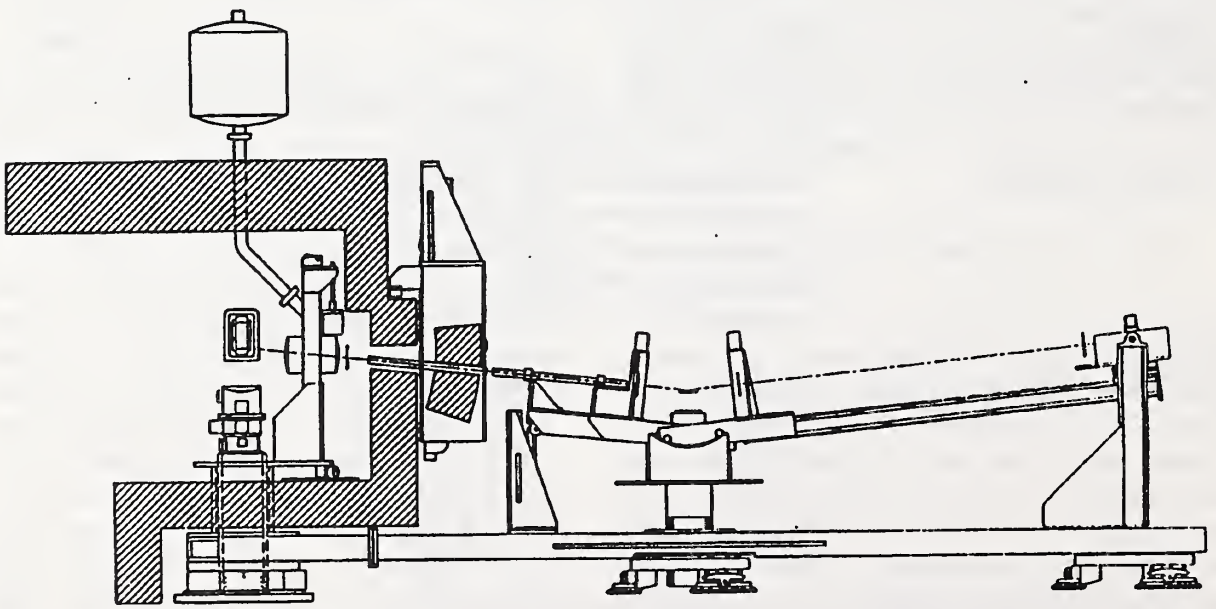

Figure 2. Side view of the NIST/IBM/U. Minn. reflectometer.

from this large cross section are Bragg-reflected using a flat first monochromator then focussed onto the sample using an adjustable vertically-curved second monochromator. To further augment the fluence rate without a degradation in vertical-focussing, both monochromators are constructed of two layers of PG(002) crystals with a horizontal angular offset of 25'. Each layer possesses an isotropic mosaic of ~25', thus yielding the same overall vertical mosaic of only 25', yet an effectively larger horizontal mosaic of ~50'. A new, larger collimator (60') is situated between the monochromators. Additional detectors have been installed in the flight path, filling all remaining gaps within the available range of scattering angles.

An oscillating radial collimator is being installed between the sample and the flight path to shield the detectors from neutrons scattered from non-sample positions. We anticipate that the instrument will become available to outside users in the next Call for Proposals (deadline Jan. '93).

- **Multiple Disk Chopper Time-of-Flight Spectrometer**

This instrument will use a set of seven chopper disks, and a partitioned guide, to produce pulses of neutrons of a single wavelength at the sample position. The first and last pairs of choppers determine the incident wavelength whereas the three intermediate choppers remove contaminant wavelengths and unwanted pulses [3]. There are three slots in each of the disks belonging to the first and last counter-rotating chopper pairs. By appropriately phasing these disks the resolution of the instrument can be changed, without having to change the incident wavelength or the speed of the choppers. The sample chamber will accept a variety of types of cryostats or furnaces, providing the capability to locate the sample at the correct position and in the desired orientation. Detectors will be placed 4 meters from the sample, in three parallel banks. Their total active area will be about 10 m^2.

The chopper system is undergoing final tests at the manufacturer (Uranit GmbH, Jülich, Germany), and should be shipped before the end of the year. The customized guide system, which includes an optical filter to remove high energy radiation, is presently being fabricated. Work has begun on the design of the sample chamber and flight chamber, and the associated shielding. A full complement of detectors and analog electronics (pre-amplifier, amplifier and discriminator in a single box) has been ordered from Transcal (formerly Xeram), Bollène, France. Extensive tests of prototype detectors have recently been completed, and a final design has been selected; the fill pressure is 6 atmospheres, and the active portion of the detector has a newly developed rectangular cross section, ~10 mm thick, ~32 mm wide, 400 mm long. The fast discriminator was designed at NIST to minimize timing dispersion associated with the broad spectrum of pulse amplitudes received from the amplifier. The design of the digital data acquisition hardware has been started, building on concepts developed by P. A. Seeger at the Los Alamos National Laboratory [4].

Capillary Neutron Optics

Materials analysis techniques involving neutron absorption can attain greater precision with a focused neutron beam. A prototype neutron lens constructed with polycapillary fibers for focusing neutrons has been measured at various stations at the NBSR. The parameters of the neutron beams from the various facilities used are summarized in Table 1. The conditions for measurements performed at the reactor in Kurchatov Institute [5] are also listed for comparison. The size and intensity of the neutron beam are recorded with a Video Radiation Detector (VRD) using a ^{6}LiF scintillation converter film and a imaging chip [6] with a pixel size of 12 μm x 13.7 μm.

The arrangement of the fibers in the lens is such that the fibers further away from the center (defined by the longitudinal axis) have more severe bending. Therefore, the transmission efficiency is lower for the fibers near the circumference than those near the center. We have studied this effect by using a series of masking apertures of various diameters at the entrance of the lens. The transmission as a function of the radius of the aperture is consistently lower than the computer simulations [7]. We attribute the losses to the surface roughness as well as other factors, such as imperfections of the fiber openings, the shape of the capillaries, and, most likely, a misalignment of the fibers.

Where higher orders are present (as on the BT-6 spectrometer), the true gain may be related to the measured gain by

$$\text{Gain}(\lambda) = \{[\alpha(\lambda) + 1]\text{Gain}_{exp}(\lambda) - 1\}/\alpha(\lambda)$$

where $\alpha(\lambda)$ is the ratio of the secondary to the primary components at a given wavelength. The gains after this correction are plotted in Figure 3. The lens has been constructed such that the maximum bending allows full transmission of wavelengths above 0.27 nm, assuming perfect collimation of the incident beam. In reality, this value is higher, since the incident beam always has a certain divergence as well as other gain reduction factors, such as reflectivity and roughness. In fact, both experimental and computer simulation indicate a continuous rise of the gain for wavelength up to 0.31 nm.

Figure 3 also shows the gain at the long wavelength range, as measured at the end position of the cold neutron guide NG3. Essentially, the gain does not vary with wavelength and is stable at about 3.6, indicating that a maximum of transmission has been reached when the wavelength is above 0.5 nm.

Computer simulations [7] have been performed under the various experimental conditions; the results are also listed in table 1. The measured gains are smaller than the simulated gains. The computer model includes the reflectivity as a function of wavelength and angle, but does not include the roughness of the inner wall. Such factors can cause a major reduction in the overall transmitted intensity. However, from the weak wavelength dependence of the gain at longer wavelengths, we conclude that the discrepancy between the predicted gain and the measured gain is attributed to other factors, such as mechanical imperfection rather than the random roughness of the inner wall of the capillaries.

The Hydrogen Cold Source

A liquid hydrogen cold neutron source has been under development to replace the current D_2O ice moderator. The preliminary design was described previously [8]; the final design is as follows. The moderator chamber is a 2-cm thick spherical shell

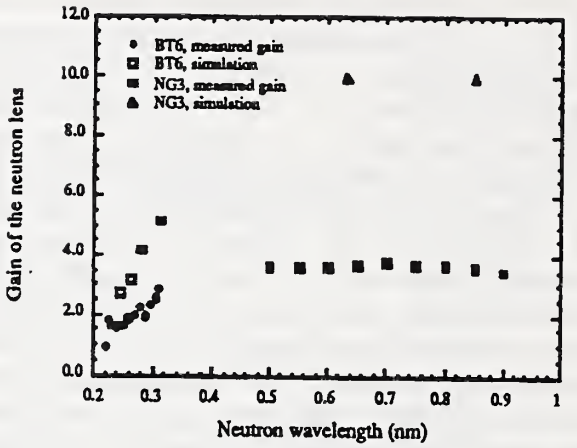

Figure 3. Lens gain as a function of neutron wavelength from the thermal to cold energy range. The gain at long wavelengths is nearly constant.

Table 3. Neutron capillary optics summary

Station	λ(nm)	Divergence (mrad)	Intensity $n\text{-}cm^{-2}s^{-1}$	Δλ/λ	Gain (exp.)	Gain (calc.)
CTW	0.2-0.9	13.5	$1x10^7$	(white)	9[b]	24
NG7	0.4-1.0	31.4	$1x10^8$	(white)	2.7	10
BT6	0.25	17.4	$1x10^6$	0.01	1.6	3
	0.31	17.4			2.7	5
NG3	0.50	20.4	$2x10^6$	0.34 or 0.15	3.6	10
	0.90	36.7	$2x10^5$		3.6	10
IR-8[a]	0.24	6.4	$1x10^6$	0.01	6.5	17

[a]Kurchatov Institute
[b]projected

with an outside diameter of 32-cm and a volume of 5 L; the interior is filled with vapor, creating a cold-neutron flux trap. A 20-cm diam reentrant hole in the back side of the chamber shell fully illuminates the guides with cold neutrons from the flux trap in the interior. Monte Carlo calculations using MCNP [9] were used to determine the shell dimensions optimizing cold-neutron production.

Figure 4 shows the location of the cold source relative to the reactor core and the neutron guides. Because of new geometry, lower temperature, and the greater efficiency of hydrogen as a moderator, the liquid hydrogen source will increase the yield of long-wavelength (> 0.4 nm) neutrons by a factor of 2 to 3 over the D_2O ice. The hydrogen source with a new, 3.5 kW refrigerator will be colder (21 K) than the D_2O (40 K).

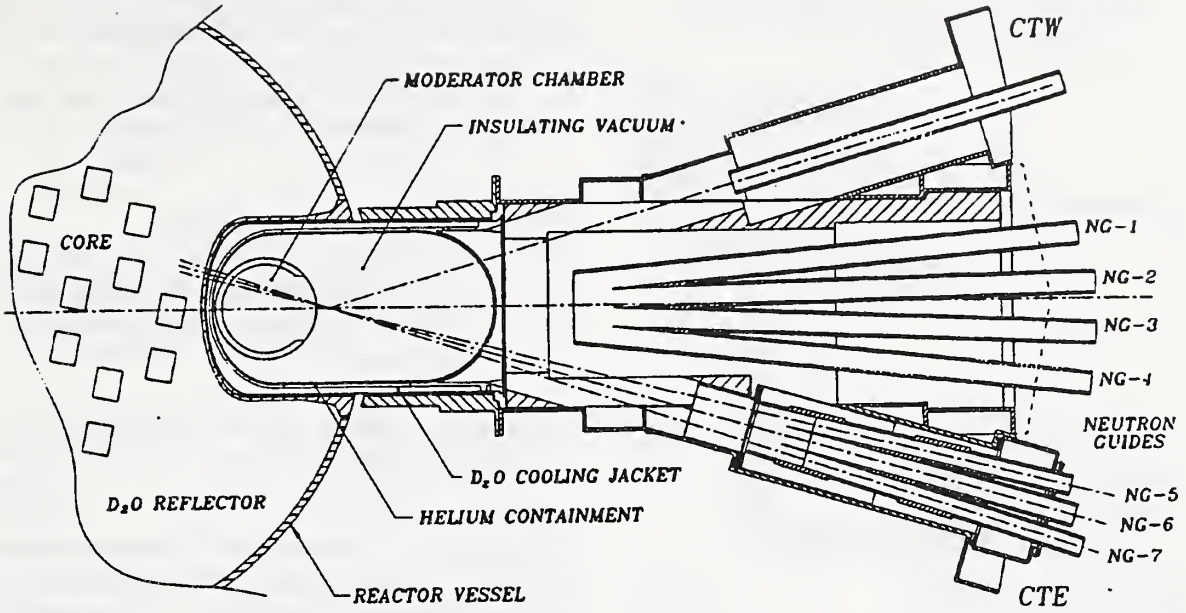

Figure 4. Plan view of the hydrogen cold source in the cryogenic beam port of the NBSR.

About 1000 W will be deposited in the cold source from neutron scattering in the moderator, from gamma-ray absorption in the moderator and Al chamber walls, and from beta- particle absorption in the walls. Hydrogen will evaporate at 2.5 g/s and rise through the outer transfer tube to the condenser as shown in Figure 5. Condensed liquid will flow by gravity through the center tube, completing the thermosiphon. The average hydrogen density in the chamber is expected to be 0.063 g/cm^3, 90% of liquid density at 150 kPa (1.5 atm). About half of the hydrogen inventory of 700 g will be liquified during normal operation, so the system pressure when warm is about 300 kPa.

Each component of the hydrogen system is surrounded by a helium containment above atmospheric pressure. The containment provides another barrier preventing air from mixing with hydrogen, and makes it possible to immediately detect insulating vacuum leaks. Containment or insulating vacuum pressures outside established limits indicate one of the barriers is compromised. The refrigerator will be shutdown, allowing the hydrogen to expand into the ballast tank. The reactor will scram when the hydrogen pressure rises so as not to overheat the moderator chamber.

The ballast tank provides many safety features. A check valve in the supply line to the condenser traps 98% of the hydrogen in the tank in the event of any system failure, even if hydrogen has leaked into an insulating vacuum or helium containment. Once the tank is initially charged with hydrogen, the cold source can be operated and shutdown any number of times without additional gas handling. Hydrogen will be removed only for major repairs, using a portable metal-hydride storage unit. An analysis of the safety issues arising from this cold moderator has been submitted to the Nuclear Regulatory Commission.

A full-scale glass model of the moderator chamber, with a heating element to simulate the reactor heat load, has been built at NIST-Boulder. The hydrogen vapor fraction has been measured as a function of heater power. Preliminary results indicate that very stable flow can be achieved and that the vapor fraction varies linearly with power at roughly 1% per 100 W.

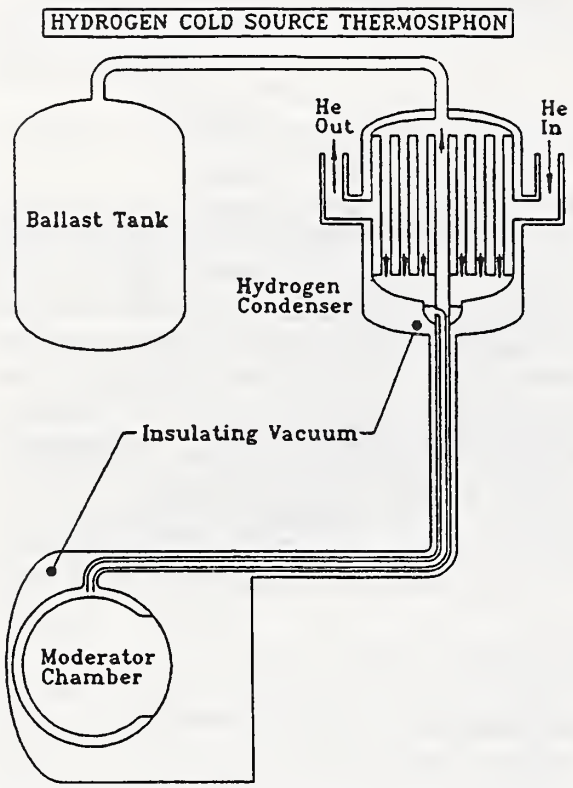

Figure 5. Schematic of the liquid hydrogen cold neutron source. Each component is completely surrounded by a helium containment, not shown.

References

[1] B. Hammouda, C. Glinka, S. Krueger, C. H. Chen, J. Moyer, and W. E. Dickerson, NIST Tech. Note 1292, 160-1 1992.

[2] S. Krueger, B. Hammouda, article in J. Res. series, NIST J. Res. 98, #1 Jan/Feb 1993.

[3] Complete instrumental details given by J.R.D. Copley and T. J. Udovic, in NIST J. Res. 98, #1 1993.

[4] P. A. Seeger, "User's Guide to the Multiple-Independent Detector System," Los Alamos National Laboratory Report LA-9764-M (1983).

[5] M. A. Kumakhov and V. A. Sharov, Nature 357, 390-391 (1992).

[6] R. G. Downing, C. J. Zeissler, and H. Chen, "Neutrons, X Rays and Gamma Rays: Imaging Detectors, Materials Characterization Techniques Applications" (eds., J. M Carpenter and D. F. R. Mildner) SPIE Proceedings 1737, paper 32 (1992).]

[7] X-ray Optics Simulation, Copyright 1992 by X-ray Optical Systems, Inc., Albany, New York.

[8] P. Kopetka, J.M. Rowe and R.E. Williams, NIST Tech. Note 1292, 167-69 (1992).

[9] "MCNP-A General Monte Carlo Code for Neutron and Photon Transport (Version 3A)", LA-7396-M, Rev. 2, J. F. Briesmeister, Ed., Los Alamos National Lab. (1986).

CNRF Instrumentation Titles

Cold Neutron Focusing Using Capillary Optics
H. Chen, R. G. Downing, D.F.R. Mildner, and V. A. Sharov.

Modeling to Optimize Neutron Focusing
D.F.R. Mildner, H. Chen, R. G. Downing, and V. A. Sharov.

The NSF/NIST Center for High Resolution Neutorn Scatterng (CHRNS) 30-m SANS Instrument
B. Hammouda, C. J. Glinka, S. Krueger, and J. G. Barker.

The High-Resolution Multiple-Disk Chopper Time-of-Flight Spectrometer
J.R.D. Copley

The Medium-Resolution Time-of-Flight Spectrometer
T. J. Udovic

The NSF/NIST (CHRNS) Triple-Axis Spectrometer
S. F. Trevino and C. F. Majkrzak

The NIST/IBM/U. of MINN. Cold Neutron Reflectometer
S. K. Satija and A. Karim

A Liquid Hydrogen Cold Neutron Source
R. E. Williams, J. M. Rowe, and P. A. Kopetka.

Fe-Si Supermirror Polarizers
C. F. Majkrzak, J. F. Ankner, and V. Nunez.

NiC-TiMn Supermirror Reflectivity Measurements
C. F. Majkrzak and J. F. Ankner.

NiC-Ti Supermirror Reflectivity Measurements
C. F. Majkrzak and J. F. Ankner.

Neutron Transmission of Bent Kumakov Capillary Tubes
D.F.R. Mildner, H. Chen, and M. A. Kumakhov.

Determination of Neutron Detector Tube Characteristics for Time-of-Flight Measurements
J.R.D. Copley, H. P. Layer, and C. F. Majkrzak.

Composite Pyrolytic Graphite Crystal Monochromator Reflectivity Measurements
D. Neumann, C. W. Brocker, and C. F. Majkrzak.

Full Scale Tests of the Thermal Performance of a Hydrogen Cold Source for the NBSR
J. Seegworth, D. Olson, J. M. Rowe, M. Jones, P. Kopetha, R. E. Williams.

Participants

Ankner, J. F.	Reactor Radiation Division
Baltic, G. M.	Reactor Radiation Division
Barker, J. G.	Reactor Radiation Division
Chen, H.	Inorganic Analytical Res. Div.
Copley, J.R.D.	Reactor Radiation Division
Dickerson, W.E.	Reactor Radiation Division
Downing, R. G.	Inorganic Analytical Res. Div.
Fravel, D. H.	Reactor Radiation Division
Glinka, C. J.	Reactor Radiation Division
Graham, P. H.	Reactor Radiation Division
Greene, G. C.	Reactor Radiation Division
Hammouda, B.	Reactor Radiation Division
Jones, M.	Chemical Sci. & Tech. Lab, NIST Boulder
Kamitakahara, W. A.	Reactor Radiation Division
Karim, A.	University of Maryland
Knill, W. C.	Reactor Radiation Division
Kopetka, P. A.	Reactor Radiation Division
Krueger, S.	Reactor Radiation Division
Kumakhov, M. A.	Inst. for Roentgen Optical Sys.
LaRock, J. G.	Reactor Radiation Division
Layer, H. P.	Reactor Radiation Division
Majkrzak, C. J.	Reactor Radiation Division
Mildner, D.F.R.	Inorganic Analytical Res. Div.
V. Nunez	University of Maryland
O'Connor, C.	Reactor Radiation Division
Olson, D.	Chemical Sci. & Tech. Lab, NIST Boulder
Pierce, D. J.	Reactor Radiation Division
Prask, H. J.	Reactor Radiation Division
Rinehart, M. J.	Reactor Radiation Division
Rowe, J. M.	Reactor Radiation Division
Satija, S. K.	Reactor Radiation Division
Schröder, I. G.	Reactor Radiation Division
Seegworth, J.	Chemical Sci. & Tech. Lab, NIST Boulder
Sharov, V. A.	X-ray Optical Systems, Inc. Albany, NY and Kurchatov Inst. of Atomic Energy, Moscow, Russia
Thai, T.	Reactor Radiation Division
Trevino, S. F.	Army Res., Dev. & Eng. Ctr.
Udovic, T. J.	Reactor Radiation Division
Williams, R. H.	Reactor Radiation Division
Williams, R. E.	Reactor Radiation Division

GUEST RESEARCHERS AND COLLABORATIONS

Interactions with non-Division users have been a feature of the programs at the NBSR since it first became operational in 1969. The first scattering instruments were constructed through cooperative programs with various other agencies, including the U.S. Navy and Army. Virtually all of the experimental programs have involved collaboration or cooperation with outside researchers from universities, industry or other government laboratories. This trend has continued and accelerated in the more recent past, both within the thermal neutron program and in the construction and operation of the CNRF (which was planned from the beginning as a national user facility). The growth and diversity of research participants over the past several years is evident in Figure 1. These numbers are now considerably larger than those of any other major neutron facility in the United States. Outside participants are generally involved in more than one experiment in any one year, but are only counted once. Of particular note is the small number of division staff compared to the total number of participants.

The participants shown in Figure 1 represent 47 U.S. industrial laboratories, 67 universities, 28 other government institutions, and 65 foreign laboratories.

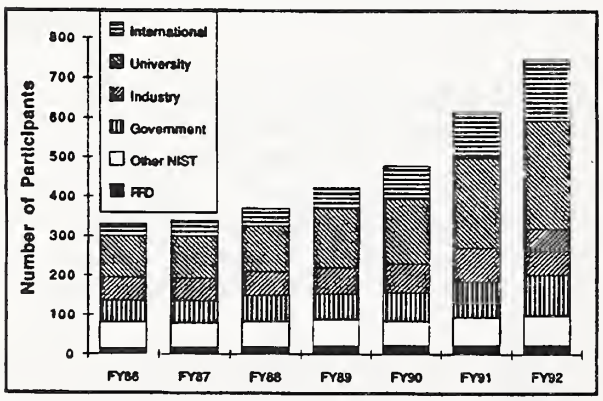

Figure 1. Research participants at the NBSR.

In addition to the rapid growth in use of the NBSR illustrated in Figure 1, there has been a change in the distribution by age of research participants, with growing participation by younger researchers. The current status is shown in Figure 2, which gives the fraction of participants by age for 1991.

It should be noted that most of the participants in the lowest age group in Figure 2 are graduate

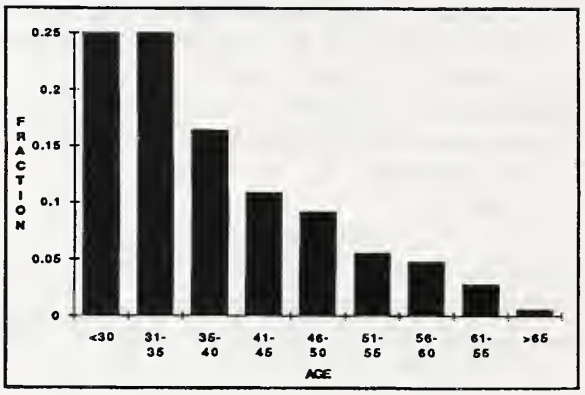

Figure 2. Age distribution of research participants at the NBSR in 1991.

students, who are being trained in the use ofneutron measurement techniques as part of their thesis projects. As a result, they will have an appreciation of the power of these methods, so that the size of the user community can be expected to continue to increase. In effect, this trend will only level off after the current facilities are saturated. We estimate that when the CNRF is complete, the NIST program will saturate near 1000 participants per year.

During the past year, a new (for NIST) mode of user access, a formal user proposal system, has been successfully launched for the facilities of the CNRF. In this mode, prospective users submit a formal written proposal for use of a particular instrument in the CNRF. These proposals are mailed out for peer review, and the final decision on time allocations for the proposals are made by the Program Advisory Committee (PAC), which meets at NIST at least twice per year. The Calls for Proposals contain information concerning available facilities, and are issued at least one month before the proposal deadline.

During the initial year of operation (October 1991 to September 1992), about 90 proposals were received, most for use of the limited time (50%) made available on the NIST/Exxon/UMn 30m SANS, and a smaller block of time on the NSF sponsored SANS facility. The time requested for the SANS facilities exceeded the time available by about a factor of two overall, a factor which will almost certainly grow. While the majority of requests were in the area of polymer research, proposals were also received for materials science, biology, condensed matter physics, and complex fluids studies.

Demand for the two analytical chemistry instruments was substantially lower, primarily reflecting, we believe, the lack of past experience with and availability of comparable facilities. There were, however, notable examples of important applications of these instruments. As the unique capabilities of these facilities becomes better known, we expect demand to increase. In order to develop the community of potential users, special efforts to demonstrate their potential are being pursued, and collaborative use is being encouraged.

For the third call, which was issued in December 1992, limited time on three additional instruments will be available—a cold neutron reflectometer, a medium resolution time-of-flight spectrometer, and the CHRNS triple-axis spectrometer. These instruments, which are being installed and commissioned now, will provide important new capabilities to the U.S. research community.

In addition to the formal outside user program for the CNRF, other modes of access to these facilities and to the other NBSR facilities are in place. Several of the CNRF instruments were built and are operated by Participating Research Teams (PRT's), which share in the cost of instrument development. In return, the PRT members receive 75% of the available time on such instruments, while providing 25% to the general community through the user program described above. Descriptions of the PRT research programs (which often involve non-PRT participants) at these instruments is provided in the other sections of this report.

There are two facilities for fundamental neutron physics at the CNRF—a dedicated cold neutron beam and a neutron interferometry station—which operate in yet another mode. Typically, experiments at these stations are of much longer duration than those at the materials and analytical chemistry stations, and involve highly specialized equipment. As an example, the first experiment scheduled for the cold neutron beam station is a measurement of the neutron lifetime, which will last more than two years, and in which most of the time is spent in developing, testing, and calibrating the necessary equipment. For this type of research, a formal user proposal system is inappropriate. In order to ensure that these facilities properly serve the entire community, an Advisory Committee has been established to advise on appropriate use and on the quality of the science performed.

The non-CNRF facilities at the NBSR are not made available through the formal user program. Nevertheless, through PRT-like and collaborative use, they are made widely available to the U.S. research community. In fact, as can be seen from the descriptions of the research programs of the division elsewhere in this report, virtually all of the research done in the division involves collaboration with outside researchers. As described earlier, many of the instruments were developed in a manner analogous to the PRT mode described above, and the experimental program is operated in the same manner. Several researchers are long term associates—for example, the group from the U.S. Army, which participated in the development of the BT-4 and BT-6 spectrometers has been stationed at NIST for more than 20 years. Other long term cooperative programs have been formed at various times. At present, these include the University of Maryland, Johns Hopkins University, and MIT among others. Similar arrangements with other universities and industrial laboratories are under discussion.

Several non-NIST programs, as well as non-division NIST mission activities are also served by the NBSR facilities in an as-needed mode for services such as irradiation, radiography, or materials characterization. In such cases, the research may be either collaborative or independent, and arrangements are made for each specific use on a case by case basis. Examples include a program with the Smithsonian Institution for autoradiography of paintings; a program with the FDA for characterization of foods or drugs; and activation analysis services for the FBI. In some cases, non-NIST researchers perform proprietary research using the facilities of the NBSR. In these cases, full cost recovery is required.

Thus, the interactions of the Reactor Radiation Division with the research community are extensive and varied. However, the growth in use is constant, and the Division considers the development of new applications of neutron measurement technologies, and encouragement of their use by the broadest possible community as one of its primary missions. In the future, additional mechanisms for interaction will undoubtedly arise, as will new uses of the unique resources provided by the NBSR and its associated experimental facilities.

For further information on the use of the facilities at the NBSR, contact Bill Kamitakahara at (301) 975-6878, or any RRD staff member.

REACTOR OPERATIONS AND ENGINEERING

Once again, reactor operations for the year was routine and uneventful with high productivity. The reactor was on-line 70% of the time which corresponds to more than 95% of scheduled operating time. There were extended shutdowns for repair and installation of guide tubes and for re-examination of licensed operators by the Nuclear Regulatory Commission (NRC). The balance of the down time was required for refueling operations and reactor maintenance. Highlights of significant items are listed below.

Advanced Fuel. The first complete core of new advanced fuel was installed in the reactor during the year. This will extend the life cycle by more than 20%. Overall, fuel utilization, which is by far the best in the United States, has improved more than five times since the original fuel design.

Main Heat Exchangers. Fabrication of major components of the new main heat exchangers will be completed in early 1993 with assembly, testing, and delivery scheduled for the end of 1993. The current heavy utilization of the reactor may require extending the installation schedule. Meantime, reactor operation continues with a single heat exchanger at a power level of 15 MW.

Control Room Upgrades. The reactor control room is nearly 30 years old. Some improvements were incorporated over the years. A complete upgrade is planned once funding becomes available. Next year, a complete replacement and modernization of the reactor annunciator system will be performed in-house.

Staffing. A new regulation by the NRC requires that all licensed operators and senior operators be re-examined prior to renewal of their licenses every six years. The comprehensive examination includes both written and operational tests. All 16 senior operators passed the written portion administered by the NRC with an average score of 94%. Operational tests will be conducted as licenses become due for renewal.

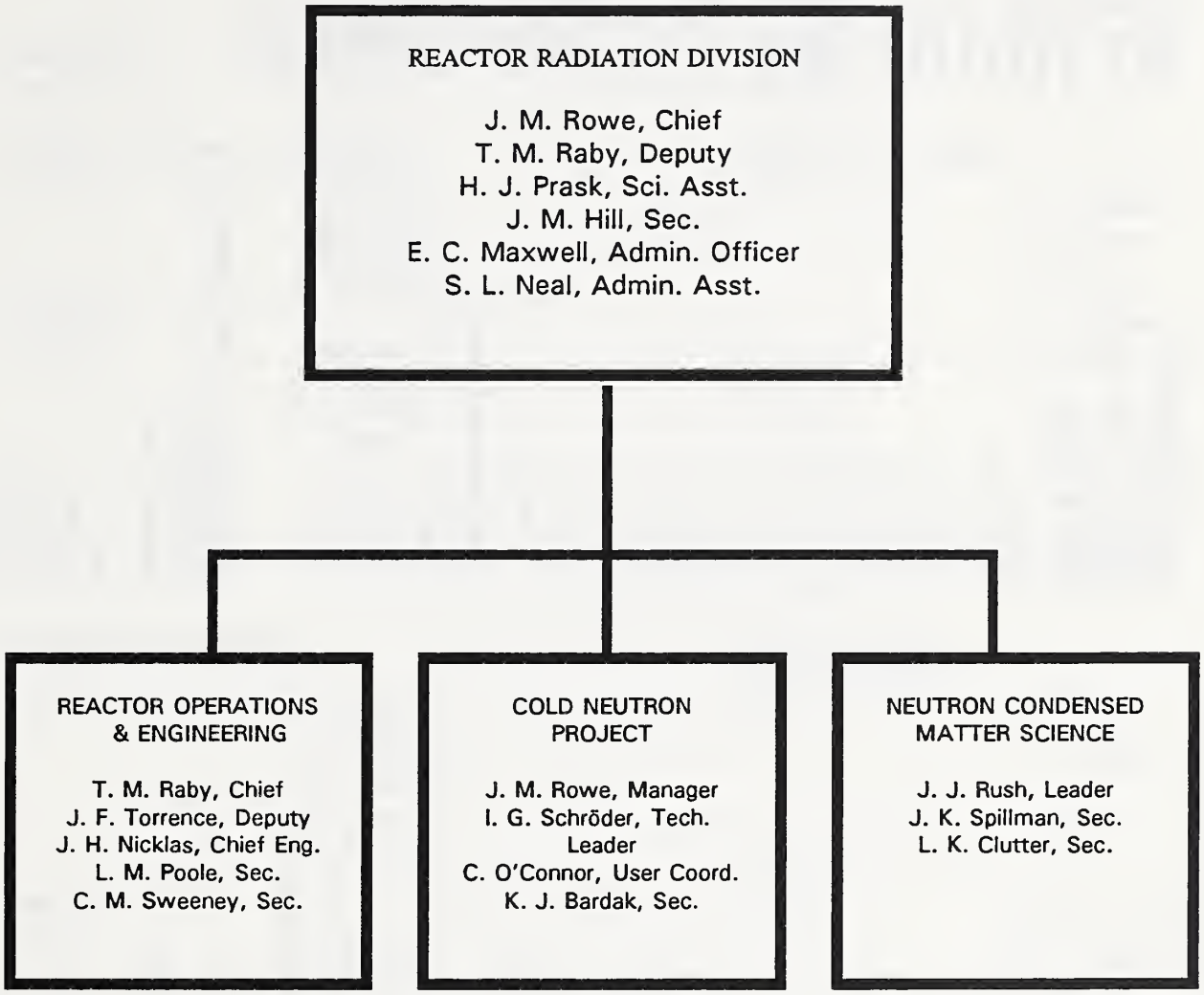

Staffing

The Division staff is organized formally into three groups, as shown in Table 1; however, staff are used where necessary, irrespective of group. Below the group level of organization, personnel are grouped into research teams according to their predominant interest. Once again, these groupings are not hard and fast—there are many overlapping interests. These teams, including long-term guest researchers, are shown in Table 2. A number of "non-resident" Ph.D. students and continuing collaborators from universities and industry are not listed.

It should be noted that members of the Cold Neutron Project are included in the teams by scientific interest, even though in most cases, their predominant responsibility is for CNRF instrument building and/or operation. In fact, they have only 30% of their time given to the conduct of research, while 70% is dedicated to the facility. Likewise, many members of the Neutron Condensed Matter Science Group have sizable CNRF responsibilities, which may amount for as much as 1/2 time when needed.

Table 1. NBSR and CNRF Resident Staff

ADMINISTRATIVE - DIVISION 856
J. M. Rowe, Chief
E. C. Maxwell, Admin. Off.
S. L. Neel, Admin. Asst.
J. M. Hill, Secretary
H. J. Prask, Physicist
D. E. Bredy, Elect. Eng.
J. M. Nicol, Res.Chemist

REACTOR OPERATIONS & ENGINEERING
Reby, T. M., Chief
Poole, L. M., Sec.

Operations
Torrenca, J. F., Deputy
Beeslay, R.D.
Bickford, N. A.
Cessells, M. G.
Clerk, F. C.
Dilks, H. W.
Flynn, D. J.
Guerin, E. L.
Lindstrom, L. T.
McDoneld, M. J.
Mueller, M. W.
Myers, T. J.
Ring, J. H.
Sprow, R. P.
Stiber, R. F.
Thompson, R. G.
Toth, A. L.
Wilkison, D. P.
Wright, K. D.

Engineering
Nickles, J. H., Chief
Sweeney, C. M., Sec.
Beetty, J. A.
Heina, C. J.
Liposky, P. J.
Suther, M.A.
Shumen, L.

Reseerch Associates
Anderson, D. (FDA)
Billos, J.
Bleu, M.
Cheng, T.(Smithsonien)
Cunninghem, W. (FDA)
Dukhen, W.
Olin, J.(Smithsonien)
Cunninghem, R.

NEUTRON CONDENSED MATTER SCIENCE
Rush, J. J., Group Ldr.
Spillmen, J. K., Sec.
Clutter, L. K., Sec.

Ankner, J. F.
Beltic, G. M.
Berk, N. F.
Borchers, J. A.
Bostien, D.
Cesella, R. C.
Clem, D.
Clow, W.
Copley, J. R.
Erwin, R. W.
Fravel, D. H.
Gahring, P.
Graen, T. A.
Karen, V. A.
Knill, W. C.
Lynn, J.
Majkrzak, C. F.
Mighell, A. D.
Neumenn, D. A.
Princa, E.
Reznik, D.
Rinehert, M. J.
Rymes, W. H.
Sentodonato, L.
Sentoro, A.
Setije, S. K.
Stalick, J. K.
Udovic, T. J.
Waisler, D.
Williems, R. H.

Guest Sciantists & Engineers
Broholm, C.
Choi, C. S.
Clinton, T. W.
Frick, B.
Giebultowicz, T.
Hueng, Q. Z.
Karim, A.
Kim, S.
Klosowski, P.
Mrose, M.
Nunez, V.
Rhyne, J.
Skenthekumer, S.
Sumerlin, I.
Trevino, S. F.
Zheng, H.

COLD NEUTRON PROJECT
Rowa, J. M., Ldr.
O'Connor, C. L., Admin.Asst.
Hill, J. M., Sec.
Berdek, K., Clk. Typ.

Berkar, J.
Dickarson, W. E.
Glinka, C. J.
Gorman, W.
Grahem, P. H.
Greene, G. C.
Hemmoude, B.
Kemitakehera W.
Kopetke, P. H.
Kruagar, S. J.
LeRock, J. G.
Layer, H. P.
Pierce, D. J.
Robeson, L.
Rosov, N.
Schrodar, I. G.
Scira, M.
Thei, T. T.
Tobin, P. L.
Williems, R. E.

Guest Sciantists & Engineers
Allen, A.
Brand, P.
Brocker, C.
Christman, R.
Heald, A. E.
Lin, M. Y.
Moyer, J. J.

NEUTRON INTERACTIONS & DOSIMETRY - DIVISION 846
Grundl, J. A., Ldr.
Mattiallo, R., Sec.

Arif, M.
Boswell, E.
Dewey, S.
Eisenheuer, C.
Gilliem, D.
Greene, G.
Littrel K.
McGerry, D.
Richerdson, J.
Schwertz, R.
Snow, M.

HEALTH PHYSICS - DIVISION 354
Slebeck, L., Ldr.
Graen, J., Secretary

Brown, D.
Cempbell, C.
Cessells, L.
Clark, J.
Deardorff, G.
Jensen, I.
Mengers, T.
Shubiek, J.

NUCLEAR METHODS GROUP - DIVISION 834
Greenberg, R., Ldr.
Wilson, J., Secretery

Beckar, D.
Blackman, J.
Chen, H.
Demirelp, R.
Downing, G.
Fitzpatrick, K.
Garrity, K.
Iyenger, V.
Koster, B.
Lamaze, G.
Langland, J.
Lindstrom, D.
Mackay, L.
Mildner, D.
Myers, E.
Normen, B.
Paul, R. L.
Sharov, V.
Truncer, J.J.

Table 2. Staffing

Surfaces and Interfaces

Staff:	J. F. Ankner
	C. F. Majkrzak
	S. K. Satija
	D. Weisler*
Long Term Visitor:	A. Karim[1,*]

Engineering and Instrument Development

Staff:	P. Kopetka*
	J. G. LaRock*
	D. J. Pierce*
	I. G. Schröder*
	R. E. Williams*
Long Term Visitors:	C. Brocker[3,*]
	R. Christman[4,*]
	A. E. Heald[4,*]
	J. J. Moyer[4,*]

Chemical Physics of Materials

Staff:	N. F. Berk
	J.R.D. Copley
	W. Kamitakahara*
	D. A. Neumann
	J. M. Nicol
	J. J. Rush
	T. J. Udovic
Long Term Visitors:	B. Frick
	S. F. Trevino[8]

Microstructure

Staff:	J. Barker*
	C. J. Glinka*
	B. Hammouda*
	S. J. Krueger*
Long Term Visitor:	M. Y. Lin[1,*]

Condensed Matter Physics

Staff:	J. A. Borchers
	R. C. Casella
	R. W. Erwin
	P. Gehring
	J. W. Lynn
	J. L. Robertson[5]
	N. Rosov*
Long Term Visitors:	C. Broholm[6]
	T. W. Clinton[1]
	T. Giebultowicz[7]
	V. Nunez[1]
	S. Skanthakumar[1]
	I. Sumarlin[6]
	H. Zhang[1]

Crystallography and Diffraction Applications

Staff:	V. Karen
	H. J. Prask
	A. D. Mighell
	E. Prince
	A. Santoro
	J.Stalick
Long Term Visitors:	P. Brand[1]
	C. S. Choi[8]
	Q. Z. Huang[1]
	M. Mrose
	I. Natali-Sora[9]

Scientific Assistance and Technical Support

G. Baltic	P. Klosowski
D. Bostian	W. C. Knill
D. Clem	H. P. Layer*
W. Clow	M. J. Rinehart
W. E. Dickerson*	L. Robeson*
D. H. Fravel	W. H. Rymes
W. Gorman	L. Santodonato
P. H. Graham*	M. Scire*
T. A. Green	R. H. Williams
G. C. Greene	T. Thai*
S. Kim*	P. Tobin*

*Primarily associated with CNRF
[1]University of Maryland
[2]Exxon Res.& Eng. Co.
[3]Institute Laue-Langevin
[4]Nesco Design Co.
[5]NRC Post-Doc; left 8/92
[6]Johns Hopkins University
[7]University of Notre Dame
[8]Army RD&E Center
[9]University of Brescia (Italy)

Research and Engineering Staff

J. F. Ankner	o Condensed matter physics o Neutron reflectometry and grazing-angle diffraction o Instrument development
J. G. Barker	o SANS instrumentation and research
N. F. Berk	o Condensed matter theory o SANS theory for microstructure analysis o Computer software for graphics and data analysis
N. A. Bickford	o Reactor operations o Reactor irradiations o Reactor utilization
J. A. Borchers	o Thin-film analysis o Artificially modulated materials o Magnetism
D. E. Brady	o Electrical/electronic engineering o Nuclear reactor instrumentation
R. C. Casella	o Condensed matter theory, including high T_c o Group theory analyses of neutron scattering from condensed matter o Fundamental physics, especially as related to reactor experiments
R. S. Conway	o Electronic engineering o Nuclear instrumentation
J. R. D. Copley	o Time-of-flight spectrometer development o Neutron instrumentation conceptual design o Condensed matter physics
W. E. Dickerson	o Neutron scattering instrumentation o Microcomputer interfacing o Nuclear and engineering physics
R. W. Erwin	o Magnetic materials o Phase transformations o Spin echo techniques o Cryogenics
P. M. Gehring	o Neutron backscattering instrumentation o Magnetic and structural phase transitions in disordered systems o Dynamics of high T_c materials
C. J. Glinka	o SANS microstructure of metals and porous media o Magnetic materials o Cold neutron instrument development

P. H. Graham	o Engineering design
G. C. Greene	o System and user software for cold neutron instrumentation o Spectrometer and data acquisition systems interfaces
B. Hammouda	o SANS from polymers, liquid crystals, and colloids o Dynamics of polymers in solution o SANS instrument development
W. A. Kamitakahara	o The CNRF guest researcher program o Dynamics of disordered solids o Condensed matter physics
V. L. Karen	o Crystal database development o X-ray crystallography
P. A. Kopetka	o Mechanical engineering o Cold source design o Electro-mechanical systems
S. Krueger	o Small angle neutron scattering instrumentation o Microstructure of materials o Biological problems
J. G. LaRock	o Mechanical engineering o Neutron instrumentation design
H. P. Layer	o Electronics and data processing o Advanced instrumentation o Fundamental physics
P. J. Liposky	o Design engineering o Nuclear systems and components
J. W. Lynn	o Condensed matter physics o Magnetic materials o Neutron scattering methods
C. F. Majkrzak	o Condensed matter physics o Polarized neutron scattering and instrumentation development o Neutron reflectivity measurements
A. D. Mighell	o Crystallographic database development o Single crystal diffraction o Theory of crystal lattices
D. A. Neumann	o Condensed matter physics o Two-dimensional materials o Neutron and x-ray scattering instrumentation

J. M. Nicol	o Properties of catalysts and adsorbates o Molecular materials o Division safety
J. H. Nicklas	o Mechanical engineering o Reactor fuel design o Reactor engineering support
D. J. Pierce	o Mechanical engineering o Neutron instrumentation design
H. J. Prask	o Residual stress measurement o Neutron NDE of hardware o Neutron NDE instrumentation
E. Prince	o Structural properties of alloys, catalysts and minerals o Advanced crystallographic refinement methods o Software for materials structure analyses
T. M. Raby	o Reactor operations o Nuclear engineering o Reactor standards
J. L. Robertson	o Quasicrystals o Structure of amorphous solids o Structural properties of alloys
N. Rosov	o Spin echo techniques o Phase transformations o Magnetic materials
J. M. Rowe	o Orientationally disordered solids o Hydrogen in metals o Cold neutron research and instrumentation
J. J. Rush	o Catalysts and molecular materials o Hydrogen in metals o Two-dimensional systems o Inelastic scattering methods
L. Santodonato	o Condensed matter physics o Cryogenics
A. Santoro	o Structure of electronic and structured ceramics o Theory of crystal lattices o Powder diffraction methods

S. K. Satija	o Low-dimensional molecular systems o Fractal aspects of microporous media o Neutron reflectometry
I. G. Schröder	o Cold neutron instrumentation development o Nuclear and engineering physics o Optical devices for neutron transport
M. A. Scire	o SANS equipment maintenance and development o Laboratory assistant
J. K. Stalick	o Neutron and x-ray diffraction o Inorganic chemistry o Crystal database development
M. A. Suthar	o Design engineering o Nuclear systems and components
J. F. Torrence	o Reactor supervision o Reactor maintenance o Nuclear engineering
T. J. Udovic	o Neutron time-of-flight instrumentation o Properties of catalysts and adsorbates o Hydrogen in metals
D. G. Wiesler	o Neutron and x-ray reflectometry o Condensed matter physics o Electrochemistry
R. E. Williams	o Cold neutron source development o Nuclear engineering

PUBLICATIONS

Albinati, A., Becker, P.J., Boggs, P.T., Collins, D.M., Coppens, P., Finger, L.W., Gjonnes, J., Konnert, J.H., Prince E., Spiegelman, C.H., Willis, B.T.M., "Refinement of Structural Parameters," Intern. Tables for Crystallg. C, edited by A.J.C. Wilson (Kluwer Academic Publishers, 1992), p. 593.

An, M., Lu, C., Prince, E., Tolimieri, R., "Fast Fourier Transform Algorithms for Real and Symmetric Data," Acta Cryst. A48, 415 (1992).

An, M., Lu, C., Prince, E., Tolimieri, R., "Fast Fourier Transforms for Space Groups Containing Rotation Axes of Order Three and Higher," Acta Cryst. A48, 346 (1992).

Anderson, R., Mighell, A.D., Karen, V.L., Jenkins, R., Carr, M.J., "Electron Diffraction Databases", Bull. Micros. Soc. Am., in press.

Ankner, J.F., Borchers, J.A., Farrow, R.F.C., Marks, R.F., "Combined Low- and High-Angle X-ray Structural Refinement of a Co/Pt(lll) Multilayer Exhibiting Perpendicular Magnetic Anisotropy," J. Appl. Phys., in press.

Ankner, J.F., Majkrzak, C.F., Homma, H., "Magnetic Dead Layer in Fe/Si Multilayer: Profile Refinement of Polarized Neutron Reflectivity Data," J. Appl. Phys, in press.

Ankner, J.F., "Profile Refinement in Neutron Reflectivity and Grazing Angle Diffraction," in Surface X-ray and Neutron Scattering, Springer Proceedings in Physics, edited by H. Zabel, I.E. Robinson, (Springer-Verlag, New York, Berlin Heidelberg, 1992), pp. 105, in press.

Ankner, J.F., Majkrzak, C.F., "Subsurface Profile Refinement for Neutron Specular Reflectivity," in Neutron Optical Devices and Applications, Proc. SPIE 1738, edited by C.F. Majkrzak, J.L. Wood, (SPIE, Bellinghem, WA) in press.

Ankner, J.F., Majkrzak, C.F., Satija, S.K., "Neutron Reflectivity and Grazing Angle Diffraction," J. Res. (NIST) 98, in press.

Barker, J.G., Glinka, C.J., "Development of a Focusing Mirror for SANS," in Neutron Optical Devices and Applications, SPIE Proc. 1738, edited by C.F. Majkrzak, J.L. Wood, (SPIE, Bellingham, WA), in press.

Beach, R.S., Matheny, A., Salamon, M.B., Flynn, C.P., Borchers, J.A., Erwin, R.W., Rhyne, J.J., "Magnetism and Epitaxy in Lu/Dy/Lu Tri-layers", J. Appl. Phys., in press.

Beach, R.S., Borchers, J.A., Erwin, R.W., Flynn, C.P., Matheny, A., Rhyne, J.J., Salamon, M.B., "Magnetic Order in Dy/Lu Superlattices", J. Magn. & Magn. Mat. 104-107, 1915 (1992).

Berk, N.F., Rush, J.J., Udovic, T.J., Anderson, I.S., "Anomalous Hydrogen Dynamics in Rare Earth Metals," J. Less-Common Metals 172-174, 496 (1991).

Berk, N.F., "Outline of Neutron Scattering Formalism," J. Res. (NIST) 98, in press.

Berliner, R., Smith, H.G., Copley, J.R.D., Trivisonno, J., "Structures of Sodium Metal," Phys. Rev. B, in press.

Borchers, J.A., Carey, M.J., Erwin, R.W., Berkowitz, A.E., Majkrzak, C.F., "Propagation of Antiferromagnetic Order Across Paramagnetic Layers in CoO/NiO Superlattices", J. Appl. Phys., in press.

Borchers, J.A., Salamon, M.B., Erwin, R.W., Rhyne, J.J., Nieuwenhuys, G.J., Du, R.R., Flynn, C.P., Beach, R.S., "Structural and Magnetic Properties of Er Thin Films and Er/Y Superlattices: Modification of the Commensurate Spin States", Phys. Rev. B44, 11814 (1991).

Casella, R.C., Werner, S.A., "Electromagnetic Acceleration of Neutrons," Phys Rev. Lett 69, 1625-1628 (1992).

Chaillout, C., Huan, Q., Cava, R.J., Chenavas, J., Santoro, A., Bordet, P., Hodeau, J.L., Krajewski, J.J., "Synthesis and Crystal Structure of $BaSrCuO_{2+x} \cdot CO_3$," Physica C., in press.

Chen, L.B., Zukoski, C.F., Ackerson, B.J., Hanley, H.J.M., Straty, G.C., Barker, J.G., Glinka, C.J., "Structural Changes and Orientational Order in a Sheared Colloidal Suspension," Phys. Rev. Lett. 69, 688 (1992).

Choi, C.S., Prask, J.J., Orosz, J., "Textures of Tantalum Metal Sheets by Neutron Diffraction," J. Mat. Sci., in press.

Choi, C.S., Prask,. H.J., Orosz, J., "Texture Study of Two Molybdenum Shaped Charge Liners by Neutron Diffraction," J. Mat. Sci., in press.

Christides, C., Neumann, D.A., Prassides, K., Copley, J.R.D., Rush, J.J., Rosseinsky, M.J., Murphy, D.W., Haddon, R.C., "Neutron Scattering Study of C_{60}^{n-} (n=3,6) Librations in Alkali-Metal Doped Fullerides," Phys. Rev. B, in press.

Clinton, T.W., Lynn, J.W., Liu, J.Z., Jia, Y.X., Shelton, R.N., "Magnetic Order of Dy in $DyBa_2Cu_3O_7$," J. Appl. Phys. 70, 5751 (1991).

Clinton, T.W., Lynn, J.W., Lee, B.W., Buchgeister, M., Maple, M.B., "Oxygen Dependecne of the Magnetic Order of Nd in $NdBa_2Cu_3O_{6+x}$," J. Appl. Phys, in press.

Clinton, T.W., Lynn, J.W., Liu, J.Z., Jia, Y.X., Shelton, R.N., "Two-Dimensional Magnetic Correlations and Magnetic Ordering of Dy and Er in $DyBa_2Cu_3O_7$ and $ErBa_2Cu_3O_7$," J. Magn. and Magn. Mater. 104-107, 625 (1992).

Collins, D.M., Prince, E., "Exponential Density: Exact Fitting of Structure Moduli by Entropy Maximization," in Crystallographic Computing 5 from Chemistry to Biology, edited by D. Moras, A.D. Podjarny, J.C. Thierry, (Oxford Univ. Press, 1991).

Composto, R.J., Mansfield, T., Beaucage, G., Stein, R.S., Iyengar, D.R., McCarthy, T.J., Satija, S.K., Ankner, J.F., Majkrzak, C.F., "The Volume Fraction Profile of Terminally Adsorbed Polymers," in Complex Fluids, Materials Research Society Symposium Proc., (MRS, Pittsburgh) in press.

Copley, J.R.D., "Scattering Effects Within an Absorbing Sphere Immersed in a Field of Neutrons," Nucl. Instr. Meth. in Phys. Res. A307, 389 (1991).

Copley, J.R.D., "Monte Carlo Calculation of Multiple Scattering Effects in Thermal Neutron Scattering Experiments: Modification to Spherical Geometry," Computer Physics Comm. 66, 403 (1991).

Copley, J.R.D., "A New Time-of-Flight Spectrometer at NIST," Physica B 180 & 181, 914 (1992).

Copley, J.R.D., Neumann, D.A., Cappelletti, R.L., Kamitakahara, W.A., "Neutron Scattering Studies of C_{60} and Its Compounds," J. Phys. Chem. Solids 53, 1353 (1992).

Copley, J.R.D., Neumann, D.A., Cappelletti, R.L., Kamitakahara, W.A., Coustel, N., McCauley Jr., J.P., Maliszewskyj, N.C., Fischer, J.E., Smith III, A.B., Creegan, K.M., Cox, D.M., "Structure and Low Energy Dynamics of Solid C_{60}," Physica B 180 & 181, 706 (1992).

Copley, J.R.D., Mildner, D.F.R., "Simulation and Analysis of the Transmission Properties of Curved-Straight Neutron Guide System," Nucl. Sci. & Eng. 110, 1-9 (1992).

Copley, J.R.D., Udovic, T.J., "Neutron Time-of-Flight Spectroscopy," J. Res. (NIST) 98, in press.

Depondt, P., Neumann, D.A., Trevino, S.F., "Neutron Scattering Study of Cs-Ammonia Intercalated Graphite," Materials Science Forum 91-93, 271 (1992).

Depondt, P., Neumann, D.A., Trevino, S.F., "Maximum Entropy as a Tool for the Determination of the C-axis Profile of Layered Compounds," Acta Cryst. B, in press.

Elsenhans, O., Buhrer, W., Anderson, I., Nicol, J.M., Udovic, T.J., Rieutord, F., Felsche, J., Sieger, P., Engelhardt, G., "Dynamics of OH and H_2O Groups in Sodalites," Physica B 180 & 181, 661-664 (1992).

Fan, Y., Solin, S.A., Kim, H., Pinnavaia, T.J., Neumann, D.A., "Elastic and Inelastic Neutron Scattering Study of Hydrogenated and Deuterated Trimethylammonium Pillared Vermiculite Clays," J. Chem. Phys. 96, 7064 (1992).

Foster, M.D., Sikka, M., Singh, N., Bates, F.S., Satija, S.K., Majkrzak, C.F., "Structure of Symmetric Polyolefin Block Copolymer Thin Films," J. Chem. Phys. 96, 8605 (1992).

Gehring, P.M., Tranquada, J.M., Shirane, G., Copley, J.R.D., Erwin, R.W., Sato, M., Shamoto, S., "Magnetic Correlations and Energy Gap in Superconducting $YBa_2Cu_3O_{6.6}$ with T_c = 53 K," Phys. Rev. B 44, 2811 (1992).

Giebultowicz, T.M., Klosowski, P., Rhyne, J.J., Samarth, N., Luo, H., Furdyna, J.K., "Incommensurate Antiferromagnetic Order in Strained Layer MnSe/ZnTe Superlattices," Physica B 180 & 181, 485 (1992).

Giebultowicz, T.M., Samarth, N., Luo, H., Furdyna, J.K., Klosowski, P., Rhyne, J.J., "Strain-Engineered Incommensurability in Epitaxial Heisenberg Antiferromagnets," Phys Rev. B 46, 12076 (1992).

Gygax, F.N., Amato, A., Anderson, I.S., Rush, J.J., Schenck, A., "Study of Localisation and Diffusion in Scandium and Yttrium," Zeitschrift für Physikalische Chemie, in press.

Hammouda, B., "SANS from Homogenous Polymer Mixtures: A Unifield Overview ," Adv. Poly. Sci., in press.

Hammouda, B., Briber, R., Bauer, B., "SANS from PSD/PVME/PSH," Polym. Comm. 33, 1785 (1992).

Hammouda, B., "Scattering From Mixtures of Flexible and Stiff Polymers," J. Chem. Phys., in press.

Hammouda, B., Nakatani, A.I., Waldow, D.A., Han, C.C., "Small Angle Neutron Scattering from Deuterated Polystyrene in Dioctyl Phthalate Solution Under Shear," Macromolecules 25, 2903 (1992).

Hammouda, B., "Practical Applications of Nuclear Research Reactors," NIST Sepcial Publication 844 (1992).

Hammouda, B., "Structure Factor for "Dendrimer" Polymer Gels," J. Poly. Sci. Poly. Phys. Edn. 30, 1387 (1992).

Hammouda, B., "Multidisk Neutron Velocity Selectors," Nucl. Instr. Methods in Phys. Res. A321, 275 (1992).

Hammouda, B., Neumann, D., "Quasielastic Scattering at the National Institute of Standards and Technology," J. Res. (NIST) 98, in press.

Hammouda, B., Krueger, S., Glinka, C.J., "Small Angle Neutron Scattering at the National Institute of Standards and Technology," J. Res. (NIST JRES) 98, in press.

Heiney, P.A., Vaughan, G.B.M., Fischer, J.E., Coustel, N., Cox, D.E., Copley, J.R.D., Neumann, D.A., Kamitakahara, W.A., Creegan, K.M., Cox, D.M., McCauley Jr., J.P., Smith III, A.B., "Discontinuous Volume Change at the Orientational Ordering Transition in Solid C_{60}," Phys. Rev. B 45, 4544 (1992).

Hempelmann, R., Richter, D., Rush, J.J., Rowe, J.M., "Hydrogen Site Distribution in the Alloy System $Nb_{100-x}V_xH_y$ Studied by Neutron Vibrational Spectroscopy," J. Less Common Metals 172, 281 (1991).

Huang, Q., Cava, R.J., Santoro, A., Krajewski, J.J., Peck, W.F., "Neutron Powder Diffraction Study of the Crystal Structure of $YSr_2CoCu_2O_7$ and $Y_{1-x}Ca_xSr_2CoCu_2O_7$," Physica C 193, 196 (1992).

Huang, Q., Karen, P., Karen, V.L., Kjekshus, A., Lynn, J.W., Mighell, A.D., Rosov, N., Santoro, A., "Neutron Powder Diffraction Study of the Nuclear and Magnetic Structures of $YBa_2Fe_3O_8$ at Room Temperature," Phys. Rev. B 45, 9611 (1992).

Huang, Q., Sunshine, S.A., Cava, R.J., Santoro, A., "Neutron Powder Diffraction Study of the Crystal Structure of $YSr_2AlCu_2O_7$," J. Solid State Chem., in press.

Kamitakahara, W.A., Copley, J.R.D., Cappelletti, R.L., Rush, J.J., Neumann, D.A., Fischer, J.E., McCauley, Jr., J.P., Smith III, A.B., "Rotations, Vibrations and Structure in Solid C_{60}: Investigations by Neutron Scattering," Mater. Res. Soc. Symp. Proc. on Novel Forms of Carbon, (San Francisco, April, 1992).

Kamitakahara, W.A., Lannin, J.S., Cappelletti, R.L., Copley, J.R.D., Li, Fang, "Vibrational Spectroscopy of C_{60} and Graphitic Carbons," Physica B 180 & 181, 709 (1992).

Karen, V.L., Mighell, A.D., "Converse Transformation Analysis", J. Appl. Cryst. 24, 1076 (1991).

Karen, V.L., Mighell, A.D., "NIST Lattice: A Program to Analyze Lattice Relationships," NIST Tech. Note 1290 (1991).

Kirchheim, R., Kieninger, W., Huang, X.Y., Filipek, S.M., Rush, J.J., Udovic, T., "Hydrogen in Amorphous Ni-Zr and Ni-Ti Alloys," J. Less-Comm. Metals 172-174, 880 (1991).

Klosowski, P., Giebultowicz, T.M., Rhyne, J.J., Samarth, N., Luo, H., "Antiferromagnetism in Epilayers and Superlattices Containing Zinc-Blende MnSe and MnTe," J. Appl. Phys. 70, 6221 (1991).

Klosowski, P., Giebultowicz, T.M., Samarth, N., Luo, H., Furdyna, J.K., Rhyne, J.J., "Investigation of ZnMnTe Weakly Diluted FCC Magnetic Semiconductor," Physica B 180 & 181, 114 (1992).

Klosowski, P., Giebultowicz, T.M., Samarth, N., Luo, H., Furdyna, J.K., Rhyne, J.J., "Magnetic Critical Phenomena in fcc Antiferromagnets Role of Strain and Dimensionality," J. Magn. & Magn. Mat. 104-107, 1795 (1992).

Knell, U., Heid, C., Wipf, H., Udovic, T.J., Rush, J.J., Lauter, H.J., "Hydrogen in $YBa_2Cu_3O_x$: A Neutron Spectroscopy and a Nuclear Magnetic Resonance Study," Zeitschrift Für Physikalische Chemie, in press.

Krueger, S., Long, G.G., Page, R.A., "The Effect of Green Body Density and the Role of MgO Additive on the Densification of Alumina Measured by Small-Angle Neutron Scattering," J. Amer. Cer. Soc. 74, 1578 (1991).

Krueger, S., Long, G.G., Black, D.R., Minor, P.R., Jemian, P.R., Nieman, W., Page, R.A., "Evolution of the Pore Size Distribution in Final Stage Sintering of Alumina Measured by Small-Angle X-Ray Scattering," J. Am. Ceram. Soc. 74, 2538 (1991).

Lieb, R.J., Trevino, S.F., "A Small Angle Neutron and X-Ray Scattering Study of the Onset and Nature of Fracture of Uniaxially Compressed Gun Propellants," Proc. of U.S. Army Science Conference, in press.

Lind, D.M., Tay, S-P, Berry, S.D., Borchers, J.A., Erwin, R.W., "Structural and Magnetic Ordering in Iron Oxide/Nickel Oxide Multilayers by X-ray and Neutron Diffraction", J. Appl. Phys., in press.

Long, G.G., Krueger, S., Gerhardt, R.A., Page, R.A., "Small Angle Neutron Scattering Characterization of Processing/Microstructure Relationships in the Sintering of Crystalline and Glassy Ceramics," J. Mat. Res. 6, 2706 (1991).

Lynn, J.W., "Magnetic Ordering in Oxide Superconductors," World Scientific. High Temperature Superconductivity, edited by S. K. Malik and S. S. Shah, (Nova Science Publishers, Inc., NY, 1992), in press.

Lynn, J.W., Rosov, N., Lin, Q., Lee, C-H, Fish, G., "Polarization Analysis of the Magnetic Excitations in Invar $Fe_{86}B_{14}$," Physica B 180 & 181, 253 (1992).

Lynn, J.W., "Two-dimensional Behavior of the Rare Earth Ordering in Oxide Superconductors," J. of Alloys and Compounds 181, 419 (1992).

Ma, S., Broholm, C. Reich, D.H., Sternlieb, B.J., Erwin, R.W., "Dominance of Long-lived Excitations in the Antiferromagnetic Spin-1 Chain NENP", Phys. Rev. Lett. 69, 3571 (1992).

Mackey, E.A., Copley, J.R.D., "Scattering and Absorption Effects in Neutron Beam Activation Analysis Experiments," J. Radioanalytical & Nucl. Chem, in press.

Majkrzak, C.F., Ankner, J.F., "Supermirror Neutron Guide Coatings," in Neutron Optical Devices and Applications, Proc. SPIE 1738, edited by C.F. Majkrzak, J.L. Wood, J.L., (SPIE, Bellingham, WA), in press.

Majkrzak, C.F., "Polarized Neutron Reflectometry," Physica B 173, 75 (1991).

Majkrzak, C.F., Kwo, J., Hong, M., Yafet, Y., Gibbs, D., Chien, C.L., Bohr, J., "Magnetic Rare Earth Superlattices," Advances in Phys. 40, 99 (1991).

Majkrzak, C.F., Nunez, Copley, J.R.D.,V., Ankner, J.F., Greene, G.C., "Supermirror Transmission Polarizers for Neutrons," in Neutron Optical Devices and Applications, Proc. SPIE 1738, edited by C.F. Majkrzak, J.L. Wood, (SPIE, Bellingham, WA), in press.

Majkrzak, C.F., Berk, N.F., Ankner, J.F., Satija, S.K., Russell, T.P., "Determination of Non-Magnetic Density Profiles Using Polarized Neutron Reflectivity," , edited by C.F. Marjkrzak, J.L. Wood, Neutron Optical Devices and Applications, (SPIE Bellingham, WA), in press.

Marezio, M., Santoro, A., Capponi, J.J., Cava, R.J., Chmasissen, O., Huang, Q., "The Crystal Structure of $Pb_2Dr_2YCu_3O_{8+\delta}$ with δ = 1.32, 1.46, 1.61, 1.71," Physica C 199, 365 (1992).

Michel, K.H., Copley, J.R.D., Neumann, D.A., "Microscopic Theory of Orientational Disorder and the Orientational Phase Transition in Solid C_{60}," Phys. Rev. Lett. 68 (19), 2929 (1992).

Mighell, A.D., Rodgers, J.R., Karen, V.L., "Protein Symmetry: Metric and Crystal", J. Appl. Cryst., (in press).

Mildner, D.F.R., Hammouda, B., "The Transmission of Curved Neutron Guides with Non-Perfect Reflectivity," J. Appl. Cryst. 25, 39 (1991).

Morris, R.E., Harrison, W.T.A., Nicol, J.M., Wilkinson, A.P., Cheetham, A.K., "Complex Structures by Powder Diffraction Methods: The Structure of $Ga_2(HPO_3)_3 \cdot 4H_2O$ from Synchrotron X-ray and Neutron Diffraction Data," Nature 359, 519 (1992).

Nakotte, H., Robinson, R.A., Lynn, J.W., Bruck, E., deBoer, F.R., "Field-Induced Transition in UpdSn at 3T," Phys. Rev. B (1992), in press.

Nenoff, T.M., Harrison, W.T.A., Gier, T.E., Nicol, J.M., Stucky, G.D., "Structural Characterization of a Dehydrated Magnesium/Sodium Beryllophosphate-X Phase," Zeolites, in press.

Nenoff, T.M., Harrison, W.T.A., Nicol, J.M., Stucky, G.D., Newsam, J.M., "The Crystal Structure of a New Sodium Zinc Arsenate Phase Solved by Simulated Annealing," Zeolites, in press.

Neumann, D.A., Copley, J.R.D., Cappelletti, R.L., Kamitakahara, W.A., Lindstrom, R.M., Creegan, K.M., Cox, D.M., Romanow, W.J., Coustel, N., McCauley, Jr., J.P., Maliszewskyj, N.C., Fischer, J.E., Smith III, A.B., "Coherent Quasielastic Neutron Scattering Study of the Rotational Dynamics of C_{60} in the Orientationally Disordered Phase," Phys. Rev. Lett. 67, 3808 (1991).

Neumann, D.A., Copley, J.R.D., Kamitakahara, W.A., Rush, J.J., Cappelletti, R.L., Coustel, N., McCauley, J.P., Fischer, J.F., Smith III, A.B., Creegan, K.M., Cox, D.M., "Rotational Dynamics and Orientational Melting of C_{60}: A Neutron Scattering Study," J. Chem. Phys. 96, 8631 (1992).

Neumann, D.A., Hammouda, B., "Ultra High Resolution Inelastic Neutron Scattering," J. Res (NIST) 98, in press.

Nicol, J.M., "Chemisorbed Hydrogen and Hydrogenous Molecules," Spectrochimica Acta 48A, 313 (1992).

Prask, H.J., Choi, C.S., "Residual Stress Characterization in Technological Samples," Proceedings of ASM Conference on Practical Applications of Residual Stress Technology, in press.

Prask, H.J., "Technical Activities 1991--Reactor Radiation Division," NISTIR No. 4698 (1991).

Prask, H.J., "Neutron Probes Tackle Industrial Problems," Roestvast Staal, (The Netherlands, May 1992), p. 35.

Prask, H.J., Rowe, J.M., "The Reactor and Cold Neutron Research Facility at NIST," Proc. of the 2nd Conference of the International Group on Research Reactors (Paris, France, May, 1992).

Prask, H.J., Choi, C.S., "Residual Stress Measurements in Armament-Related Components," in Measurement of Residual and Applied Stress Using Neutron Diffraction, edited by M.T. Hutchings, A.D. Krawitz, (Kluwer Acad. Publ., The Netherlands, 1992), p. 503.

Prask, H.J., Rowe, J.M., Rush, J.J., Schröder, "The NIST Cold Neutron Research Facility," J. Res. (NIST) 98, in press.

Prince, E., "Construction of Maximum Entropy Density Maps, and Their Use in Phase Determination and Extension," Acta Cryst., in press.

Prince, E., Stalick, J.K., editors Accuracy in Powder Diffraction II, Proceedings of the International Conference, NIST Spec. Publ. 846 (1992), in press.

Reis, K.P., Prince, E., Whittingham, S.M., "Rietveld Analysis of $Na_{x/2} \cdot yH_2O$ Which has the Hexagonal Tungsten Bronze Structure," Solid State Ionics., in press.

Robertson, J.L., "Random Cluster Model for Icosahedral Phase AlMnSi," in Physics and Chemistry of Finite Systems: From Clusters to Crystals 1, edited by P. Jena, S.N. Khanna, B. K. Rao, NATO ASI Series C: Mathematical and Physical Sciences-Vol. 374 (Kluwer Academic Publishers, Boston, 1992), p. 299.

Robertson, J.L., "Cluster Models for Incasahedral Phase Alloys," in Methods of Structural Analysis of Modulated Structures and Quasicrystals, edited by J. M. Pèrez-Mato, F. J. Zaniga, and G. Madariaga (World Scientific Singapore, 1991), p. 521.

Robertson, J.L., Moss, S.C., "Diffuse Scattering in Icosahedral Phase AlMnSi," J. Non-Crystalline Solids, in press.

Robertson, J.L., Jiang, X., Moss, S.C., Hashimoto, S., Kreider, K.G., Jacobson, D.C., Poate, J.M., "Ion Damage of Quasicrystalline Thin Films of Al_{83} Mn_{17}," in Statics and Dynamics of Alloy Phase Transformations, edited by A. Gonis, (Plenum Publishing Corp., New York) in press.

Robinson, R.A., Lynn, J.W., Nunez, V., Buschow, K.H.J., Nakotte, H., Lawson, A.C., "Crystallographic and Magnetic Properties of UAuSn," Phys. Rev. B, in press.

Robinson, R.A., Lawson, A.C., Lynn, J.W., Buschow, K.H.J., "Incommensurate Magnetic Order in UPtGe," Phys. Rev. B, in press.

Robinson, R.A., Lawson, A.C., Lynn, J.W., Buschow, K.H.J., "Temperature Dependence of Magnetic Order in UPdSn," Phys. Rev. B 45, 2939 (1992).

Rosov, N., Lynn, J.W., Lin, Q., Cao, G., O'Reilly, J.W., Pernambuco-Wise, P., Crow, J.E., "Antiferromagnetic Ordering of $BaPrO_3$ via Neutron Diffraction," Phys. Rev. B 45, 982 (1992).

Rosov, N., Lynn, J.W., Williams, J.J.M., Landee, C.P., "Quasi-Elastic and Inelastic Neutron Scattering Studies of $[(CD_3)_3ND]FeCl_3 \bullet 2D_2O$: A One-Dimensional Ising Ferromagnet," J. Appl. Phys., in press.

Rowe, J.M., Prask, H.J., "Status of Research Reactor Instrumentation in the USA," Physica B 174, 421 (1991).

Rowe, J.M., "NIST Reactor: Summary of Activities July 1990 - June 1991," NIST Tech. Note 1292, edited by C. O'Connor, January, 1992.

Russell, T.P., Menelle, A., Hamilton, W.A., Smith, G.S., Satija, S.K., "The Width of Homopolymer Interfaces in the Presence of Symmetric Diblock Copolymers," Macromolecules 24, 5721 (1991).

Russell, T.P., Menelle, A., Anastasiadis, S.H., Satija, S.K., Majkrzak, C.F., "Unconventional Morphologies of Symmetric, Diblock Copolymers Due to Film Thickness Constraints," Macromolecules (1992), in press.

Russell, T.P., Menelle, A., Anastasiadis, S.H., Satija, S.K., Majkrzak, C.F., "Ordering of Thin Films of Symmetric Diblock Copolymers," J. Colloid. Poly. Sci., in press.

Salamon, M.B., Beach, R.S., Borchers, J.A., Erwin, R.W., Flynn, C.P., Matheny, A., Tsui, F., Rhyne, J.J., "Magnetism of Rare-Earth/Y and Rare-Earth/Lu Superlattices and Films," J. Magn. & Magn. Mater. 104-107, 1729 (1992).

Samarth, N., Klosowski, P., Luo, H., Giebultowicz, T.M., Furdyna, J.K., Rhyne, J.J., Larson, B.E., Otsuka, N., "Antiferromagnetism in ZnSe/MnSe Strained Layer Superlattices," Phys. Rev. B 44, 4701 (1991).

Santoro, A., "Description of Layered Structures - Applications to High T_c Superconductors," Proc. of the Workshop on Irregularities, Classification and Predictions of Advanced Materials (Italy, April 13-15, 1992), in press.

Sanyal, M.K., Sinha, S.K. Gibaud, A., Satija, S.K., Majkrzak, C.F., Homma, H., "X-Ray Scattering Studies of Multilayer Interfaces," Proc. of MRS Mntg. (Boston, Fall, 1991).

Sanyal, M.K., Sinha, S.K., Gibaud, A., Satija, S.K., Majkrzak, C.F., Homma, H., "Specular and Diffuse Scattering Studies of Multilayer Interfaces," Proc. 2nd International Conference on Surface X-Ray and Neutron Scattering (Bad Honnef, Germany, June 25-28, 1991).

Saslow, W.M., Erwin, R., "Normal Modes and Structure Factor for a Canted Spin System: The Generalized Villain Model," Phys. Rev. B 45, 4759 (1992).

Satija, S.K., "Neutron Reflectivity Studies of Polymers Adsorbed at Solid-Air and Solid-Liquid Interfaces," in Neutron Optical Devices and Applications, Proc 1738, edited by C.F. Majkrzak and J.L. Wood (SPIE, Bellinghem, WA), in press.

Schaefer, D.W., Olivier, B.J., Ashley, C.S., Richter, D., Fargo, B., Frick, B., Hrubesh, L., van Bommel, M.J., Long, G., Krueger, S., "Structure and Topology of Silica Aerogels," J. Non-Crystalline Solids 145, 105 (1992).

Schreyer, A., Metoki, N., Zeidler, Th., Bödeker, P., Abromeit, A., Morawe, Ch., Romahn, U., Sonntag, P., Bröhl, K., Zabel, H., Ankner, J.F., Majkrzak, C.F., "Exchange Coupling in Single Crystalline Co/Cu (lll) Superlattices," J. Magnet. and Magnet. Mater, in press.

Sikka, M., Singh, N., Karim, A., Bates, F.S., Satija, S.K., Majkrzak, C.F., "Entropy Driven Surface Segregation in Block Copolymer Melts," Phys. Rev. Lett, in press.

Skanthakumar, S., Lynn, J.W., Peng, J.L., Li, Z.Y., "Magnetic Order of Cu in $Nd_{2-x}Ce_xCuO_4$," J. Mag. Mater. 104-107, 519 (1992).

Skanthankumar, S., Lynn, J.W., Peng, J.L., Li, Z.Y., "Field Dependence of the Magnetic Ordering of Cu in R_2CuO_4," J. Appl. Phys., in press.

Slade, R.C.T., Forano, C.R.M., Pressman, H.A., Nicol, J.M., Peraio, A., Alberti, G., "Neutron Scattering from Films of Pellicular Zirconium Phosphate," J. Mater. Chem. 2, 583 (1992).

Stalick, J.K., "Quantitative Phase Analysis with the Rietveld Method," NIST Special Publ. 846, in press.

Sumarlin, I.W., Lynn, J.W., Neumann, D.A., Rush, J.J., Peng, J.L., Li, Z.Y., Hagen, S.J., "Phonon Density of States in $Pr_{2-x}Ce_xCuO_4$ and Pr_2CuO_4," Physica C 185-187, 2571-2572 (1991).

Sumarlin, I.W., Skanthakumar, S., Lynn, J.W., Peng, J.L., Li, Z.Y., Greene, R.L., "Magnetic Ordering of Sm in Sm_2CuO_4," Phys. Rev. Lett. 68, 2228 (1992).

Trevino, S.F., Choi, C.S., Neumann, D.A., "The Methyl Torsional Levels of Solid Acetonitrile (CH_3CN)-A Neutron Scattering Study," J. Chem. Phys, in press.

Trevino, S.F., "The Triple Axis and Spins Spectrometer," J. Res. (NIST) 98, in press.

Tsui, F., Flynn, C.P., Beach, R.S., Borchers, J.A., Erwin, R.W., Rhyne, J.J., "Magnetic Structure in Dy/Sc Superlattices," J. Appl. Phys., in press.

Tsui, F., Flynn, C.P., Salamon, M.B., Borchers, J.A., Erwin, R.W., Rhyne, J.J. "Layer Thickness Dependence of Anisotropic Coupling in Gd/Y Superlattices", J. Magn. & Magn. Mat. 104-107, 1901 (1992).

Tu, Z., Lussier, J-G., Erwin, R.W., Lynn, J.W., Harrison, A., "A Polarization Analysis of Magnetic Excitations in $CsMnI_3$," Phys. Rev., in press.

Udovic, T.J., Nicol, J.M., Elsenhans, O., Buhrer, W., Felsche, J., Sieger, P., Wiebcke, M., "Neutron Vibrational Spectroscopy of an $H_3O_2^-$ Anion in Sodium Hydroxosodalite Dihydrate $Na_8[Al_6Si_6O_{24}](OH) \cdot 2H_2O$," Chem. Mater, in press.

Udovic, T.J., Rush, J.J., Berk, N.F., Anderson, I.S., "Evidence of Mode-Splitting for C-Axis-Polarized Hydrogen Vibrations in a-$ScH_{0.34}$," Phys. Rev. B 45, 12573 (1992).

Udovic, T.J., Rush, J.J., Berk, N.F., Anderson, I.S., Daou, J.N., Vajda, P., Blaschko, O., "Neutron Spectroscopic Comparison of Rare-Earth/Hydrogen α-Phase Systems," Zeitschrift für Physikalische Chemie, in press.

Williams, R.E., Rowe, J.M., Kopetka, P., "A Liquid Hydrogen Cold Neutron Source for the NBSR," Trans. Am. Nucl. Soc. 66, 169 (1992).

Wu, W., Majkrzak, C.F., Satija, S.K., Ankner, J.F., Orts, W.J., Satkowski, M., Smith, S.D., "The Density Profile at a Polymer/Solid Interface," Polymer Comm, in press.

Zhang, H., Lynn, J.W., Morris, D.E., "Magnetic Order of the Rare Earth in $Dy_2Ba_4Cu_7O_{15}$," J. of Magnet. and Magnet. Mater. 104-107, 821 (1992).

Zhang, H., Lynn, J.W., Morris, D.E., "Coupled-Bilayer Two-Dimensional Magnetic Order of the Dy Ions in $Dy_2Ba_4Cu_7O_{15}$," Phys. Rev. B 45, 1022 (1992).

Independent Programs

Akcasu, A.Z., Bahar, I., Drman, B., Feng, Y., Han, C.C., "Theoretical and Experimental Study of Dissolution of Inhomogeneities Formed During Spinodal Decomposition in Polymer Mixtures," J. Chem. Phys 97, 5782 (1992).

Anderson, D.L., Mackey, E.A., "Neutron Scattering-Induced Background Enhancement Prompt-gamma Activation Analysis," J. Radioanal. and Nucl. Chem., in press.

Anderson, D.L., Cunningham, W.C., "Determination of Boron and Other Elements in Food and Agricultural Products by PGAA," Trans. Am. Nucl. Soc. 65, 140 (1992).

Anderson, D.L., Cunningham, W.C., Alvarez, G.H., "Multielement Analysis of Foods by Neutron Capture Prompt γ-Ray Activation Analysis," J. Radioanal. Nucl. Chem., in press.

Arif, M., Dewey, M.S., Greene, G.L., Snow, W.M., "Facilities for Fundamental Neutron Physics Research at the NIST Cold Neutron Research Facility," J. Res. (NIST) 98, in press.

Balsara, N.P., Fetters, L.J., Hadjichristidis, N., Lohse, D.J., Han, C. C., Graessley, W.W., Krishnamoorti, R., "Thermodynamic Interactions in Model Polyolefin Blends Obtained by Small Angle Neutron Scattering," Macromol. 25, p. 6137 (1992).

Balsara, N.P., Lohse, D.J., Sissano, J.A., Schulz, D.N., Graessley, W.W., Krishnamoorti, R., "Thermodynamics of Random Copolymer Mixtures by SANS," ACS Division of Polymeric Materials: Science and Engineering 67, 203 (1992).

Barr, R.M., Clarke, W.B., Clarke, R.M., Venturelli, J., Downing, R.G., "Regulation of Lithium and Boron Levels in Normal Human Blood-Environmental and Genetic Considerations," J. Laboratory and Clinical Medicine, in press.

Becker, D.A., "Determination of Trace Element Impurities in High Temperature Superconductor Starting Materials," Trans. Am. Nucl. Soc. 64, 228 (1991).

Becker, D.A., "Problems and Errors in NAA Irradiations," Trans. Am. Nucl. Soc. 64, 8 (1991).

Becker, D.A., Chrintensen, R., Currie, L., Diamondstone, B., Eberhardt, K., Gills, T., Hertz, H., Klouda G., Moody, J., Parris, R., Schaffer, R., Steel, E., Taylor, J., Watters, R., Zeisler, R., "Use of NIST Standard Reference Materials for Decisions on Performance of Analytical Chemical Methods and Laboratories," NIST Spec. Publ. 829 (1992).

Becker, D.A., Anderson, D.L., Lindstrom, R.M., Greenberg, R.R., Garrity, K.M., Mackey, E.A., "Use of INAA, PGAA, and RNAA to Determine 30 Elements for Certification of an SRM: Tomato Leaves, 1573a," J. Radioanal. and Nucl. Chem., in press.

Becker, D.A., "Results of the ASTM Nuclear Methods Intercomparison on NIST Apple and Peach Leaves SRMS," J. Radioanal. and Nucl. Chem., in press.

Becker, D.A., "Unique Quality Assurance Aspects of INAA for CRM Homogeneity and Certification," Fresenius J. Anal. Chem., in press.

Becker, D.A., Greenberg, Robert R., Stone, Susan, "The Use of High Accuracy Neutron Activation Analysis for the Certification of NIST Standard Reference Materials," J. Radioanal. and Nucl. Chem. 160, 41 (1992).

Becker, D.A., Navarro, J.A., Kenna, B.T., Kossack, C.F., "A General Testing Protocol for Bulk Explosive Detection Systems," Proceedings of the 1st International Symposium on Explosive Detection Technology (1992).

Becker, P.R., Koster, B.J., Wise, S.A., Zeisler, R.M., "Biological Specimen Banking in Arctic Research: An Alaska Perspective," Science of the Total Environment, in press.

Becker, D.A., "INAA Errors and Interferences During the Certification Analysis of NIST SRM 1573a, Tomato Leaves (Renewal)," Trans. Am. Nucl. Soc. 65, 168 (1992).

Bode, P., Lindstrom, R. M., "Advanced Detector Systems: What Do They Have to Offer for Activation Analysis?," J. Radioanal. and Nucl. Chem., in press.

Carpenter, J.M., Mildner, D.F.R., "Improving the Resolution of Chopper Spectrometers at Pulsed Neutron Sources," Nucl. Instrum. Meth. A, in press.

Chen, H., Downing, R.G., Mildner, D.F.R., Gibson, W. M., Kumakhov, M. A., Ponomarev, I. Yu, Gubarev, M.V., "Guiding and Focusing Neutron Beams Using Capillary Optics," Nature 357, 391 (1992).

Chen, H., Downing, R.G., Mildner, D.F.R., Sharov, V.A., "Characterizing a Neutron Lens: Study of Capillary Optics," in Neutron Optical Devices and Applications, Proc. SPIE 1738, edited by Majkrzak, C.F. Wood, J.L., (SPIE, Bellinghem, WA) in press.

Chen, H., Heald, S.M., "Comparison of Glacing Angle EXAFS Obtained from Fluorescence and Reflectivity Measurements," J. Appl. Phys. in press.

Cunningham, W.C., Anderson, D.L., "Multielement Analysis of Foods and Related Materials by NAA," Trans. Am. Nucl. Soc. 65, 141 (1992).

Demiralp, R., Guinn, V.P., Becker, D.A., "Fluorine Determinations in Biological Materials by Instrumental Neutron Activation Analysis," Trans. Am. Nucl. Soc. 65, 168 (1992).

Dewey, M.S., "Current Results and Future Prospects for a Neutron Lifetime Determination Using Trapped Proton," in Capture Gamma-Ray Spectroscopy and Related Topics: Seventh International Symposium (1991), p. 774.

Dewey, M.S., Greene, G.L., Snow, W.M., "Neutron Beta Decay as a Test of the Standard Model,"in Proc. of the X(¦II Moriond Conf., edited by J. Tran Than Van, in press.

Dewey, M.S., Greene, G.L., Snow, W.M., "Neutron Beta Decay as a Test of the Standard Model," in Proc. of the XII Moriond Conf., edited by J. Tran Than Wan, in press.

Di Marizo, E.A., Han, C.C., "Workshop on Polymer Blends," J. Res. (NIST) 97, 1 (1992).

Downing, R.G., Lamaze, G.P., "Non-destructive Determination of Weight Percent Boron in Dielectric Films," Trans. Am. Nucl. Soc. 65, 171 (1992).

Downing, R.G., Lamaze, G.P., Langland, J.K., Hwang, S.T., "Neutron Depth Profiling: Overview and Description of NIST Facilities," J. Res. (NIST) 98, in press.

Downing, R.G., Lamaze, G.P., "Neutron Depth Profiling Technique and Facilities," Neutron News, in press.

Downing, R.G., Zeissler, C.J., Chen, H., "High Resolution Charged Particle and Neutron Imaging Using Charge Injection Devices," in Neutron X Rays and Gamma Rays: Imaging Detectors, Materials Characterization Techniques and Applications, edited by J.M. Carpenter and D.F.R. Mildner, SPIE 1737 (San Diego, CA), in press.

Dozier, W.D., Huang, J.S., Fetters, L.J., "Colloidal Nature of Star-Branched Polymer in Dilute and Semi-Dilute Solutions," Macromolecules 24, 2810 (1991).

Eisenhauer, C., "Two-Component Analytical Model to Calculate Room-Return Corrections for Calibration of Neutron Instruments," Radiation Protection Dosimetry, in press.

Evans, D.J., Cu, S.T., Hanley, H.J.M., Straty, G.C., "Conditions for Existance of a Reentrant Solid Phase in a Sheared Atomic Fluid", Phys. Rev. A 46, 6731 (1992).

Greene, G. G., Golub, R., Richardson, D., Lamoreaux, S.K., "Ultra Cold Neutrons," Science 256, 1836 (1992).

Greene, G. G., Dewey, M.S., Snow, J.M., "Neutron Beta Decay as a Test of the Standard Model," in Proc. of the XII Moriond Conference, edited by J. Tran Than Van, in press.

Graessley, W.W., Krishnamoorti, R., Balsara, N.P., Lohse, D.J., "Effect of Deuterium Substitution on Thermodynamic Interactions in Polymer Blends," ACS Division of Polymeric Materials: Science and Engineering 67, 193 (1992).

Greenberg, R.R., "Accuracy in Standards Preparation for Neutron Activation Analysis," J. Radioanal. and Nucl. Chem., in press.

Greenberg, R.R., "Quality Assurance in Standards Preparation for Neutron Activation Analysis," Trans. Am. Nucl. Soc. 64, 4 (1991).

Grundl, J.A., Eisenhauer, C.M., McGarry, E.D., Hawari, A.I., Simpson, P.A., Venkataraman, R., "The Matrials Dosimetry Reference Facility (MDRF)," ANS Trans 66, 172 (1992).

Grüning, U., Magerl, A., Mildner, D.F.R.., "Neutron Guidance by Internal Reflections in Thin Silicon Wafers," Nucl. Instrum. Meth. A314, 171 (1992).

Guinn, V.P., Demiralp, R., "Arsenic in Hair: Recent Murder Case," J. Radioanal. and Nucl. Chem., in press.

Hair, D.W., Hobbie, E.K., Nakatani, A.I., Han, C.C., "Deviation from Mean-field Behavior in a Low Molecular Weight Polymer Blend," J. Chem. Phys. 96, 9133 (1992).

Hair, D.W., Hobbie, E.K., Douglas, J., Han, C.C., "Critical Dynamics of an Asymmetric Binary Polymer Mixture," Phys. Rev. Lett 68, 2476 (1992).

Hair, D.W., Hobbie, E.K., Douglas, J., Han, C.C., "Static and Dynamic Critical Behavior of an Asymmetric Binary Polymer Blend," Poly. Preprints (ACS) 33, 120 (1992).

Hamley, I.W., Koppi, K.A., Rosedale, J.H., Bates, F.S., "Fluctuation Induced Phase Transitions in an Ordered Mesomorphic System," Nature, in press.

Han, C.C., Akcasu, A.Z., "Phase Decomposition in Polymers,"Phase Decomposition in Polymers," Annu. Rev. Phys. Chem. 43, 61 (1992).

Hanley, H.J.M., Straty, G.C., Linder, P., "Structure of a Binary Suspension, Langmuir," in press.

Hobbie, K.E., Hair, D.W., Nakatan, A.I., Han, C.C., "Crossover to Strong Shear in a Low Molecular Weight Critical Polymer Blend," Polymer Preprints (ACS) 33, 120 (1992).

Huang, J.S., Fetters, L.J., Lin, M.Y., Richter, D., Hadjichistidis, N., Gast, A.P., "Structure of Diblock Copolymer Aggregates in Solution," in Complex Fluids, edited by E. Sirot, D. Weitz, T. Witten, and I Israelachivili, (Mater. Sci. Proc., 1992),p. 355.

Huang, J.S., Park, T.S., Downing, R.G., Lamaze, G.P., Chang, C.G., Song, J.Y., "^{10}B Surface Contamination for CdTe by the Cold Neutron Depth Profiling Technique," J. of Korean Soc. of Anal. Sci. 4, 241 (1991).

Iyengar, G.V., Wolf, W.R., Greenberg, R.R., Demiralp, R., "Mixed Total Diet Slurry as a Proposed Reference Material," submitted to Fresenius J. Anal. Chem. (1992).

Jinnai, H., Hasegawa, H., Hashimoto, T., Han, C.C., "Inversion of Phase Diagram from UUCST to LCST in Deuterated Polybutadiene Blends," Macromolecules 25, 6078 (1992).

Kitto, M.E., Anderson, D.L., Gordon, G.E., Olmez, I., "Rare Earth Distributions in Catalysts and Airborne Particles, Environ, Sci. Technol. 26, 1368 (1992).

Kitto, M.E., Faller, S.H., Anderson, D.L., McCarthy, L.E., "Airborne Chernobyl Radioactivity in College Park, Maryland," Radiochimica Acta 55, 43 (1991).

Koppi, K.A., Tirrell, M., Bates, F.S., "Shear-Induced Isotropic-to-Lamellar Transition," Phys. Rev. Lett., in press.

Lamaze, G.P., Downing, R.G., Langland, J.K., Hwang, S.T., "The New Cold Neutron Depth Profiling Instrument at NIST," J. Radioanal. and Nucl. Chem. 160, 315 (1992).

Lamaze, G.P., Downing, R.G., Pilione, L., Badzian, A., Badzian, T., "Analysis of Boron in CVD Diamond Surfaces Using Neutron Depth Profiling," Appl. Sur. Sci., in press.

Lauenstein, G., Schantz, M.M., Zeisler, R., Wise, S.A., "Comparison of Data From a U.S. Coastal Monitoring Program and Its Specimen Banking Activity: Specimen Banking as a Quality Assurance Element," Science of the Total Environment, in press.

Lin, M.Y., Abeles, B., Huang, J.S., Stasiewski, H.E., Zhang, Q., "Viscous Flow and Diffusion of Liquids in Microporons Glasses," Phys. Rev. B 46, 10701 (1992).

Lindstrom, R.M., "Prompt-Gamma Activation Analysis," J. Res. (NIST), in press.

Lindstrom, R.M., Norman, B.R., "Determination of Iodine and Iodine-129 in Several New Botanical SRMs by NAA," Trans. Am. Nucl. Soc. 64, 11 (1991).

Lindstrom, R.M., Paul, R.L., Vincent, D.H., Greenberg, R.R., "Measuring Hydrogen by Cold-Neutron Prompt-Gamma Activation Analysis," J. Radioanal. and Nucl. Chem., in press.

Lindstrom, R.M., Blaauw, M., "Local Area Networks for Use in Neutron Activation Analysis: Advantages and Pitfalls," J. Radioanal. and Nucl. Chem., in press.

Lindstrom, R.M., Zeisler, R., Vincent, D. H., Greenberg, R.R., Stone, C.A., Mackey, E. Z., Anderson, D.L., and Clark, D.D., "Neutron Capture Prompt Gamma-Ray Activation Analysis at the NIST Cold Neutron Research Facility," J. Radioanal. and Nucl. Chem., in press.

Lindstrom, R.M., "High-Sensitivity Gamma Counting in Activation Analysis," Appl. Radiat. Isot. 43, 263 (1992).

Lindstrom, R.M., "Advanced Detector Systems: What Do They Have to Offer for Activation Analysis?," J. Radioanal. and Nucl. Chem, in press.

Lindstrom, R.M., Garrity, K.M., "Control of High Count Rate and Decay Effects," Trans. Am. Nucl. Soc. 64, 7 (1991).

Mackey, E.A., Copley, J.R.D., "Scattering and Absorption Effects in Neutron Beam Activation Analysis Experiments," J. Radioanal. and Nucl. Chem., in press.

Mackey, E.A., Gordon, G. E., Lindstrom, R. M., Anderson, D. L., "Use of Spherical Targets to Minimize Effects of Neutron Scattering by Hydrogen in Neutron Capture Prompt Gamma-Ray Activation Analysis," Anal. Chem., in press.

Mackey, E.A., Gordon, G., Lindstrom, R.A., "Accuracy in Neutron Capture Prompt Gamma-Ray Activation Analysis by Hydrogenous Materials," Trans. Am. Nucl. Soc. 64, 7 (1992).

Matsushita, Y., Shimizus, K., Noda, I., Chang, T., Han, C.C., "Chain Conformation of Block Copolymer Copolymers in Dilute Solutions Measured by Small-Angle Neutron Scattering," Polymer 33, 2412 (1992).

Mays, C.W., Aamodt, R.L., Inn, K.G.W., Brown, D.R., Greenberg, R.R., Iyengar, V.G., Schima, F.J., Slaback, L.S., Tracy, J.W., Mossman, K.L., and Lynch, T.P., "External Gamma Ray Counting of Selected Tissues from a Thorotrast Patient," J. Health Phys. 63, 33 (1992).

Mildner, D.F.R., "Neutron Focusing Using Converging Guides," Capture Gamma-Ray Spectroscopy, AIP Conf. Proc., edited by R.W. Hoff (Pacific Grove, CA) 238, 1003 (1992).

Mildner, D.F.R., Arif, M., Stone, C.A., Crawford, R.K., "The Neutron Transmission of Single Crystal Sapphire Filters," Nucl. Instrum. Meth. A, in press.

Mildner, D.F.R., Chen, H., Downing, R.G., Sharov, V.A., "Developing a Focused Neutron Probe for Materials Analysis", Proc. 50th Annual meeting of Electron Microscopy Society of America, edited by G.W. Bailey, J. Bentley & J.A. Small, San Francisco Press Inc., 1728, 1992 (Boston, MA).

Mildner, D.F.R., Chen, H., Downing, R.G., Sharov, V.A., "Neutron Focusing: A Point to be Made,", Neutron News, in press.

Mildner, D.F.R., Chen, H., Magerl, A., Grüning, U., "Promise of Silicon Wafer Microguides for Future Neutron Optical Elements," in Neutron Optical Devices and Applications, Proc. SPIE 1738, edited by C.F. Majkrzak and J.L. Wood, (SPIE, Bellinghem, WA), in press.

Mildner, D.F.R., Hammouda, B., "The Transmission of Curved Neutron Guides With Non-Perfect Reflectivity," J. Appl. Cryst. 25, 39 (1992).

Norman, B.R., Iyengar, V., "Determination of Iodine in Diverse Botanical and Dietary Matrices by Preirradiation Combustion Followed by Neutron Activation Analysis," Fresenius J. Anal. Chem., in press.

Paul, R.L., Lindstrom, R.M., Vincent, D.H., "Cold Neutron Prompt Gamma Activation Analysis at NIST--A Progress Report," J. Radioanal. and Nucl. Chem., in press.

Richter, D., Juchnischke, O., Willner, L., Fetters, L.J., Lin, M.Y., Huang, J.S., Roovers, J., Toporowski, P., Zhou, L.L., "Structure and Ordering Phenomena of Star Polymers in Solutions," Poly. Maters. Sci. and Eng. 67, 425 (1992).

Schirmer, A., Mildner, D.F.R., "Calculation of the Transmission of Neutron Benders," Meas. Sci. & Tech. 2, 1059 (1991).

Scott, R.D., Pauwels, J., Eykens, R., Bryne, J., Dawber, P.G., Gilliam, D.M., "The Characterization of ^{10}B and ^{6}LiF Reference Deposits by the Measurement of Neutron Induced Charged Particle Reactions," Nucl. Instr. and Meth. in Phys. Rev. A 314, 163 (1992).

Shibayama, M., Tanaka, T., Han, C.C., "Small Angle Neutron Scattering Study oon Weakly Charged Temperature Sensitive Polymer Gels,", J. Chem. Phys., in press.

Shibayama, M., Tanaka, T., Han, C.C., "Small Angle Neutron Scattering Study on Poly(N--Isopropyl Acrylamide) Gels Near Their volume-Phase Transition Temperation," J. Chem. Phys., in press.

Snow, W.M., Wang, Y, Sokol, P.E., "Neutron Diffraction from Liquid and Solid ^{2}D in Vycore Glass, Appl. Phys. Lett., in press.

Soni, K.K., Williams, D.B., Newbury, D.E., Chi, P., Downing, R.G., Lamaze, G.P., "Depth-distribution of Lithium in Oxidized Binary Aluminum-Lithium Alloys Determined by Secondary Ion Mass Spectrometry and Neutron Depth Profiling," Corrosion, in press.

Stone, C.A., Mildner, D.F.R., Zeisler, R., Crammer, D.C., "Capture Gamma-Ray Spectroscopy Using Cold Neutron Beams," Capture Gammma-Ray Spectroscopy, edited by R. W. Hoff, AIP Conf. Proc. 238, 929 (1991).

van Well, A.A., de Haan, V.O., Mildner, D.F.R., "The Average Number of Reflections in a Curved Neutron Guide," Nucl. Instrum. & Meth. A309, 284 (1991).

Wasserman, E.G., Richardson, J.M., Thompson, A.K., Coulter, K.P., Freeedman, S.J., Bowles, T.J., Elliott, S.R., Nico, J.S., Spencer, T.C., Robertson, R.G.H., Wilkerson, J.F., Chupp, T.E., Dewey, M.S., Gilliam, D.M., Greene, G.L., Snow, W.M., "Development of an Experiment to Search for Time Reversal," Invariance Violation," Bull. Am. Phys. Soc. 37, 1273 (1992).

Willner, L., Richter, D., Jucknischke, O., Farago, B., Fetters, L.J., Huang, J.S., "Incipient Ordering of Star Polymer in Solutions by SANS, Euro. Phys. Lett. 19, 297 (1992).

Weider, T., Glasser, M.A., Hanley, H.J.M., Clark, N.A., "Shear Melting ofTwo Dimensional Solids," Phys. Rev., in press.

Wise, S.A., Schantz, M.M., Koster, B.J., Demiralp, R., Mackey, E.A., Greenberg, R.R., Burow, M., Ostapczuk, P., and Lillistolen, T.I., "Development of Frozen Whale Blubber and Liver Reference Materials for the Measurement of Organic and Inorganic Contaminants," Fresenius A. Anal. Chem., in press.

Wu, W., Wignall, G.D., Madelkern, L., "A SANS Study of the Plastic Deformation Mechanism in Polyethylene," Polymer 33, 4137 (1992).

Wu, W., "Off-Specular Reflection from Flat Interfaces with Density or Compositional Fluctuations," J. Chem. Phys. 98, in press.

Zeisler, R., Wise, Stephen, Koster, Barbara, "Specimen Banking at the National Institute of Standards and Technology," in Analytical Approaches As Related to Specimen Banking, M. Rossbach, P. Ostapczuk, and J.D. Schladot, Eds., Springer Verlag, Stuttgart, Germany, 37 (1992).

Zeisler, R., Demiralp, R., Koster, B., Becker, P., Ostapczuk, P., Wise, S.A., "Determination of Inorganic Constituents in Marine Mammal Tissues," Science of the Total Environment, in press.

Zeisler, R., Demiralp, R., Makarewicz, M., "High Count Rate Gamma Spectrometry: A Recent Experiment in High Accuracy NAA Applications," J. Radioanal. and Nucl. Chem., in press.

Zirkel, A., Urban, V., Richter, D., Fetters, L.J., Huang, J.S., "Polymer Materials: Science and Engineering 67, 215 (1992).